MULTIDISCIPLINARY CENTER FOR EARTHQUAKE ENGINEERING RESEARCH
A National Center of Excellence in Advanced Technology Applications

ISSN 1520-295X

Behavior of Underground Piping Joints Due to Static and Dynamic Loading

by

Ronald D. Meis, E. Manos Maragakis and Raj Siddharthan
University of Nevada, Reno
Civil Engineering Department
Reno, Nevada 89557

Technical Report MCEER-03-0006

November 17, 2003

This research was conducted at the University of Nevada at Reno and was supported primarily by the Earthquake Engineering Research Centers Program of the National Science Foundation under award number EEC-9701471.

NOTICE

DISCLAIMER

- This document has been reproduced from the best copy furnished by the sponsoring agency. It is being released in the interest of making available as much information as possible.

MULTIDISCIPLINARY CENTER FOR EARTHQUAKE ENGINEERING RESEARCH
A National Center of Excellence in Advanced Technology Applications

Behavior of Underground Piping Joints Due to Static and Dynamic Loading

by

Ronald D. Meis[1], E. Manos Maragakis[2] and Raj Siddharthan[3]

Publication Date: November 17, 2003
Submittal Date: April 1, 2003

Technical Report MCEER-03-0006

Task Numbers 1.6 and 4.1

NSF Master Contract Number EEC-9701471

1 Graduate Research Assistant, Civil Engineering Department, University of Nevada, Reno
2 Professor and Chair, Civil Engineering Department, University of Nevada, Reno
3 Professor, Civil Engineering Department, University of Nevada, Reno

MULTIDISCIPLINARY CENTER FOR EARTHQUAKE ENGINEERING RESEARCH
University at Buffalo, State University of New York
Red Jacket Quadrangle, Buffalo, NY 14261

Preface

The Multidisciplinary Center for Earthquake Engineering Research (MCEER) is a national center of excellence in advanced technology applications that is dedicated to the reduction of earthquake losses nationwide. Headquartered at the University at Buffalo, State University of New York, the Center was originally established by the National Science Foundation in 1986, as the National Center for Earthquake Engineering Research (NCEER).

Comprising a consortium of researchers from numerous disciplines and institutions throughout the United States, the Center's mission is to reduce earthquake losses through research and the application of advanced technologies that improve engineering, pre-earthquake planning and post-earthquake recovery strategies. Toward this end, the Center coordinates a nationwide program of multidisciplinary team research, education and outreach activities.

MCEER's research is conducted under the sponsorship of two major federal agencies: the National Science Foundation (NSF) and the Federal Highway Administration (FHWA), and the State of New York. Significant support is derived from the Federal Emergency Management Agency (FEMA), other state governments, academic institutions, foreign governments and private industry.

MCEER's NSF-sponsored research objectives are twofold: to increase resilience by developing seismic evaluation and rehabilitation strategies for the post-disaster facilities and systems (hospitals, electrical and water lifelines, and bridges and highways) that society expects to be operational following an earthquake; and to further enhance resilience by developing improved emergency management capabilities to ensure an effective response and recovery following the earthquake (see the figure below).

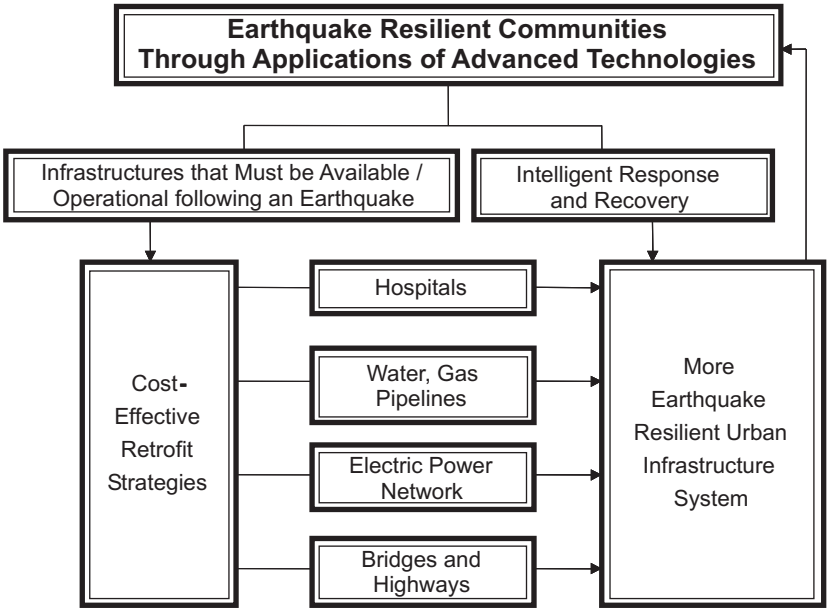

A cross-program activity focuses on the establishment of an effective experimental and analytical network to facilitate the exchange of information between researchers located in various institutions across the country. These are complemented by, and integrated with, other MCEER activities in education, outreach, technology transfer, and industry partnerships.

This report describes the procedures and results of an empirical data research program designed to determine the static and dynamic behavior of some typical restrained and unrestrained underground pipe joints. Pipelines have suffered damage and failure during past earthquakes, and it is well-documented that a majority of these failures occurred at unrestrained pipe joints, while restrained joints have a capacity to resist pull-out. Therefore, both unrestrained and restrained pipe joints need to be examined, and their axial and rotational stiffness, and strength characteristics need to be investigated to help mitigate potential damage and failure. Five different material types with eight different joint types and several different pipe diameters were used in this testing program. The test results are given as load-displacement plots, moment-rotation plots, and tables listing the axial and rotational stiffness, force capacities, and bending moment capacities. A comparison is made between static and dynamic results to determine if static testing is sufficient to characterize the dynamic behavior of pipe joints. This report also suggests methods to use the test results for a finite element pipeline system analysis and for risk assessment evaluation.

ABSTRACT

This report describes the procedures and results of an empirical data research program designed to determine the static and dynamic behavior of some typical restrained and unrestrained underground pipe joints, such as their axial and rotational stiffness, axial force capacity, and moment bending capacity. Pipelines have suffered damage and failure from past earthquakes and have been shown to be vulnerable to seismic motions. It has been well documented that a majority of pipeline failures have occurred at unrestrained pipe joints while restrained joints have a capacity to resist pull-out, and therefore, both unrestrained and restrained pipe joints need to be examined and their axial and rotational stiffness and their strength characteristics need to be investigated in order to help mitigate potential damage and failure. Five different material types with eight different joint types and several different pipe diameters were used in this testing program. The test results are given as load-displacement plots, moment-rotation plots, and tables listing the axial and rotational stiffness, force capacities, and bending moment capacities. A comparison is made between static results and dynamic results to determine if static testing is sufficient to characterize the dynamic behavior of pipe joints. This report also suggests methods to use the test results for a finite element pipeline system analysis and for risk assessment evaluation.

ACKNOWLEDGMENTS

The project described in this report was funded by the Multidisciplinary Center for Earthquake Engineering Research (MCEER) located at the State University of New York at Buffalo under a grant from the National Science Foundation (NSF). The authors are grateful for this funding and support. However, it must be noted that the opinions expressed in this report are those of the authors and do not necessarily reflect the views of MCEER.

TABLE OF CONTENTS

LIST OF ILLUSTRATIONS

FIGURE TITLE PAGE

LIST OF TABLES

SECTION 1
INTRODUCTION

1.1 Background

Pipelines transporting water, gas, or volatile fuels are classified as part of the infrastructure "lifeline" system and are critical to the viability and safety of communities. Disruption to these lifelines can have disastrous results due to the threat they pose in the release of natural gas and flammable fuels, or in the restriction of needed water supply required to fight fires and for domestic use. M. O'Rourke (1996), Iwamoto (1995), Kitura and Miyajima (1996), T. O'Rourke (1996) and other authors have documented pipeline damage and failures caused by wave propagation of seismic motions, surface faulting, and by permanent ground deformations resulting from liquefaction and landslides. Figures 1-1 to 1-8 show examples of joint failures during the Northridge and Kobe earthquakes. A large number of pipeline failures have occurred at joints due to pull-out of unrestrained bell and spigot type joints and the fracture and buckling of welded joints on steel pipes. Singhal (1984) performed testing on 100 mm, 150 mm, 200 mm and 250 mm diameter ductile iron pipe with push-on rubber gasket joints to determine their structural and stiffness characteristics when subjected to axial pull-out loads. He showed that the resistance to pull-out of unrestrained push-on joints is quite low, less than 2 kN (500 lbs) in magnitude, which suggests that the cyclic nature of the forces induced by earthquakes and by the resulting ground deformations is an important design concern for pipelines with unrestrained joints. The use of commercially available joint restraining devices such as retaining rings, gripper gaskets, and bolted collars can greatly increase a joint's capacity to resist pull-out, and therefore, decrease the probability of joint failure.

The resulting interruption in service and the economic consequences of repair and replacement of damaged pipe can be severe for communities as well as for pipeline owners. Some preliminary strategies have been implemented to address the problem of

service disruption. Some pipeline owners are willing to let the inevitable damage occur and to by-pass the damaged area with temporary flexible hosing until repair to the pipeline can be made. This strategy is based on two assumptions: 1) the time of disruption until the by-pass can be installed is tolerable, and 2) the redundant lines will have the capacity to provide vital services. Another strategy employed for seismic damage mitigation is to develop a long-term program of pipeline upgrade to a more seismic resistant design. If this is in conjunction with regular replacement of older and corroded pipes, it may be part of a normal maintenance program and the cost can be incorporated into an annual maintenance expense. Other pipeline owners may select to develop a seismic upgrade program for pipelines that still have remaining economic life, with the cost budgeted in a special seismic upgrade account. In either case, there is a possibility that the time-span to complete the upgrade may be excessive and the probability of a major earthquake occurring during this time-span may be high. However, if pipeline owners were able to assess the damage potential of zones within their service area, certain portions of their system and corresponding upgrade plans could be prioritized according to the damage potential which would reduce the probability of major earthquake damage occurring within that zone. A comprehensive program of this type can help in mitigating potential damage and the consequence of failures.

This report discusses an empirical research project designed to determine the static and dynamic axial and rotational stiffness and the strength characteristics of a number of common types of pipe joints, both restrained and unrestrained. It must be recognized that a pipe joint, especially one with a restraining device, is an assembly of structural mechanisms, each with highly non-linear properties such as friction sliding, compressive behavior, tensile restraint, and surface gouging and extrusion. As such, the examination of the behavior of pipe joints requires empirical testing of the joint assembly as a whole. The results of this testing can help in assessing the response of pipelines to seismic motion and ground deformation and identify areas of potential damage. The data from this research can be used in a computer based finite element pipeline system analysis or in a risk assessment evaluation to determine probable joint failure (see Section 5). A complete evaluation of the effects of seismic motions on pipelines must also include the

evaluation of the soil-pipe interaction and how strains in the soil are transferred to the pipe (see Appendix E).

This experimental project included testing of different types of pipe joints and materials and was divided into three phases: 1) static axial loading, 2) dynamic axial loading, and 3) static and dynamic bending loading. Static axial loading was initially done, not only to obtain static axial behavior characteristics, but also to get a benchmark of the maximum force level capacities of the individual pipe joints so that the dynamic axial testing phase of the project could be properly planned and designed. Since static actuators are able to deliver a greater level of loading to a specimen than dynamic actuators, static axial loading was performed on a larger number of pipe joints and diameters, while the diameters of pipe for axial dynamic loading and bending loading were limited due to the load capacity limitations of the loading assemblies. The results of the experiments produced extensive empirical data on the static and dynamic axial and bending stiffness and failure levels of the specimens tested. They also allowed comparisons between restrained and unrestrained joints, between different pipe diameters, and between static and dynamic loadings. However, the characterization of the behavior of joints are limited to the specimens tested and should not be extrapolated to other joint types or pipe diameters.

1.2 Past Performance of Pipelines

Pipeline damage that occurred during recent earthquakes has been well documented. T. O'Rourke (1996) reviewed the performance and damage of pipelines for various earthquakes and its effects on different lifeline systems. Table 1-1 summarizes the amount of damage that occurred to pipelines in some recent earthquakes. In the 1989 Loma Prieta earthquake, the major damage was concentrated in areas of soft soils, such as in the Mission district in San Francisco. In the San Francisco, Oakland, Berkeley, and the Santa Cruz areas, there were almost 600 water distribution pipeline failures. In the 1994 Northridge earthquake, over 1400 failures were reported including 100 failures to

critical large diameter lines. In the 1995 Kobe earthquake, 1610 failures to distribution water mains were reported along with 5190 failures to distribution gas mains.
Figures 1-1 to 1-8 are field photographs of some typical types of failures that occurred in the Northridge and the Kobe earthquakes.

TABLE 1-1 Earthquake Damage Data Summary (O'Rourke 1996)

1989 Loma Prieta Earthquake	
San Francisco, Oakland, Berkeley	350 repairs to water lines
Santa Cruz	240 repairs to water lines
Overall area	>1000 repairs to gas lines
1994 Northridge	
Los Angeles area	1400 repairs to water lines 107 repairs to gas lines
1995 Kobe Earthquake	
Kobe City	1610 repairs to water lines 5190 repairs to gas lines

The evidence and documentation shows that earthquakes will cause damage and failure of pipelines due to transient wave motion and ground deformation, resulting in disruption to communities and utility services, and risking the life-safety of citizens. Research into the behavior of pipelines and in particular, pipe joints, both restrained and unrestrained, must be done in order to understand how and where piping systems fail, and to develop mitigation methods to reduce the damaging results of earthquakes.

1.3 Past Research

Extensive research studies have been performed in the past, investigating the effects of seismic motions and ground deformations on buried pipelines, focusing on the extent and causes of failures, and the determination of their structural properties. Current testing conducted by manufacturers has been limited to determining the pressure capacity and pressure rating of pipes and pipe fittings, and is essentially a proof-testing procedure to a pre-specified level. Past earthquakes have shown that pipelines will fail during seismic

events and ground movements, and that research into pipeline behavior is essential. Past research can be divided into three areas: 1) review and extent of pipeline damage, 2) theoretical and analytical evaluation of pipelines and pipe joint behavior, and 3) empirical testing of pipe joints to determine their structural properties.

Iwamatu et al. (1998) document failures and the failure rate per km in the 1995 Kobe earthquake. They provide a comprehensive summary on pipeline damage in terms of pipe material, joint type, and the failure mechanisms that were observed. They also report that the majority of pipeline failures were at the joints, and the predominant modes of failure were slip-out of the joints and the intrusion of the spigot into the bell end. They observed that in steel pipes, failure occurred in the welded joints.

Kitura and Miyajima (1996) document failures in the 1995 Kobe earthquake. They report that the majority of pipeline failures were at the joints and the predominate modes of failure were slip-out of the joints and the intrusion of the spigot into the bell end, especially in small diameter cast iron pipes. These researchers provide a comprehensive summary on pipeline damage in terms of pipe material type, joint type, and the failure mechanisms that were observed.

Wang and Cheng (1979) state that " most literature on pipeline failure due to earthquakes indicated joints being pulled out and crushed are the most common modes of failures".

Trifunac and Todorovska (1997) have a detailed investigation for the amount and types of pipe breaks occurring during the 1994 Northridge earthquake. They report that the "occurrence of pipe breaks in those areas during earthquakes can be correlated with the recorded amplitudes of strong ground motion....". In their paper, they note the distribution of pipe breaks and present empirical equations which relate the average number of water pipe breaks per km of pipe length with the peak strain in the soil or intensity of shaking at the site.

T. O'Rouke and Palmer (1996) review the performance of gas pipelines in Southern California over a 61 year period. Statistics are provided for 11 major earthquakes starting from the 1933 Long Beach earthquake up to the 1994 Northridge earthquake. The paper states "an evaluation is made of the most vulnerable types of piping, failure mechanisms, break statistics, and the threshold of seismic intensity to cause failure, and damage induced by permanent ground displacements".

Newmark (1967), in a seminal paper on wave propagation in soil, develops the relationship between seismic motions and the resulting soil strains and curvatures, and shows that the strains induced in the soil are related to the velocity of the seismic motion and the shear wave velocity of the soil. This paper is cited by almost all subsequent research publications that focus on the evaluation of pipeline behavior and earthquakes.

Wang (1979) summarizes the seismic motion and soil strain relationships. Using these relationships as a basis, Wang develops a simplified quasi-static approach to determine the relative pipeline displacements and rotations, and proposes design criteria and a methodology to resist seismic wave propagation effects.

Singhal (1984) performed a number of experiments on rubber gasketed ductile iron pipe joints to determine their structural and stiffness characteristics. The joints were subjected to axial and bending static loading for pipes that were encased in a "sand box" that allowed the soil-pipe interaction and overburden pressures to be included. The author gives failure criteria in terms of deformations for various sizes of pipes and suggests a modified joint detail to provide greater deformation capacity. His results showed that the resistance to pull-out of the spigot end from the bell end is low.

Wang and Li (1994) conducted studies on the damping and stiffness characteristics of flexible pipe joints with rubber gaskets, both axial and lateral, and subjected to dynamic cyclic loading. They provide expressions for energy dissipation and for equivalent axial and lateral stiffness.

Figure 1-1 Ruptured 150 mm Dia. Cast Iron Pipe from the Northridge Earthquake (Ref: LADWP 1999)

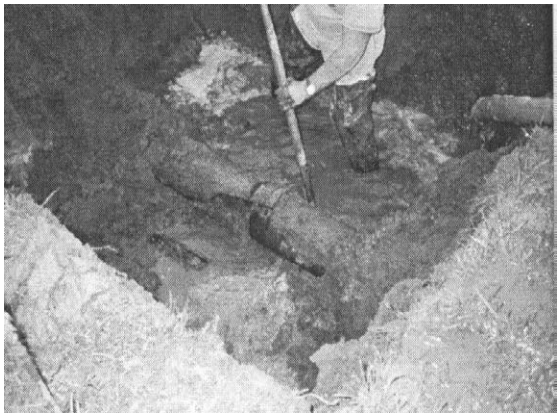

Figure 1-2 Cracked Bell on 200 mm Dia. Cast Iron Pipe from the Northridge Earthquake (Ref: LADWP 1999)

Figure 1-3 Slip-Out of Joint on 450 mm Dia. Cast Iron Pipe from the Kobe Earthquake Kobe (Ref: Iwamoto 1995)

Figure 1-4 Slip-Out of Joint on 200 mm Dia. Ductile Iron Pipe from the Earthquake (Ref: Iwamoto 1995)

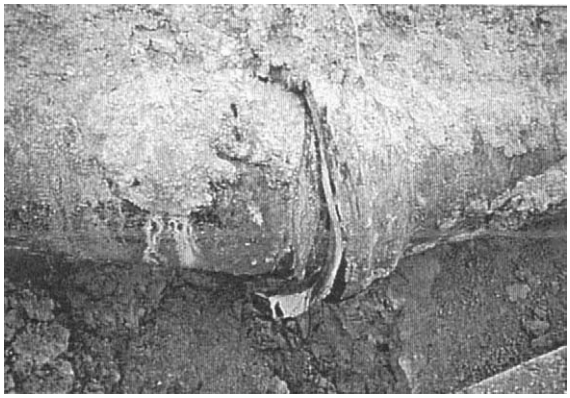

Figure 1-5 Slip-Out of Joint on 450 mm Dia. Cast Iron Pipe from the Kobe Earthquake (Ref: Iwamoto 1995)

Figure 1-6 Shear Failure on 200 mm Dia. Cast Iron Pipe from the Kobe Earthquake (Ref: Iwamoto 1995)

Figure 1-7 Slip-Out of Joint on 300 mm Dia. Ductile Iron Pipe from the Kobe Earthquake (Ref: Iwamoto 1995)

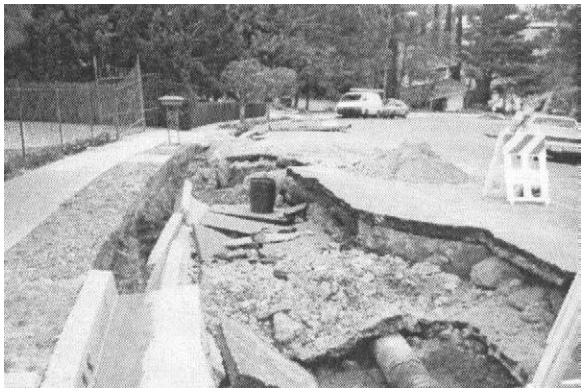

Figure 1-8 Failure of 300 mm Dia. Steel Main from the Northridge Earthquake (Ref: LADWP 1999)

1.4 Test Specimen Descriptions

Common pipe material and joint types of various diameters were used in this experimental project. The material types tested were: 1) cast iron, 2) ductile iron (DIP), 3) steel, 4) PVC, and 5) polyethylene (PE). Several different types of joints and pipe diameters were tested. The most common joint type used for water distribution is ductile iron pipe with "push-on" joints that is comprised of a plain pipe or "spigot" end, which is

inserted into an enlarged or "bell" end. A rubber ring gasket, which is compressed during the insertion of the spigot end, provides a water-tight seal at the joint. Figure 1-9 shows a sketch of the ductile iron pipe tested with the following joint configurations:

1) unrestrained push-on joint with rubber gasket seal (Figure 1-9a),
2) bell-spigot joint restrained with retaining ring (Figure 1-9b),
3) bell-spigot joint restrained with gripper gasket seal (Figure 1-9c), and,
4) bell-spigot joint restrained with bolted collar (Figure 1-9d)

The restraining mechanisms shown, as well as other restraining devices are commercially available and are commonly used on ductile iron pipe with unrestrained push-on type joints, especially as a replacement for conventional thrust blocks. Other pipe materials and joints, such as welded steel joints and PE fused joints, have an inherent capacity to resist tension due to the continuity of material through the joint. The types and description of restrained pipe joints tested in this project are briefly described below.

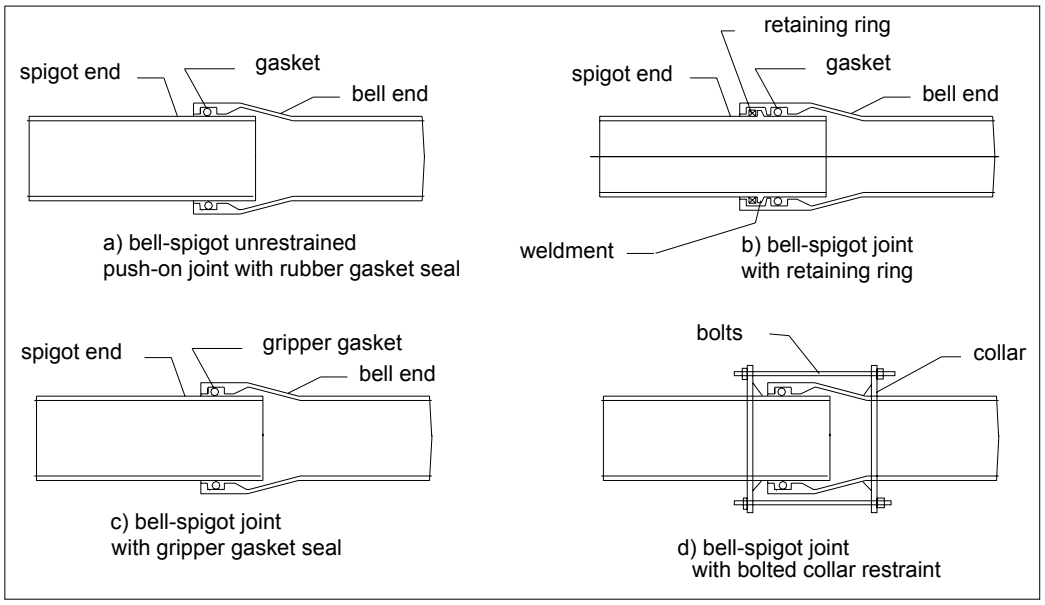

Figure 1-9 Joint Types for Ductile Iron Pipe

Cast iron pipe with bell and spigot lead caulked unrestrained joint (Figure 1-10). Cast iron has been used for water transportation for many years, and was first introduced in the United States around 1817. Today, more than 350 U.S. utilities have had cast iron distribution mains in continuous service for more than 100 years and cast iron is currently the most common type of pipe material in service for water distribution systems. Graphite flakes are distributed evenly throughout the material. They have a darkening effect on the material, giving it its proper name of "gray cast iron". Historically, the most common type of caulking at the bell and spigot joint has been poured lead with tightly tamped oakum material. These joint caulkings tend to become rigid with age, making it susceptible to damage during earthquake motion.

Figure 1-10 Cast Iron Pipe with Lead-Caulked Joint

Ductile iron pipe with bell and spigot push-on rubber gasket unrestrained joint (Figure 1-11). Ductile iron pipe is one of the most commonly used materials for new water distribution installations today. It differs from cast iron in that its graphite is spheroidal or nodular in form instead of flakes, resulting in greater strength, ductility, and toughness due to this change in microstructure. It is manufactured by a centrifugally casting system as opposed to the pit casting for cast iron. Ductile iron was first introduced in about 1955, and has been recognized as the standard for modern water systems. Normally, ductile iron pipe is furnished with cement-mortar interior lining. The specifications for water transportation using ductile iron pipe are governed by the American Water Works Association (AWWA) C151.

Figure 1-11 Ductile Iron Pipe Segments

Ductile iron pipe with bell and spigot retaining ring restrained joint. Figure 1-12 shows a ductile iron pipe joint with a retaining snap-ring and a weldment on the spigot end, both with beveled faces, ready to be inserted into the bell end. A weldment is a steel bar bent to fit around the circumference of the spigot end and welded to the pipe surface. After the joint is assembled, the retaining snap-ring snaps into a groove in the bell end behind the weldment. When a tension force or withdrawal motion is applied to the joint, the weldment bears against the retaining ring and prevents the two ends from pulling apart. This results in an outward radial pressure on the bell.

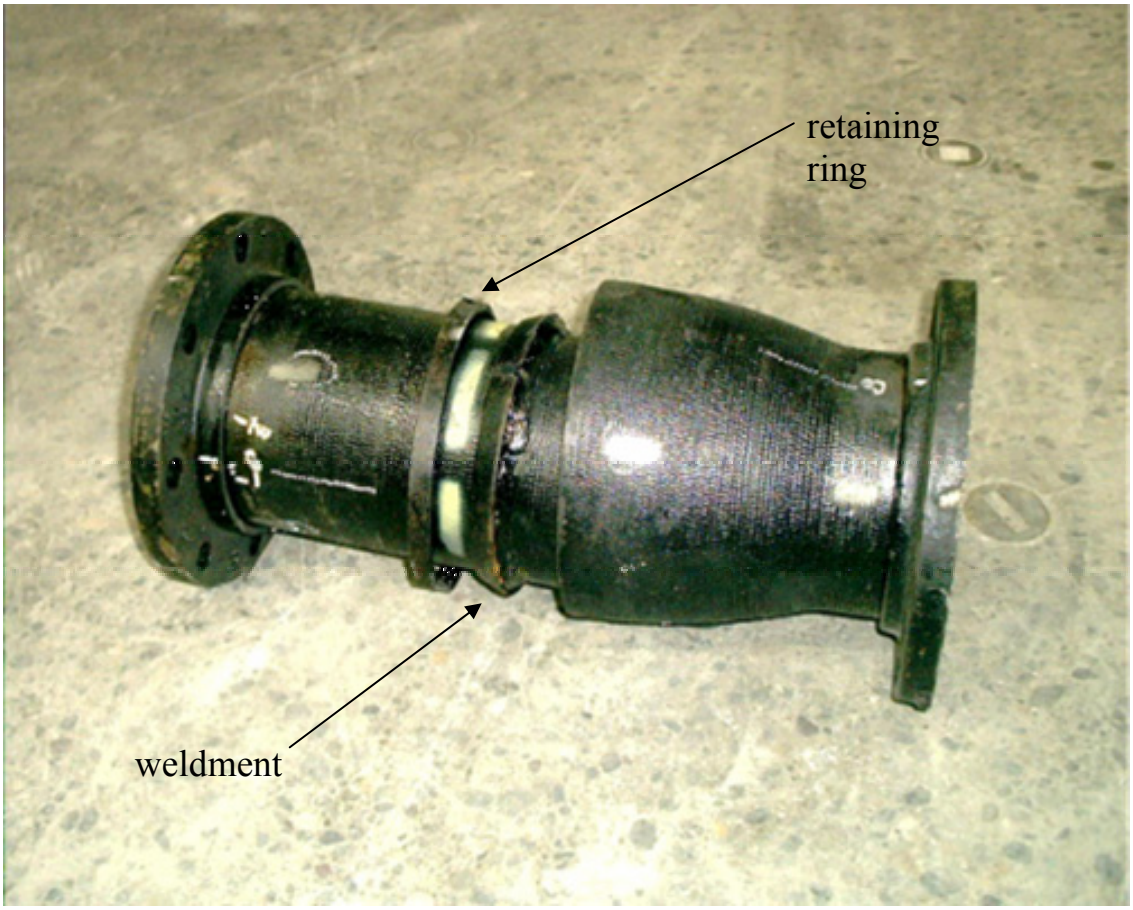

Figure 1-12 Ductile Iron Pipe with Retaining Ring

Ductile iron pipe with bell and spigot gripper gasket restrained joint. Figure 1-13 shows a ductile iron pipe with a gripper type gasket, which provides joint restraint against pull-out for ductile iron pipe joints. Stainless steel locking segments in the form of angled teeth, which are embedded in the rubber gasket, grip and prevent the spigot end from withdrawing from the bell end. By inserting this gasket into the bell socket, restraint is achieved when the joint is assembled.

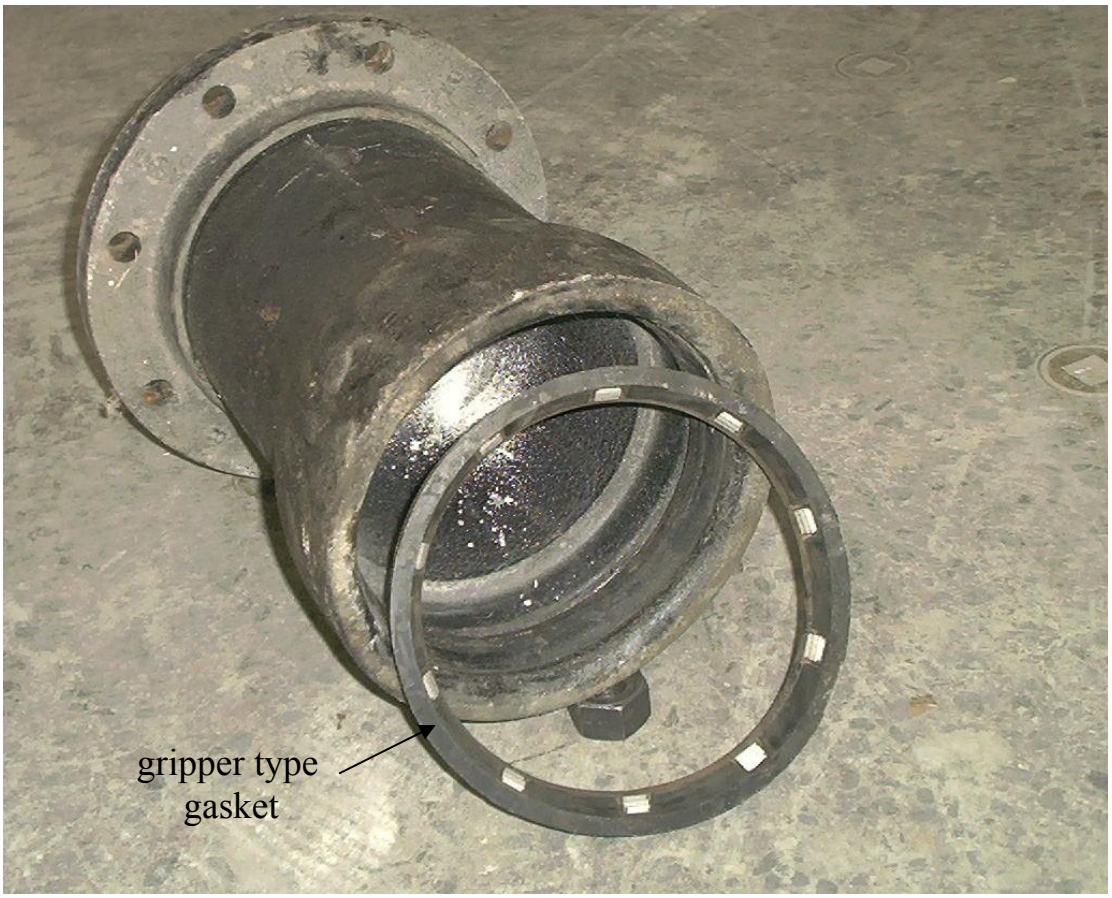

Figure 1-13 Ductile Iron Pipe with a Gripper Gasket Joint

Ductile iron pipe with bell and spigot bolted collar restrained joint (Figure 1-14). This type of assembly provides a restraining system for a pipe joint using a cast iron collar with wedge screws fitted with slanted teeth that is tightened firmly against and digs into the pipe surface. One collar is bolted to a similar collar on the opposite side of the joint, preventing the joint from pulling apart.

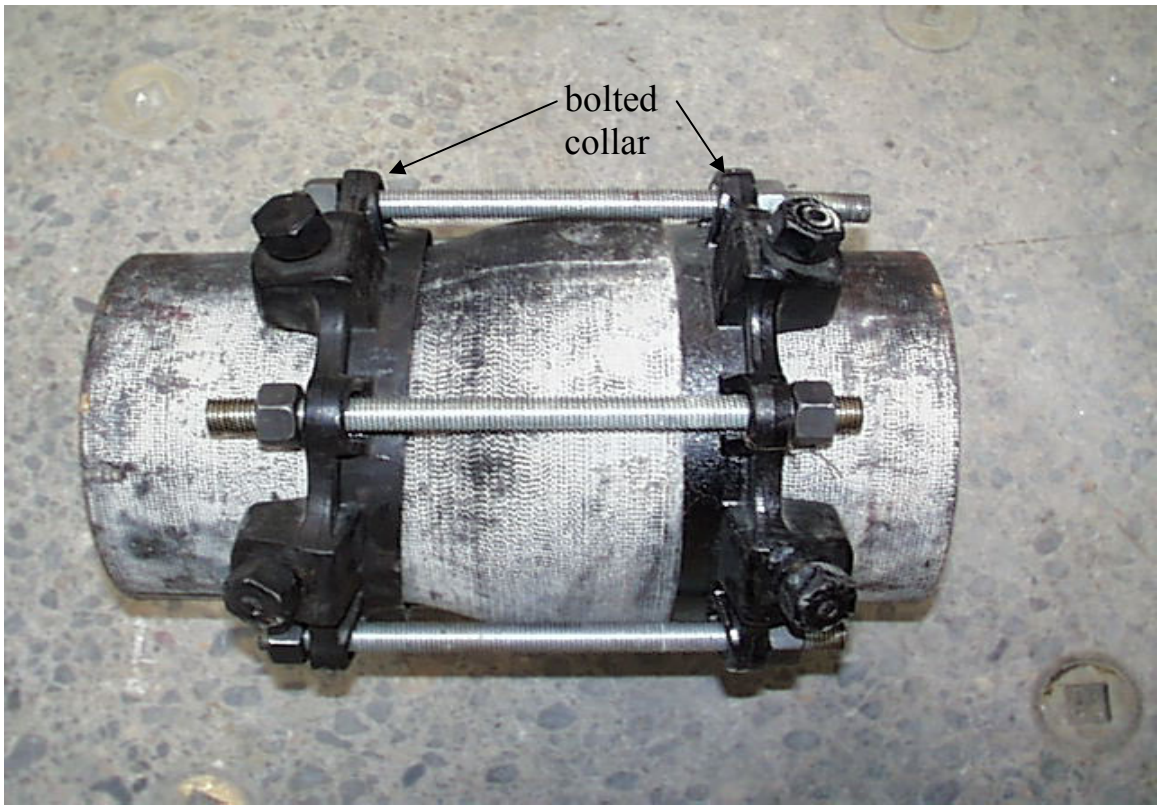

Figure1-14 Ductile Iron Pipe with Bolted Collar Joint

Steel pipe with bell and spigot lap-welded restrained joint (Figure 1-15). The joint is created by enlarging one end segment with a swedge so that it has an inside diameter that allows the other segment end to be inserted, forming a bell and spigot joint. The joint is joined and sealed by fillet welding the overlap of the two segment ends. Steel pipe is used for both water distribution lines and gas transmission lines. The specifications for steel used for water supply are governed by the American Water Works Association (AWWA) C200.

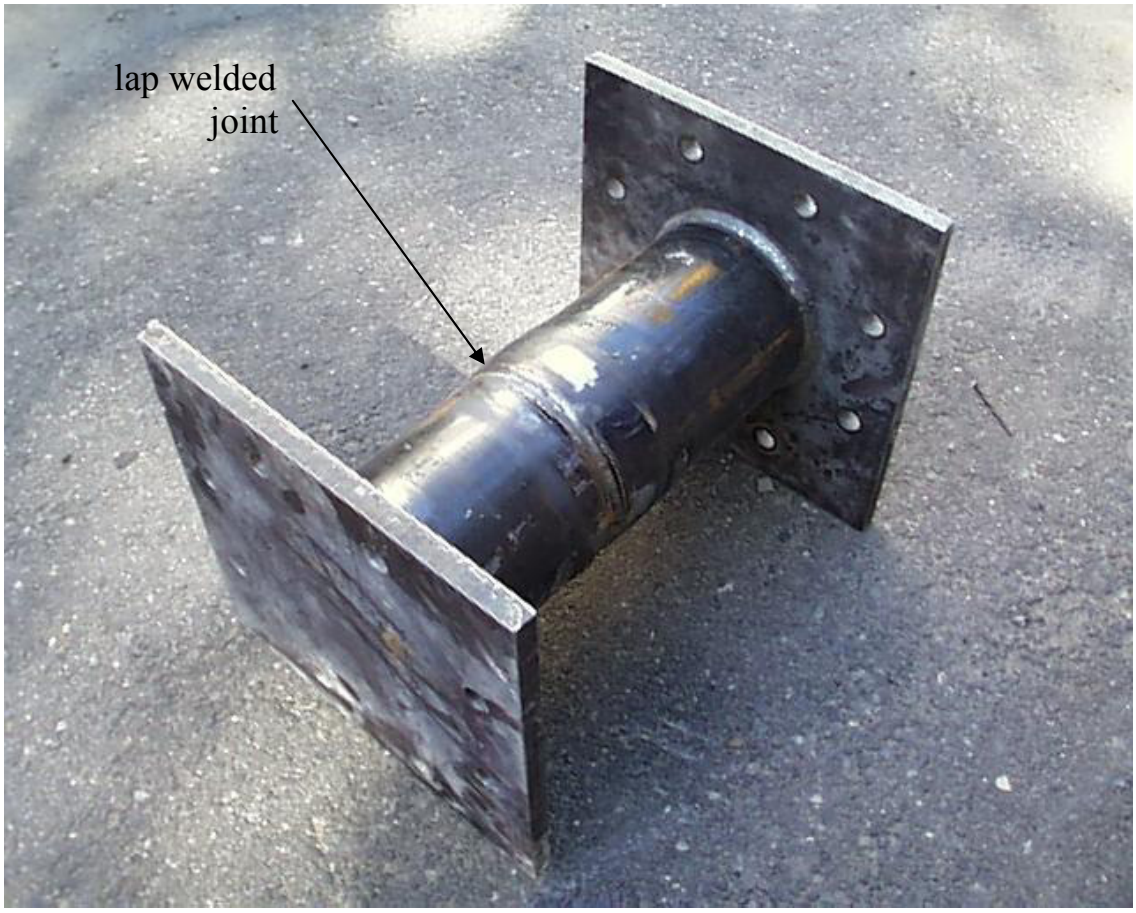

Figure 1-15 Steel Pipe with Lap-Welded Joint

PVC pipe with bell and spigot push-on rubber gasket unrestrained joint (Figure 1-16). PVC pipe outside diameter dimensions are equivalent to the comparable sizes of cast iron outside diameters, so that they are interchangeable and can replace existing cast iron systems and connections. The most obvious benefit of using PVC is its lower weight, which makes it easier to handle and place than the heavier ductile iron pipe. Joint connections are similar to ductile iron pipe joints with a bell and spigot joint and rubber gasket seal. PVC pipe is manufactured to meet the requirements for the American Water Works Association (AWWA) C900 "Polyvinyl Chloride Pressure Pipe".

Figure 1-16 PVC Pipe with Push-on Rubber Gasket Joint

Polyethylene (PE) pipe with butt-fused restrained joint (Figure 1-17). The joint connection for PE pipe is made by "fusing" the ends of two pipe sections. PE pipe is made from high density extra high molecular weight material and has advantages similar to PVC pipe in that it is much lighter in weight than metal pipe, and therefore, it is easier to handle and install. Segment lengths are joined by a fusion process using a special fusing device which is similar to the welding of steel sections. PE pipe is used for both water distribution lines and gas transmission lines. The governing specification for water transportation using PE pipe is American Water Works Association (AWWA) C906.

Figure 1-17 Polyethylene Pipe with Butt-Fused Joint

SECTION 2
AXIAL STATIC EXPERIMENTS

2.1 Description

This phase of testing was designed to determine the axial stiffness characteristics and force capacities of some common types of underground piping joints due to static loading conditions. The types of joints tested fall into three categories: 1) unrestrained bell and spigot push-on joints with gasket seals, 2) bell and spigot joints with restraining devices to resist pull-out, and 3) welded or fused joints that have a continuity across the joint and can resist both compressive and tensile motions.

The primary objective of this axial static testing was to develop values that can be used to provide stiffness as well as yield and failure force data which can be used for the development of analytical finite element modeling of pipeline networks and for risk analysis evaluation such as the risk assessment procedure proposed by T. O'Rourke (1996) (see Section 5).

Another goal of this experimental phase was to determine the magnitude of force capacities to be used in the planning and design of the subsequent axial dynamic experiments. Dynamic experiments can provide dynamic properties and characteristics of the joints which may be sensitive to the frequency content and loading rate of the seismic loading. Static testing is more controlled and predictable and can impose higher levels of force from a hydraulic actuator than can be imposed in dynamic testing, and therefore, it can better achieve yield and failure conditions in the specimen. The actual joint behavior due to seismic motions can be extrapolated from the results of both the static and dynamic experiments.

2.2 Test Assembly Configuration and Instrumentation

The first part of the static testing phase was done on ductile iron pipe (DIP) of four different diameters, 100 mm (4”), 150 mm (6”), 200 mm (8”), and 250 mm (10”), with unrestrained push-on rubber gasket joints. The DIP joints have a spigot end that is inserted into a bell end with a rubber gasket to create a water-tight seal. There is no device or other method to provide restraint against pull-out of the two ends. The specimens were tested in a SATEC compression testing machine with 500k capacity and were loaded axially in compression until noticeable fracture and load-shedding occurred. The instrumentation consisted of a Novatechnic LVDT (linear variable displacement transducer) to measure displacement and a load-cell internal to the SATEC to measure force levels. Load-displacement values were recorded and stored using a Megadac data acquisition system.

The remaining specimens were tested using a different test configuration and assembly. Figures 2-1 and 2-2 show the self-contained steel loading frame designed for the experiments which allows a hydraulic actuator to apply axial compression and/or tension load to a test specimen without the use of external reaction walls or blocks. The assembly consisted of two end plates, one end to attach the actuator and the other to attach the test specimen. The two end plates were connected by steel wide-flange members to create a frame. The loading and the anchoring setup were designed to readily accept various diameters of pipe specimens and to assemble them within a reasonable amount of time. Axial loads, both in tension and compression, were applied under incremental displacement control by a MTS 450k hydraulic actuator. Figure 2-3 is a sketch of the instrumentation on a specimen. The instrumentation consisted of a Novatechnic LVDT placed between the end flanges of the specimen to measure the actual displacement in the specimen, a LVDT and a load-cell internal to the MTS actuator, and strain gages placed circumferentially and along the length of the specimen barrel (normally at about 5 mm from the ends and at the bell section). The specimens were filled with water and a pressure transducer was inserted into the specimen. A low level of internal water pressure was applied at about 20 to 28 kPa (3 to 4 psi) in order to

monitor loss of pressure and water leakage without creating a substantial artificial hydrostatic restraining force that would alter the actual load applied to the specimen. Data was recorded and stored using a Megadac data acquisition system.

Figure 2-1 Load Frame and Actuator Configuration for Static Load Testing

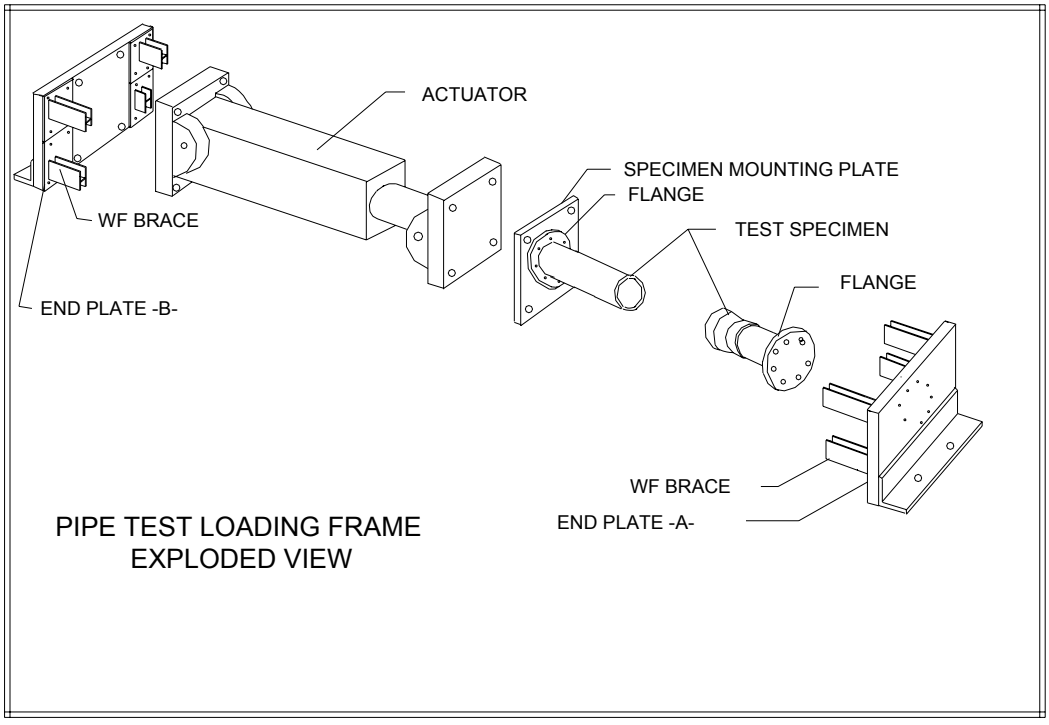

Figure 2-2 Exploded View of Actuator, Test Specimen, and Loading Frame

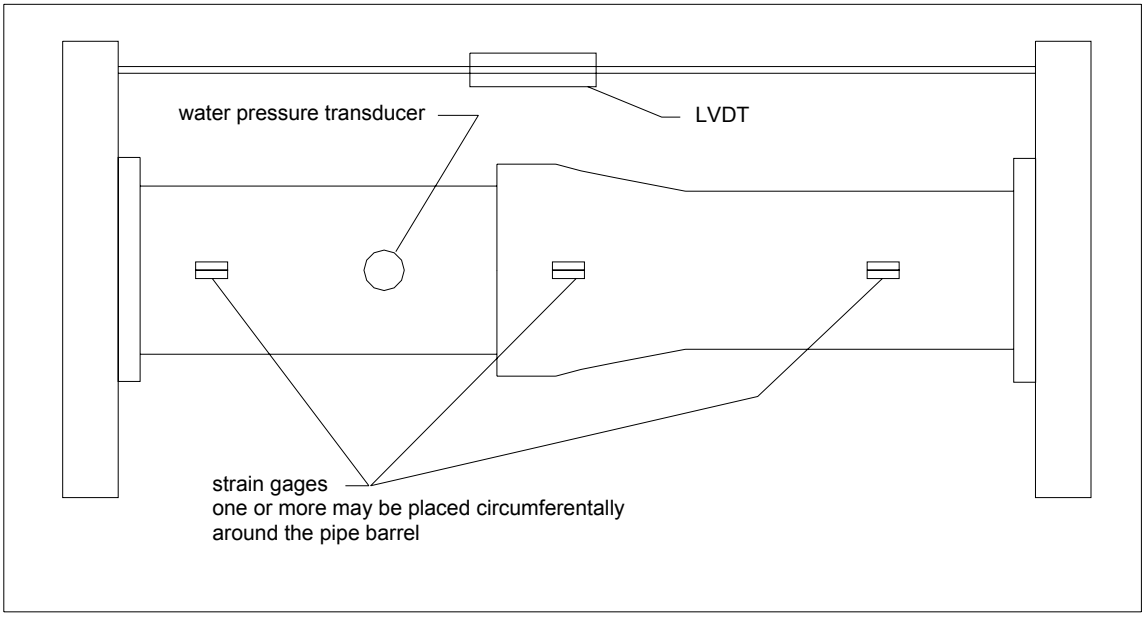

Figure 2-3 Location of External Instrumentation for Static Load Testing

2.3 Test Methodology and Loading

The loading procedure consisted of applying an axial displacement for a small increment, letting the load rest and relax or partially unload, then continuing to increase the displacement for the next increment. Compressive displacements only were applied to those specimens that did not have tension restraint capacity (unrestrained), tension displacements only for specimens that had tension restraint devices (restrained), and both tension and compression displacements in cyclic loading for specimens that were able to inherently resist both tension and compression, such as steel pipe and PE pipe joints.

The data obtained from this testing phase consisted of load-displacement values, barrel strains, and internal water pressures of the joint assembly. Typically, at some level of loading, noticeable fracture and buckling, or major leaking, or a very noticeable load-shedding occurred, indicating severe pipe damage and a probable failure condition. A description of each individual test and the plot of the raw load-displacement data from each test are given in Appendix A.

2.4 Test Results

For graphical representation and comparison purposes, the resulting load-displacement curves for each specimen are combined into single plots for similar pipe material and joint type (Figures 2-6 and 2-8 to 2-14). A "smoothened" load-displacement curve was created from the raw data by eliminating the noise and chatter in the data. A typical smoothened plot is shown in Figure 2-4, which shows the key zones and specific points that define the smoothened curve. The actual smoothened plots have a similar shape to a load-displacement curve for typical metals, which increases at a constant slope to a yield point, and either continues at a substantially lower slope or at a negative slope until failure. In some cases they failed at the yield point. The smoothened load-displacement curve for each specimen was used to develop a straight-line "approximated" bi-linear curve. An example of a typical approximated bi-linear curve is shown in Figure 2-5.

The load-displacement plots for the compression testing of unrestrained ductile iron pipe with push-on rubber gasket joints are shown in Figure 2-6. It was observed during the testing that there were measurable amounts of seating distance that had to be overcome before the joints exhibited any resistance to the compression load. As expected, the strengths of these pipe joints are proportional to the pipe diameter. At the conclusion of the tests, the 200 mm (8 in.) specimen was cut in half longitudinally to observe the failure mechanism (Figure 2-7). The failure mechanism can be described as a telescoping and intrusion of the spigot end into the bell end and a subsequent buckling and fracture of the spigot end. It cannot be determined precisely when leakage would have occurred, however, the fracturing and buckling of the spigot end had severely damaged the rubber gasket seal.

The testing of the remaining specimens was done using a 450k MTS hydraulic actuator which recorded load-displacement data as shown in Figures 2-8 to 2-14. The load-displacement plot for the cast iron specimen is shown in Figure 2-8 and as it can be seen, has a very high compression force capacity. This indicates that it would be difficult to have a pure axial compressive load failure from seismic motions.

Most ductile iron pipe specimens typically exhibited a load-displacement behavior with a distinguishable yield point, a post-yield zone, and a failure point. However, some specimens, for example the 300 mm ductile iron pipe with a gripper gasket joint (Figure 2-9) and the 150 mm, 200 mm, and 300 mm ductile iron pipe with a retaining ring joint (Figure 2-10), failed at their yield load level without any post-yield behavior.

For steel pipe (Figure 2-12) and polyethylene (PE) pipe (Figure 2-14), the load-displacement plots are hysteretic type curves due to the bi-directional cyclic loading. The smoothened curves for these specimens were created by joining the peak values of the hysteretic curves and show an elastic zone, a yield point, and a post-yield zone.

Table 2-1 provides a summary of the results of the testing for each material, joint type and pipe diameter and gives the maximum force capacities and brief comments about each test. It must be noted that the data from the instrumentation were in standard English units and were converted to SI units. The maximum force capacity F_{max}, as listed in Table 2-1, is the maximum force level that was achieved during the test and is the maximum of either the force level at yield or at failure, whichever is greater. For bi-directional loading, the maximum force capacity listed is the lesser of the F_{max} values from the tension and compression directions. For compression only tests, F_{max} is the maximum compression force level, but it must be noted that in the tension direction for these specimens, the force capacity is essentially zero.

Table 2-2 lists the results of the testing in terms of yield force level and corresponding displacement, computed elastic stiffness, failure force level and corresponding displacement, and the computed post-yield stiffness values for each restrained specimen. Both the elastic stiffness and the post-yield stiffness values were calculated directly by determining the slope of the corresponding elastic and post-yield portions of the approximated bi-linear curve. Table 2-3 provides similar information for unrestrained joints. In some cases, the post-yield stiffness is a negative value indicating a degradation prior to failure. The symbol "---" in the table indicates that the specimen failed at its yield point, without any post-yield behavior.

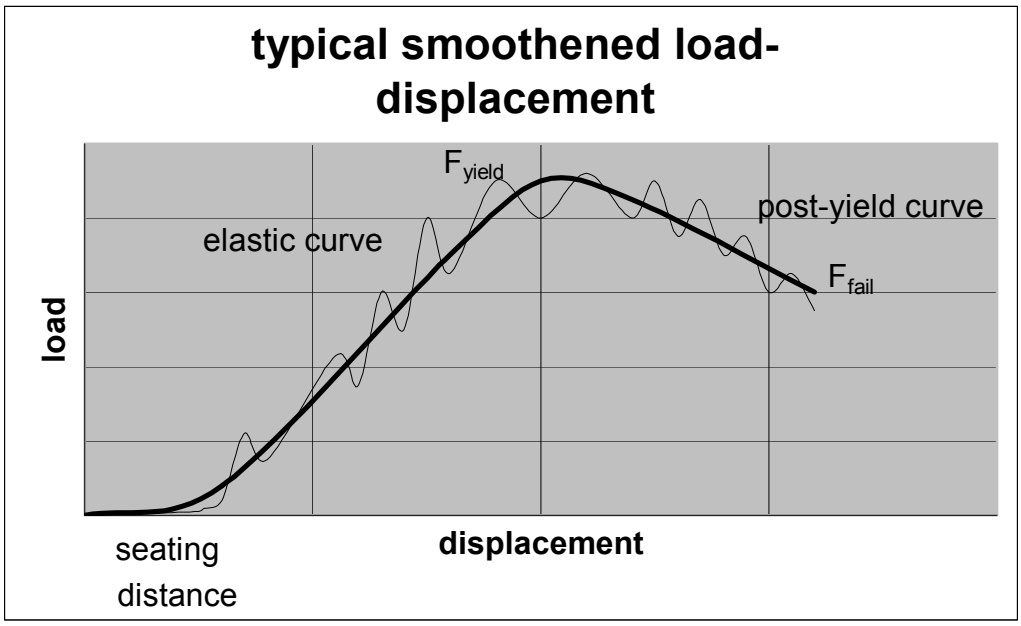

Figure 2-4 Typical Smoothened Load-Displacement Plot Showing Key Zones and Points

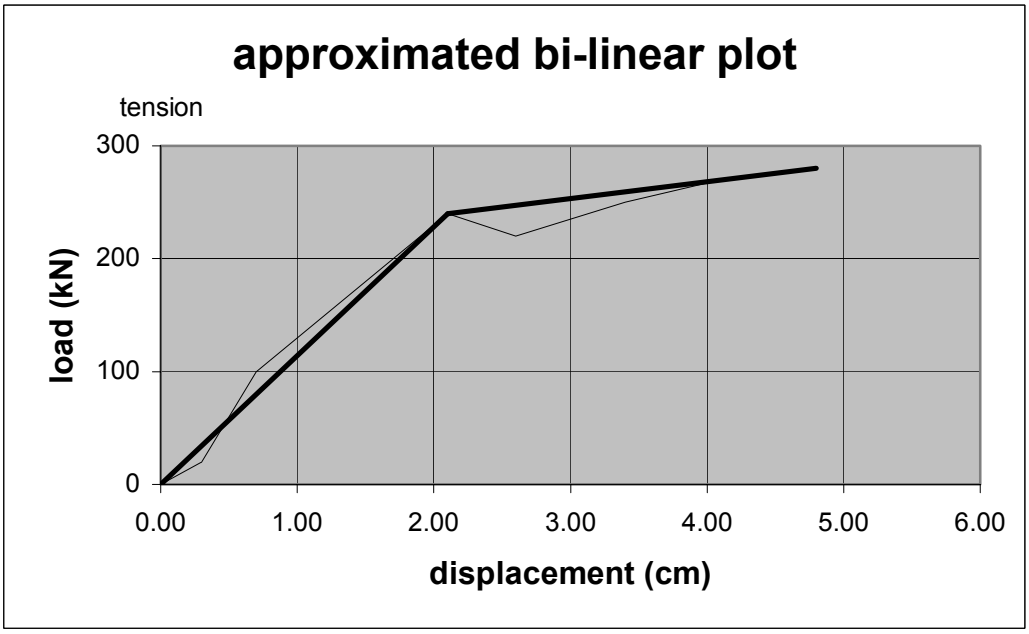

Figure 2-5 Example of Load-Displacement Plot with Approximated Bi-Linear Curve

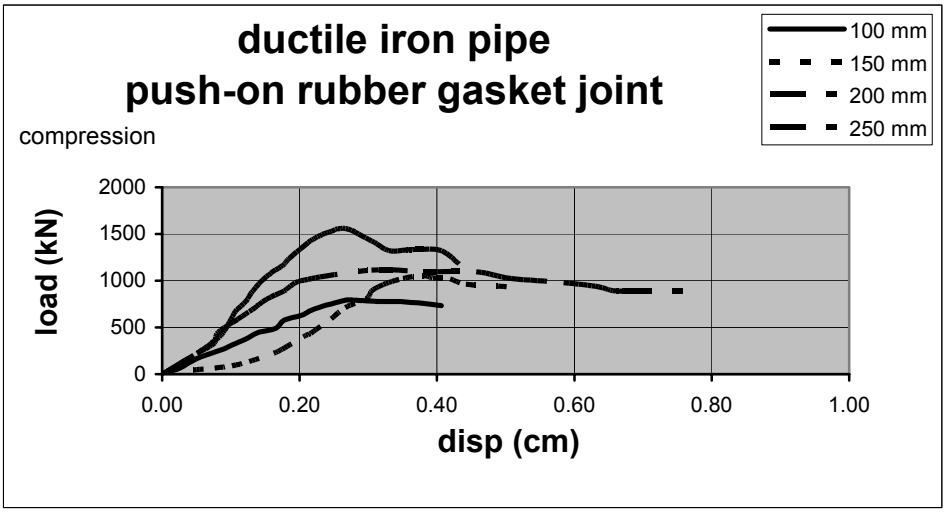

Figure 2-6 Load-Displacement for Ductile Iron Pipe with Push-On Rubber Gasket Joints

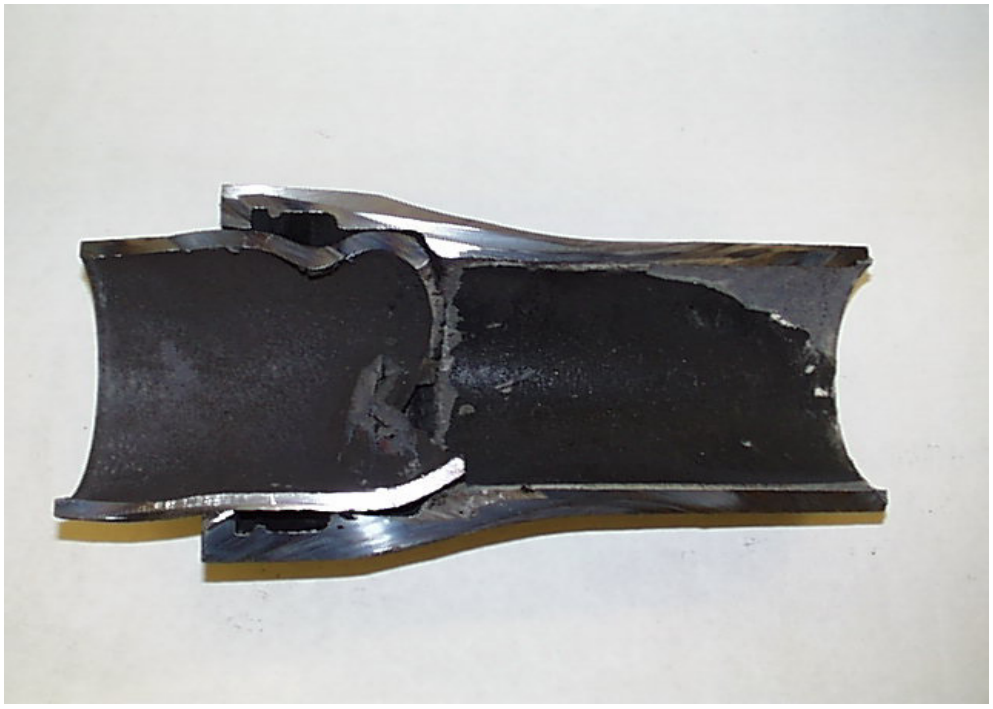

Figure 2-7 Cut Section of Ductile Iron Pipe with Push-On Rubber Gasket Joint

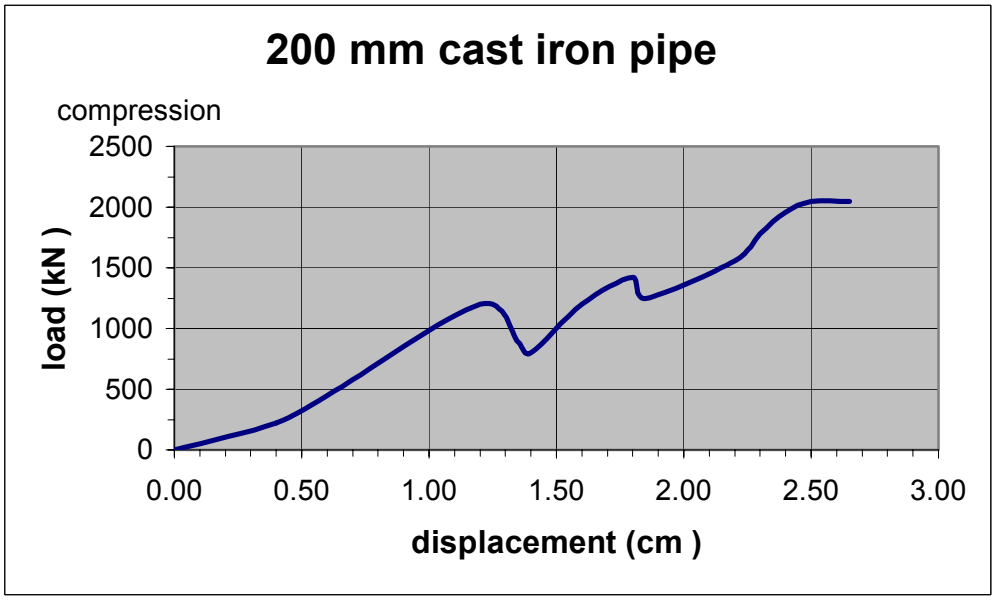

Figure 2-8 Load-Displacement for Cast Iron Pipe

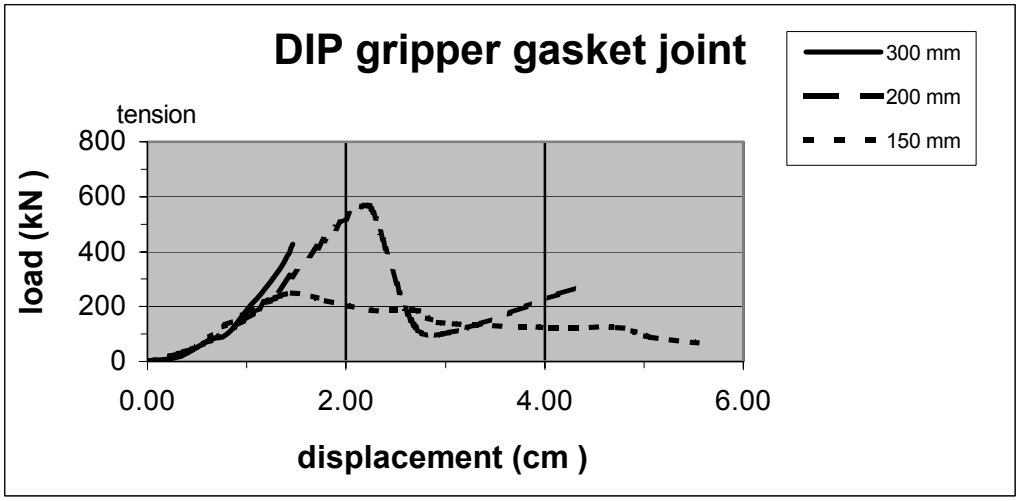

Figure 2-9 Load-Displacement for Ductile Iron Pipe with Gripper Gasket Joints

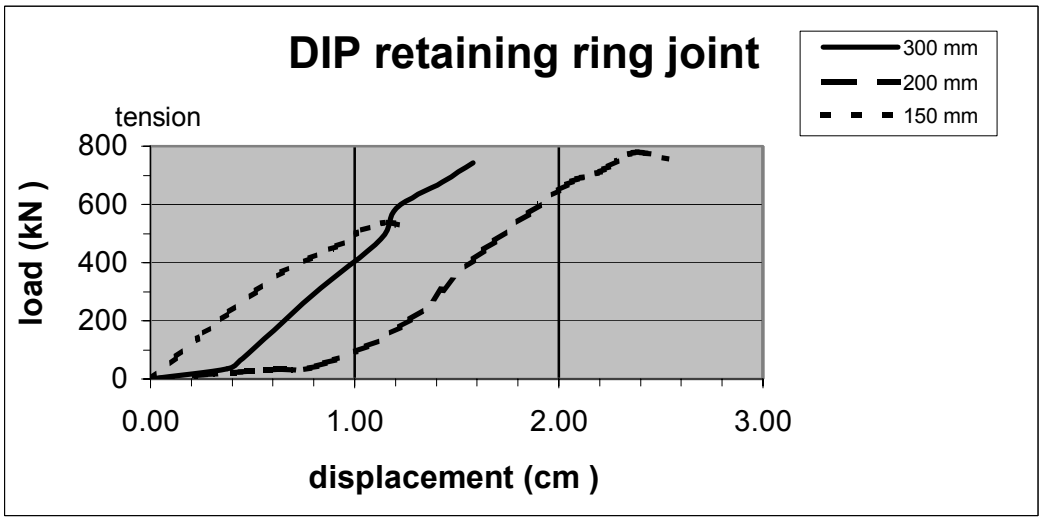

Figure 2-10 Load-Displacement for Ductile Iron Pipe with Retaining Ring Joints

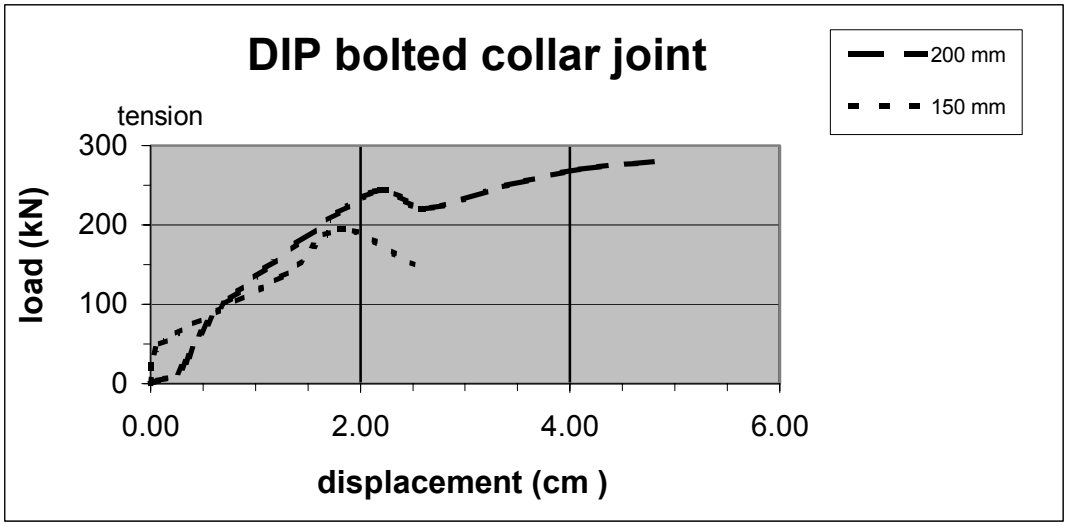

Figure 2-11 Load-Displacement for Ductile Iron Pipe with Bolted Collar Joints

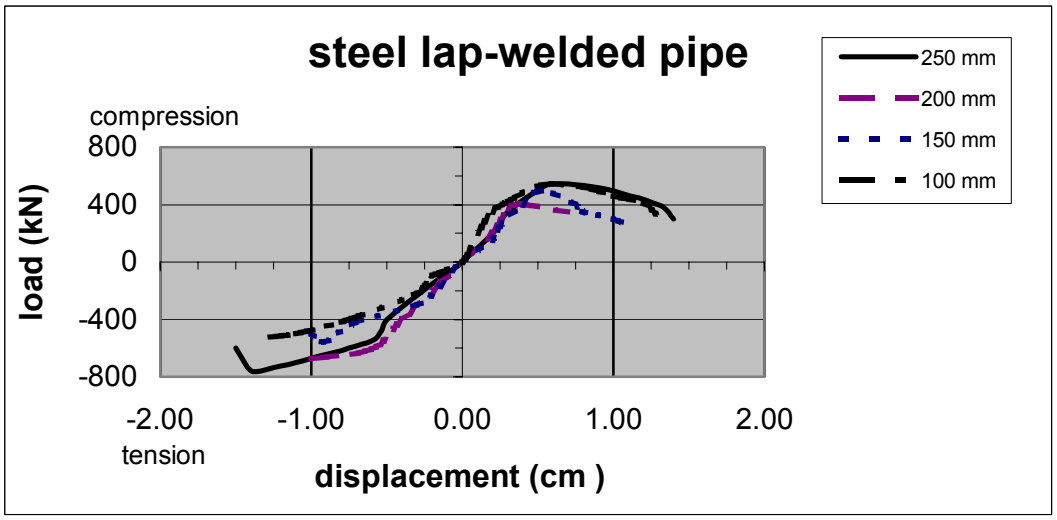

Figure 2-12 Load-Displacement for Steel Pipe with Lap-Welded Joints

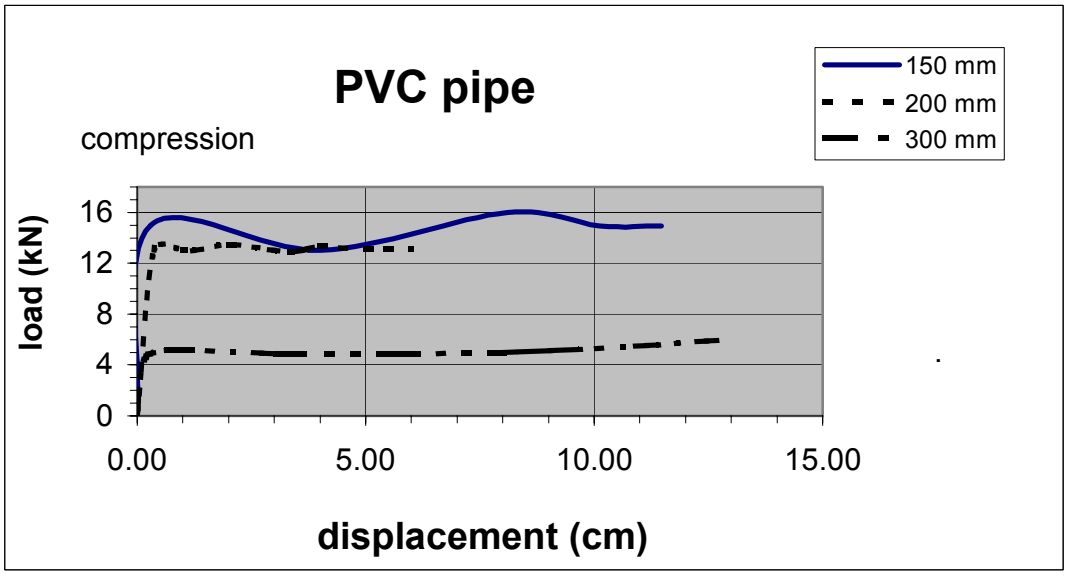

Figure 2-13 Load-Displacement for PVC Pipe with Push-On Rubber Gasket Joints

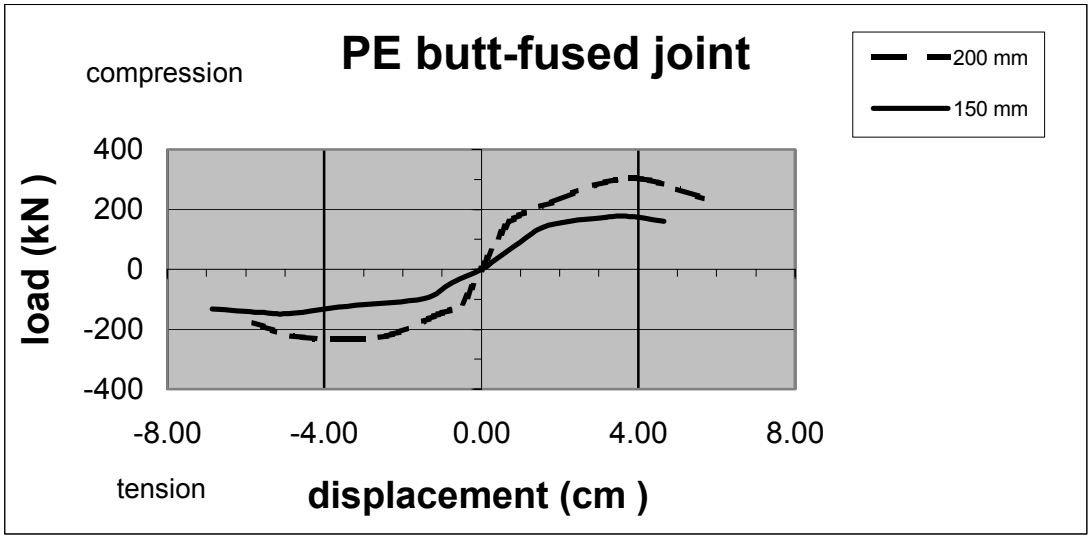

Figure 2-14 Load-Displacement for PE Pipe

Table 2-1 Test Results Summary for Static Axial Loading

Material	Diameter	Joint Type	F_{max} (kN)	Comments
cast iron	200 mm (8”)	bell-spigot lead calked joints	2046 C	compression load only; probable fracture of the spigot end inside bell end
ductile iron	100 mm (4”) 150 mm (6”) 200 mm (8”) 250 mm (10”)	bell-spigot, push-on rubber gasket joint	792 C 1054 C 1112 C 1557 C	compression load only; spigot end telescoped into bell end; fracture of spigot end inside bell end
ductile iron	150 mm (6”) 200 mm (8”) 300 mm (12”)	bell-spigot, gripper gasket	253 T 539 T 488 T	tension load only; ultimate failure of metal teeth in gasket
ductile iron	150 mm (6”) 200 mm (8”) 300 mm (12”)	bell-spigot, retaining ring joint	538 T 795 T 750 T	tension load only; ultimate failure in bell end at retaining ring groove
ductile iron	150 mm (6”) 200 mm (8”)	bell-spigot, bolted collar	195 T 280 T	tension load only; fracture at collar wedge screw holes
steel	100 mm (4”) 150 mm (6”) 200 mm (8”) 250 mm (10”)	bell-spigot, lap welded	522 B 491 B 401 B 546 B	bi-directional load; fracture occurred at weld and barrel adjacent to weld; severe buckling at bell.
PVC	150 mm (6”) 200 mm (8”) 300 mm (12”)	bell-spigot, push-on rubber gasket joint	15 C 13 C 6 C	compression load only; spigot end extruded into bell end; water seal maintained; no fracture
PE polyethylene	150 mm (6”) 200 mm (8”)	butt-fused joint	157 B 232 B	bi-directional load; fused joint remained ductile; severe bucking of pipe; failure occurred at end flange

C = compression T = tension B = bi-directional

Table 2-2 Joint Static Axial Stiffness Values and Force Levels for Restrained Joints

1	2	3	4	5	6	7	8	9
Pipe Material Joint type	**Pipe Diameter (mm)**	**Test Load Direction**	**Yield Force (kN)**	**Yield Disp. (cm)**	**Elastic Stiffness (kN/cm)**	**Failure Force (kN)**	**Failure Disp. (cm)**	**Post-yield Stiffness (kN/cm)**
DIP bell-spigot gripper gasket	150 (6”)	tension	253	1.64	154	78	5.90	-41
	200 (8”)	tension	539	2.31	233	300	4.60	-104
	300 (12”)	tension	488	1.87	261	---	---	---
DIP bell-spigot retaining ring	150 (6”)	tension	360	.60	600	538	1.16	320
	200 (8”)	tension	795	2.70	294	---	---	---
	300 (12”)	tension	750	1.55	484	---	---	---
DIP bell-spigot bolted collar	150 (6”)	tension	195	1.90	103	150	2.50	-75
	200 (8”)	tension	220	2.01	109	280	4.94	20
Steel bell-spigot lap-welded	100 (4”)	tension	342	.53	647	522	1.27	243
		compression	535	.52	1029	309	1.29	-294
	150 (6”)	tension	400	.50	800	554	.94	350
		compression	491	.57	861	243	1.18	-407
	200 (8”)	tension	316	.24	1317	711	1.00	520
		compression	401	.40	1003	350	.68	-182
	250 (10”)	tension	343	.52	660	761	1.38	486
		compression	546	.60	913	400	1.20	-243
PE butt-fused	150 (6”)	tension	133	1.50	89	157	6.20	5
		compression	186	3.90	48	125	5.50	-38
	200 (8”)	tension	125	.87	144	232	4.30	31
		compression	307	3.90	79	250	6.00	-27

Table 2-3 Joint Static Axial Stiffness Values and Force Levels for Unrestrained Joints

1	2	3	4	5	6	7	8	9
Pipe Material Joint type	**Pipe Diameter (mm)**	**Test Load Direction**	**Yield Force (kN)**	**Yield Disp. (cm)**	**Elastic Stiffness (kN/cm)**	**Failure Force (kN)**	**Failure Disp. (cm)**	**Post-yield Stiffness (kN/cm)**
Cast Iron	200 (8")	compression	1108	1.27	872	2046	2.46	788
DIP bell-spigot push-on rubber gasket joint	100 (4")	compression	792	.267	2966	734	.406	-417
	150 (6")	compression	1054	.305	3456	934	.460	-120
	200 (8")	compression	1112	.372	2989	890	.829	-486
	250 (10")	compression	1557	.312	4990	1179	.477	-2290
PVC bell-spigot push-on rubber gasket joint	150 (6")	compression	15	.30	50	---	---	---
	200 (8")	compression	13	.37	35	---	---	---
	300 (12")	compression	6	.16	38	---	---	---

The comparisons of maximum force capacity and of elastic stiffness for different types of pipe joints and diameters are shown in Figures 2-15 and 2-16. From Figure 2-15, it can be seen that the force capacities for steel pipe with lap-welded joints, ductile iron pipe with retaining ring joints, and ductile iron pipe with gripper gasket joints generally increase with an increase in pipe diameter, while the force capacities for ductile iron pipe with bolted collar joints and for polyethylene pipe joints are independent of the pipe diameter.

Figure 2-16 shows the comparison of the elastic stiffnesses for different joints and different pipe diameters. It can be seen that the elastic stiffness values for ductile iron pipe with gripper gasket joints and steel pipe with lap-welded joints have some dependence on the pipe diameter. The elastic stiffness of ductile iron pipe with bolted collar joints, ductile iron pipe with retaining ring joints, and polyethylene pipe joints appear to be independent of the pipe diameter.

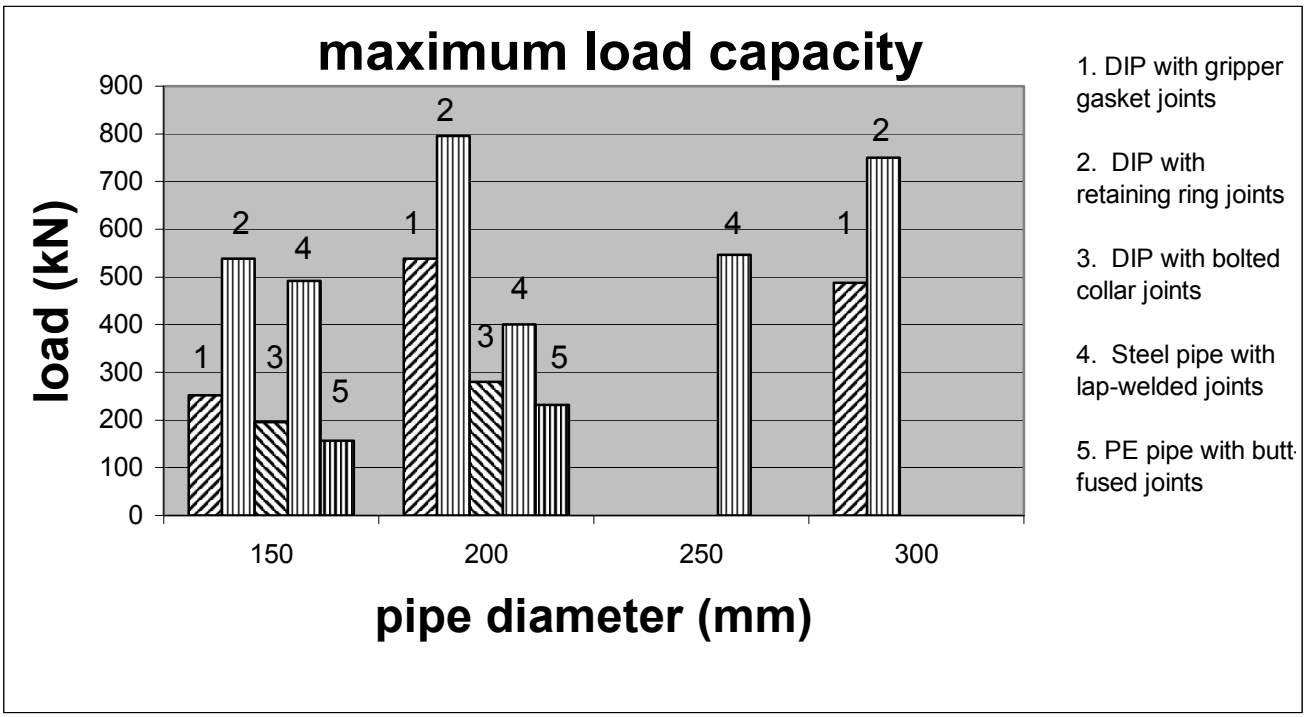

Figure 2-15 Maximum Load Capacity for Different Pipe Diameters of Restrained Joints

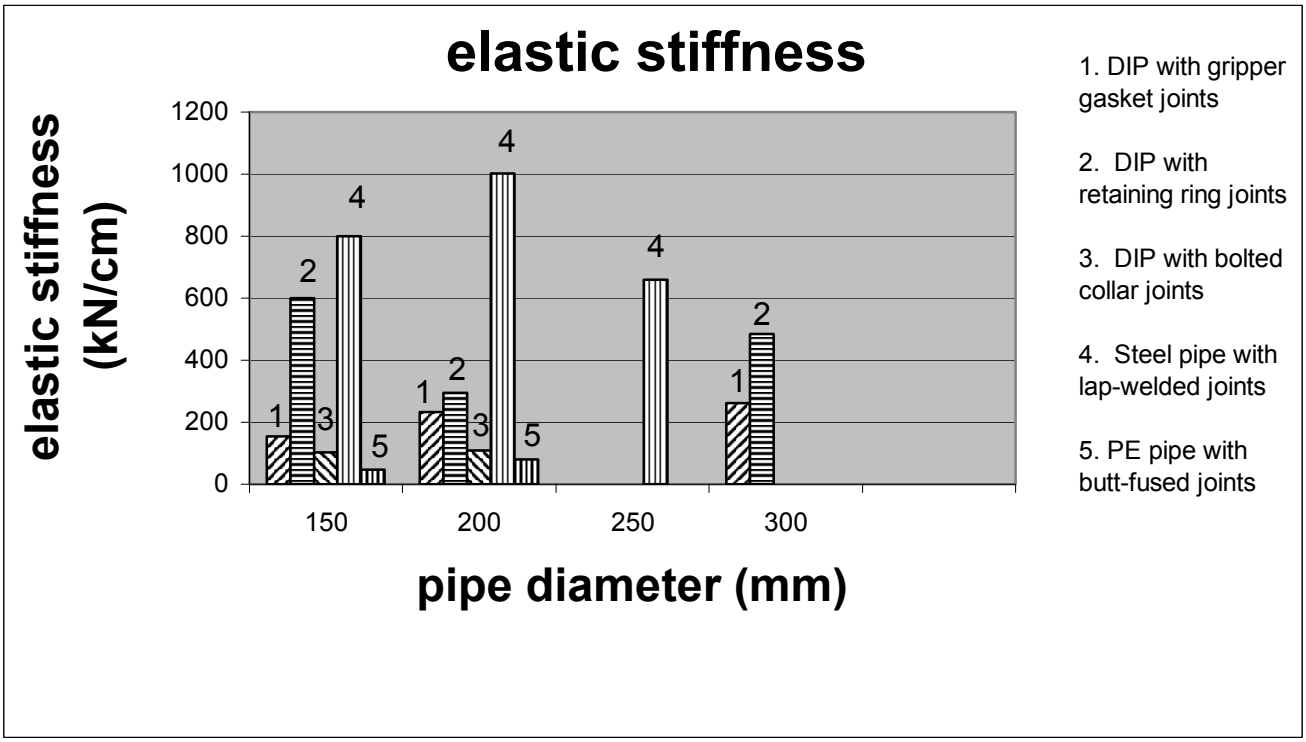

Figure 2-16 Elastic Stiffness for Different Pipe Diameters of Restrained Joints

SECTION 3
AXIAL DYNAMIC EXPERIMENTS

3.1 Description

The overall objective of this phase of testing was to determine the axial stiffness characteristics and force capacities of some common types of underground piping joints due to dynamic loading conditions. The types of joints tested fall into three categories: 1) unrestrained bell and spigot push-on joints with gasket seals, 2) bell and spigot joints with restraining devices to resist pull-out, and 3) welded or fused joints that have a continuity across the joint and can resist both compressive and tensile motions. The diameters of pipe tested were determined from the axial static experiments, and were the diameters that could be tested with the available equipment. The diameters of pipe joints tested were limited to 150 mm and 200 mm diameters.

One goal of this experimental phase of testing was to determine whether dynamic testing is required to capture the dynamic behavior of pipe joints or is static testing sufficient. Included in this experimental phase is a comparison of the static results with the dynamic results to determine if dynamic effects such as the cyclic loading, loading rate, and frequency content have noticeable effects on the final results.

In order to develop an effective dynamic testing program, a test assembly was designed, fabricated, and assembled, utilizing one of the shake-tables at the University of Nevada, Reno, Large Scale Testing Structures Laboratory. The shake-table was used to simulate actual seismic motions with realistic frequency content and was operated under displacement control from actual earthquake records which can impart displacements to the specimen. These displacements caused dynamic strains and forces in the specimens that were equivalent to the strains and forces that would be imposed on the specimen from the soil during an earthquake. The shake-table can also impart these motions with a fixed head mount, so that any rotational motions which may cause bending strains were eliminated.

3.2 Test Assembly Configuration and Instrumentation

The dynamic pipe joint testing assembly consisted of one of the lab's shake-tables, concrete reaction blocks post-tensioned to the lab's strong floor and used to provide end anchorage for the pipe joint specimens, a steel rectangular tube restraint frame used to maintain lateral stability for the pipe specimen during testing, and a 150 mm diameter steel pipe loading arm that connected the specimens to the shake table (Figures 3-1 and 3-2). The loading arm was divided into two sections with a load-cell installed in-between them.

The instrumentation (Figure 3-3) consisted of a Novatechnic LVDT (linear variable displacement transducer) placed between the end flanges of the specimen to measure actual displacements in the specimen, a 150k load-cell located between the two loading arm sections to measure the applied load, and strain gages placed circumferentially and along the length of the specimen barrel (usually at about 5 mm from the ends and at the bell section). The specimens were filled with water and a pressure transducer was inserted into the specimen. A low level of internal water pressure was applied at about 20 to 28 kPa (3 to 4 psi) in order to monitor water leakage without creating a substantial artificial hydrostatic restraining force that would alter the actual load applied to the specimen.

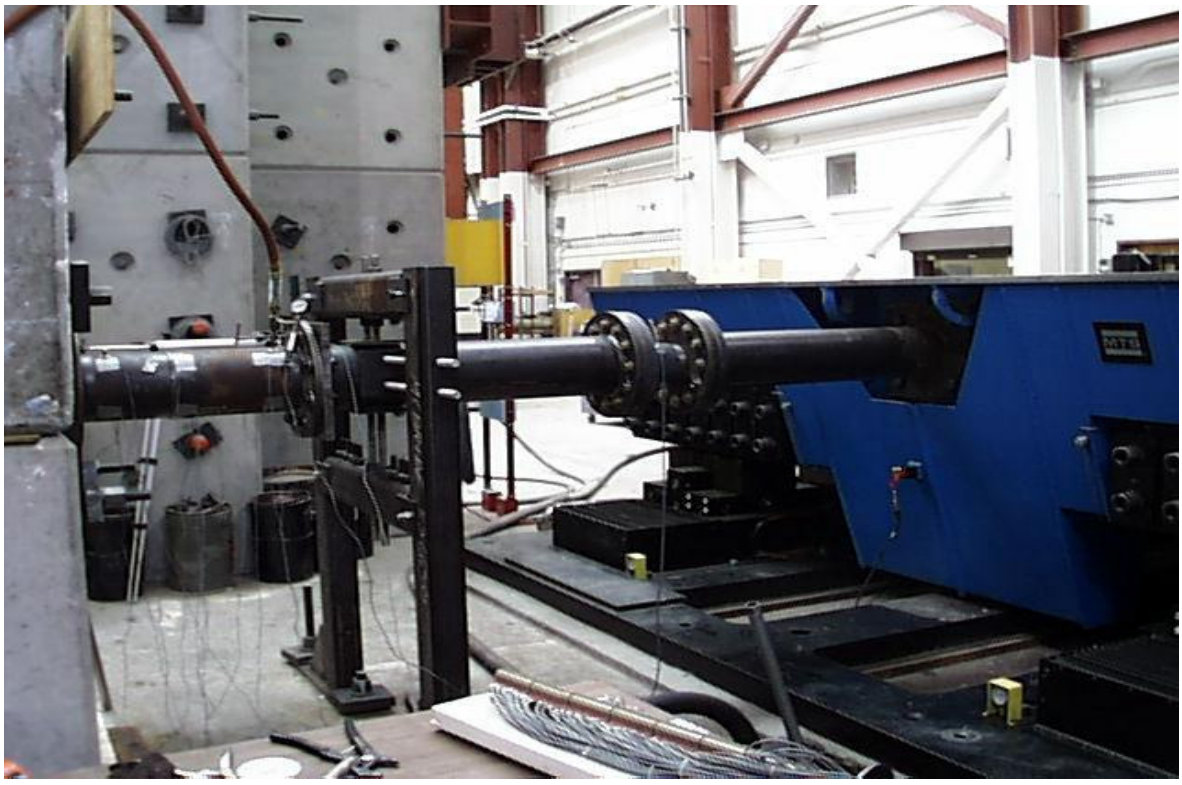

Figure 3-1 Dynamic Test Assembly and Shake-Table

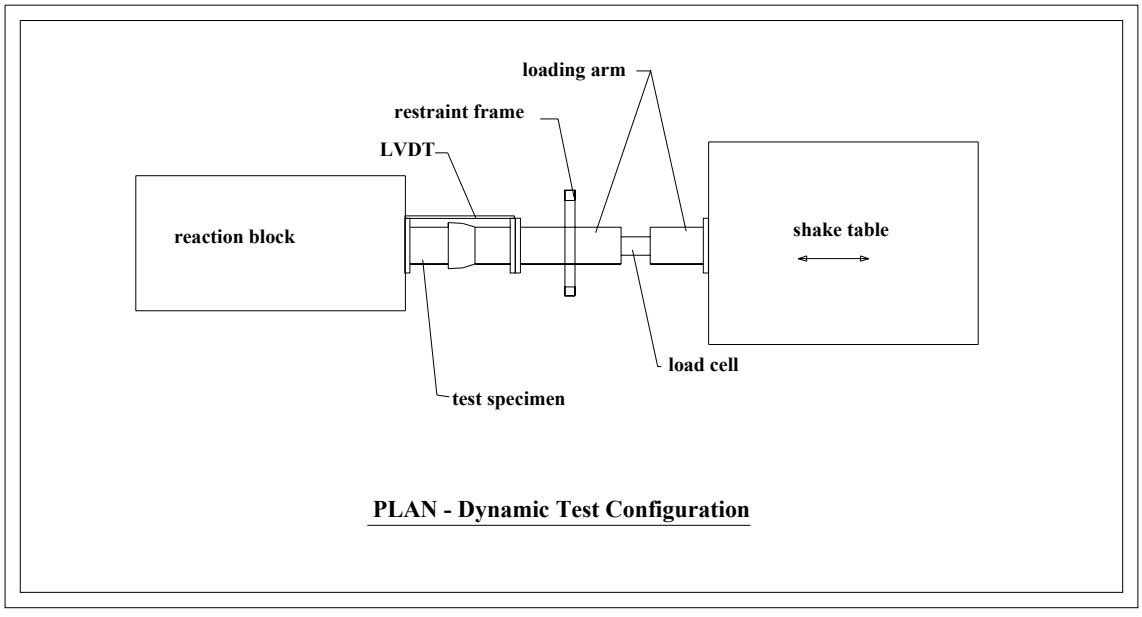

Figure 3-2 Plan View of Shake-Table, Specimen, Restraint Frame and Loading Arm

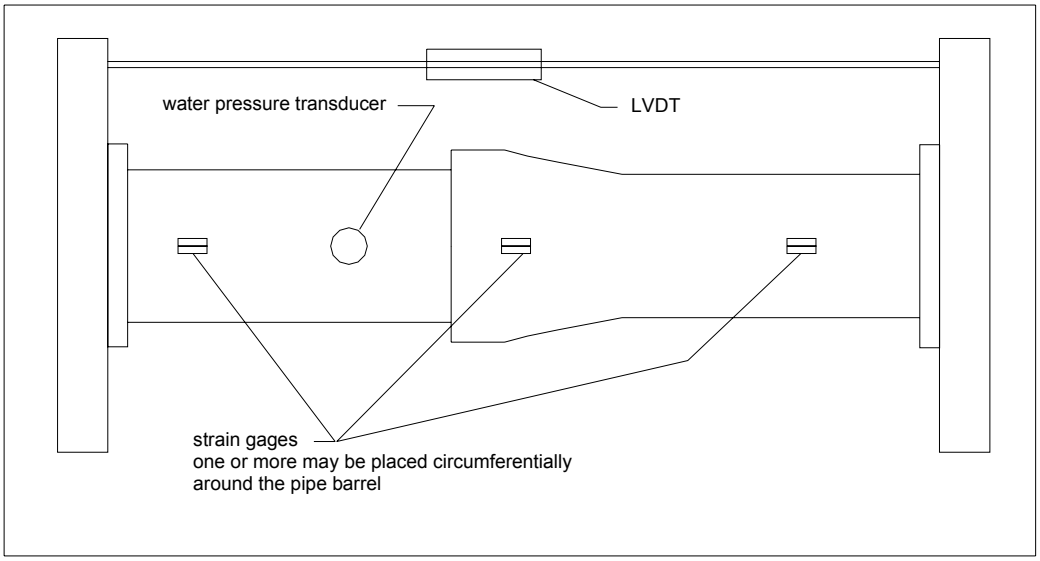

Figure 3-3 Location of External Instrumentation for Dynamic Load Testing

3.3 Test Methodology and Loading

Bi-directional dynamic axial loadings were applied to the specimens using actual seismic time-history records as displacement control. Seismic motion records used in the testing were selected from a database of motions recorded during the 1994 Northridge earthquake which occurred in the Los Angeles area on January 7, 1994 (see Section 3-4). The specimens were tested using three separate station records: 1) Arleta station (Figure 2-13), a near-field station, 2) Sylmar station (Figure 2-15), a far-field station, and 3) Laholl station (Figure 2-17), another far-field station. It can be shown that the strains and applied forces on the pipe from the soil are a function of the velocity of the seismic motion (Newmark, 1967) (see Appendix E). The shake-table was operated under displacement control using velocity time-history records, which applied displacements to the specimen that resulted in strains in the specimen containing the same shape and frequency content as would occur from seismic motions. The motion magnitudes were applied starting at a low level amplitude and continued at increasing levels of amplitude for subsequent runs until a failure condition occurred or the limit of the shake-table was reached. The resulting load-displacement values and the barrel strains were recorded using a Pacific data acquisition system and were used to produce test results. Typically,

at some level of loading, noticeable fracture and buckling, or major leaking, or very noticeable load shedding occurred indicating severe pipe damage and a failure condition.

3.4 Seismic Motion Records

The dynamic testing was done using three separate seismic time-history velocity records from the Northridge earthquake which were used as displacement control for the shake-table. The records have different cyclic and amplitude properties and were selected on the basis of their proximity to the epicenter and the shape and cyclic frequency of their velocity record. Table 3-1 gives specific data on the epicentral distance, direction component, predominate period, duration, maximum acceleration, and maximum velocity amplitude for each station record. The actual recorded amplitudes were not critical in this testing since the records used for the table control were normalized to one, and the testing was done by ramping-up the amplitude of the displacement control on successive tests.

The Arleta record (Figure 3-4) is a near-field record with fairly evenly-spaced cycles and without a relatively high individual peak amplitude. The predominant period of the motion was determined from the corresponding response spectra developed from the time-history record (Figure 3-5). The primary testing case was done using this record, simulating a near-field event which would have the most severe effects on pipelines. This record was also used to bring the specimen to its ultimate loading state.

The second motion was from the Sylmar station (Figure 3-6), a far-field record with a relatively high single peak amplitude at the beginning of the motion and relatively low

level amplitude for the remaining portion of the motion. The predominate period of the motion was determined from the corresponding response spectra (Figure 3-7).

The third motion used was the Laholl station (Figure 3-8), a far-field record with evenly-spaced cycles and a relatively uniform level of amplitude. The record appearance has distinguishable points of "P" wave, "S" wave, and coda waves. The predominate period of this motion was determined from the corresponding response spectra (Figure 3-9).

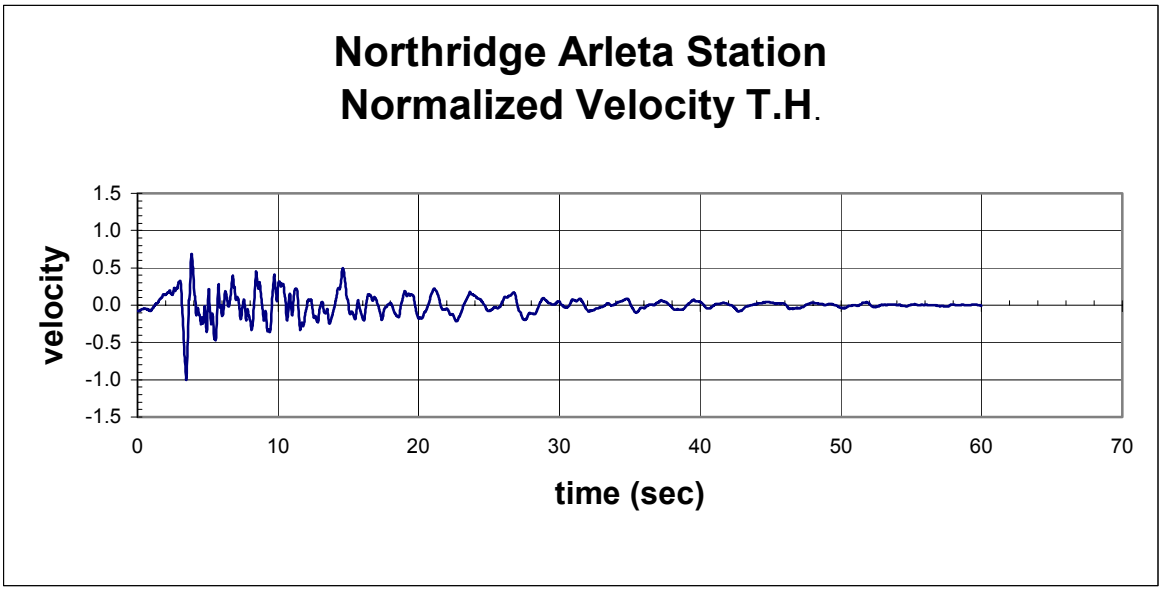

Figure 3-4 Northridge Arleta Station Normalized Velocity Time-History

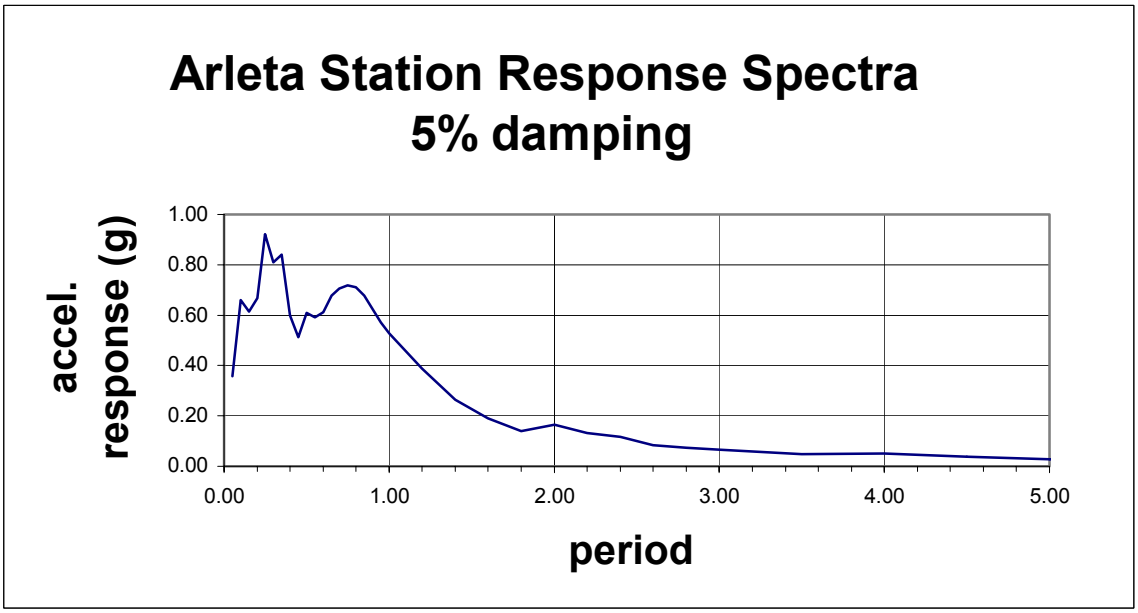

Figure 3-5 Northridge Arleta Station Response Spectra

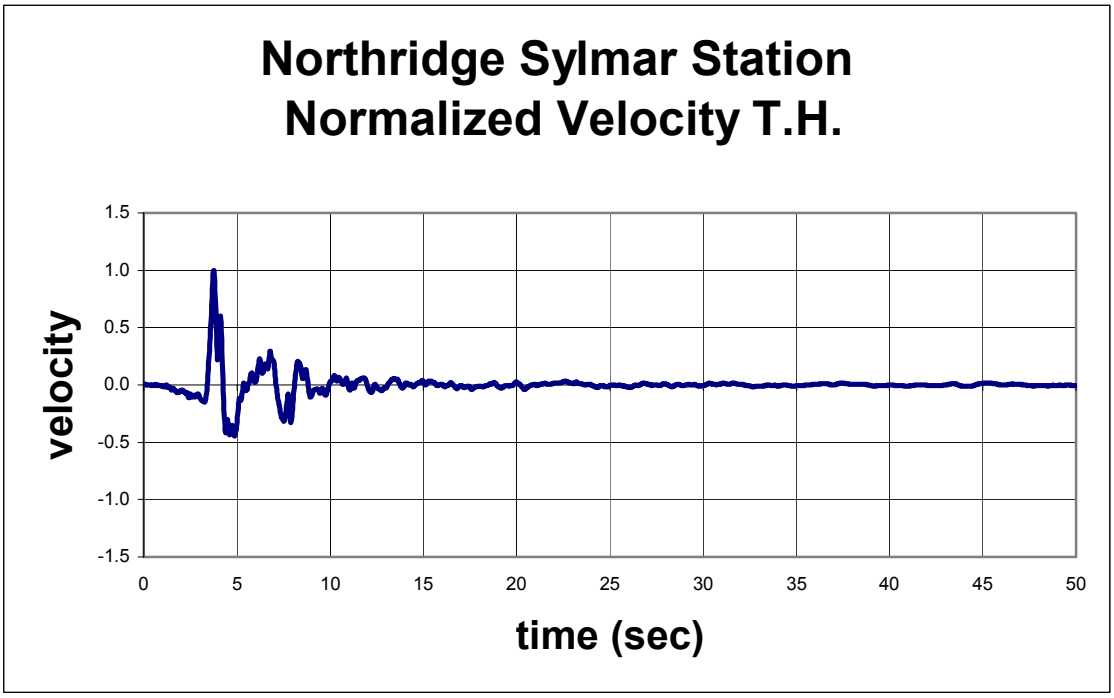

Figure 3-6 Northridge Sylmar Station Normalized Velocity Time-History

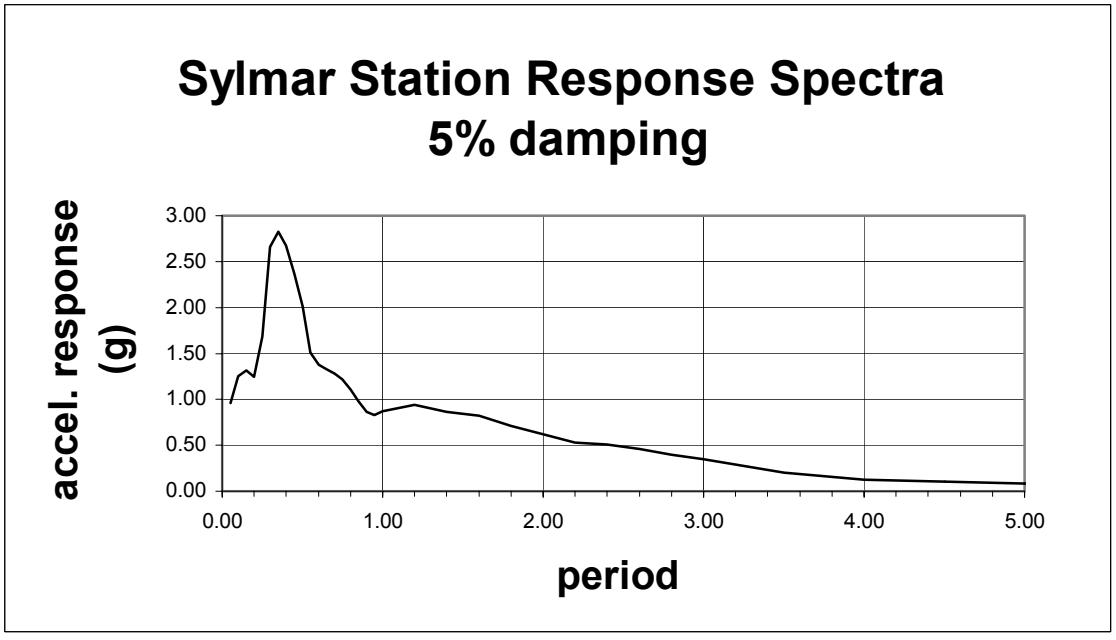

Figure 3-7 Northridge Sylmar Response Spectra

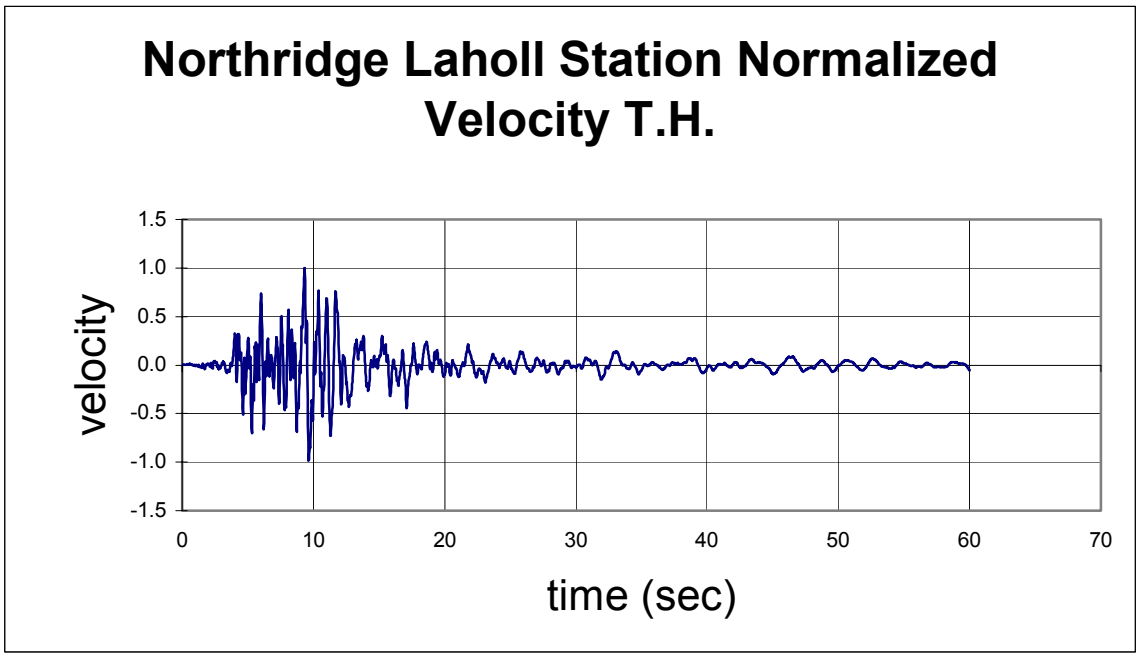

Figure 3-8 Northridge Laholl Station Normalized Velocity Time-History

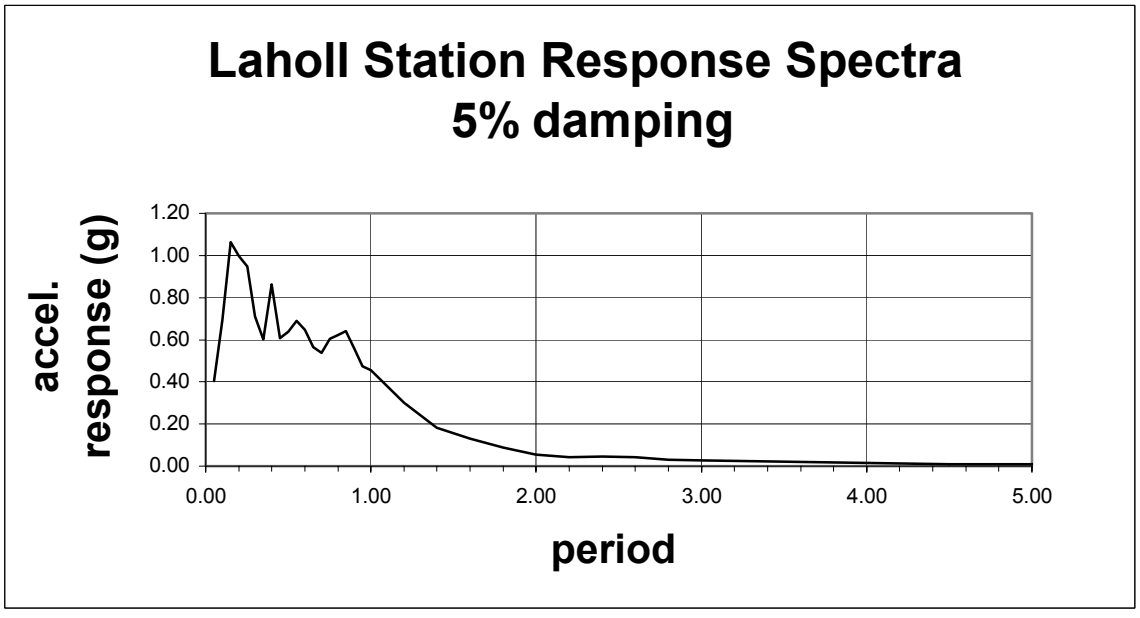

Figure 3-9 Northridge Laholl Station Response Spectra

TABLE 3-1 Northridge Earthquake Station Record Data

Station	Epicentral dist.	Component	Predominant period	Duration	Max. accel. amplitude	Max. velocity amplitude
Arleta	9 km	90 deg	.25 sec	59.98 sec	.347g	40.362 cm/s
Sylmar	16 km	360 deg	.35 sec	59.98 sec	.401g	22.263 cm/s
Laholl	23 km	360 deg	.15 sec	59.98 sec	.892g	128.884 cm/s

3.5 Test Results

Each specimen was tested by dynamic loading imposed by one of the shake-tables located in the UNR Large Scale Testing Structures Laboratory and operated under displacement control. A description of each test and the plot of the raw load-displacement data for the loading of the highest level reached from the Arleta Station record are given in Appendix B. "Approximated" straight line elastic stiffness curves were developed using the raw data hysteretic curves from the Artleta Station, the Sylmar Station, and the Laholl Station and were used to determine the dynamic stiffness of the joint due to the different input motions. A typical approximated elastic stiffness curve for a restrained joint specimen is shown in Figure 3-10 and indicates the point of engagement of the restraint device and the straight line elastic stiffness curve. The resulting elastic stiffness curves for each unrestrained and restrained specimen from the three stations as well as for the elastic portion of the static loading are shown in Figures 3-11 to 3-25. It must be noted that the data from the instrumentation were in standard English units and were converted to SI units

The dynamic stiffness curve for cast iron pipe is shown in Figure 3-11, for ductile iron pipe with unrestrained push-on joints in Figures 3-12 and 3-13, and PVC pipe with push-on joints in Figures 3-22 and 3-23. These joint specimens have no restraining devices for tensile load, and therefore, the tensile elastic stiffness is essentially zero and only the compressive elastic stiffness is shown. For these tests, the imposed displacement was

limited to approximately 25 mm (1 in.) to ensure that there was no possibility that a pull-out separation would occur during the test and potentially cause problems with the test assembly. The objective was to obtain the elastic stiffness for these unrestrained joints, not to reach a failure load condition. It can be seen from the load-displacement curves that the compressive dynamic elastic stiffness (slope of the load-displacement curve) for these specimens is greater by about twice or more than the compressive static elastic stiffness, and therefore, shows that the dynamic effects are an important consideration for design purposes.

Load displacement curves for ductile iron pipe joints with tensile restraint devices are shown in Figures 3-14 and 3-15 for gripper gasket joints, Figures 3-16 and 3-17 for retaining ring joints, and Figures 3-18 and 3-19 for bolted collar joints. For these joints, the plots show the tension elastic stiffness curves for the Arleta Station, the Sylmar Station, and the Laholl Stations, as well as the static elastic stiffness curves determined from the static phase of testing. It can be seen that in all cases, similar to unrestrained joints, the dynamic elastic stiffness is greater by approximately twice or more than the static elastic stiffness. For ductile iron pipe with gripper gasket joints (Figures 3-14 and 3-15) and for bolted collar joints (Figures 3-18 and 3-19), the Sylmar and Laholl elastic stiffnesses are greater than the Arleta results. For retaining ring joints (Figures 3-16 and 3-17), the Sylmar and Laholl elastic stiffnesses are lower than the Arleta results. The raw data load-displacement plots in Appendix B show that the tension load increases when the restraining devices are engaged, and in the compressive direction, the elastic stiffness is zero until the compressive resistance is engaged. The actual compressive elastic stiffness for these joints can be obtained from the compressive results of the unrestrained push-on joint testing.

Results for steel pipe joints (Figures 3-20 and 3-21) and PE pipe joints (Figures 3-24 and 3-25) are similar to the ductile iron pipe joints in the sense that the dynamic elastic stiffness is greater than the static stiffness. For these two joint types, both tensile and compressive elastic stiffness curves are shown since they have resistance in both directions.

A summary of the tensile results for restrained joints in terms of tensile yield force, yield displacement, and elastic stiffness is given in Table 3-2. These results were computed from the approximated straight line elastic stiffness curves. Tensile stiffness prior to engagement of the restraint is essentially zero when compared with the stiffness after engagement. As it can be seen from the raw data plots in Appendix B, the yield force level for restrained joints in tension is also the ultimate force level, without any post-yield behavior. Table 3-3 is a similar summary for unrestrained joints. It must be noted that the data acquisition values were in English units and were converted to SI units.

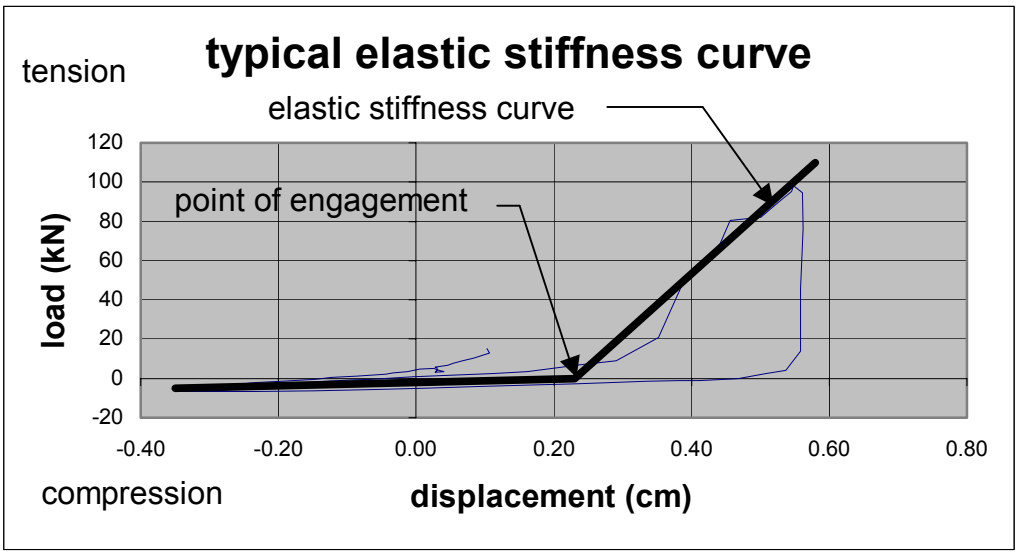

Figure 3-10 Typical Elastic Stiffness Curve for Restrained Joints

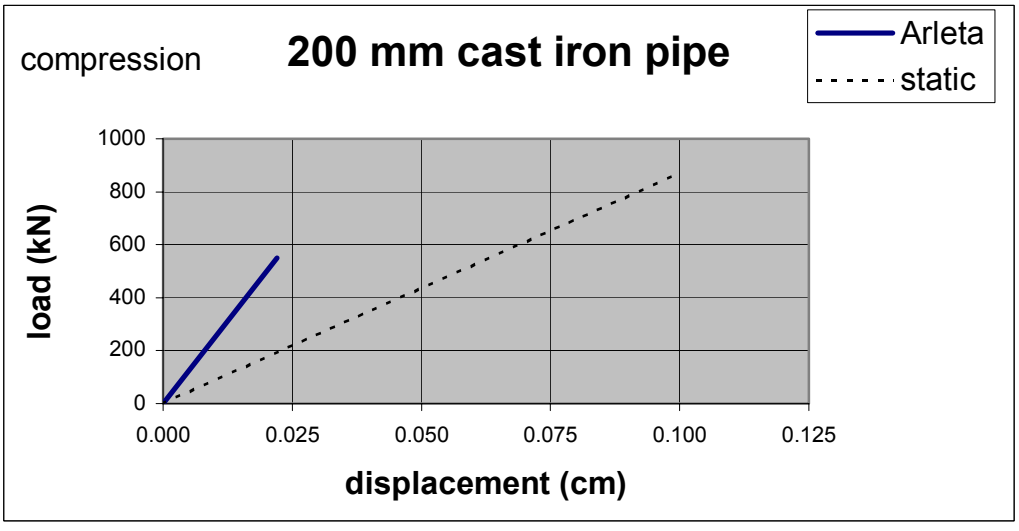

Figure 3-11 Load-Displacement Curves for 200 mm Cast Iron Pipe (after compressive engagement)

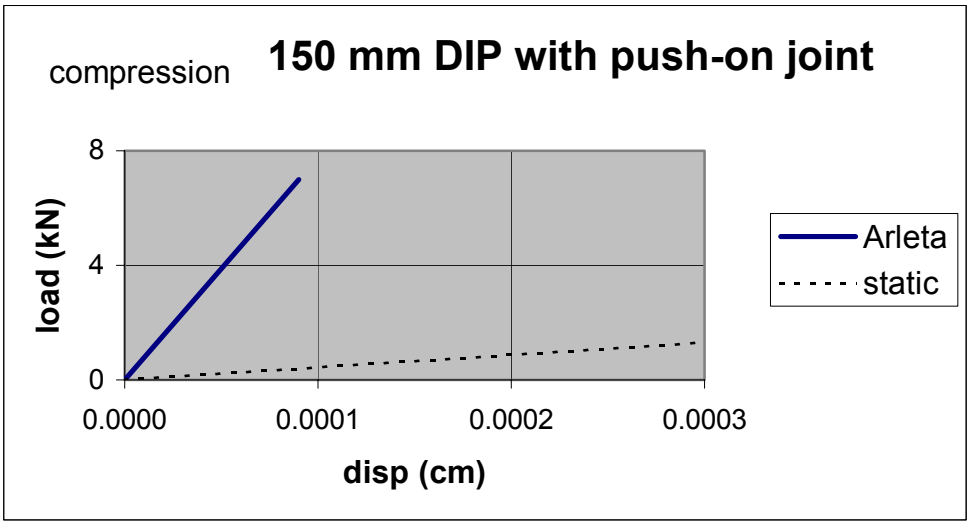

Figure 3-12 Load-Displacement Curves for 150 mm DIP with Push-on Joint (after compressive engagement)

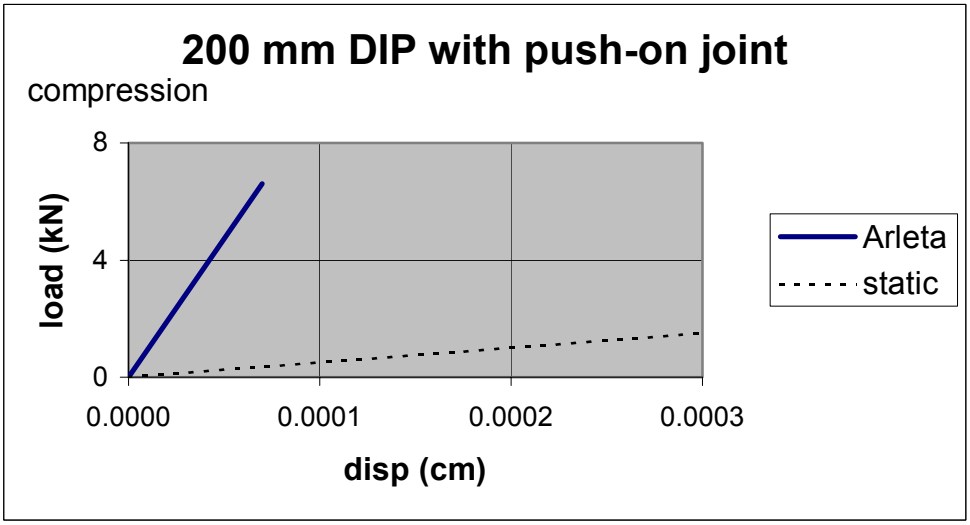

Figure 3-13 Load-Displacement Curves for 200 mm DIP with Push-on Joint (after compressive engagement)

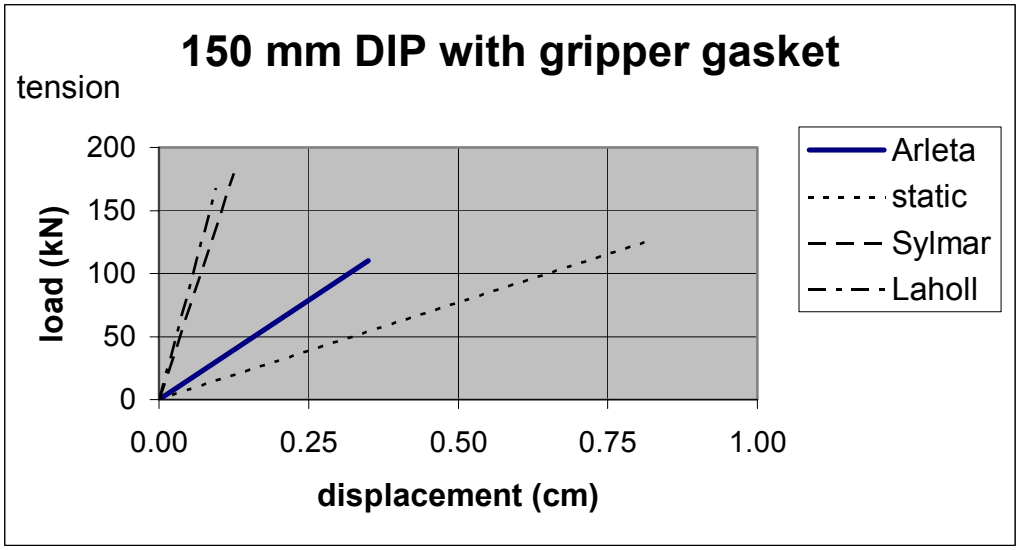

Figure 3-14 Load-Displacement Curves for 150 mm DIP with Gripper Gasket Joint

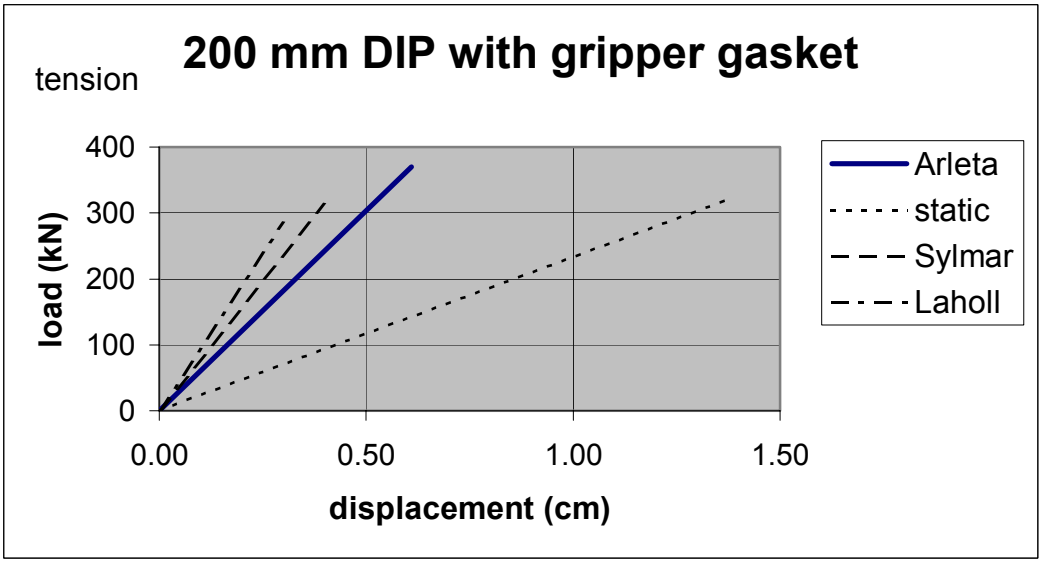

Figure 3-15 Load-Displacement Curves for 200 mm DIP with Gripper Gasket Joint

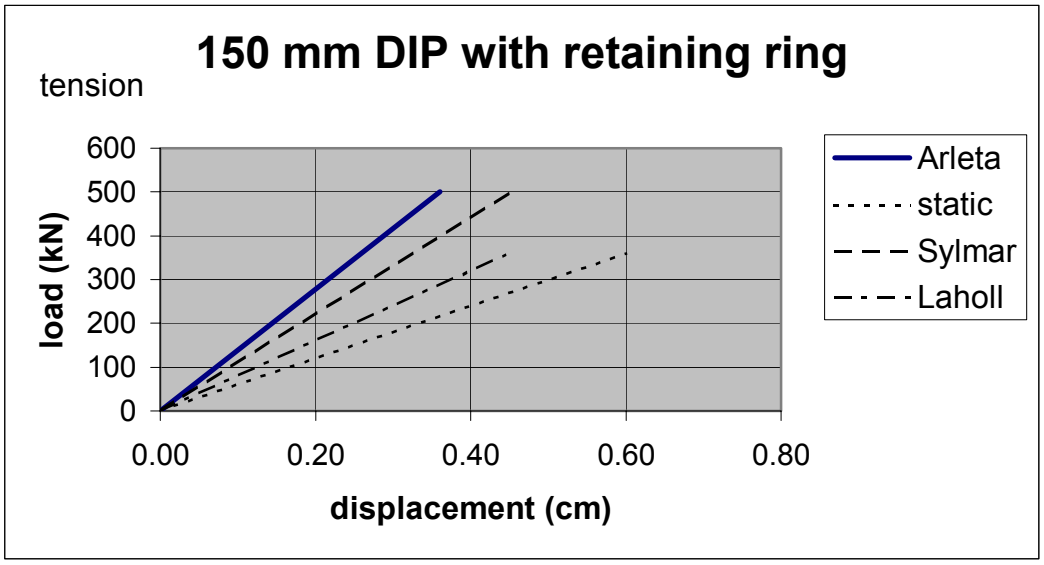

Figure 3-16 Load-Displacement Curves for 150 mm DIP with Retaining Ring Joint

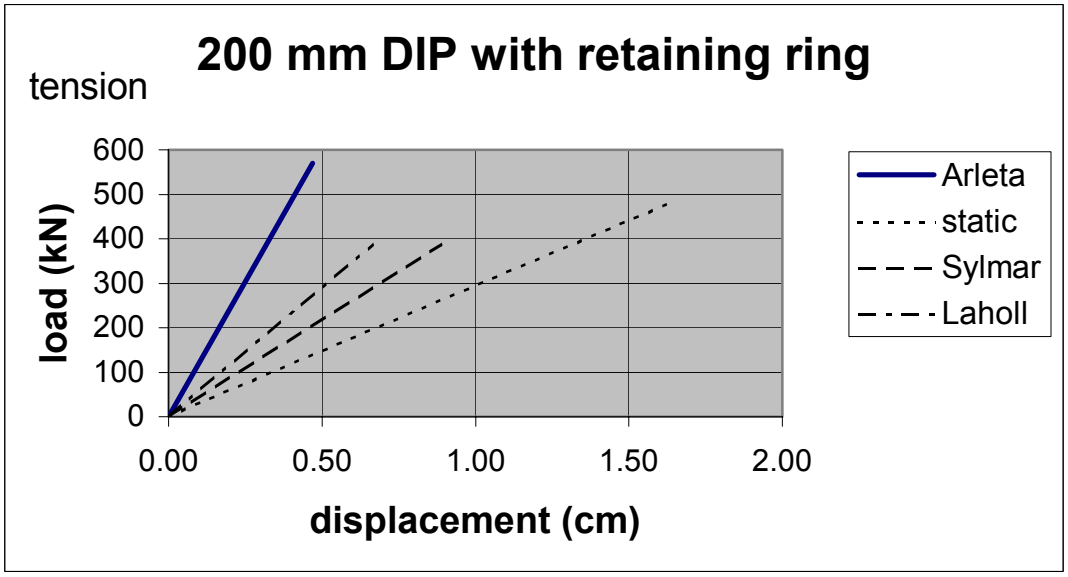

Figure 3-17 Load-Displacement Curves for 200 mm DIP with Retaining Ring Joint

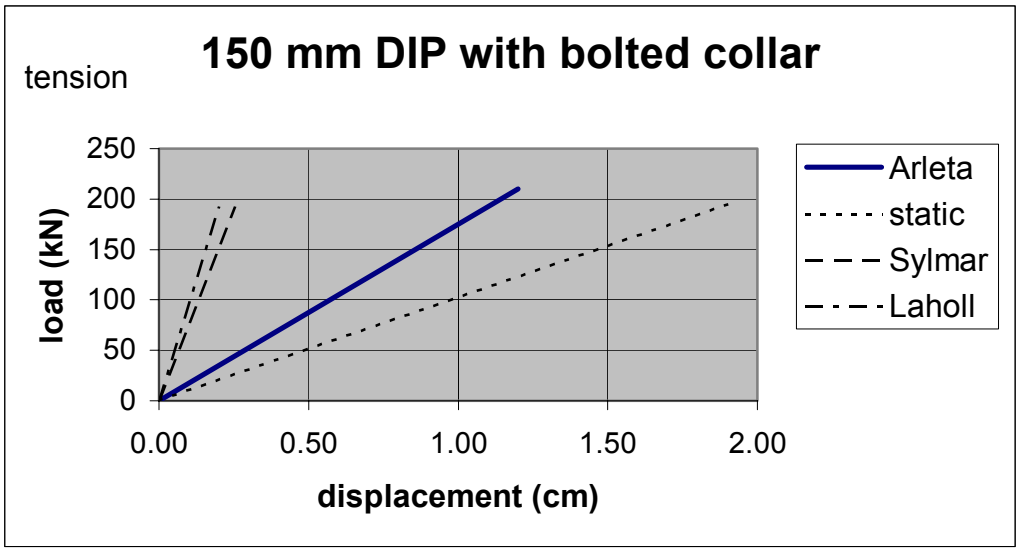

Figure 3-18 Load-Displacement Curves for 150 mm DIP with Bolted Collar Joint

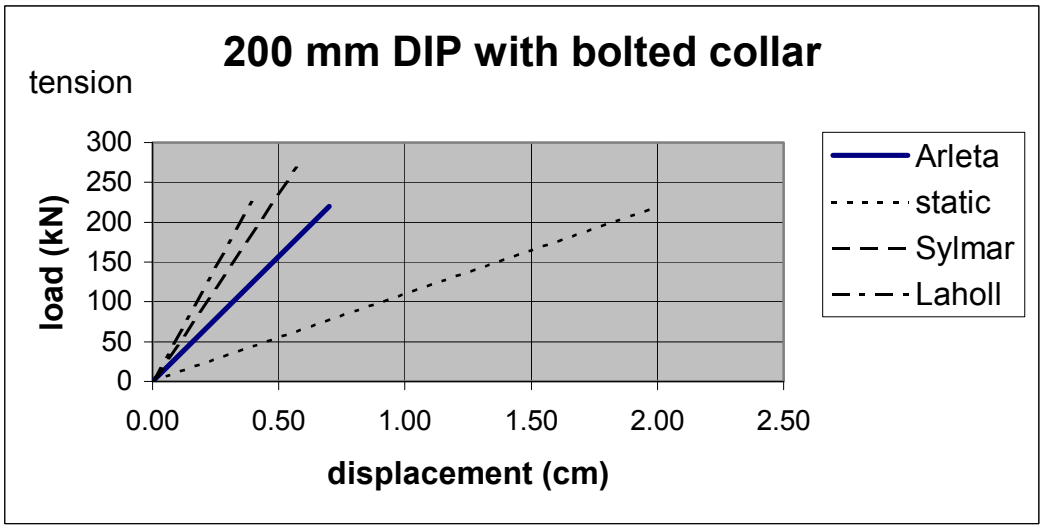

Figure 3-19 Load-Displacement Curves for 200 mm DIP with Bolted Collar Joint

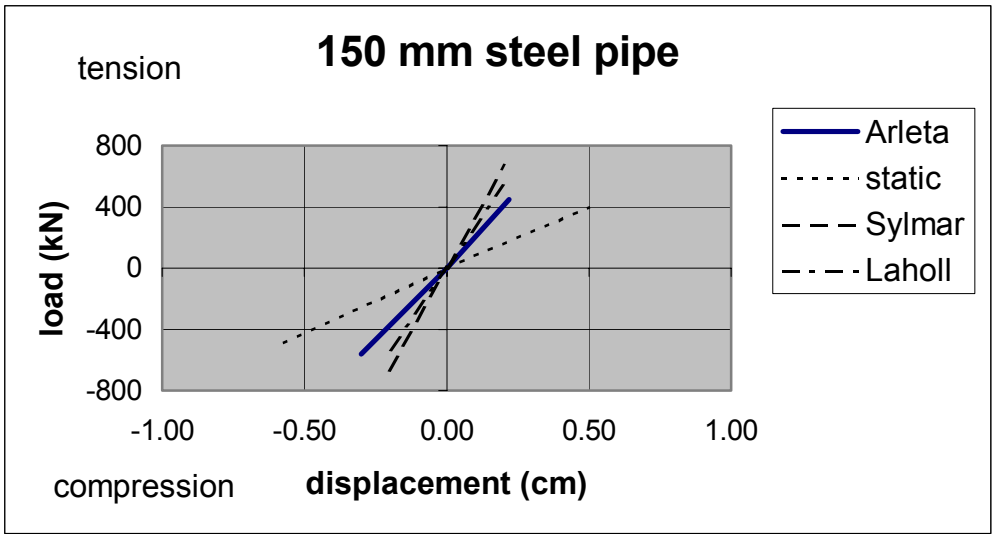

Figure 3-20 Load-Displacement Curves for 150 mm Steel Pipe

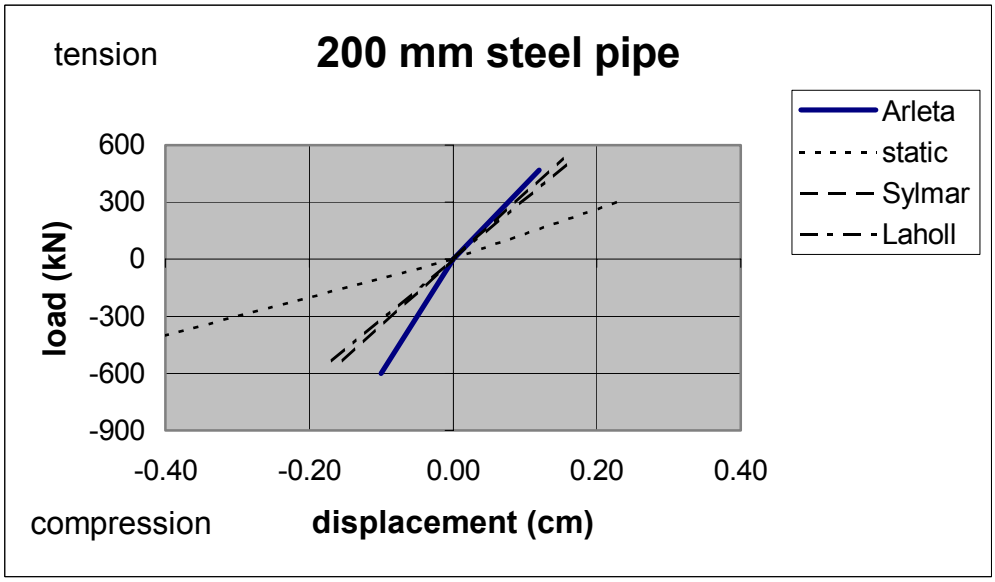

Figure 3-21 Load-Displacement Curves for 200 mm Steel Pipe

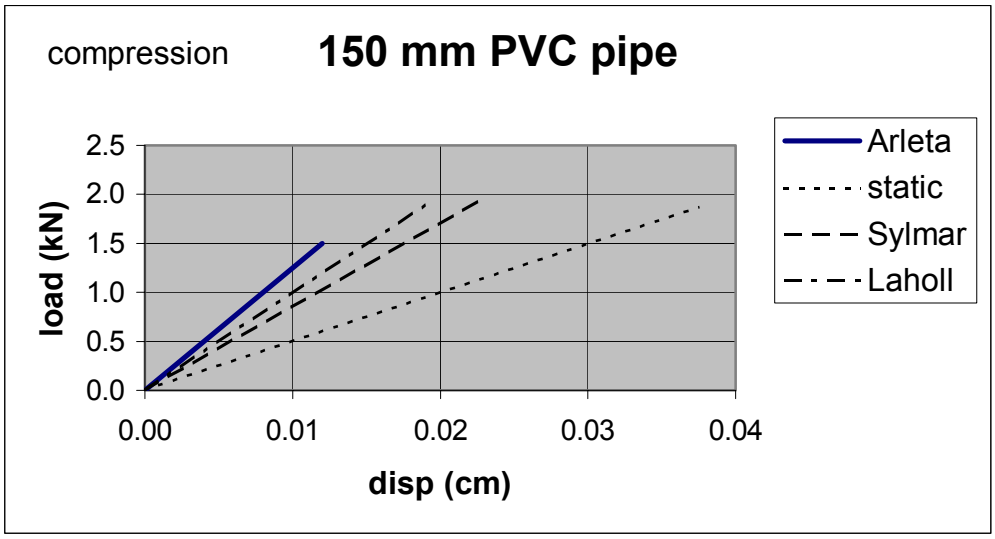

Figure 3-22 Load-Displacement Curves for 150 mm PVC Pipe

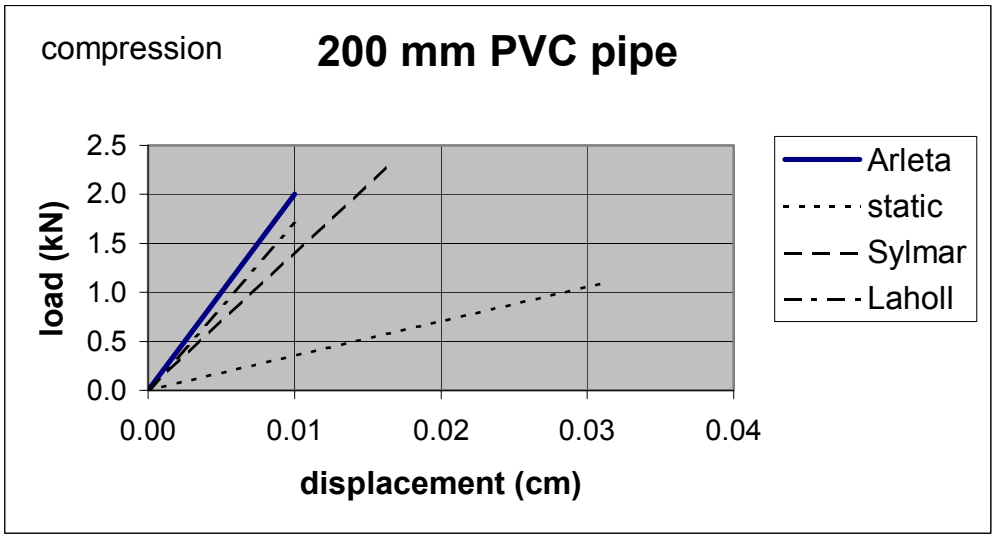

Figure 3-23 Load-Displacement Curves for 200 mm PVC Pipe

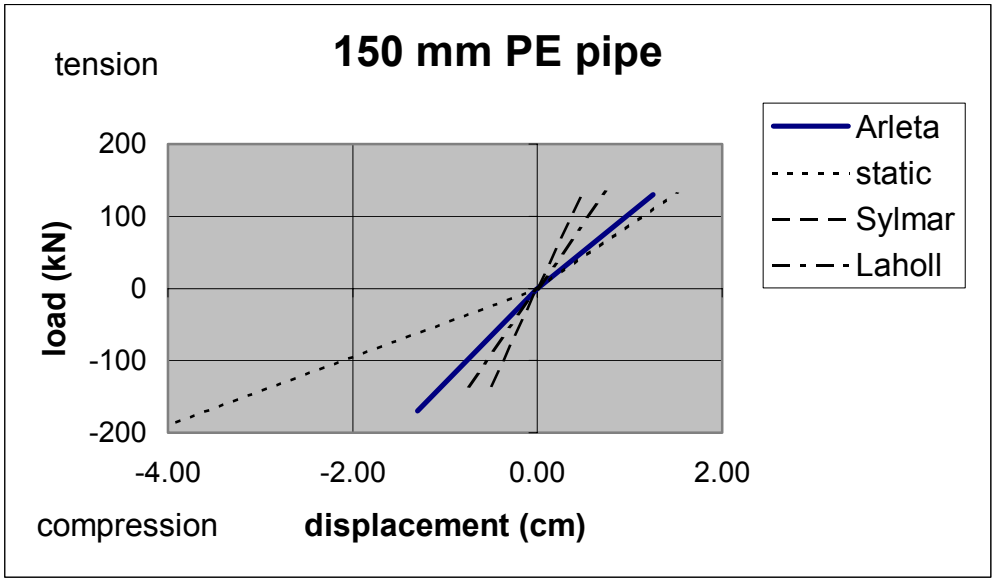

Figure 3-24 Load-Displacement Curves for 150 mm PE Pipe

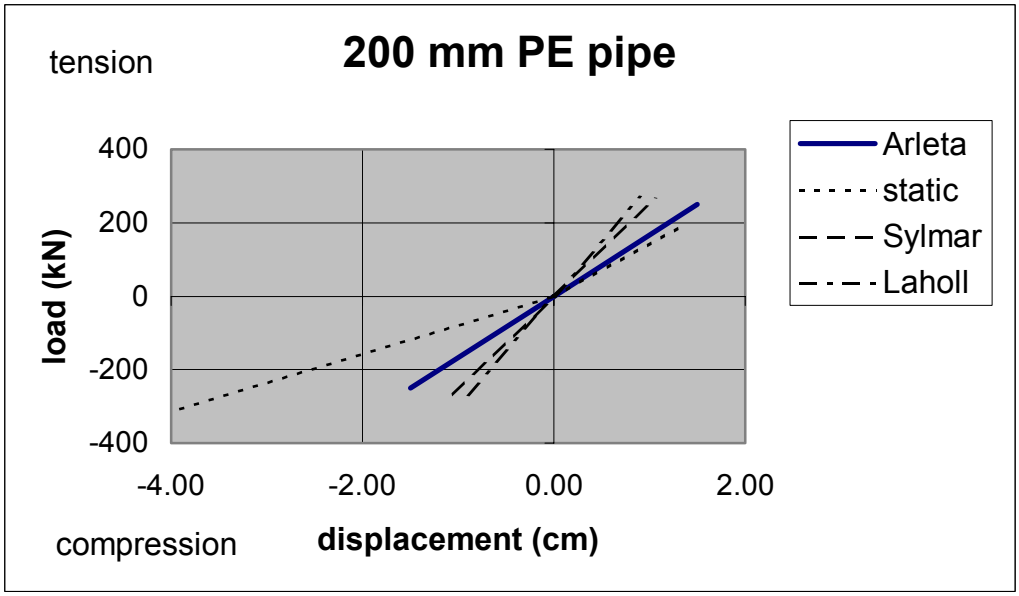

Figure 3-25 Load-Displacement Curves for 200 mm PE Pipe

Table 3-2 Joint Dynamic Stiffness Values and Yield Force Levels for Restrained Joints

1	2	3	4	5	6
Pipe Material Joint type	**Pipe Diameter (mm)**	**Test Load Direction**	**Yield Force (kN)**	**Yield Disp. (cm)**	**Elastic Stiffness (kN/cm)**
DIP bell-spigot gripper gasket	150 (6”)	tension	110	.350	314
	200 (8”)	tension	343	.565	607
DIP bell-spigot retaining ring	150 (6”)	tension	441	.317	1390
	200 (8”)	tension	551	.455	1210
DIP bell-spigot bolted collar	150 (6”)	tension	201	1.149	175
	200 (8”)	tension	212	.675	314
Steel bell-spigot lap-welded	150 (6”)	tension	472	.252	1870
		compression	516	.252	2050
	200 (8”)	tension	551	.092	6000
		compression	558	.142	3920
PE butt-fused	150 (6”)	tension	150	1.153	130
		compression	151	1.51	100
	200 (8”)	tension	220	1.244	170
		compression	286	1.682	170

Table 3-3 Joint Dynamic Stiffness Values and Final Force Levels for Unrestrained Joints

1	2	3	4	5	6
Pipe Material Joint type	**Pipe Diameter (mm)**	**Test Load Direction**	**Final Force (kN)**	**Final Disp. (cm)**	**Elastic Stiffness (kN/cm)**
Cast Iron	200 (8")	compression	549*	0.022	24954**
DIP push-on rubber gasket joint	150 (6")	compression	7*	.00009	77777**
	200 (8")	compression	6.6*	.00007	94285**
PVC push-on rubber gasket joint	150 (6")	compression	2.8*	0.022	125
	200 (8")	compression	7*	0.060	116

* compressive failure force level not reached during test
** after compressive engagement

3.6 Combined Load-Displacement Plots

Figures 3-26 to 3-32 show plots of each joint type for the 150 mm and 200 mm diameter pipe joints combined into single plots. Ductile iron pipe with unrestrained push-on joints (Figure 3-26) and ductile iron pipe with retaining ring joints (Figure 3-28) show that the unrestrained stiffnesses are approximately equal for the two diameters of pipe. For ductile iron pipe with gripper gasket joints (Figure 3-27), ductile iron pipe with bolted collar joints (Figure 3-29), steel pipe (Figure 3-30), and PVC pipe (Figure 3-31), the larger diameter pipe has about twice the stiffness of the smaller diameter pipe.

Figure 3-33 shows a bar chart comparing joint stiffnesses for each restrained joint type and each pipe diameter. Except for ductile iron pipe with restraining ring joints, the larger diameter pipes have a greater stiffness value. Figure 3-34 shows the ultimate load capacity for each restrained joint type, and it can be observed that for each case, the larger diameter pipe has a greater ultimate force capacity.

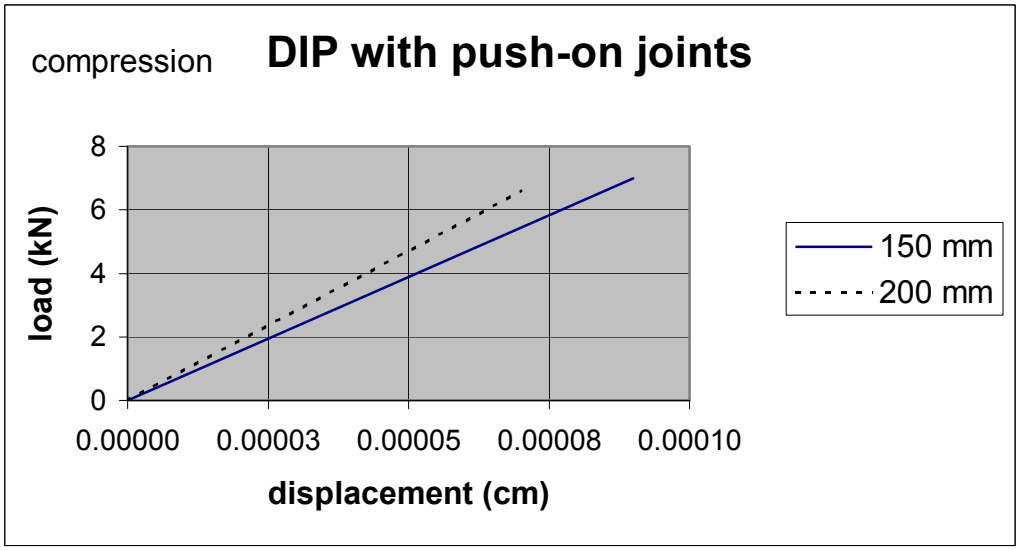

Figure 3-26 Load-Displacement Curves for DIP with Push-On Joints (after compressive engagement)

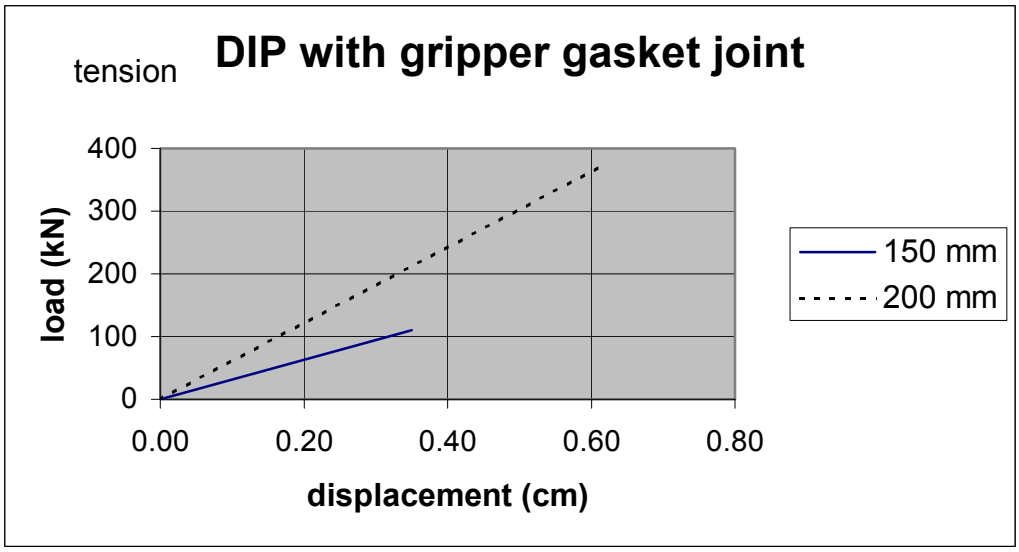

Figure 3-27 Load-Displacement Curves for DIP with Gripper Gasket Joints

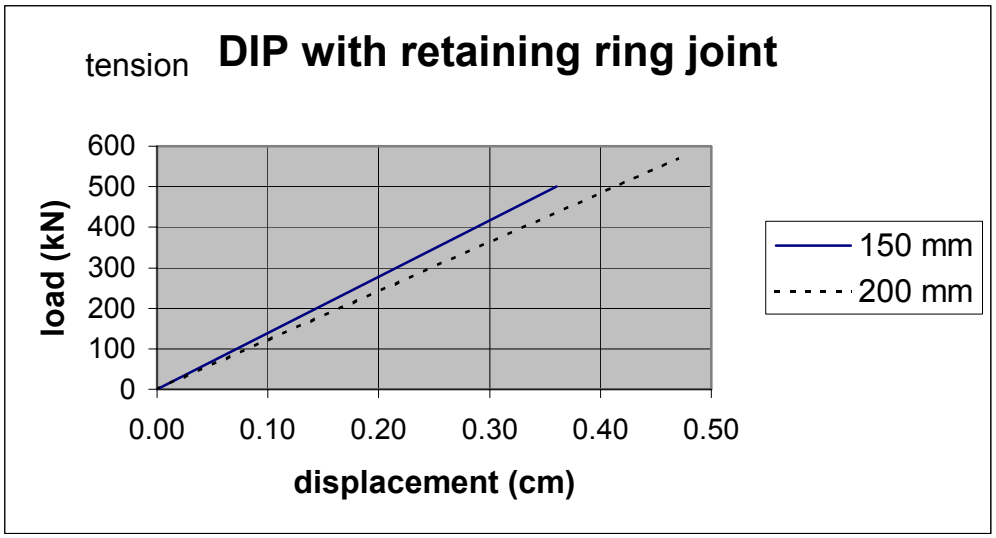

Figure 3-28 Load-Displacement Curves for DIP with Retaining Ring Joints

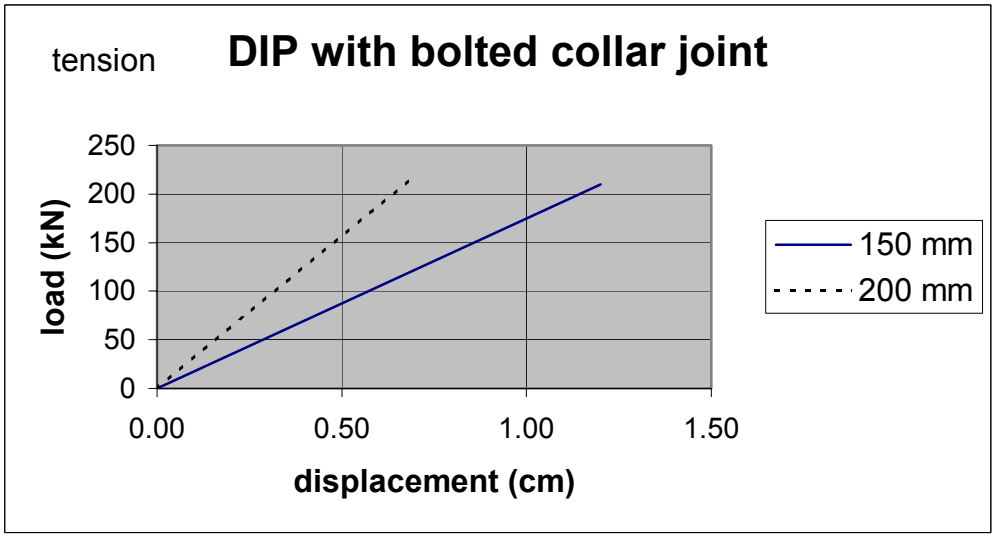

Figure 3-29 Load-Displacement Curves for DIP with Bolted Collar Joints

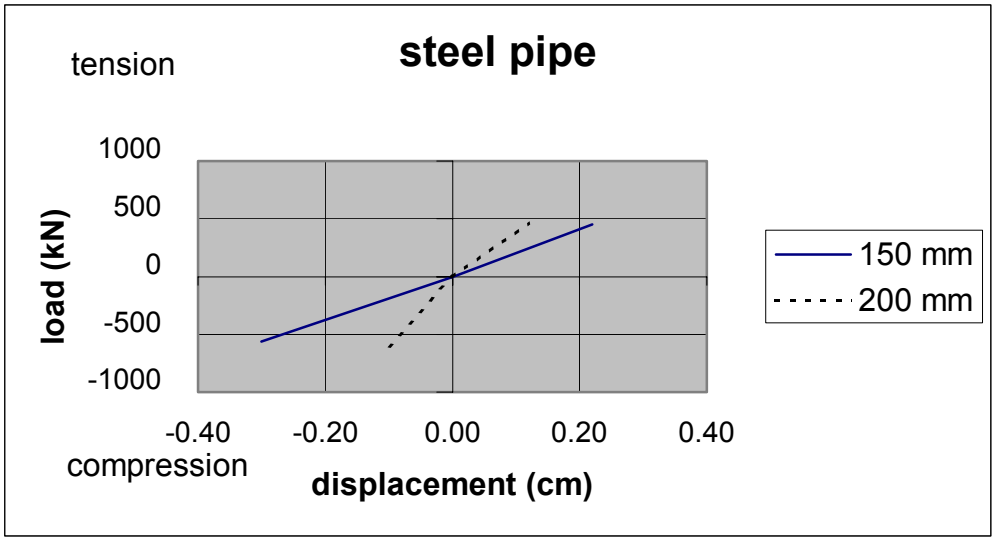

Figure 3-30 Load-Displacement Curves for Steel Pipe with Lap-Welded Joints

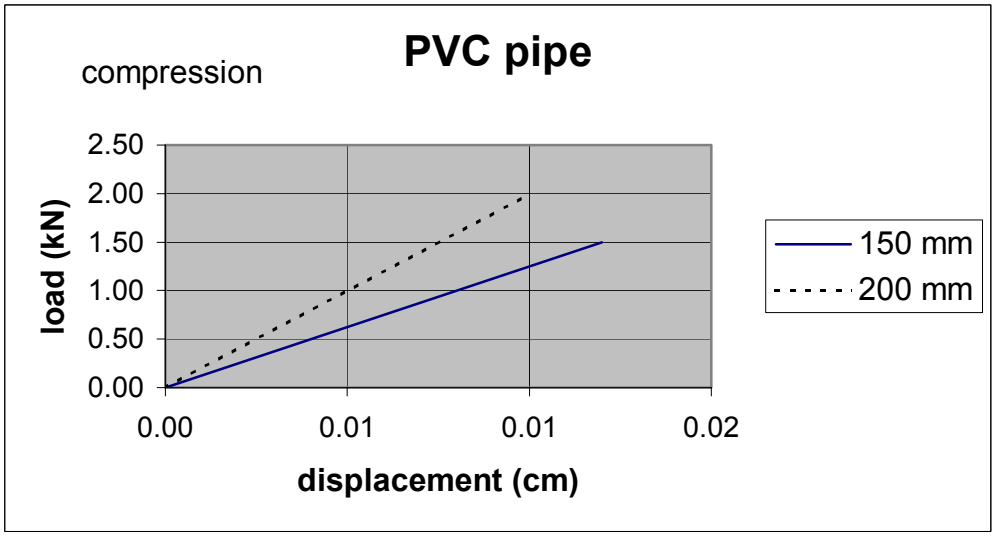

Figure 3-31 Load-Displacement Curves for PVC Pipe with Push-On Joints

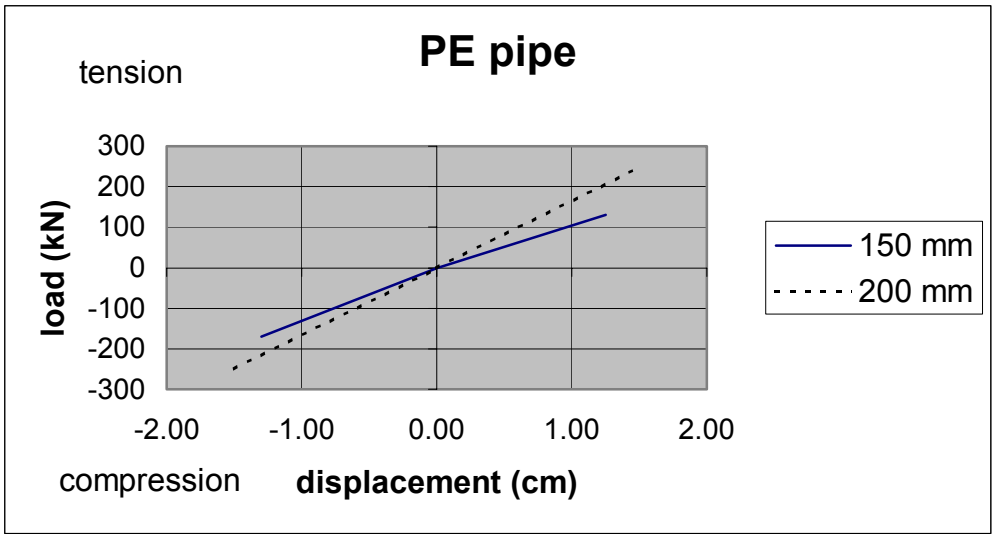

Figure 3-32 Load-Displacement Curves for PE Pipe with Butt-Welded Joints

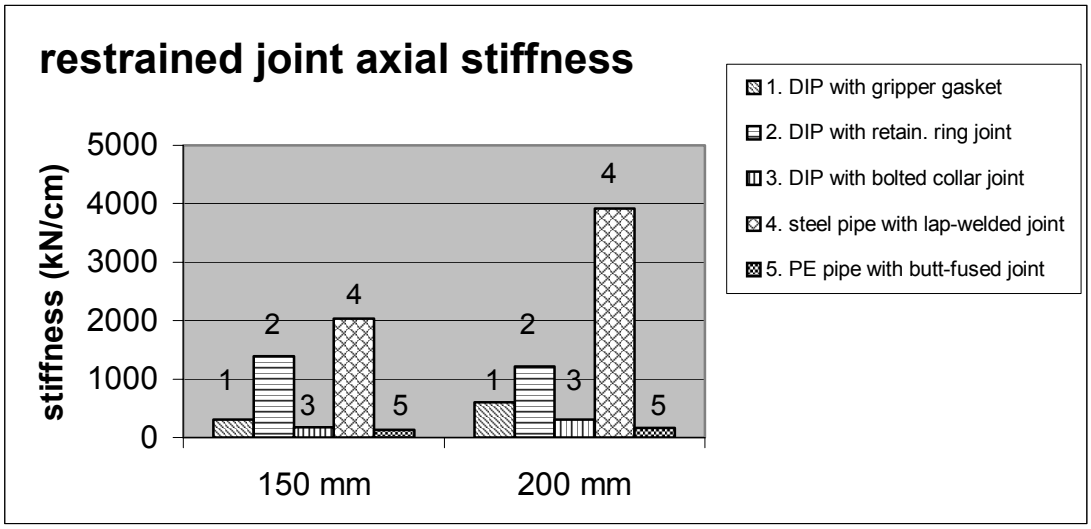

Figure 3-33 Restrained Joint Axial Stiffness

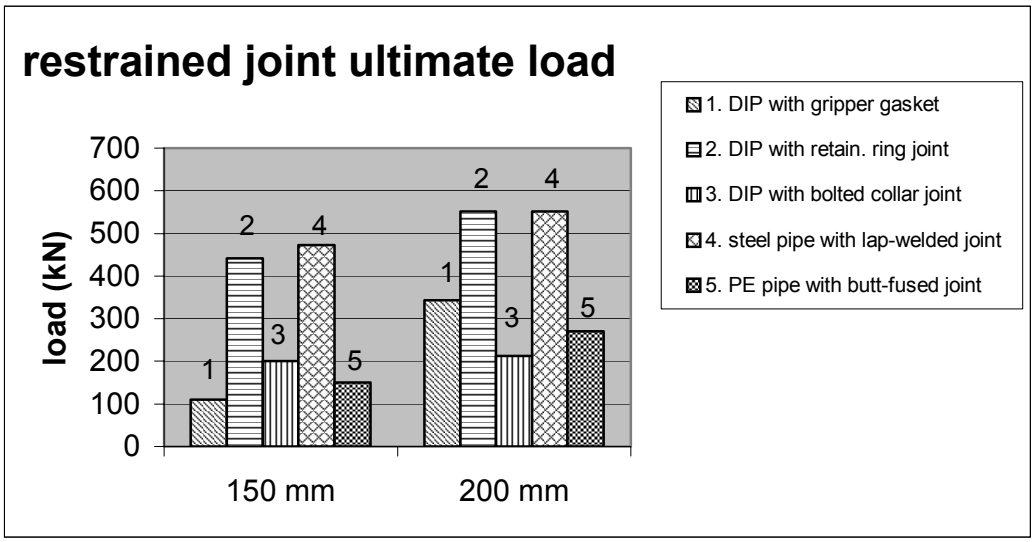

Figure 3-34 Restrained Joint Ultimate Load

3.7 Comparison Between Dynamic Loading and Static Loading Results

One of the objectives of this testing program is to compare the results of the static and dynamic testing and determine whether dynamic testing is necessary in order to characterize the seismic behavior of pipe joints. Table 3-4 shows the comparative results for static and dynamic loadings.

For unrestrained joints, the compressive loading results are for conditions that have the spigot end engage the bell end and a true compression force transfer occurs through the pipe walls. The maximum load applied for the dynamic compressive load was much less than the maximum compressive load for static loading by design, and a direct comparison of the maximum or ultimate loading for these specimens cannot be made.

Figures 3-35 and 3-36 show the comparison of the ultimate load of the various joint types and the two diameters of pipe for static and dynamic loadings. For restrained joints, the ultimate loading values are approximately the same for both cases which indicates that the dynamic effects on the force capacities are not significant and that the static testing is

able to capture the joint behavior under dynamic loading conditions. The comparison of the elastic stiffness behavior for static and dynamic loadings is shown in Figures 3-37 and 3-38. The elastic stiffness values show that the dynamic stiffness values are greater by about twice or more than the static elastic stiffness, which indicates that the frequency content and the higher loading rate of the dynamic loading condition will increase the elastic axial stiffness. Therefore, in terms of elastic axial stiffness, the static testing cannot capture the joint behavior under dynamic loading conditions.

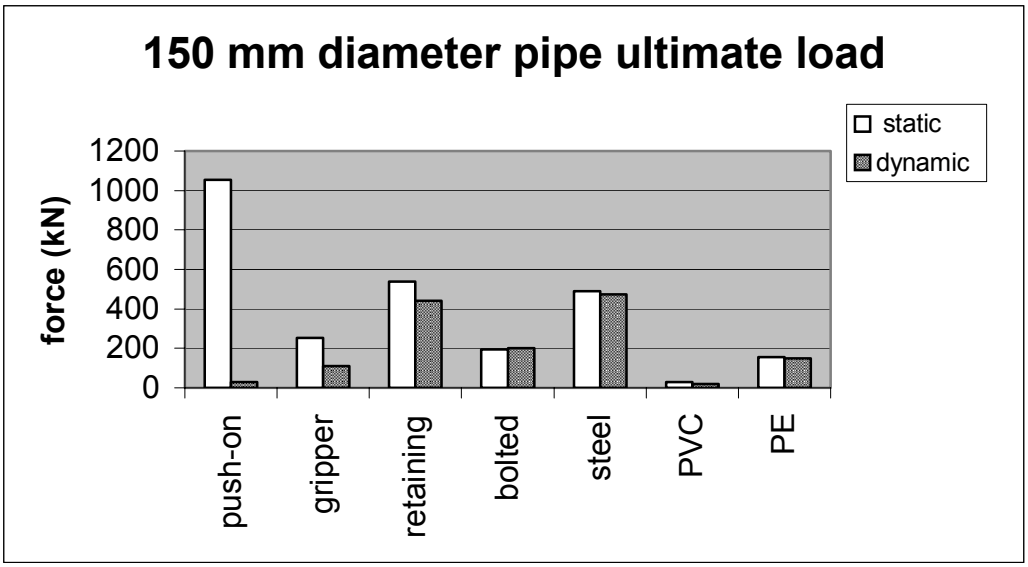

Figure 3-35 Static-Dynamic Ultimate Load Comparison for 150 mm Diameter Pipe

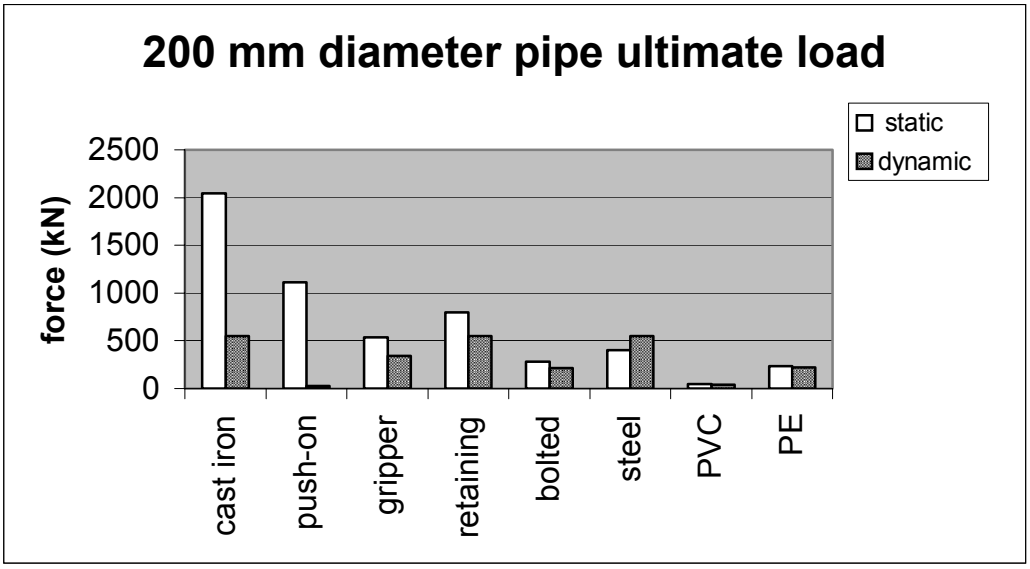

Figure 3-36 Static-Dynamic Ultimate Load Comparison for 200 mm Diameter Pipe

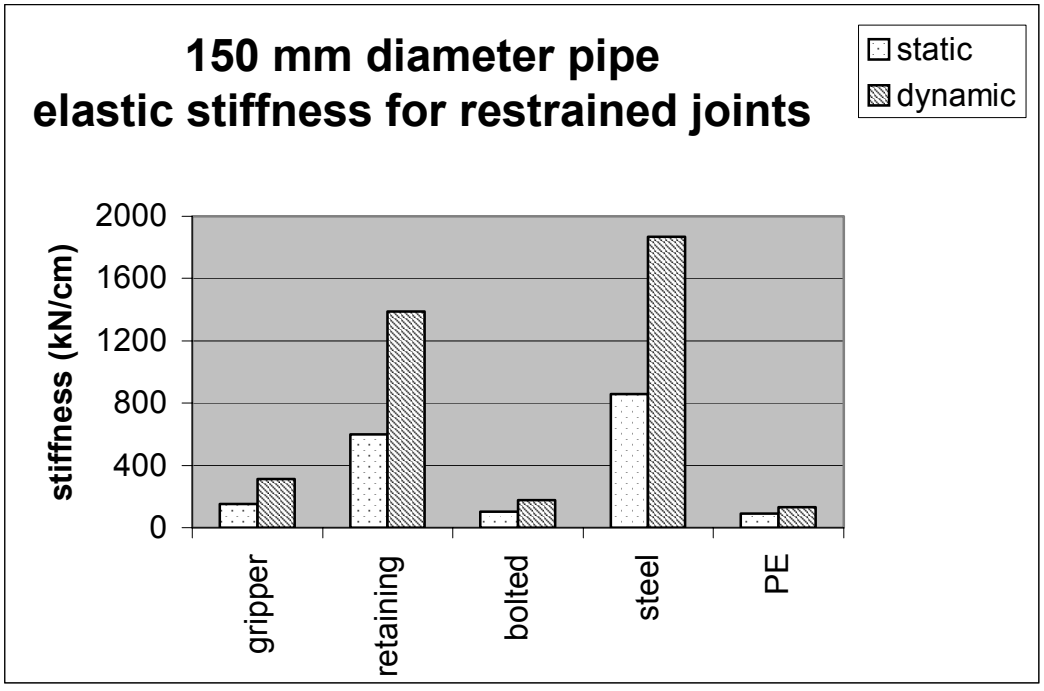

Figure 3-37 Static-Dynamic Elastic Stiffness Comparison for 150 mm Diameter Restrained Joints

TABLE 3-4 Comparison of Dynamic and Static Yield Force and Elastic Stiffness

Specimen	Type	Dir.	Dia (mm)	Ultimate Force (kN)		Elastic Stiffness (kN / cm)	
				static	dynamic	static	dynamic
cast iron	unrestrained	comp	200	2046	549*	8724	24954**
DIP push-on joint	unrestrained	comp	150	1054	7*	4348	77777**
			200	1112	6.6*	8724	94285**
DIP gripper gasket	restrained	ten	150	253	110	154	314
			200	539	343	233	607
DIP retain.ring	restrained	ten	150	538	441	600	1390
			200	795	551	294	1210
DIP bolted collar	restrained	ten	150	195	201	103	175
			200	280	212	109	314
steel lap-welded	restrained	ten	150	554	472	860	1870
		comp		491	516	800	2050
		ten	200	711	551	1317	6000
		comp		401	558	1000	3920
PVC push-on joint	unrestrained	comp	150	15	2.8*	40	125
			200	13	7*	30	116
PE butt-fused	restrained	ten	150	157	150	89	130
		comp		186	151	50	100
		ten	200	232	220	144	170
		comp		307	286	80	170

* compressive failure force level not reached during test

** after compressive engagement

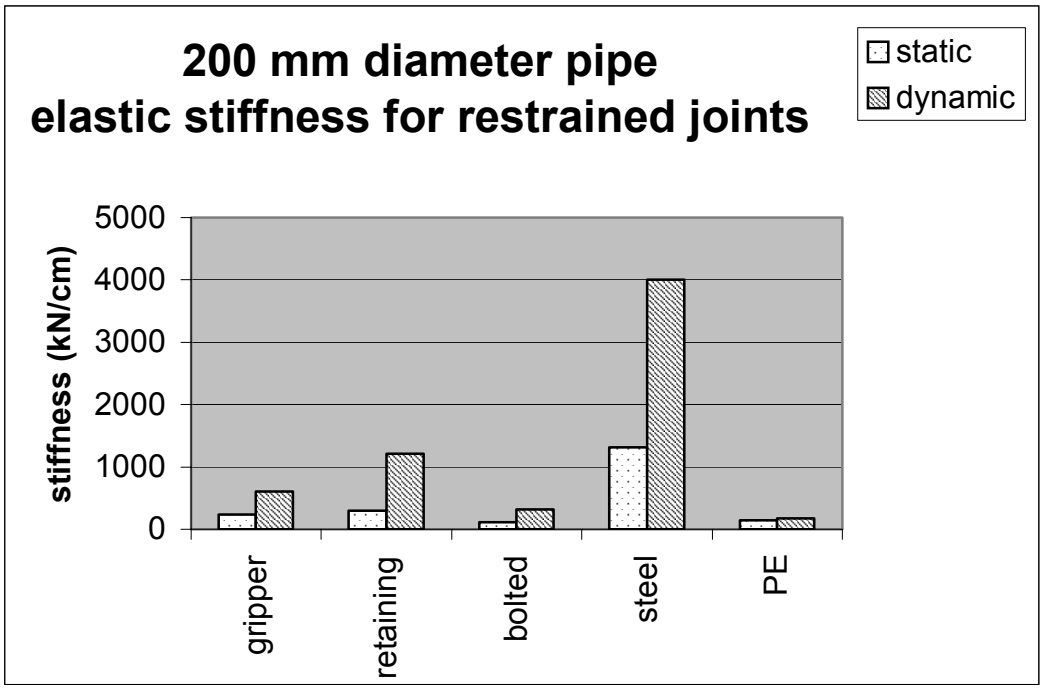

Figure 3-38 Static-Dynamic Elastic Stiffness Comparison for 200 mm Diameter Restrained Joints

SECTION 4
STATIC AND DYNAMIC BENDING EXPERIMENTS

4.1 Description

This phase of testing was designed to determine the rotational stiffness characteristics of some common types of underground piping joints due to both static and dynamic loading conditions. The types of joints tested fall into three categories: 1) unrestrained bell and spigot push-on joints with gasket seals, 2) bell and spigot joints with restraining devices to resist pull-out, and 3) welded or fused joints that have a continuity across the joint and can resist both compressive and tensile motions. Seismic motions can result in soil movements of different displacements over a particular section of a piping system, which can cause bending in the system and rotation in the joints. Piping systems that have a change of direction in their alignment will have a portion of their system in the general direction of the seismic motion while another portion will be at some angle to the seismic motion. As a seismic motion travels through the system, bending moments can be imposed on a joint at the junction of the two directions which are connected by either "tee" or "elbow" sections. Rigid anchor points in the system such as risers to fire hydrants or connections to rigid structures resist both displacements and rotations, which results in bending moments at the joint connection. Permanent ground deformations which are caused by seismic events or by other conditions such as slope failures, can cause differential movements in a localized area normal or near normal to a piping system, resulting in bending or curvatures at the joints.

While the first two phases of this testing program were concerned with the axial behavior, a failure condition of the joint most likely will be a combination of concurrent axial forces and bending, and therefore, to understand and properly analyze and design piping systems, both the axial and rotational stiffnesses of the joints need to be known. The rotational stiffness of joints, as determined from this phase of testing, can be used as part of the input data required in a finite element analysis of a piping system subjected to seismic motions or to permanent ground deformations. Because of the limitations of the

testing assembly, the diameters of pipe tested in this phase were limited to 150 mm and 200 mm.

4.2 Test Assembly Configuration and Instrumentation

A test assembly was designed and fabricated that can apply a four point simple beam cyclic bending load to a test specimen with a joint at the mid-span of the specimen. The span length of the specimen was 122 cm (Figure 4-1). For this loading, the concentrated load points, both upward and downward, were at the ¼ span points with the reaction at the specimen ends. A 220k MTS dynamic actuator and its support frame was used to provide the loading force. The actuator and its support frame are in a vertical position so that the loading was applied in a vertical direction. Two steel tube frames (Figure 4-2), each consisting of two columns and a cross beam were fabricated to provide the end support and restraint in both the upward or downward directions, while allowing the end of the specimen to rotate. These support frames were located outside the actuator frame and were post-tensioned to the lab's strong floor.

The assembly from the actuator head to the specimen consisted of: 1) a bolting plate with a welded bar forming a "tee" shape, 2) a load-cell with end flanges, 3) a spreader-beam to distribute the load to the load points, and 4) loading round bars that applied the load to the specimen. The actuator head contains a hydraulically driven gripping jaw that is able to grab a specimen for tension or compression loading. In order to provide a bolting surface to the actuator head, a steel plate with a steel bar welded vertically to the flat surface of the plate was fabricated. The hydraulic jaws were clamped onto this bolting plate making a bolting surface for both compressive and tensile loadings. A 150k load-cell with end flanges was attached to the bolting surface, and a load spreader-beam was bolted to the load-cell's other end flange. Loading round bars above and below the specimen were bolted to the spreader-beam and provided the upward and downward loading points to the test specimen. The restraint round bars at the end supports were

also above and below the specimen and were bolted to the support frame which constrained the upward and downward cyclic loading (see Figure 4-2).

The instrumentation for this testing phase consisted of a LVDT internal to the dynamic actuator, a 150k load-cell placed between the actuator and the spreader beam, a laser extensionometer to measure mid-span vertical displacement at the pipe's spring-line, and Celesco LVDTs placed under the specimen at the loading points to measure vertical displacements. Strain gages were attached to the specimen's top surface at about 35 cm from each of the end supports, and at the start of the bell at the joint (Figure 4-3). The specimens were filled with water at a very low level of pressure in order to detect any leakage that would occur at the joint during the loading process.

Figure 4-1 Test Specimen and Actuator Configuration for Bending Testing

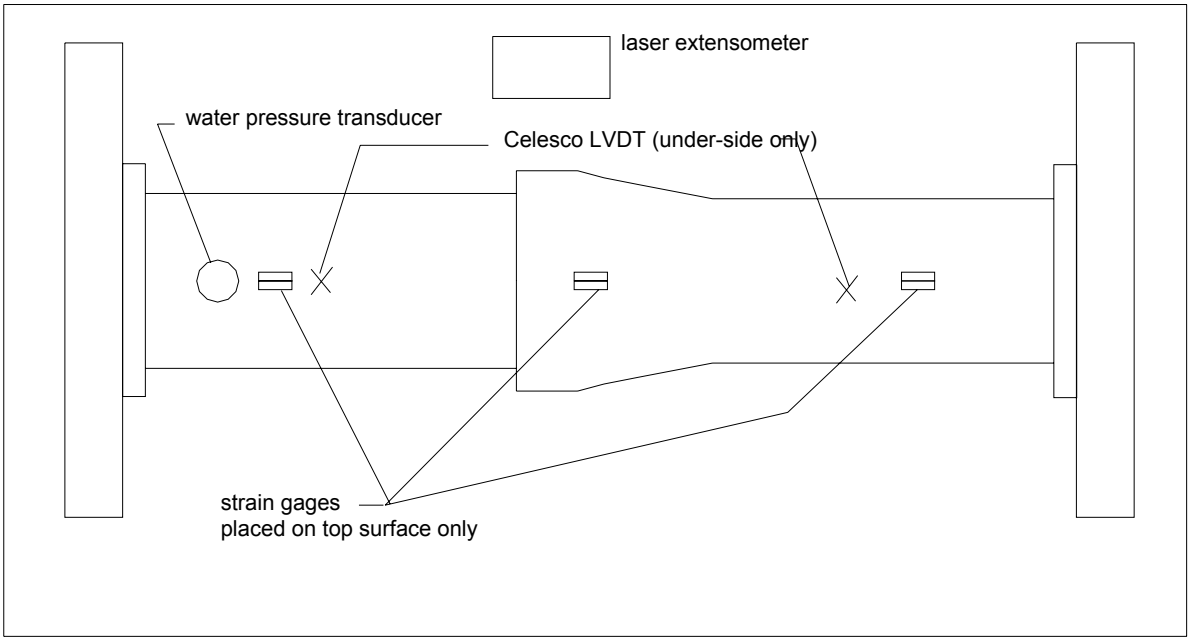

Figure 4-2 Bending Test Assembly Elevation

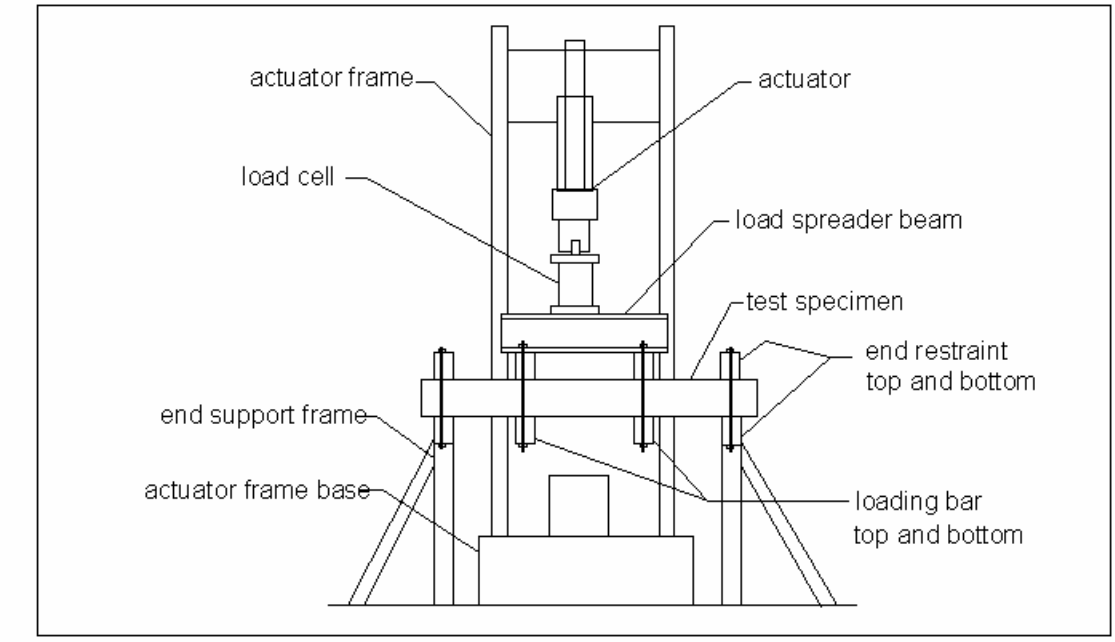

Figure 4-3 Location of External Instrumentation for Bending Testing

4.3 Test Methodology and Loading

The loading procedure for the bending phase of testing consisted of both a dynamic loading step and a static loading step. A four point bending configuration with two load points and two end reaction points was used to apply simple beam bending moments without any shear component at the mid-span. For dynamic loading, the Arleta Station velocity record from the Northridge earthquake (see Section 3-5) was used for displacement control to the actuator to achieve a dynamic loading with a realistic frequency content, but at a low level of displacement amplitudes. Displacements were applied by a 220k MTS actuator using the input earthquake record. In order to maintain a comparison of testing results between the various specimens, and because only one specimen for each type of joint was available, it was important that failure did not occur during the dynamic step. However, the dynamic load amplitude needed to be of sufficient level to provide useful data from the loading to determine dynamic behavior characteristics. The dynamic loading results were used only to determine a trend of the initial unrestrained rotational stiffness under dynamic conditions.

For the static loading, cyclic displacements were applied by the actuator in bi-directional loading, starting at a low level amplitude and increasing by incremental steps until a failure condition occurred, or it was obvious that other behavior was occurring and that a failure condition could not be reached. The static loading provided rotational stiffness characteristics at higher displacement amplitudes than was imposed by the dynamic loading.

4.4 Test Results

Data were recorded and stored using a Megadac data acquisition system and consisted of load values, vertical displacement values at the mid-span and at the load points, and longitudinal barrel strain. The load-displacement values were used to compute the corresponding mid-span moment and the mid-span rotation. Each individual test is

documented in Appendix C along with the moment-rotation curves. It should be noted that the rotation is computed at the mid-span.

Each specimen was subjected to both dynamic and static loadings. The dynamic loading resulted in data points with a large amount of scatter and non-uniform hysteretic curves, and therefore, "approximated" straight-line curves for the dynamic testing were developed, but with a high degree of subjectivity. In order to maintain a consistency of the testing for comparative purposes of the various joint types and pipe material, the failure level or the last test amplitude reached for all specimens was reached during the static testing. Figure 4-4 shows a typical moment-theta curve for a bell and spigot type joint, with "approximated" straight-line curves. Theta is the rotational angle of the deflected specimen under loading. The approximated straight-line curves were developed from the moment-theta curves and show critical zones such as the initial "unrestrained" rotational stiffness, the point of surface contact engagement, and the "restrained" rotational stiffness. The initial unrestrained curve shows relatively low stiffness of the joint rotating about the gasket without any other restraint mechanism. As the spigot end rotates in the bell end, and the point of contact engagement occurs, the outer tip of the spigot end contacts the inner surface of the bell end at the same time the inner tip of the bell end contacts the outer surface of the spigot end, forming a force couple and a restraining moment. Once this couple is formed, the rotational stiffness increases

Figure 4-5 shows the moment-theta curve for the 200 mm cast iron pipe. The water seal of this specimen is a leaded caulking which had hardened over its service life. This hardening resulted in a relative rigid joint condition even in its unrestrained rotational stiffness. The specimen ultimately failed in its barrel due to the specimen assembly configuration. The dynamic unrestrained rotational stiffness is noticeably larger than the static unrestrained stiffness.

Figures 4-6 and 4-7 show the moment-theta curves for the two different diameters of ductile iron pipe with push-on rubber gasket joints. The plots show that the dynamic

unrestrained stiffness is noticeably greater than the static stiffness. In the static cyclic loading, these joints exhibited an incremental creep of withdrawal of the specimen's spigot end from the bell end, where at each cycle of loading, the spigot end incrementally slipped out of the bell end and would have eventually lead to a complete separation and joint failure. This phenomenon is likely due to the surface contact between the spigot end and the bell end in its rotated state. The spigot end is able to slide on the inner surface of the bell end during the withdrawal motion, while in the inward motion, the spigot tip will dig into the bell's rough inner surface, restraining the movement in that direction. The result is that the withdrawal movement is essentially free to move while the inward movement is restricted. This ratcheting effect caused the spigot end to incrementally move outward at each loading cycle and the static testing was stopped when it was apparent that the spigot end was in danger of completely separating from the bell end. The dynamic unrestrained rotational stiffness is noticeably larger than the static unrestrained stiffness

Ductile iron pipe with gripper gasket joints (Figures 4-8 and 4-9) and ductile iron pipe with retaining ring joints (Figure 4-10 and 4-11) have similar characteristics as the ductile iron pipe with push-on joints. However, due to the restraining devices of these joints that hold the spigot end and the bell end together, the incremental creep of withdrawal did not occur. The restraining mechanism creates a greater rotational stiffness because the contact surface slippage is prevented or at least restrained. Similar to a push-on joint, the dynamic unrestrained stiffness is greater than the static unrestrained stiffness.

Bolted collar restrained joints show a different behavior (Figures 4-12 and 4-13). The restraint mechanism is on the outer surface of the pipe, not inside the joint. Due to the bolted collar assembly, the compressive motion of the bending is completely unrestrained which allows free movement in the compressive or inward direction, while the tensile motion is restrained. For both the gripper gasket and the retaining ring joints, the restraining mechanism is evenly distributed around the circumference for the pipe, while for bolted collar joints, the restraining mechanism is at the points where the four wedge screws contact and dig into the pipe surface. This imposes a greater localized stress level

and allows greater slippage to occur. For this reason, the rotational stiffness of bolted collar joints for dynamic loading and for static loading are much closer together.

The moment-theta curves of steel pipe joints are shown in Figures 4-14 and 4-15. It can be seen that the bending behavior of these joints resembles that of simple beam action. Since the pipe is thin wall and the fillet lap-weld provides only a minor increase in thickness, the joint has only a slight eccentricity in the stress load-path. Unlike bell and spigot joints where the joint itself acts like a rotational spring connected by rigid pipe segments, the joint of the steel pipe is continuous and maintains a zero rotational slope at the mid-span similar to simple beam bending. The joint rotation is determined from the difference of the slopes at the load point and the mid-span location. The rotational stiffness would be linear up until a plastic hinge is formed, however this level was not reached in the testing. As the vertical load increased, surface crushing at the load point limited the force amplitude that would be required to produce the plastic hinge moment and the testing was terminated when the loading resulted in major local surface deformations. It can be seen that the dynamic rotational stiffness is noticeably larger than the static rotational stiffness. PVC pipe (Figures 4-16 and 4-17) with push-on rubber gasket joints has the same assemblage as ductile iron pipe with push-on joints. However, the plastic material for both the spigot surface and the bell end surface is extremely smooth, and therefore, the restraint of slippage in the compressive or inward direction did not occur and the incremental creep of withdrawal did not happen. In addition, the ductility of the PVC material allows large strains to occur without fracture or permanent deformations. The difference between the dynamic and the static rotational stiffnesses is not as great as for the case of ductile iron pipe.

Similar to steel pipe, PE pipe (Figures 4-18 and 4-19) shows the behavior of a simple beam bending, but with a much higher level of ductility. The specimen acted as a beam mechanism and the rotational stiffness was linear for the entire range of the loading amplitude. As with steel pipe, the dynamic rotational stiffness is close to the static rotational stiffness. It was observed during the testing that large deformations and displacements occurred without any fracture or joint failure.

Table 4-1 summarizes the results of the static loading step for each specimen tested and lists its initial unrestrained moment and rotation, unrestrained rotational stiffness, restrained moment and rotation, and restrained rotational stiffness. It must be noted that the data acquisition values were in English units and were converted to SI units for this report. In this table, the symbol "---" indicates that there were only restrained moments and rotations and no unrestrained values for the steel pipe and PE pipe specimens.

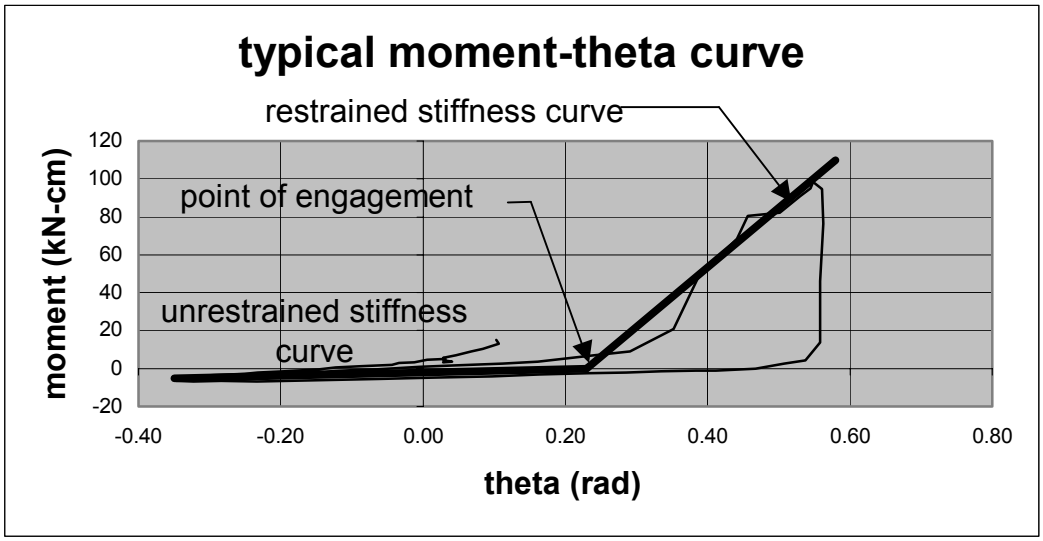

Figure 4-4 Typical Moment-Theta Plot with Approximated Straight-Line Curves

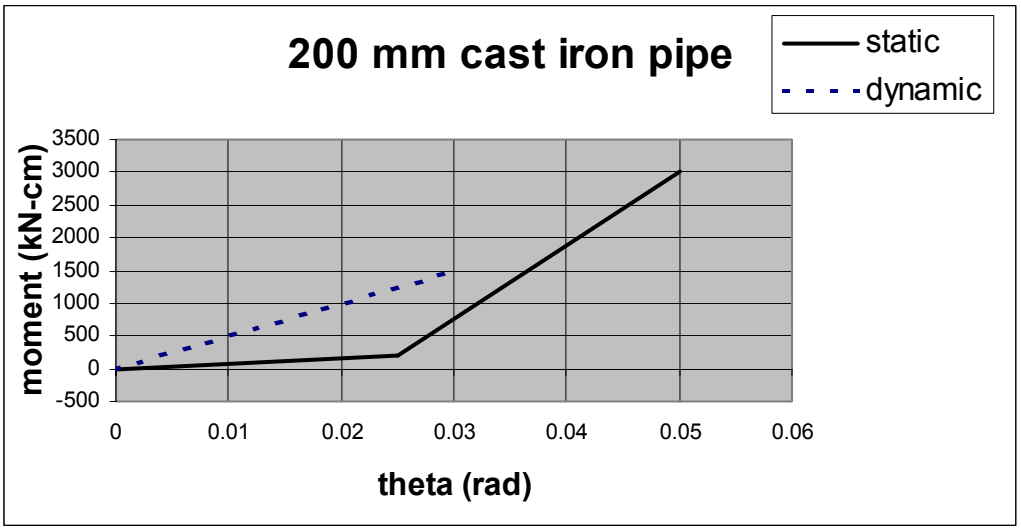

Figure 4-5 Moment-Theta Plot for 200 mm Diameter Cast Iron Pipe

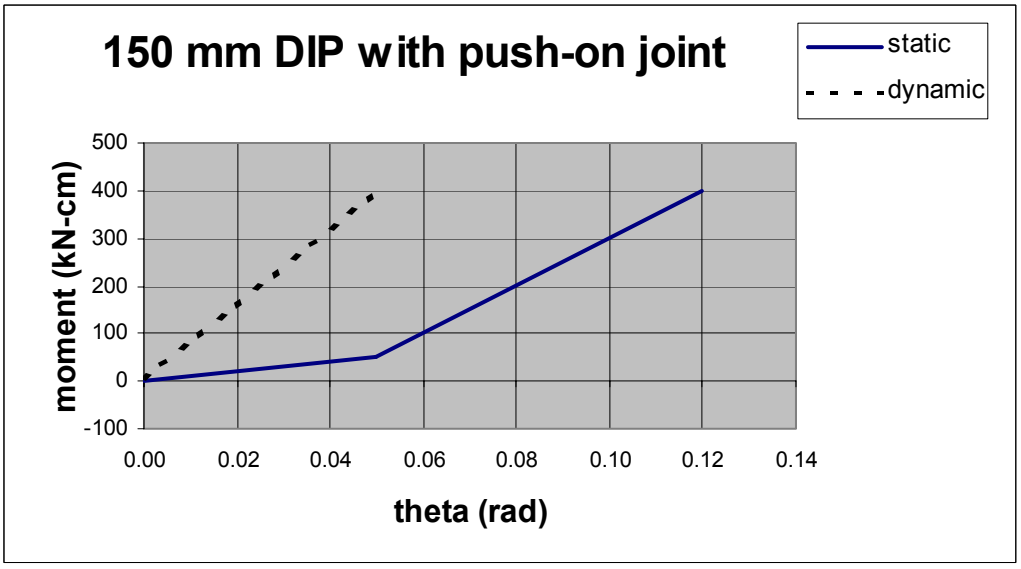

Figure 4-6 Moment-Theta Plot for 150 mm Diameter Ductile Iron Pipe with Push-On Joint

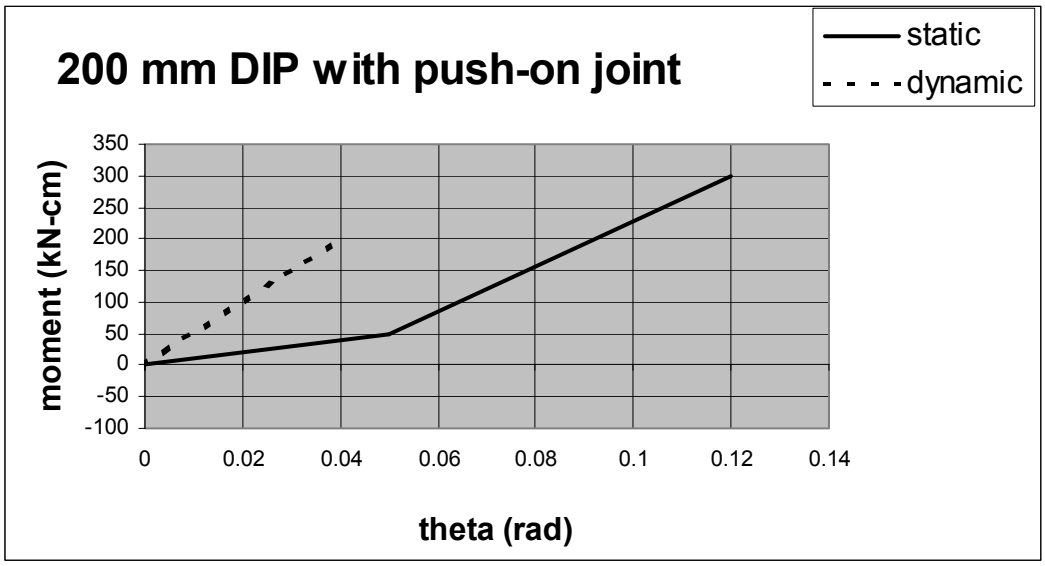

Figure 4-7 Moment-Theta Plot for 200 mm Diameter Ductile Iron Pipe with Push-On Joint

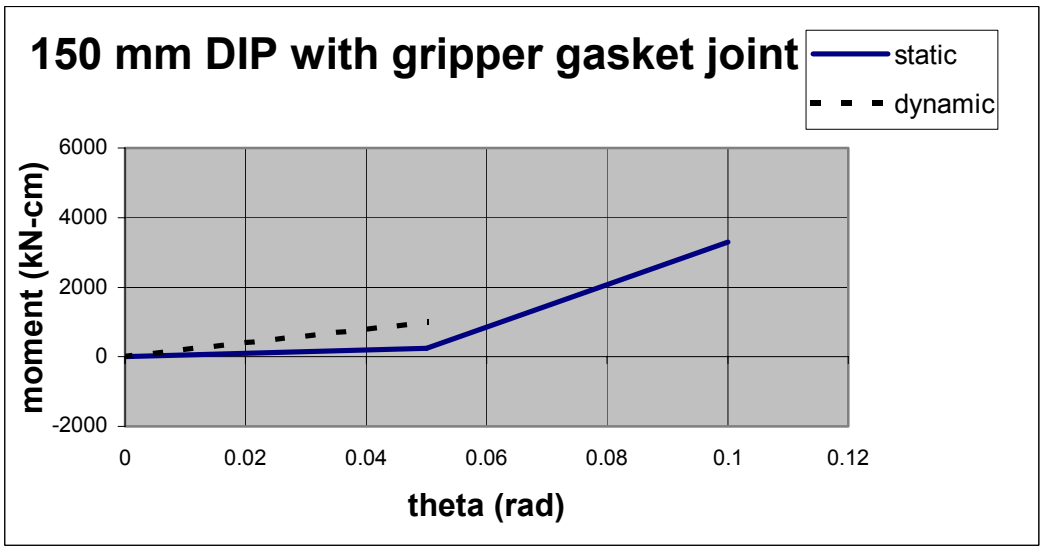

Figure 4-8 Moment-Theta Plot for 150 mm Diameter Ductile Iron Pipe with Gripper Gasket Joint

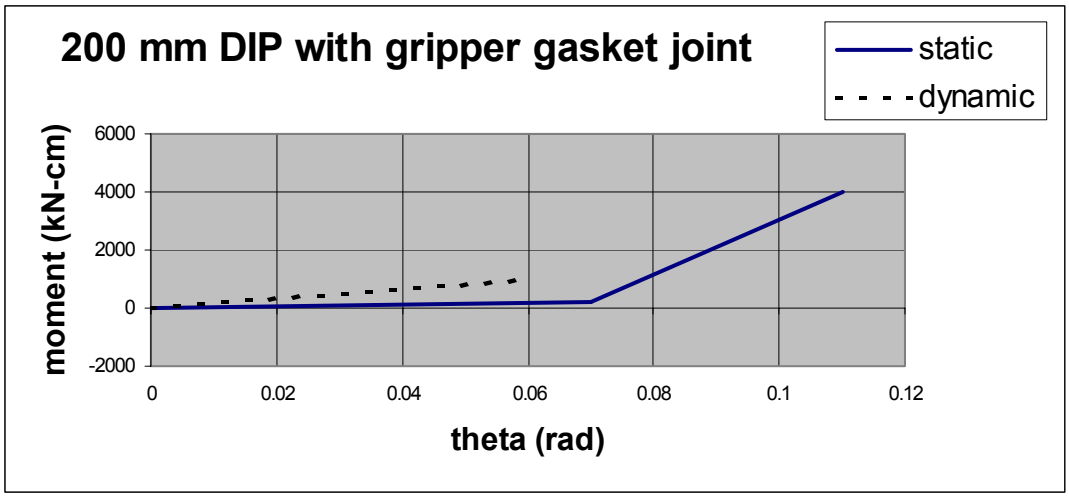

Figure 4-9 Moment-Theta Plot for 200 mm Diameter Ductile Iron Pipe with Gripper Gasket Joint

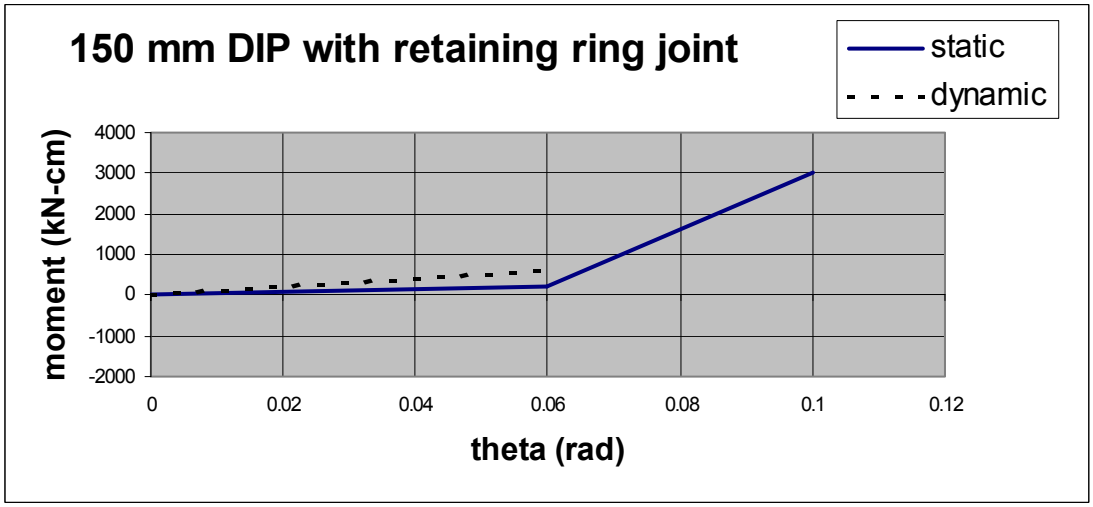

Figure 4-10 Moment-Theta Plot for 150 mm Diameter Ductile Iron Pipe with Retaining Ring Joint

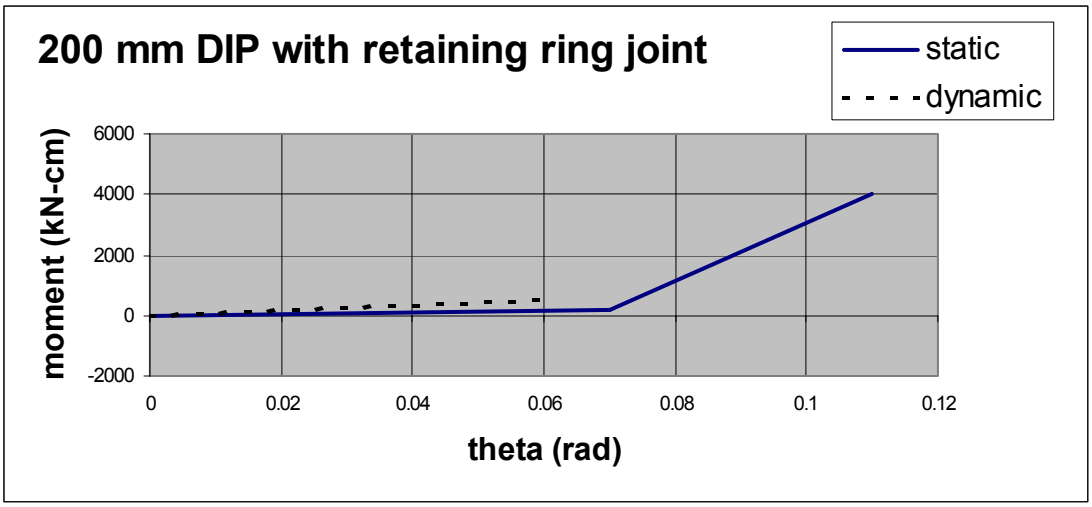

Figure 4-11 Moment-Theta Plot for 200 mm Diameter Ductile Iron Pipe with Retaining Ring Joint

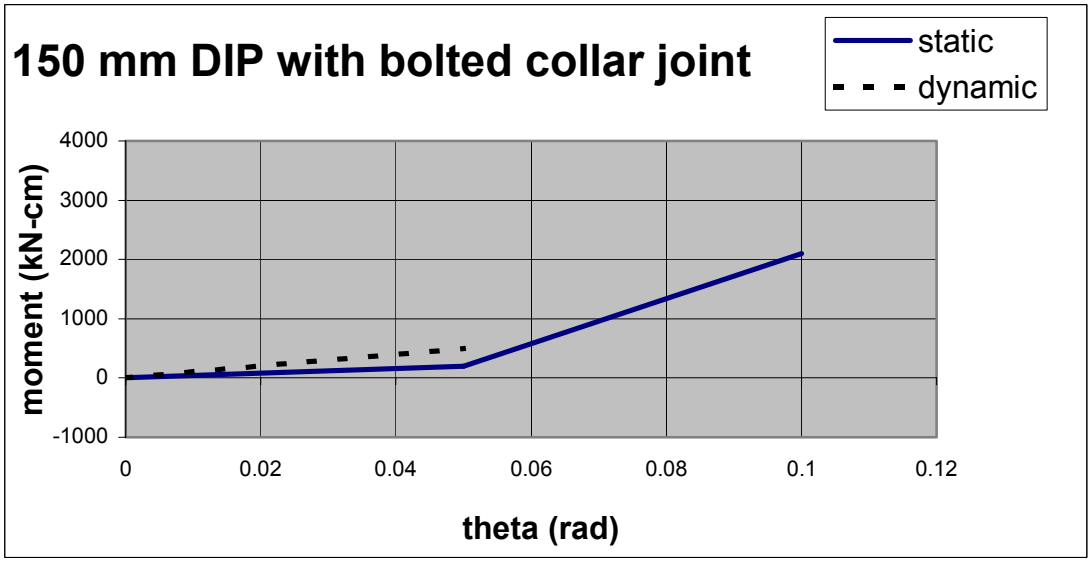

Figure 4-12 Moment-Theta Plot for 150 mm Diameter Ductile Iron Pipe with Bolted Collar Joint

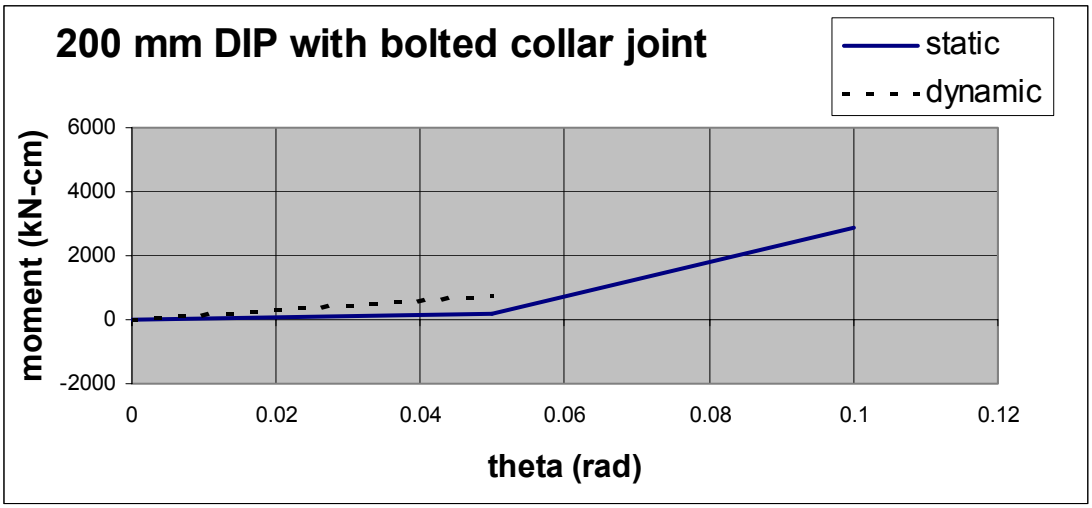

Figure 4-13 Moment-Theta Plot for 200 mm Diameter Ductile Iron Pipe with Bolted Collar Joint

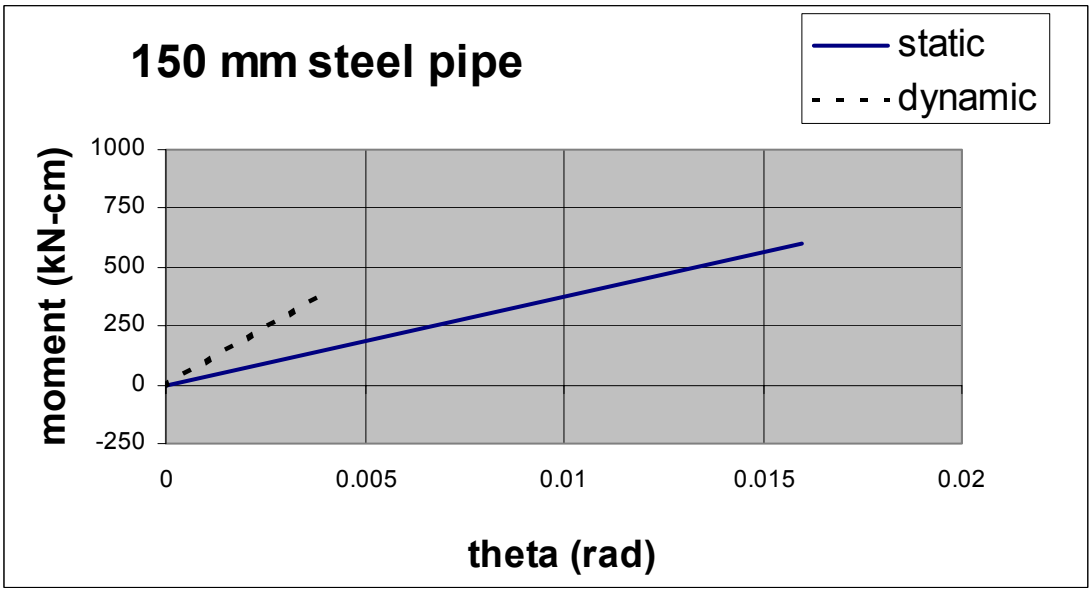

Figure 4-14 Moment-Theta Plot for 150 mm Diameter Steel Pipe

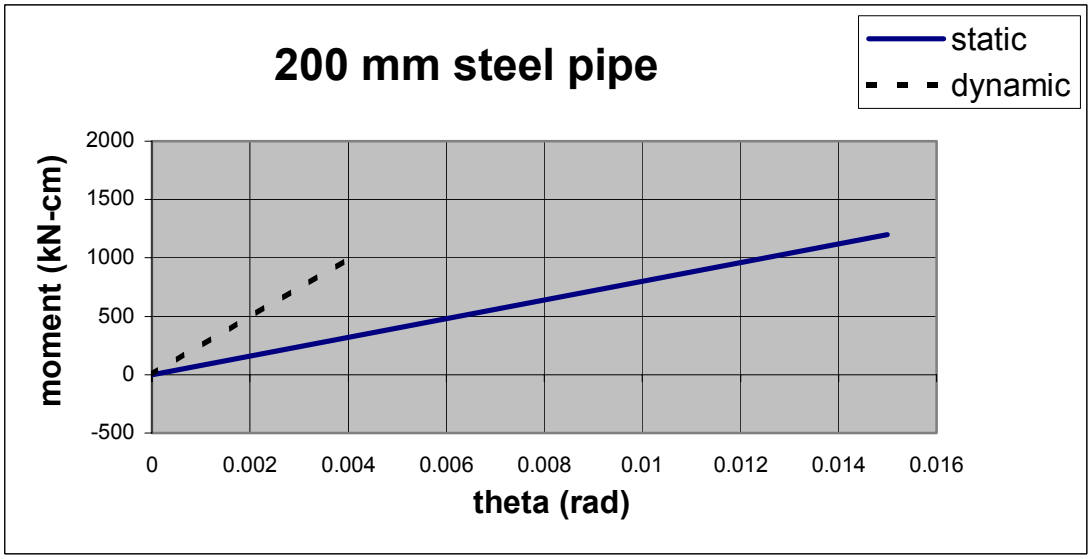

Figure 4-15 Moment-Theta Plot for 200 mm Diameter Steel Pipe

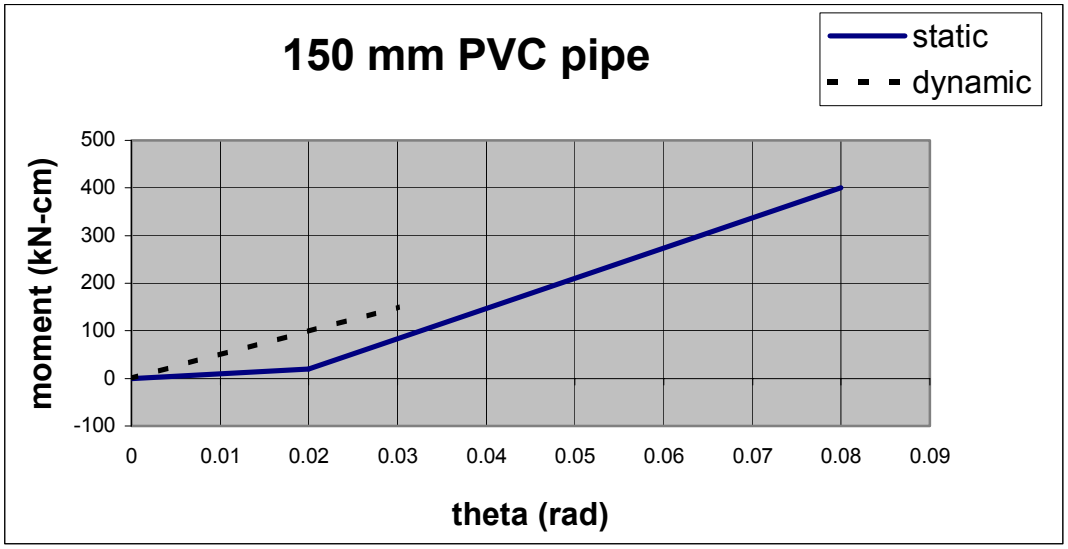

Figure 4-16 Moment-Theta Plot for 150 mm Diameter PVC Pipe

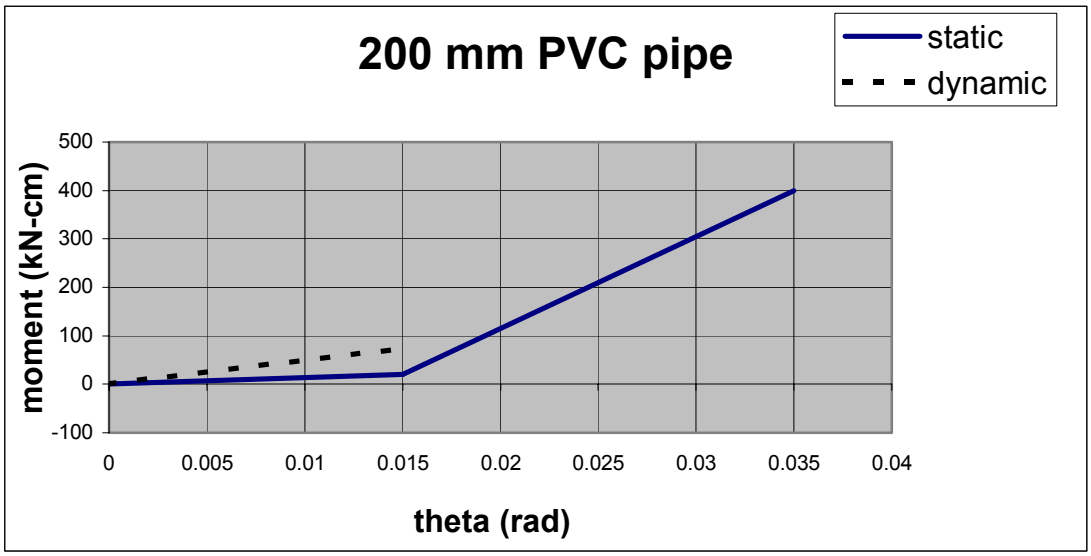

Figure 4-17 Moment-Theta Plot for 200 mm Diameter PVC Pipe

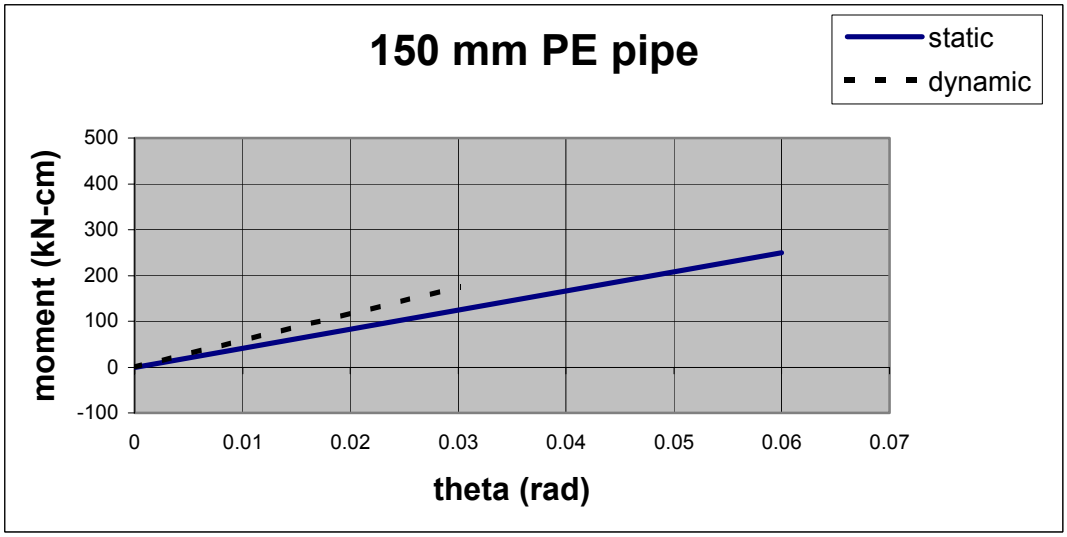

Figure 4-18 Moment-Theta Plot for 150 mm Diameter PE Pipe

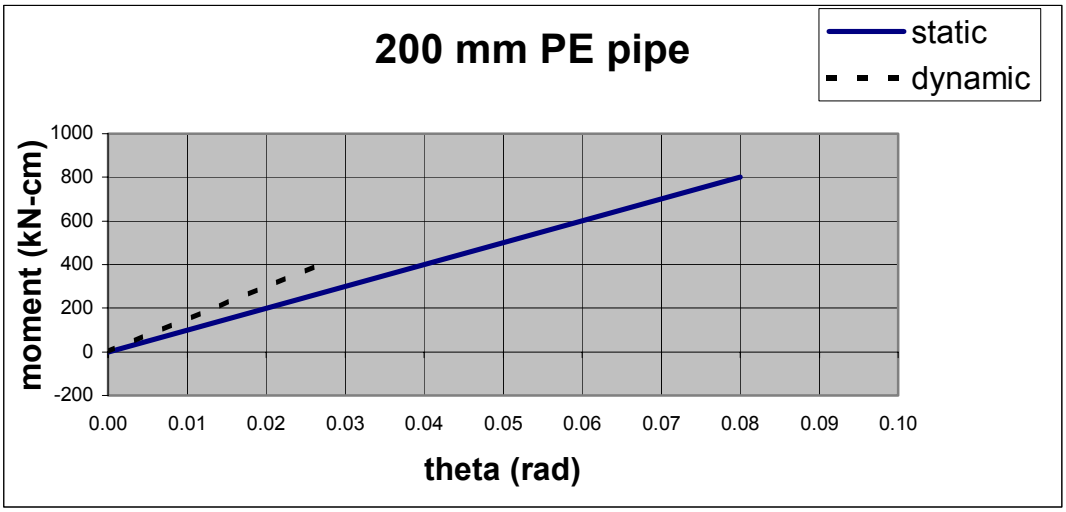

Figure 4-19 Moment-Theta Plot for 200 mm Diameter PE Pipe

4.5 Combined Moment-Theta Plots

Figures 4-20 to 4-26 show the static loading moment-theta plots for the 150 mm and the 200 mm diameter pipes. In these figures, similar material and joint types are combined into a single plot in order to see the comparable behavior of the larger and smaller pipe diameters. Except for ductile iron pipe with push-on rubber gasket joints, the larger diameter pipe had a higher level of rotational stiffness than the smaller pipe. This would be expected since in a bending mode, the specimen with a larger equivalent section modulus, i.e. deeper section, would have a larger resistance to bending and a larger rotational stiffness.

A comparison of static loading rotational stiffnesses for all specimens is given in the bar chart shown in Figure 4-27. It can be seen that the restrained joints have a higher rotational stiffness than unrestrained joints, except for the cast iron pipe, which had a level of joint restraint due to the hardening of the gasket material. It can also be seen that in general, larger diameter pipes have a higher rotational stiffness than smaller diameter pipes.

Table 4-1 Joint Static Rotational Stiffness Values

1	2	3	4	5	6	7	8
Pipe material joint type	**Pipe diameter (mm)**	**Unrestrained moment (kN-cm)**	**Unrestrained rotation (rad)**	**Unrestrained stiffness (kN-cm/rad)**	**Restrained moment (kN-cm)**	**Restrained rotation (rad)**	**Restrained stiffness (kN-cm/rad)**
Cast iron	200 (8”)	200	.025	8000	3000	.050	112000
DIP bell-spigot push-on joint	150 (6”)	50	.050	1000	301	.100	5000
	200 (8”)	50	.050	1000	300	.120	4236
DIP bell-spigot gripper gasket	150 (6”)	250	.050	5000	2580	.090	65000
	200 (8”)	200	.070	2857	3150	.100	98333
DIP bell-spigot retaining ring	150 (6”)	200	.060	3333	3000	.110	56000
	200 (8”)	200	.070	2857	3000	.100	93333
DIP bell-spigot bolted collar	150 (6”)	200	.050	4000	1950	.090	43750
	200 (8”)	200	.050	4000	2950	.100	55000
Steel bell-spigot lap-welded	150 (6”)	---	---	---	560	.017	27765
	200 (8”)	---	---	---	1264	.016	72500
PVC push-on joint	150 (6”)	20	.020	1000	384	.080	5567
	200 (8”)	20	.015	1333	410	.035	19000
PE butt-fused	150 (6”)	---	---	---	254	.060	4233
	200 (8”)	---	---	---	814	.080	10175

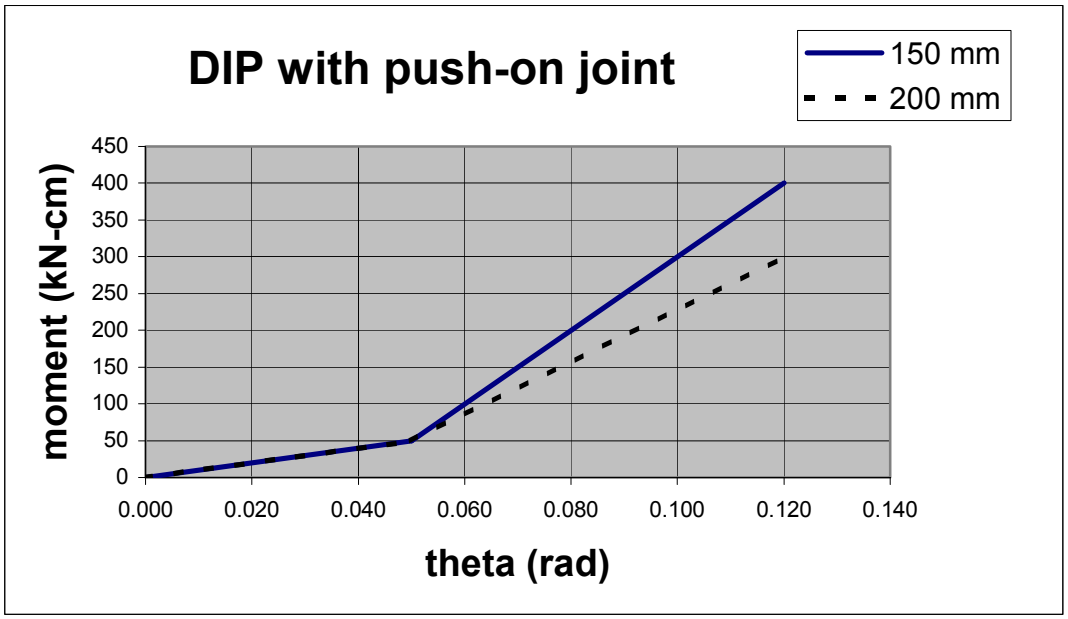

Figure 4-20 Static Moment-Theta Plot for Ductile Iron Pipe with Push-On Joints

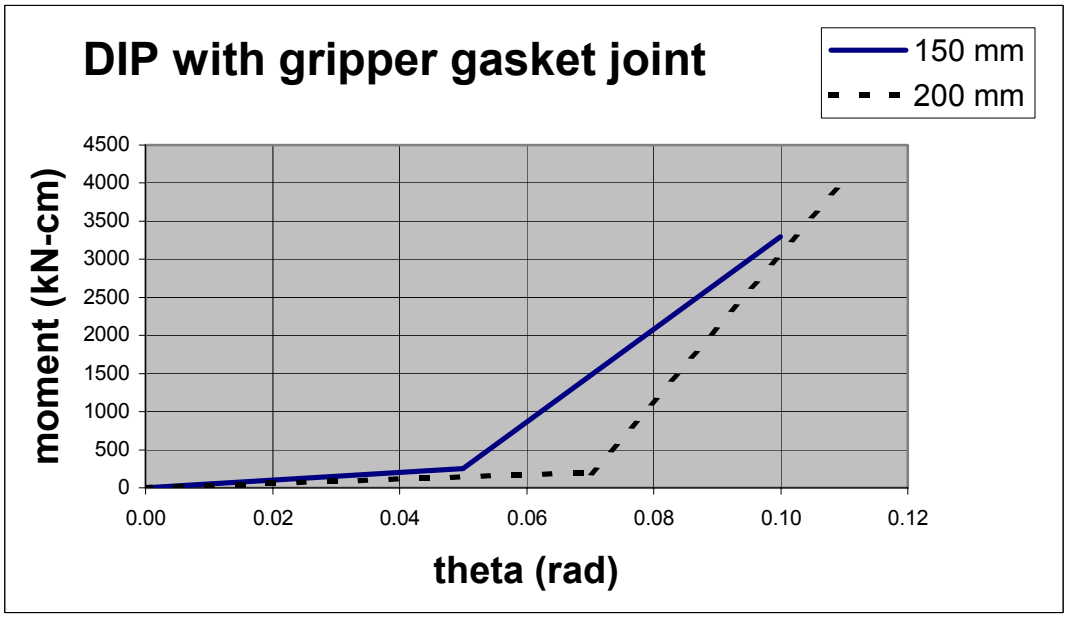

Figure 4-21 Static Moment-Theta Plot for Ductile Iron Pipe with Gripper Gasket Joints

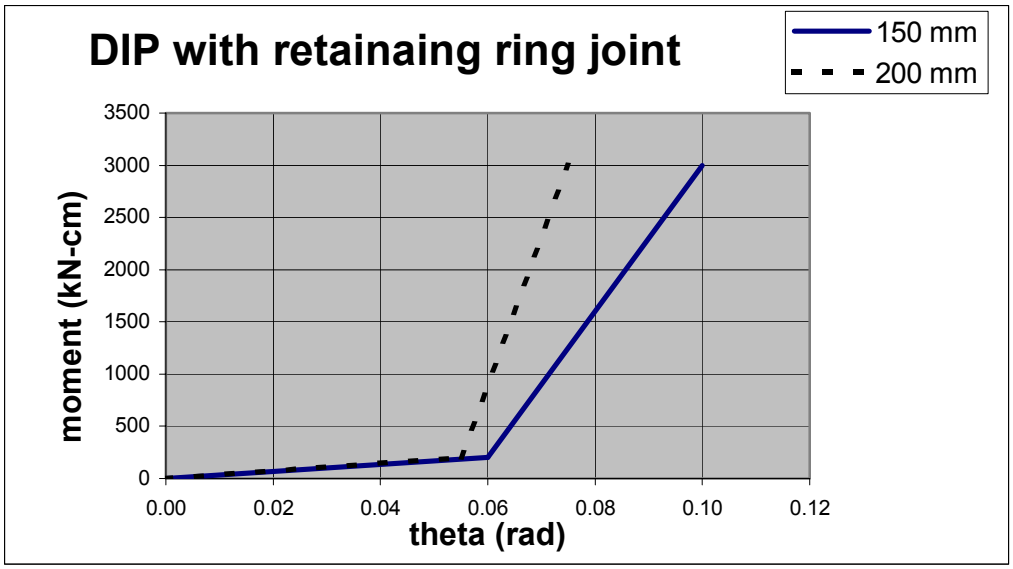

Figure 4-22 Static Moment-Theta Plot for Ductile Iron Pipe with Retaining Ring Joints

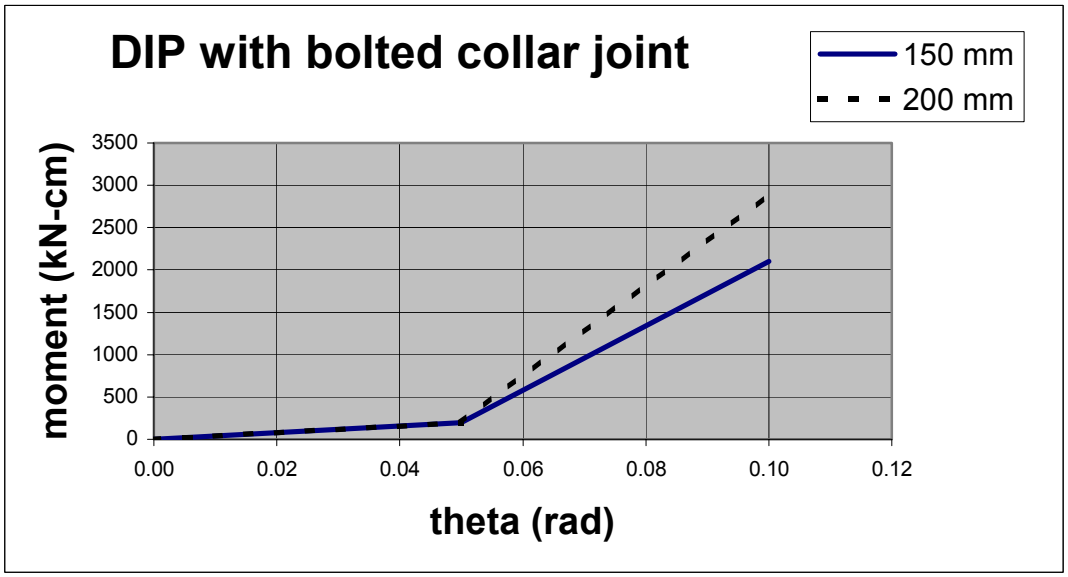

Figure 4-23 Static Moment-Theta Plot for Ductile Iron Pipe with Bolted Collar Joints

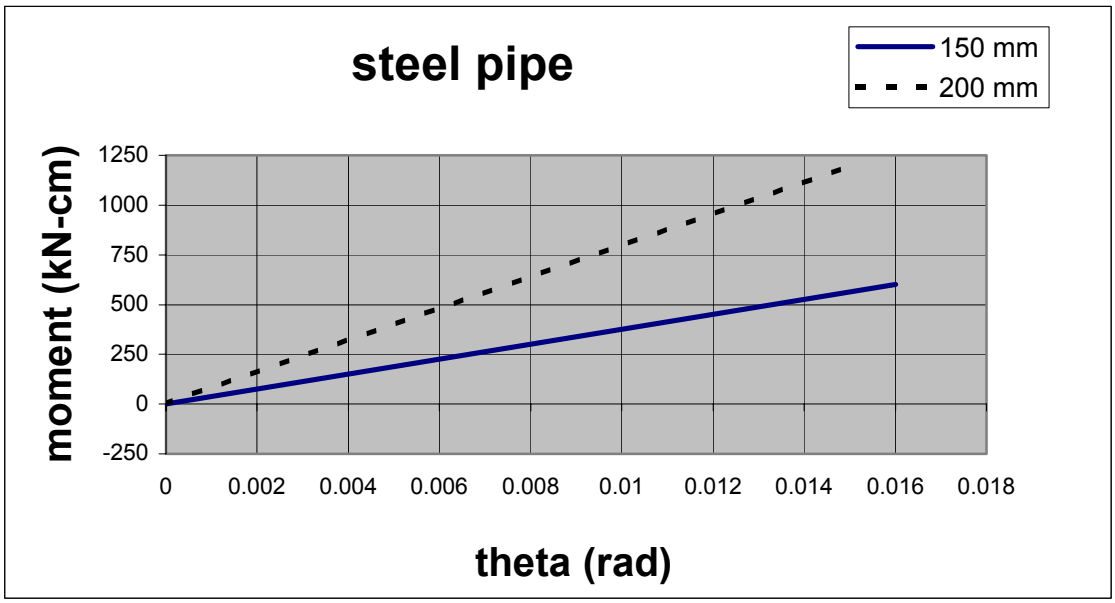

Figure 4-24 Static Moment-Theta Plot for Steel Pipe with Lap-Welded Joints

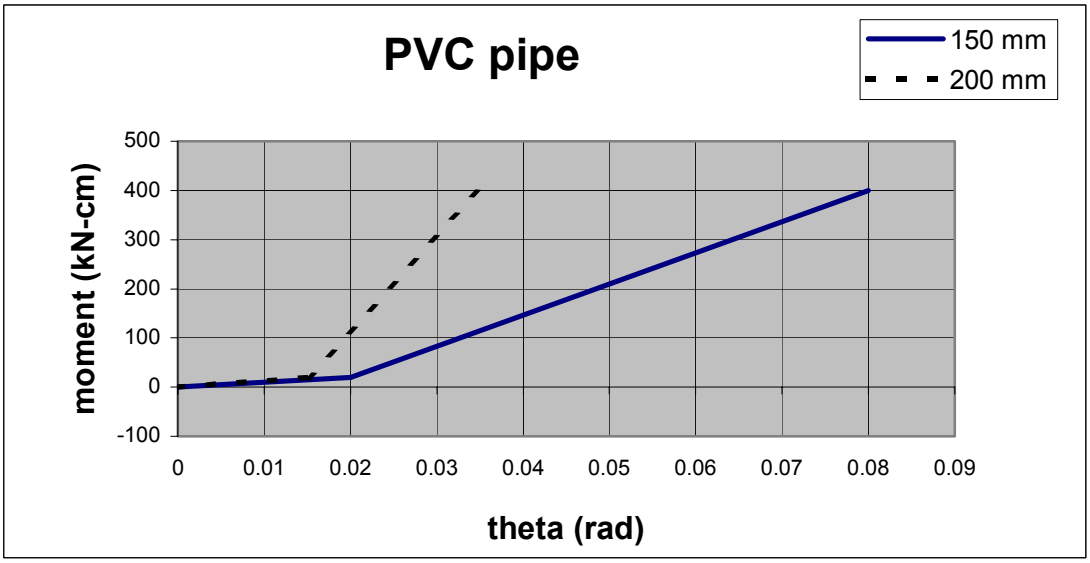

Figure 4-25 Static Moment-Theta Plot for PVC Pipe with Push-On Joints

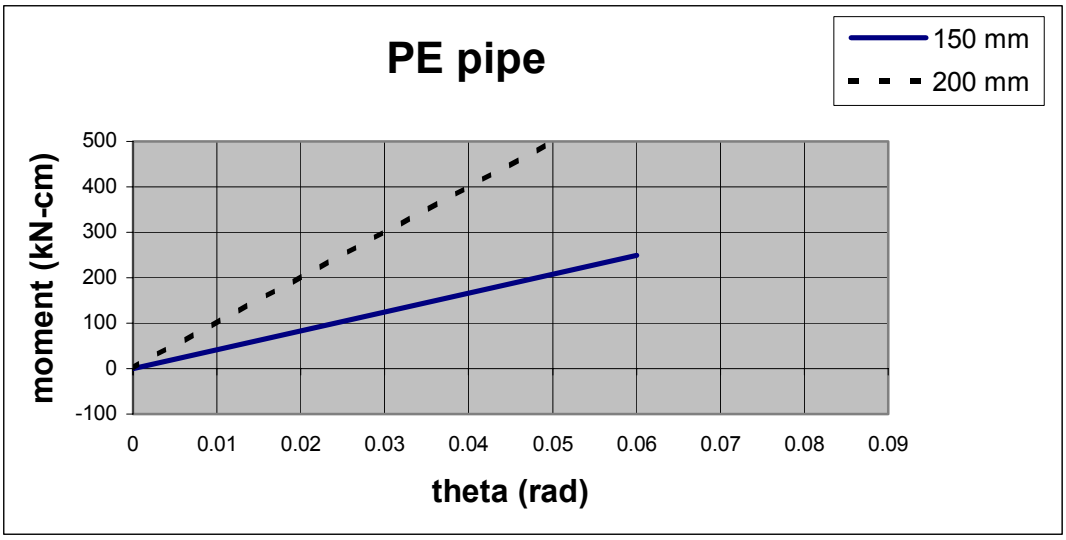

Figure 4-26 Static Moment-Theta Plot for PE Pipe with Butt-Fused Joints

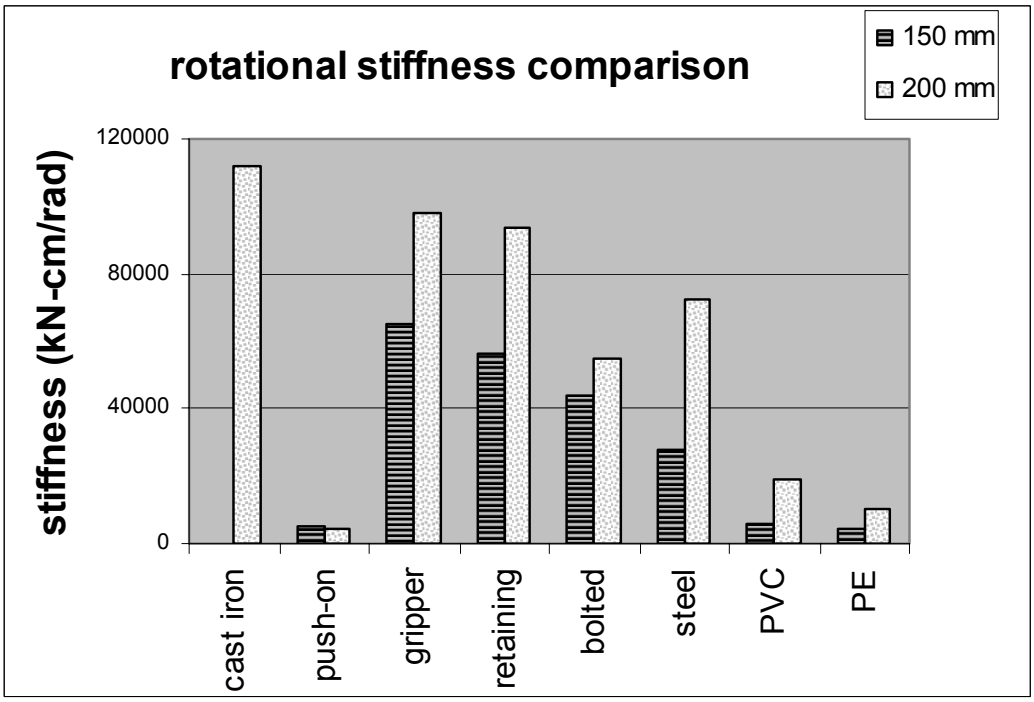

Figure 4-27 Comparison of Static Rotational Stiffness

SECTION 5
APPLICATION OF TEST RESULTS

5.1 Description

The results of this testing program can be used directly for the design and analysis of pipeline systems subjected to seismic loading or permanent ground deformation, or for a simplified pipeline risk assessment analysis. For computerized analytical studies of pipeline network systems (e.g. finite element analysis), the stiffness properties of all pipe segments including the joints and the surrounding soil medium must be known. The elastic and post-yield stiffness properties of the pipe joints, as determined by this testing program, can be used as input data in such a numerical investigation. For risk assessment evaluation, the maximum force capacities of the joint as determined by this research must be known.

5.2 Risk Assessment Evaluation

The results of this testing can be used in a simplified risk assessment procedure (see Appendix D) as described below. This simplified procedure requires estimates on the maximum force capacities of the pipe joints. Newmark (1967) showed that for simple traveling waves with a constant and coherent wave shape, the soil strain and thus the axial pipe strain can be computed using the expression (see Appendix E):

$$\varepsilon_{pipe} = \frac{V}{c} \qquad (5\text{-}1)$$

where:

ε_{pipe} = pipe or soil strain

V = particle velocity from the seismic motion

c = soil wave propagation velocity

Using this relationship, T. O'Rouke (1996) developed a simple risk assessment methodology based on comparing a pipe's joint force capacity with the force level resulting from the soil strain that may be imposed on the pipe due to seismic motion. Although this procedure was originally designed for piping systems with continuous joints, it is also applicable to systems with segmented joints that have a tensile restraint capacity. There is a limit to the force that can be transmitted from the soil to the pipe, since this force needs to be transmitted through interface friction, and if the imposed force is beyond the frictional limit, slippage will occur. If the level of force induced by seismic motion is greater than the pipe joint force capacity, and if this force is able to be transferred from the soil to the pipe by friction, then a "probable failure" condition exists (see Appendix D).

A modification to the T. O'Rourke (1996) procedure has been developed in this project that makes use of the pipe force capacities determined in this research. Using the above relationships, an analyst is able to determine the probable "fail" or "no fail" condition of a piping system. Analysis parameters consists of the particle velocity from the earthquake V, the predominant earthquake period T, soil wave propagation velocity c, the maximum possible frictional transfer force per unit length of pipe f, the pipe's cross-sectional area A, the pipe's material property Young's modulus E, and the maximum joint force capacity F_{max}. The maximum joint force capacity values are provided by the results of the static testing phase (Table 2-1) or from the dynamic testing phase (Table 3-2 and 3-3). Two expressions are provided, each indicating its own probable "fail" condition.

$$\left(\frac{V}{c}\right)\cdot\left(\frac{A\,E}{F_{max}}\right) \geq 1 \quad \text{for fail condition} \qquad (5-2)$$

$$(T\,c)\cdot\left(\frac{f}{4\cdot F_{max}}\right) \geq 1 \quad \text{for fail condition} \qquad (5-3)$$

Equation 5-2 is a criterion for the imposed force from the seismic motion. Equation 5-3 is a criterion for the maximum possible frictional force transfer between the soil and the pipe surface. The risk assessment criteria requires that both equations must have a "fail" condition for the pipe joint to have an overall probable "fail" condition. This procedure is graphically represented by the use of two separate design charts shown in Figures 5-1 and 5-2. Figure 5-1 is a chart of the joint force capacity for different curves of imposed soil strains (V/c). Figure 5-2 is a chart of the friction transfer force for different earthquake wave lengths (T x c). These charts are applicable for any pipe material and configuration as well as any consistent geological site and seismic conditions. It should be noted that the units of each expression must be consistent. The parameters for Figure 5-1 are unitless while the units for the parameters in Figure 5-2 are in meters.

Example

This example shows how results from this testing program may be utilized in a risk assessment analysis of transient seismic motion. Consider a 200 mm (nominal) ductile iron pipeline with bolted collar restrained joints. The pipe has a Young's modulus E of 165480 MPa and a cross-sectional area A of 4457 mm^2. The probable "fail" or "no fail" conditions need to be determined. The pipeline is to be placed in a soil with a wave propagation velocity c of 800 m/s. A postulated earthquake for the region has a peak particle velocity V of 32 cm/s with a predominant period of seismic motion T of 2.5s. The maximum possible friction transfer force between the soil and the pipe f is 18.3 kN/m, and the dynamic force capacity of a 200 mm DIP bolted collar joint from Table 3-2 is 212 kN. After converting all values to consistent units, the following parameters are computed:

1) Parameters: $\frac{V}{c} = .00040$ and $\frac{A\,E}{F_{max}} = 3474$

Using these values in Figure 5-1, it can be seen that the point falls in the "fail" zone, which means that the imposed force on the joint from the earthquake is greater than the force capacity of the joint.

2) Parameters: $T \times c = 1250$ m and $\frac{f}{4 F_{max}} = .0215$ (1/m)

Using these values in Figure 5-2, it can be seen that the point also falls in the "fail" zone, which means that the force level is able to be transferred from the soil to the pipe.

Since both conditions indicate a "fail" condition, the joint has an overall probable "fail" condition, which is unacceptable.

However, if the joint type were to be changed to a gripper gasket, which has a dynamic force capacity from Table 3-2 of 343 kN, the following parameters are computed:

1) Parameters: $\frac{V}{c} = .00040$ and $\frac{A E}{F_{max}} = 2147$

Using these values in Figure 5-1, it can be seen that the point falls in the "no fail" zone, so that the imposed force from the earthquake is less than the force capacity of the joint.

Since at least one condition in this case has an overall "no fail" condition, the joint has an overall "no fail" condition, and is satisfactory.

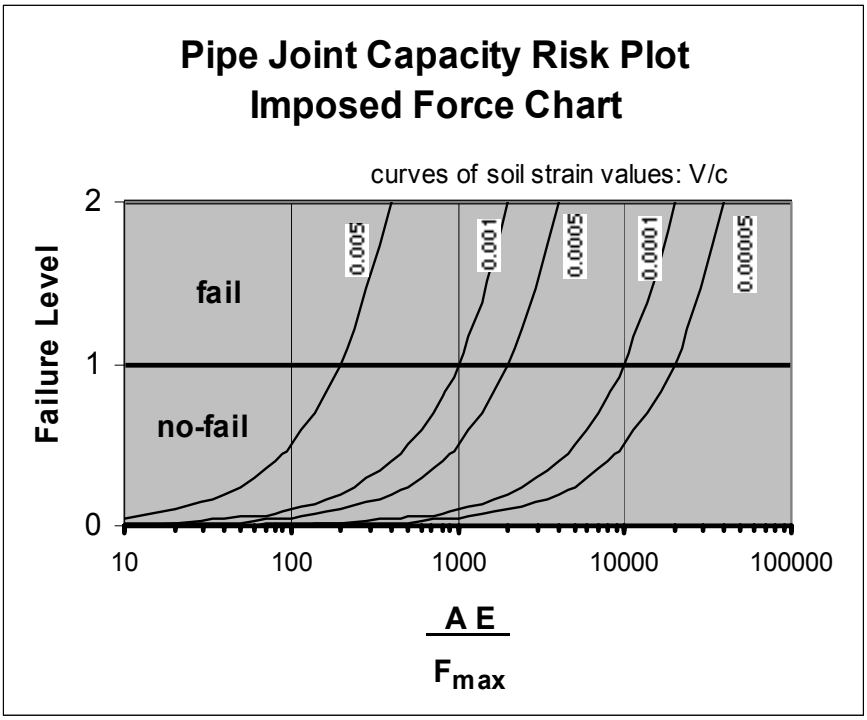

Figure 5-1 Pipe Joint Capacity Chart (see Eq. 5-2)

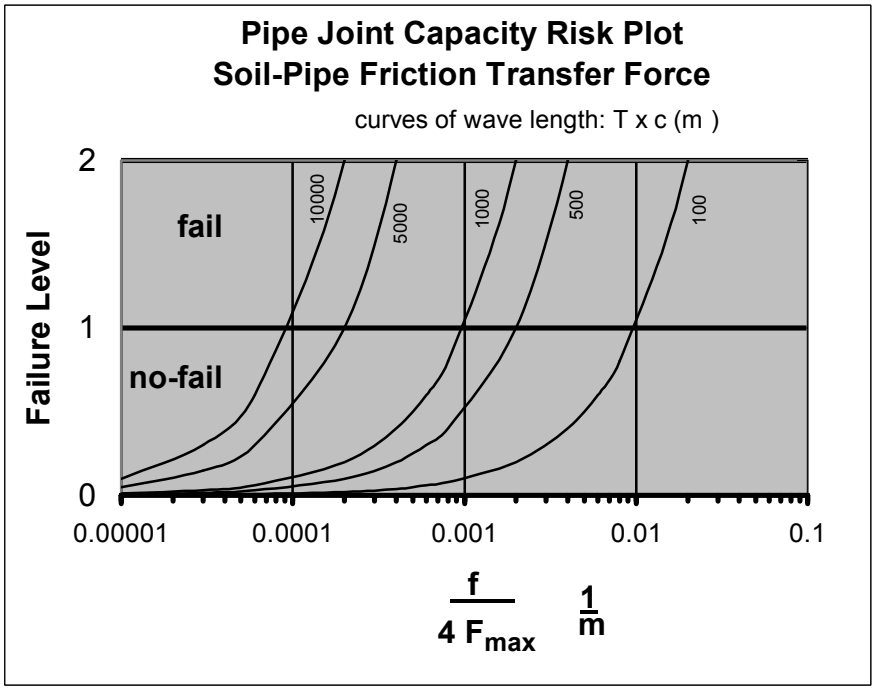

Figure 5-2 Pipe-Soil Friction Transfer Chart (see Eq. 5-3)

5.3 Analytical Finite Element Analysis

Current computerized methods of finite element analysis are very powerful and can provide the response of a complex two-dimensional pipeline system subjected to loading conditions such as transient motions or imposed ground deformations. The use of these computational methods can indicate areas of possible pipeline failure and allow pipeline owners to prioritize upgrade plans to a more seismic resistant configuration. An example of a finite element computer analysis of a pipeline system is given in Section 5.4.

There are a number of different software products that are capable of performing the proper analysis which requires consideration of non-linear material properties and a load-stepping process. Typically, joints would be modeled as a finite element member with bi-linear material properties in both the tension and compression directions, as well as providing for a gap distance. Also, the joint member must have a rotational stiffness property. In most cases, a single member type will not be able to have all the stiffness properties required, but must be made up of several members, each with a specific behavior characteristic so that the total of these members can correctly model the joint assembly.

The imposed loading can be either a time-varying seismic motion or a static nodal displacement loading representing permanent ground deformations using a load-stepping process. Loading forces and displacements are applied to the system through nodes representing the soil with connecting members to the pipe that have properties of the soil such as described by the ASCE Technical Council on Lifeline Earthquake Engineering (ASCE, 1984). The joint response from the imposed loading can be compared with specific criteria to determine if forces or relative separation displacements exceed acceptable conditions. The value of computerized analysis is that several different scenarios can be run in a relatively short period of time, changing problem parameters and investigating a wide range of physical conditions.

A system model may be limited to a small physical area bounded by anchor points, or may include a much larger system encompassing a wide area and a larger number of anchor points Anchor points or boundary nodes may consist of fixed nodes or may include soil spring elements with a prescribed displacement (including zero displacement) at its end node. In either case, if a fail condition is detected, mitigating configurations and modifications can be investigated until a satisfactory condition is reached.

5.4 Example: Computer Analysis of a Pipeline System

5.4.1 Description

The ultimate purpose of any empirical research project is its application to practical engineering analysis and design. As an illustration of the use of the data derived from this experimental testing project, an example analysis of a simplified piping network consisting of a single straight run with a tee branch (Figure 5-3) subjected to a permanent ground deformation (PGD) is presented. Note that piping systems can also be subjected to transient seismic motions, which can be analyzed using a similar approach to the one described here using a true time-domain dynamic analysis procedure.

Buried pipelines can be subjected to several types of loading conditions. Seismic events can cause forces and displacements to be transferred from the soil environment to the pipe surface due to transient motions passing through the piping system and causing differential strains. The resulting expansions and contractions in the piping will cause tensile and compressive forces in the joint. The seismic motions can also result in large permanent ground movements in the supporting soil. These displacements in turn will cause piping joints within that zone to have differential displacements. Permanent ground deformation, or PGD, is often a localized problem for pipelines and has the potential to cause major damage. Similar to ground movements caused by seismic activity, non-seismic events such as slope failures can also cause substantial ground

movement, and therefore, can cause differential joint displacements. Ground movement may happen in any orientation to the major axis of the piping system so that differential displacements may have longitudinal and transverse components.

The example and the data used below are based on the work done by Kuruswamy (2002) at the University of Nevada, Reno. The objective of Kuruswamy's work was to do a study of a straight pipeline system and to investigate the influence of various parameters on the overall response of the system. He has developed a methodology and procedure to use the data derived in this experimental testing project as input data to the non-linear computer program, ADINA.

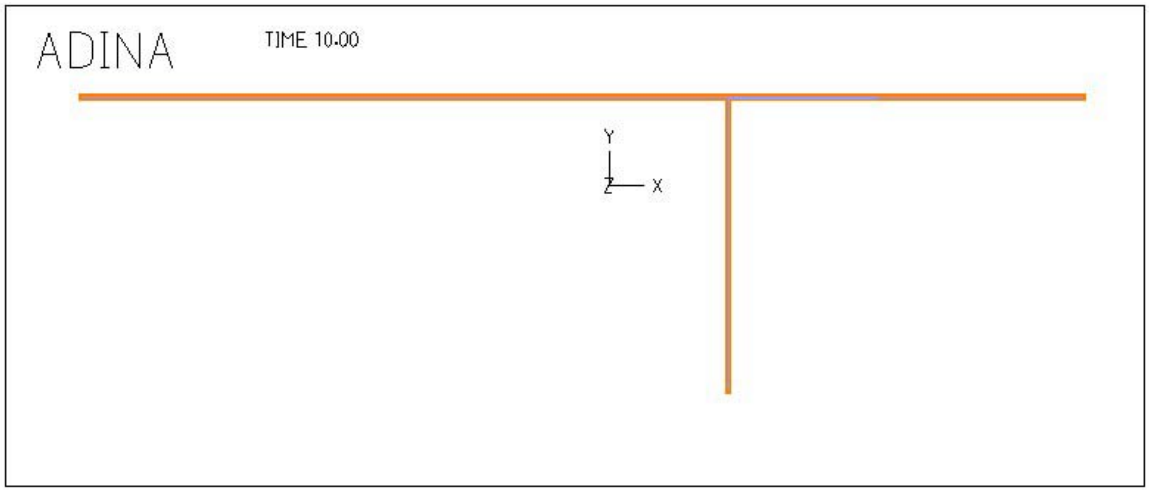

Figure 5-3 Plan of Piping System Geometry

The following discussion is a summary of Kuruswamy's procedure (Kuruswamy 2002). The loading configurations consisted of permanent ground deformations with varying displacement amplitudes, load directions, and loading patterns along the straight pipeline system. The displacements that are applied to the piping system are defined by a lateral permanent deformation of the surrounding soil (Figure 5-4). The soil deformation can be caused by many factors such as slope movement and lateral spreading resulting from liquefaction. The parameters that define the applied displacement loading (Figure 5-4) and the piping system response are:

1. amount of PGD movement, δ
2. transverse width of the PGD zone, W
3. longitudinal length of the PGD zone, L, and
4. pattern or distribution of the ground movement across and along the PGD zone

The requirements of the ADINA program had to be considered and the input data were prepared so that they were acceptable and interpreted properly by the program. The model consisted of pipe section (body) elements connected by joint section elements (Figure 5-5). A procedure to link the stiffness of the various elements comprising the joint to account for a tension direction restraint and a compressive direction restraint was developed so that the cumulative behavior of the several different elements represented the actual measured behavior of the joint as a whole.

A significant influence on the response of a piping system is the surrounding soil deformation and the soil properties. Much of the development in this area is based on research by M. O'Rourke and Liu (1999), in which they describe the behavior of piping networks subjected to permanent ground deformations and the effect of various elements in the system. The interaction of the soil and pipe can be modeled using linear or non-linear springs and the analysis of the interaction can be undertaken using a "beam on an elastic foundation" approach (Figure 5-5).

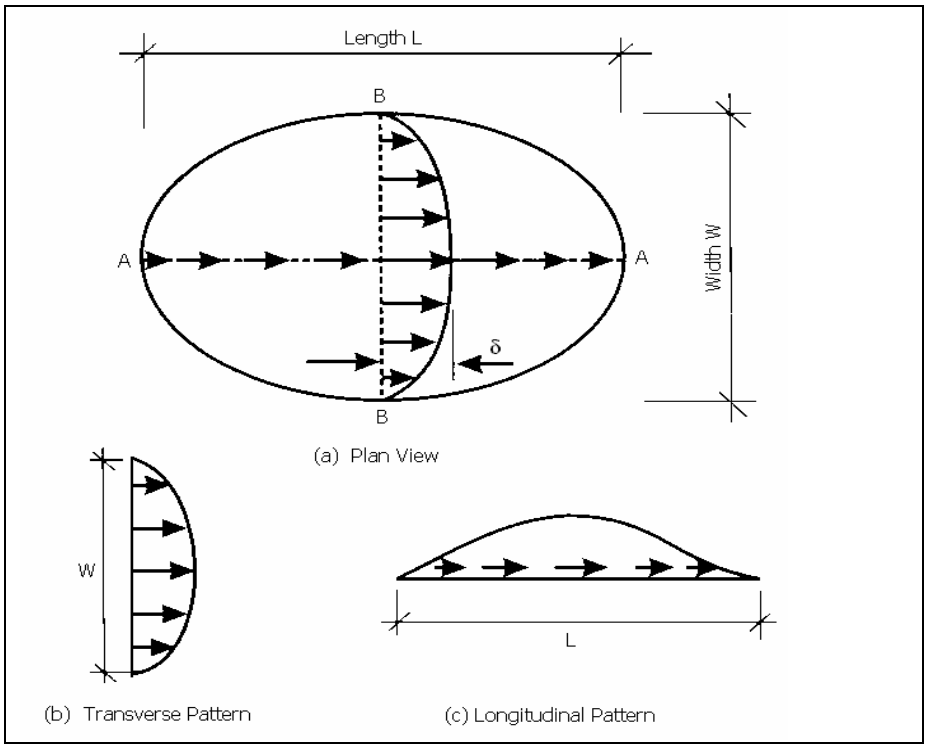

Figure 5-4 Diagram of Lateral Spread Displacement Distribution (Ref: O'Rourke and Liu 1999)

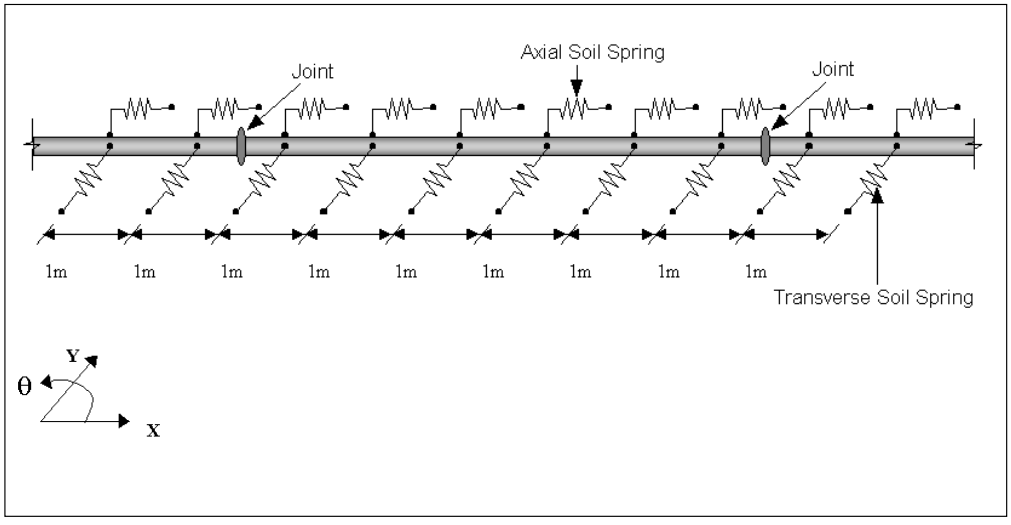

Figure 5-5 Piping System Elements (Ref: Kuruswamy 2002)

For Kuruswamy's work and for this example, the axial and transverse soil spring stiffnesses were developed from the guidelines of the ASCE Technical Council on Lifeline Earthquake Engineering (TCLEE) (ASCE, 1984) (see Figures 5-11 and 5-12). The soil spring stiffnesses are determined from parameters of force resistance and elastic deformation as defined by the following expressions:

For axial soil-spring: $$Ka = \frac{t_u}{x_u/2} \quad (5\text{-}4)$$

For transverse soil-spring: $$Kt = \frac{p_u}{y_u/2} \quad (5\text{-}5)$$

where: Ka = soil stiffness in the axial direction per unit length

Kt = soil stiffness in the transverse direction per unit length

t_u = max. force resistance in the axial direction per unit length

x_u = max. elastic deformation in the axial direction

p_u = max. force resistance in the transverse direction per unit length

y_u = max. elastic deformation in the transverse direction

The parameters for sand are defined as follows:

$$t_u = \frac{\pi}{2} D \gamma H (1+k_0) \tan k\phi \quad (5\text{-}6)$$

and $$x_u = (2.54 \text{ to } 5.08)\ 10^{-3} \quad (5\text{-}7)$$

where: t_u = force resistance

x_u = elastic soil deformation

D = pipe diameter

γ = effective unit weight of the soil

H = depth of the center-line of the pipe

ϕ = angle of the shear resistance of the sand

k_0 = coefficient of lateral pressure

k = reduction factor depending on the surface of the pipe

The x_u value used for this analysis was: $x_u = 3.8\ 10^{-3}$

The stiffness parameters for sand for the transverse soil spring, from the ASCE guidelines are:

$$p_u = \gamma H\ Nqh\ D \qquad (5\text{-}8)$$

and

$$y_u = (1.78 \text{ to } 2.54)(H+D/2)\ 10^{-3} \quad \text{loose sand} \qquad (5\text{-}9)$$

$$(.76 \text{ to } 1.27)\ (H+D/2)\ 10^{-3} \quad \text{medium sand} \qquad (5\text{-}10)$$

$$(.50 \text{ to } .76)\ (H+D/2)\ 10^{-3} \quad \text{dense sand} \qquad (5\text{-}11)$$

where: Nqh = horizontal bearing capacity factor for sand

The y_u value used for this example was: $y_u = 0.5\ (H+D/2)\ 10^{-3}$

These relationships are valid for relative displacements less than one-half of the maximum elastic deformations. Above these levels of relative displacements, the soil is considered rigid plastic. For pipelines placed in a liquefied soil, the response is dependent on the stiffness of the soil springs. The soil spring stiffness increases as a function of the effective soil stress and is a decreasing function of excess pore water pressures.

For the maximum amplitude of the displacement pattern in a liquefied soil, Hamada et al. (1986) propose an empirical relation as:

$$\delta = .75\sqrt{h}\sqrt[3]{\theta} \qquad (5-12)$$

where: δ = maximum amplitude of the displacement pattern (m)

h = thickness of the liquefied soil layer (m)

θ = larger of the slope of the lower soil boundary or the ground surface (%)

The soil-induced loading was defined using spatially distributed longitudinal and transverse PGD (Figure 5-4). The deformation value is zero at the edge of the pattern, increasing to the maximum displacement amplitude, and then decreasing back to zero at the other edge of the pattern. This displacement pattern is used for both longitudinal and transverse applied displacements. Nodes outside the loading pattern and nodes with low amplitude of applied displacement become anchor points for the system. Several pattern variation functions have been proposed, but most of them involve some trigonometric function. M. O'Rourke and Liu (1999) proposed the following displacement function (Figure 5-6):

$$u(x) = \frac{\delta}{2}\left(1 - \cos\frac{2\pi x}{W}\right) \qquad (5\text{-}13)$$

where: $u(x)$ = displacement function along the pattern

δ = maximum displacement amplitude

x = distance from start of the loading pattern

W = total width (or length) of the loading pattern

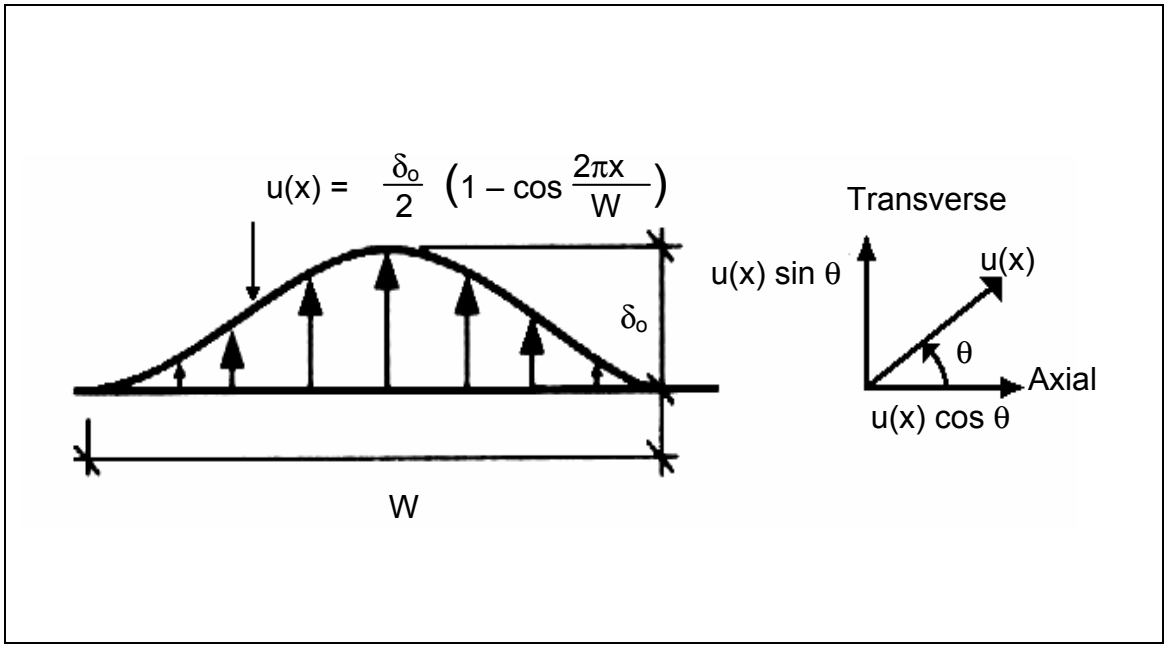

Figure 5-6 Load Pattern Distribution (Ref: M. O'Rourke and Liu 1999)

The ADINA non-linear step-wise processing computer program was used for the analysis. It must be noted that other non-linear step-wise processing computer programs could have been used and would have produced similar results. For the ADINA program, data is entered through a user interface pre-processor call ADINA-AUI (ADINA User Interface). Menus and toolbars are provided to allow the user to enter data directly, while some of this data can be imported into ADINA from external files. There are specific data generation capabilities within AUI, especially for nodal coordinates, member connectivity, and loading configurations. Graphical plotting is available to aid in verifying the structure's geometry and loading. This program has the capability of doing load-stepping or time-stepping analysis on structures containing members with non-linear material properties.

The analysis for Kuruswamy's work used a load-stepping procedure where the final applied displacement was reached in ten steps with a sub-step increment being controlled by the program. Each sub-step requires meeting a convergence criteria. If convergence during a sub-step cannot be reached, the program automatically decreases the sub-step increment until convergence is reached, or if convergence cannot be reached within a specified tolerance, the program will terminate due to structure instability. Structural members can have their material properties defined in several ways. For Kuruswamy's work, member properties were defined as being either linear or non-linear with the non-linear properties being defined by either load-displacement curves or by stress-strain curves. Each member type such as trusses, beams, or springs has its own method of defining material properties.

The actual analysis was performed by invoking the ADINA program. Specific analysis results were requested from the program and stored in an external file. Data was reviewed using an ADINA post-processing program called ADINA-PLOT. The ADINA output can be graphically plotted and tabular results such as nodal displacements and member forces can be specified and exported to an external file for processing by other programs such as Microsoft's EXCEL spread-sheet program. Nodal displacements for each start node and end node at a joint were requested and exported into an external text

file. Joint separations or contractions were then computed from the relative nodal displacements from the analysis.

However, the ADINA analysis was run using small displacement analysis only, and therefore, any large displacements occurring from a transversely applied displacement pattern were not accounted for. To account for large displacement analysis, arc-length effects, which is the axial elongation resulting from the curvature of the displacement pattern, were computed independently and added to the computed joint separation. The expression defining the arc-length effects from M. O'Rourke and Liu (1999) is:

$$\Delta x = \frac{Lo}{2}\left[\frac{\pi\delta}{W}\sin\frac{2\pi x}{W}\right]^2 \qquad (5-14)$$

where: Δx = joint elongation resulting from arc-length effects
Lo = pipe segment length
δ = maximum applied displacement amplitude from PGD
x = distance from the start of the load displacement pattern
W = total width (or length) of the load pattern

The total joint separation of pipes loaded transversely to their axis is the summation of the computed nodal separations of the joint from the ADINA analysis and the arc-length effects computed from Eq. 5-14. It should be noted that Eq. 5-14 assumes that the pipeline displacement exactly conforms with the specified transverse soil displacement (no pipeline resistance). The summation of the pipe joint deformation as determined by this method will result in a conservative estimate. The displacement results and the joint elongation can be plotted for each analysis configuration along with plots of the number of joints in the model exceeding a specific separation amount. Such results are presented independently.

5.4.2 Example Model Geometry and Boundary Conditions

The model for this example analysis has a geometry which consists of a main branch approximately 800 m long and a tee branch approximately 200 m long, connected at about the 500 m point on the main branch (Figure 5-3). The main branch is designated as the branch running in the global X direction and the tee branch is designated as the branch running in the global Y direction. It must be noted that the units for all input data to the ADINA program for this example analysis are in meters and newtons. The primary member is a pipe segment of 6 m long with a joint segment connecting the pipe segments of 0.2 m long. The pipe is further divided into seven sub-segments at which soil springs are connected to the nodal points (Figure 5-5). Several different ductile iron pipe joints, both restrained and unrestrained, were used in this example. The soil springs are in pairs, one in the longitudinal direction and another in the transverse direction. The far ends of the soil springs (designated "Axial Soil Spring" and "Transverse Soil Spring" in Figure 5-7) have a boundary condition of an applied displacement (or zero displacement) in the direction of the soil spring member.

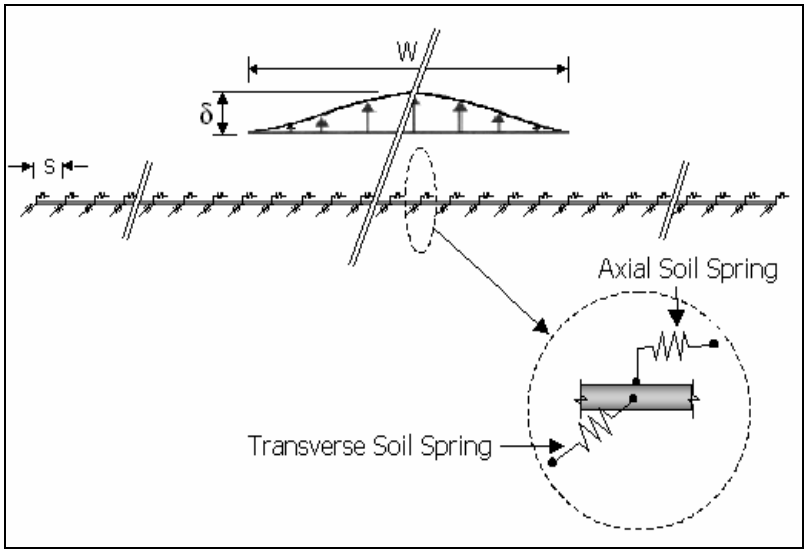

Figure 5-7 Straight Piping System Model with Soil Springs (Ref: Kuruswamy 2002)

The joint segment is made up of four individual truss members, each with its own behavior characteristics, but in combination, they model the behavior of the joint as a whole (Figure 5-8). One member represents the tension behavior, another member represents the compressive behavior, a third member links the tension and compression members, and the fourth member accounts for the rotational stiffness. The compression truss member is connected at points 1 and 2 in Figure 5-8, and the tension truss member is connected at points 3 and 4. In the model, points 2 and 3 are the same node which is the end node for one of the connected pipe barrel sections. The rigid link is represented by the member connecting points 1 and 4 and the rotational spring is connected by points 1 and 2, similar to the compression member. The joint is modeled to have a gap condition for both tension and compression conditions. However, the capabilities of the ADINA program allow gap specifications only for compressive loading conditions, and therefore, in order to have the tension members to be placed in a compressive state when the joint itself is in a tensile state, Kuruswamy (2002) developed this configuration. Member properties were input to have compression-only behavior (zero tension) and as can be seen for this configuration, when the joint is placed in compression (pushed together), the compressive member (member 1-2) will resist the compression, and when the joint is placed in tension (pulled apart), the member representing the tension behavior (member 3-4) will be put in a compressive state, which resists the tension movement of the joint. In this way, any pipe joint behavior (tension, compression, and rotational) can be incorporated so that the overall behavior of the joint matches the behavior measured in the laboratory.

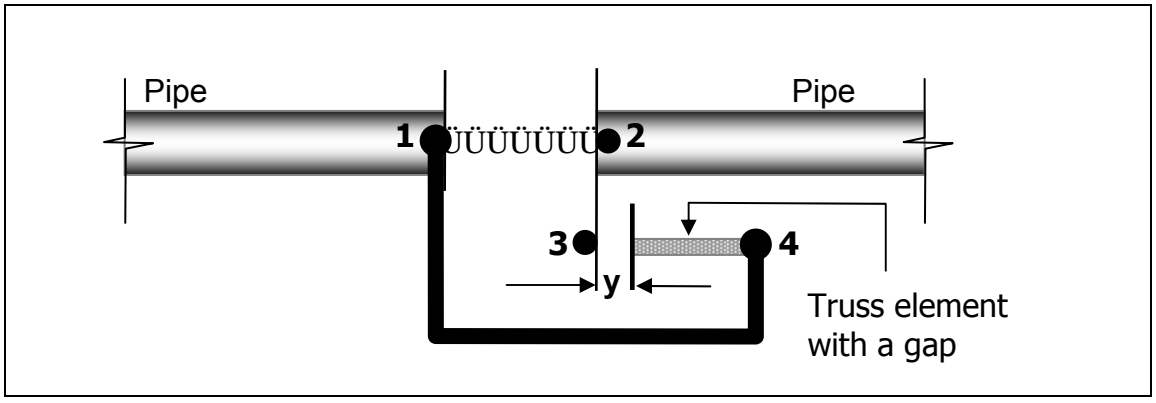

Figure 5-8 Joint Configuration (Ref: Kuruswamy 2002)

5.4.3 Member Section and Material Properties

The piping system for this example is comprised of several different element types, each one selected for its unique structural behavior. Element types have been formulated in such a way that they model the buried pipeline system in a realistic manner. Table 5-1 is a list of the members in the structural system, its element type, and its material behavior.

Table 5-1 Example Analysis Member Types and Material Behavior

Member	Element type	Supported DOF	Material behavior
pipe barrel (body)	beam	6 DOF	non-linear
joint compression	truss	2 DOF	non-linear with gaps
joint tension	truss	2 DOF	non-linear with gaps
joint rigid link	truss	2 DOF	linear elastic
joint rotational	spring	1 DOF	non-linear
soil spring transverse	truss	2 DOF	non-linear
soil spring longitudinal	truss	2 DOF	non-linear

Each member has specific material behavior attributes. The results of this experimental testing project determined the overall joint assembly stiffness for axial compression, axial tension, and rotational response. Since each of these stiffness characteristics can only be represented by a single member in the pipe-joint model, these characteristics are assigned to the individual members. Therefore, the stiffness of each of the individual members is specified by a unique material property.

Figure 5-9 is a load-displacement plot for ductile iron pipe joints showing both axial tension and axial compression. Values for both restrained and unrestrained joints are provided. The equivalent elastic Young's modulus and post-yield strain-hardening modulus that were determined from the laboratory investigation were used as input to ADINA The Young's modulus and strain-hardening modulus for the compression direction are the same for all the pipe joint types. The figure shows a gap distance under compression of about 13 mm, while in tension, only the retaining ring has a gap distance before engagement. Figure 5-10 shows a similar plot for the moment-rotational values of a typical joint. The moment-rotational data was entered into ADINA as non-linear

moment-rotation (or moment-theta, where theta is the rotational angle) values similar to the load-displacement input. Table 5-2 lists the numerical values of the load-displacement behavior for beam and truss members and Table 5-3 is a similar list for rotational moment-theta values. Figures 5-11 and 5-12 are force-displacement plots for the axial and transverse soil springs respectively with data entered into ADINA as the equivalent stress-strain values which were derived from the force-displacement values by Kuruswamy (2002) using references from M. O'Rourke and Liu (1999). The pipe barrel beam section property values were defined by inputting dimensions into ADINA of a pipe shape with the diameter specified as .2297 m (200 mm nominal) and wall thickness of 0.00635 m. It was necessary that the rigid link member to be extremely stiff in order to transfer loads without significant deformations. To accomplish this, the value of the Young's modulus of this member was set very high.

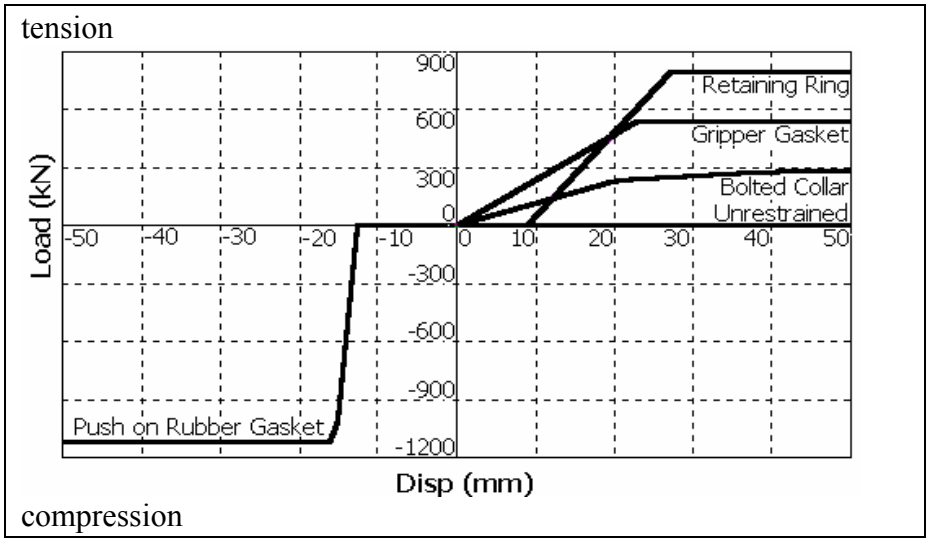

Figure 5-9 Laboratory Measured Load-Displacement Plots for DIP Joints (Ref: Kuruswamy 2002)

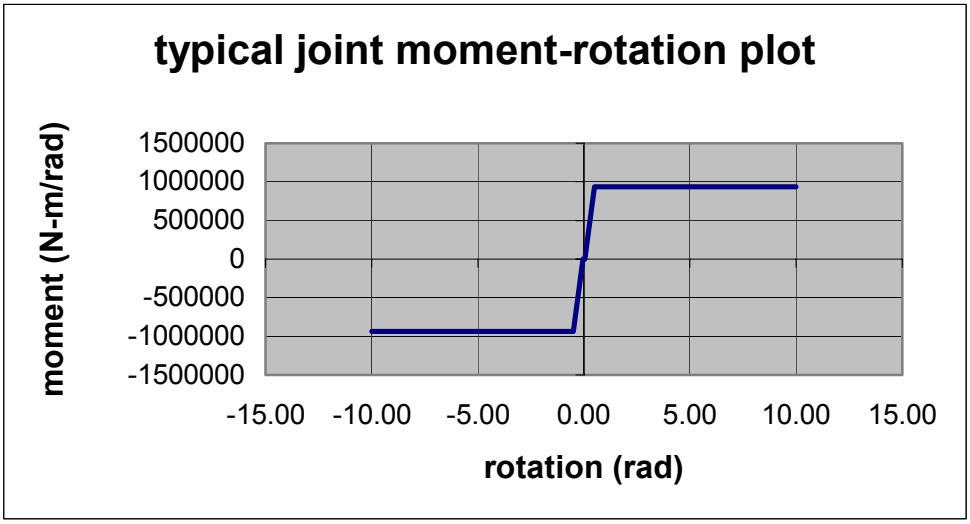

Figure 5-10 Laboratory Measured Typical Joint Moment-Rotation Plot

Table 5-2 Joint and Member Axial Properties

Member or joint type	Member type	Young's modulus (N/m^2)	Yield stress (N/m^2)	Strain-hardening modulus (N/m^2)
pipe barrel		1.7E10	2.9E8	7E9
unrestrained joint	joint compression	1.7E10	2.9E8	7E9
	joint tension	5.0E3	1.4E3	5.0E3
retaining ring joint	joint compression	1.7E10	2.9E8	7E9
	joint tension	8.7E6	8.0E5	1.0E4
bolted collar joint	joint compression	1.7E10	2.9E8	7E9
	joint tension	22.2E6	2.2E5	1.0E4
gripper gasket joint	joint compression	1.7E10	2.9E8	7E9
	joint tension	4.7E6	5.4E5	1.0E4
joint rigid link		1E20		

Table 5-3 Joint Rotational Properties from Laboratory Results

Joint type	Yield moment (N-m)	Yield rotation (rad.)
unrestrained joint	4.2E4	0.12
retaining ring	9.3E5	0.10
bolted collar	5.5E5	0.10
gripper gasket	9.8E5	0.10

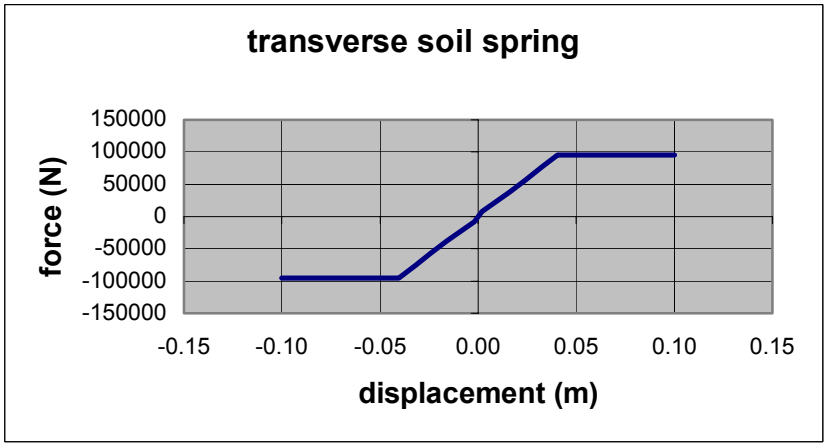

Figure 5-11 Load-Displacement Plot for Axial Soil Spring Input Data

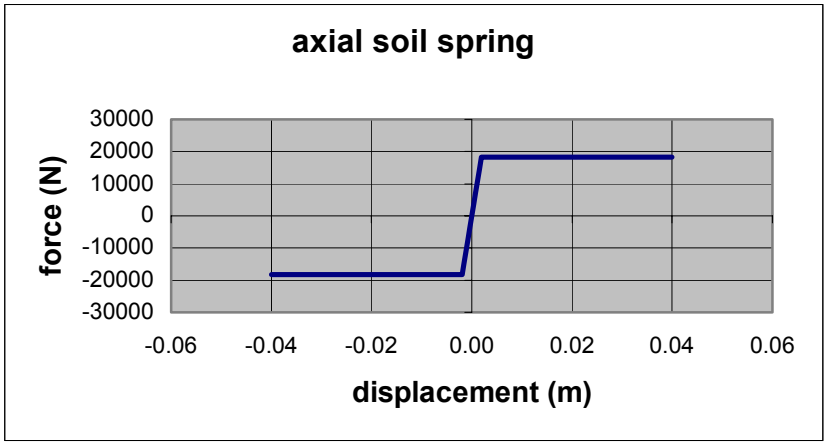

Figure 5-12 Load-Displacement Plot for Transverse Soil Spring Input data

5.4.4 Model Loading Configurations

This example analysis considered a loading condition resulting from a PGD pattern as defined in Figure 5-4. Table 5-4 lists the parameters for each analysis performed. Figure 5-13 shows the displacement amplitude pattern on the main branch which is the amplitude pattern for both longitudinally applied displacements (global X direction) and for transversely applied displacements (global Y direction). The angle "θ" in Table 5-4 is defined as being zero degrees in the positive global X direction and 90 degrees in the negative global Y direction. Figure 5-14 is a similar figure for the tee branch, but in this case, the displacements applied longitudinally to the member are in the negative global Y direction and the transversely applied displacements are in the positive global X direction. The displacement pattern on the tee branch is only a half distribution pattern since, at the intersection with the main branch, the amplitude is at its peak value and is equal to the amplitude on the main branch at that point.

Table 5-4 Loading Configurations Considered

Piping system joint type	Applied displacement load direction, θ	Maximum displacement amplitude, δ	Loading pattern width, W
unrestrained	0 degrees	2.5 m	550 m
	90 degrees	2.5 m	550 m
retaining ring	0 degrees	2.5 m	550 m
	90 degrees	2.5 m	550 m
bolted collar	0 degrees	2.5 m	550 m
	90 degrees	2.5 m	550 m
gripper gasket	0 degrees	2.5 m	550 m
	90 degrees	2.5 m	550 m

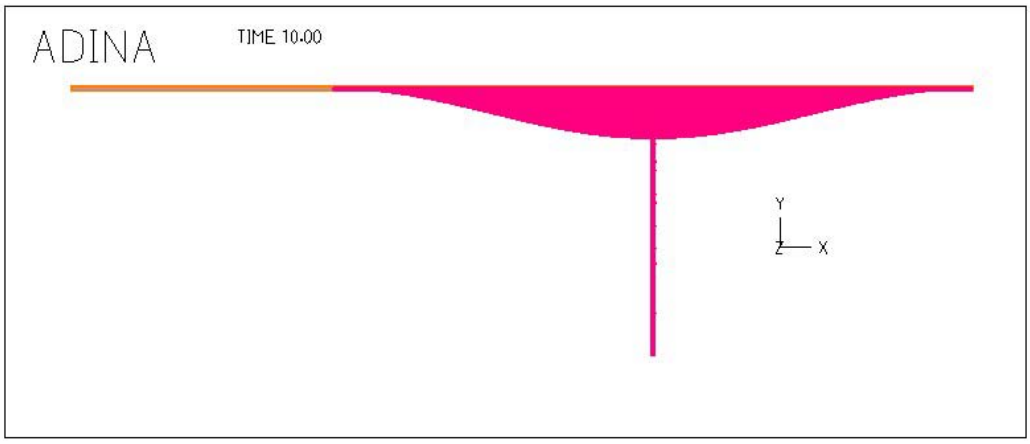

Figure 5-13 Applied Displacement Amplitude Pattern on Main Branch

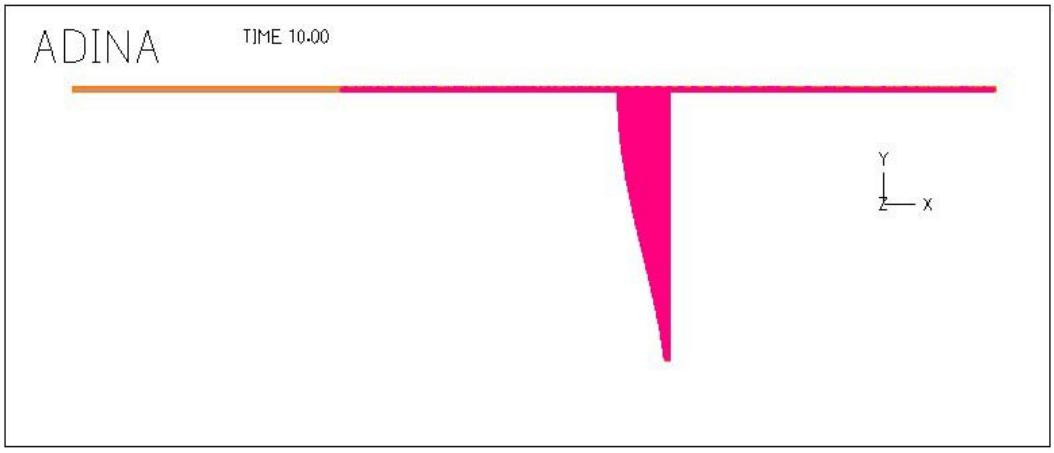

Figure 5-14 Applied Displacement Amplitude Pattern on Tee Branch

5.4.5 Analysis and Results

Once all data were input and verified, the ADINA program was invoked to perform the analysis. The load-step to ramp-up from zero displacement to the final amplitude was initially set at ten, but because the automatic time stepping (ATS) capability of ADINA was specified, each defined step was further sub-divided until the load-stepping increment was able to converge. If a sub-step was not able to reach convergence, the ATS further decreased the load-step increment until convergence was achieved.

Analysis results were specified and retrieved by executing the associated program ADINA-PLOT. Results from the analysis were stored in a binary file called a "porthole"

file, which contained the primary analysis results such as nodal displacements. Secondary results, such as element stresses and strains, are only computed upon request using the primary results. For this analysis, nodal displacements at the end nodes of the joint compression members were requested and exported to an external text file. The text file was then imported into Microsoft's EXCEL spread-sheet program for post-processing. The objective of the post-processing was to compute the relative joint separations using the X and Y nodal displacements from the ADINA analysis. In addition to these computed joint separations, large displacement effects, or arc-length effects, due to the curvature of the loading pattern had to be accounted for when displacement loading was transverse to the pipe axis (see Eq. 5-14). The total joint separations were then computed as the sum of the analysis joint separations and the arc-length effects.

The nodal displacements for each branch resulting from the applied displacement in the θ=0 direction (global X) are shown in Figures 5-15 and 5-16, and from the applied displacement in the θ=90 direction (global Y) in Figures 5-17 and 5-18. Table 5-5 lists the maximum nodal displacements for each joint type and load direction. As it can be seen, the resulting nodal displacements are approximately the same as the applied displacement pattern, and therefore, are within the arc-length equation's stated criteria.

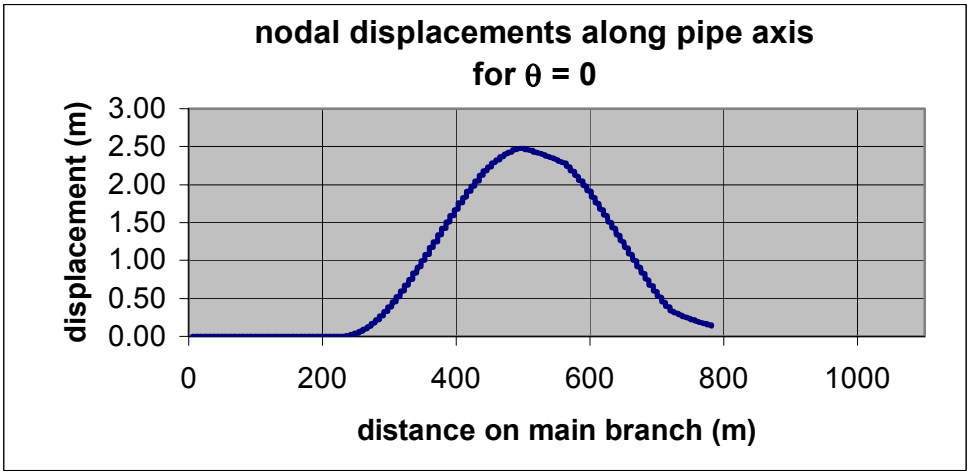

Figure 5-15 Computed Main Branch Nodal Displacements Along Pipe Axis From Applied Displacements in the θ = 0 Direction

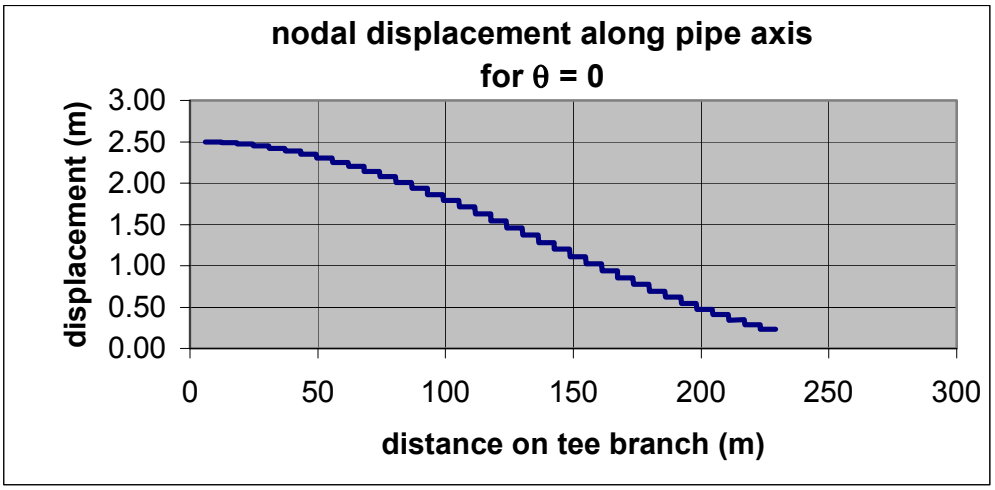

Figure 5-16 Computed Tee Branch Nodal Displacements Along Pipe Axis From Applied Displacements in the θ = 0 Direction

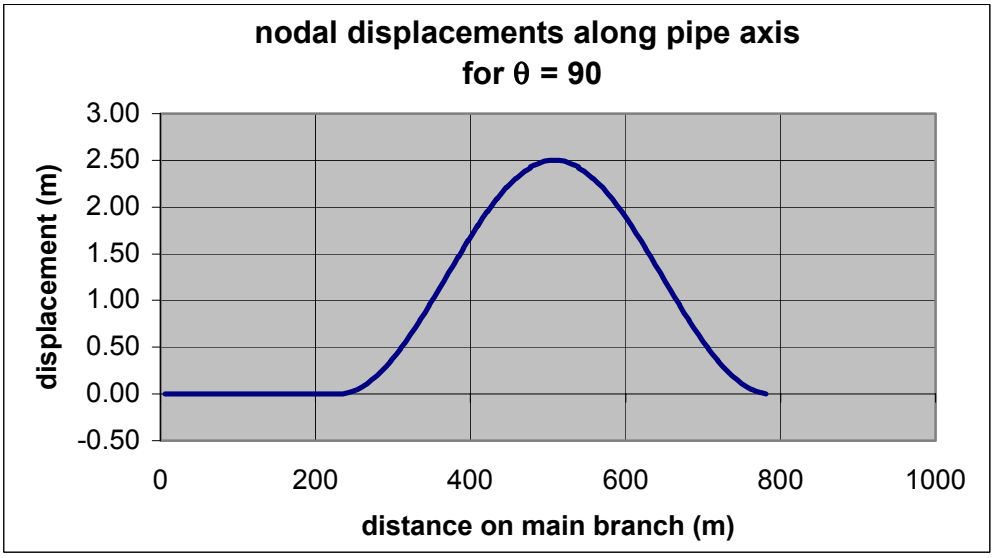

Figure 5-17 Computed Main Branch Nodal Displacements Along Pipe Axis From Applied Displacements in the θ = 90 Direction

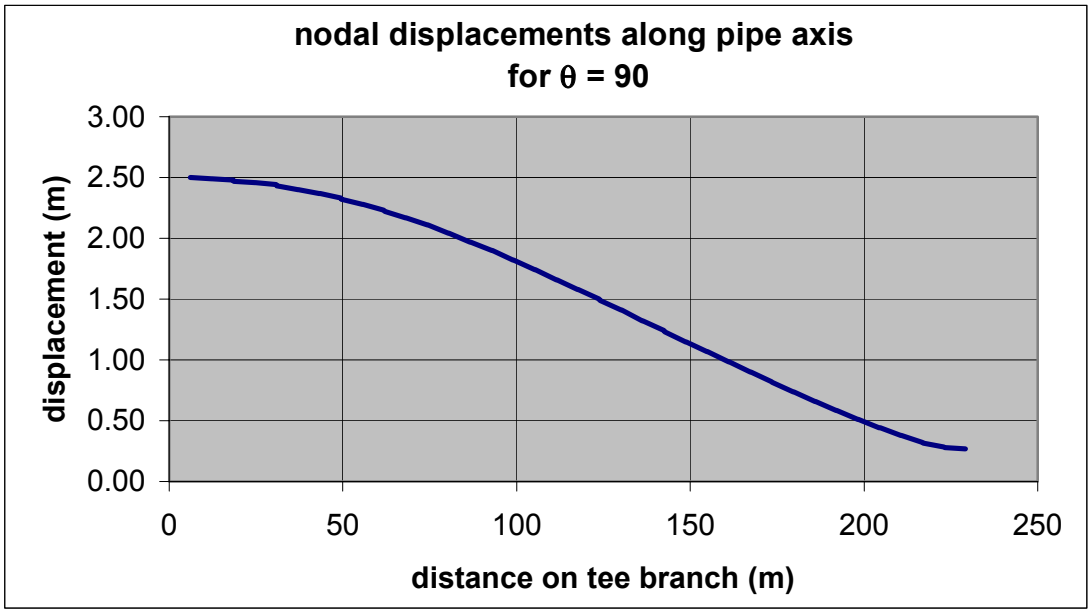

Figure 5-18 Computed Tee Branch Nodal Displacements Along Pipe Axis From Applied Displacements in the θ = 90 Direction

Table 5-5 Resulting Maximum Nodal Displacements Along Pipe Axis

Joint type	Load direction, θ	Main branch displacements (m)	Tee branch displacement (m)
unrestrained	0 degrees	2.48	2.50
	90 degrees	2.50	2.50
gripper	0 degrees	2.47	2.50
	90 degrees	2.50	2.49
retaining ring	0 degrees	2.44	2.50
	90 degrees	2.50	2.45
bolted collar	0 degrees	2.48	2.50
	90 degrees	2.50	2.50

For a practical analysis of a pipeline system, failure criteria must be established in order to determine the potential for damage and failure. For this example analysis, a specific failure criteria was not considered, however, plots were made in terms of the magnitude of joint separation along the length of each branch (Figure 5-19 to 5-34) and for the number of joints in the model having a joint separation exceeding a specific amount (Figures 5-35 to 5-38). Considering each branch separately, when applied loadings are

parallel to the axis of the pipe, arc-length effects are not present. However, when the applied displacements are transverse to the pipe's axis, arc-length effects are substantial and in fact, are dominant, accounting for about 95 to 99% of the total separation value. In examining the joint separation plots (Figures 5-19 to 5-34), the shape and magnitude of the separations for the various joint types loaded transverse to the pipe axis are similar due to this dominance. Arc-length effect values are identical for each joint type since each has the same applied displacement amplitude and pattern. It must be noted that the joint separation displacements due to the arc-length effects are a function of the transversely applied displacements, and therefore, will vary at each load step as the applied displacements are ramped-up from zero to the maximum amplitude.

For displacements applied in the θ=0 direction (global X), unrestrained joints in the main branch, where the applied displacement is axial, have little resistance from the anchor points because of their inability to transfer tension across the joint, and therefore, each joint moves exactly as the applied displacement at that joint. The separation is therefore limited to the difference of applied displacements at each end of the joint element, which is extremely small. In contrast, a restrained joint system is restricted in its movement due to the anchor points (nodes with prescribed zero or near zero applied displacement) and their capability of limiting differential movement due to the tensile restraint across a joint. Nodes further away from the anchor points are more likely to have displacements the same as the surrounding soil movement due to slippage that occurs in the restraining mechanisms over the length of the pipe branch. Nodes closer to the anchor points are more restrained in their displacements relative to the soil. The end result is that a restrained joint system, contrary to what might be expected, can have larger joint separations than an unrestrained joint system in some localized areas. It must be noted that the tensile restraint capacity of each of the restrained joint types is not significantly different so that the similarity of their results would be expected. In the tee branch, when applied displacements are transverse to the pipe axis, arc-length effects dominate the separation values resulting in a similarity of results for all joint types.

For loading in the θ=90 direction (global Y), the separations in the main branch, which is loaded transverse to the pipe axis, are dominated by arc-length effects and are therefore similar in shape and magnitude for all joint types except for some anomalies at the intersection of the main branch with the tee branch. The shape of the separation curves for the joints on the tee branch, which is loaded in its axial direction, are similar except for the unrestrained joints for reasons explained above.

Figures 5-35 to 5-38 show the total separation values and the number of joints that have a separation exceeding a specific amount for similar loading directions and along each branch. Again, the similarities of the different joint types for the same branch and loading direction can be seen.

Once an analysis of a piping system has been completed, the analyst is able to use a specific failure criteria based on the joint's total separation values. Overall system failure may be based on the percentage of the joints exceeding the individual failure criteria or on the magnitude of separation of a selected number of joints. The analyst can also look at the separation plots to see what areas of the system have joints exceeding the failure criteria. By evaluating the extent and location of potential problems, a strategy to mitigate the problem may be proposed and evaluated.

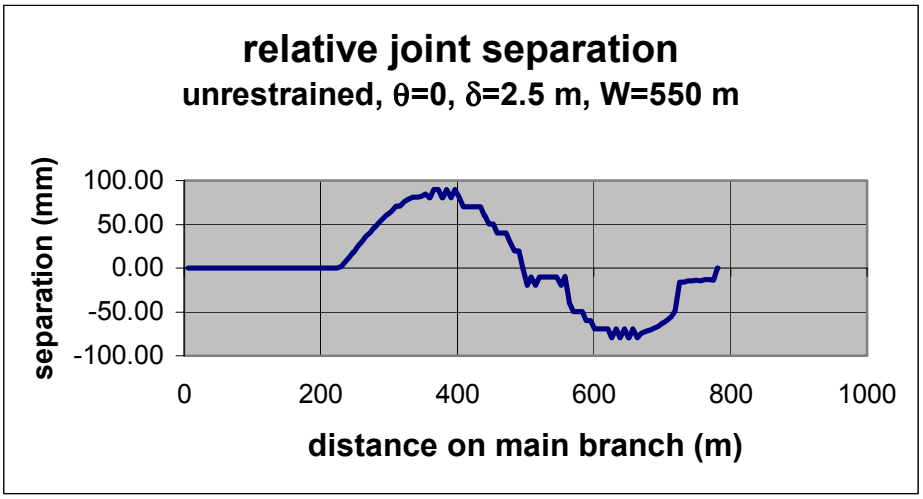

Figure 5-19 Joint Separation for Unrestrained Joints on the Main Branch Loaded in the θ = 0 Direction (Global X)

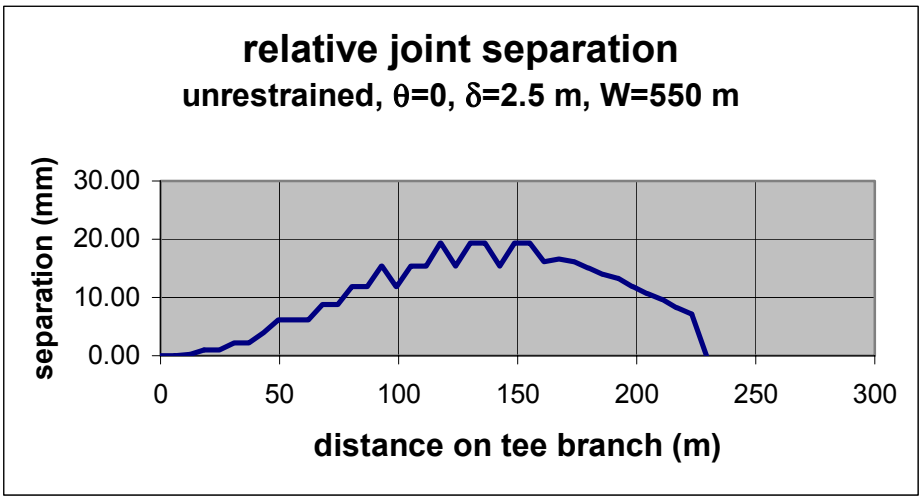

Figure 5-20 Joint Separation for Unrestrained Joints on the Tee Branch Loaded in the θ = 0 Direction (Global X)

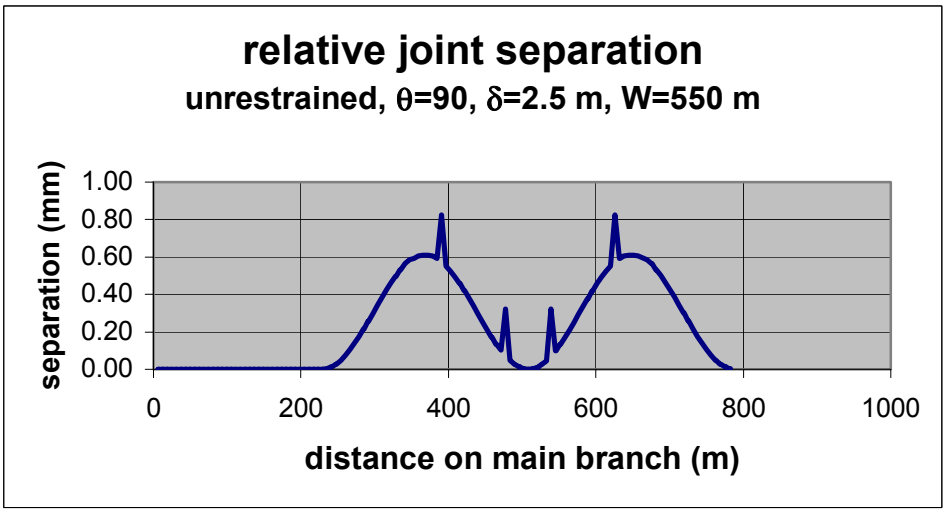

Figure 5-21 Joint Separation for Unrestrained Joints on the Main Branch Loaded in the θ = 90 Direction (Global Y)

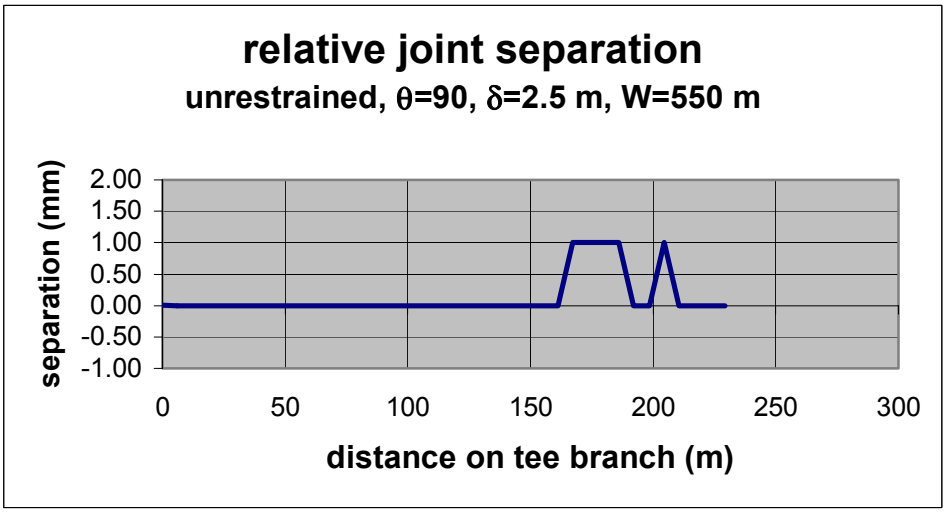

Figure 5-22 Joint Separation for Unrestrained Joints on the Tee Branch Loaded in the θ = 90 Direction (Global Y)

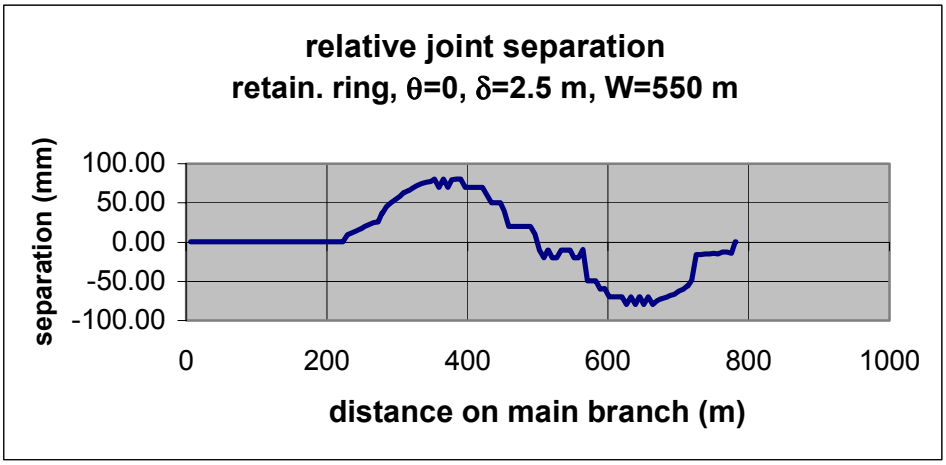

Figure 5-23 Joint Separation for Retaining Ring Joints on the Main Branch Loaded in the θ = 0 Direction (Global X)

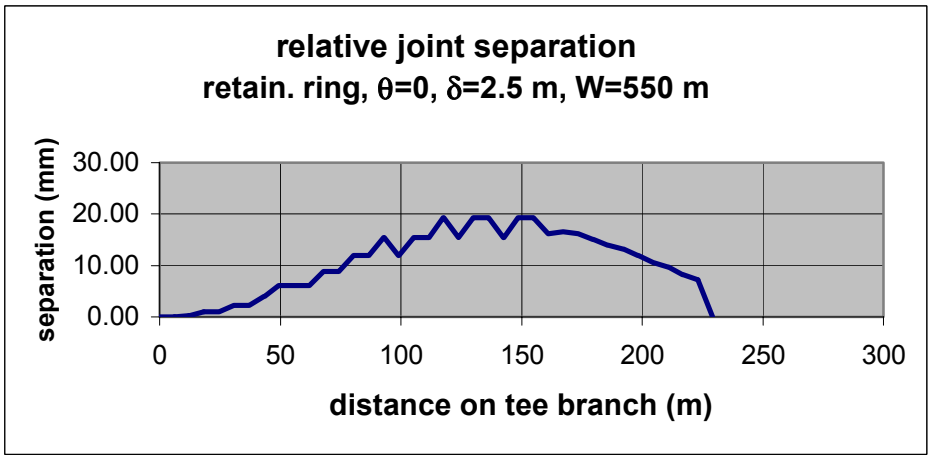

Figure 5-24 Joint Separation for Retaining Ring Joints on the Tee Branch Loaded in the θ = 0 Direction (Global X)

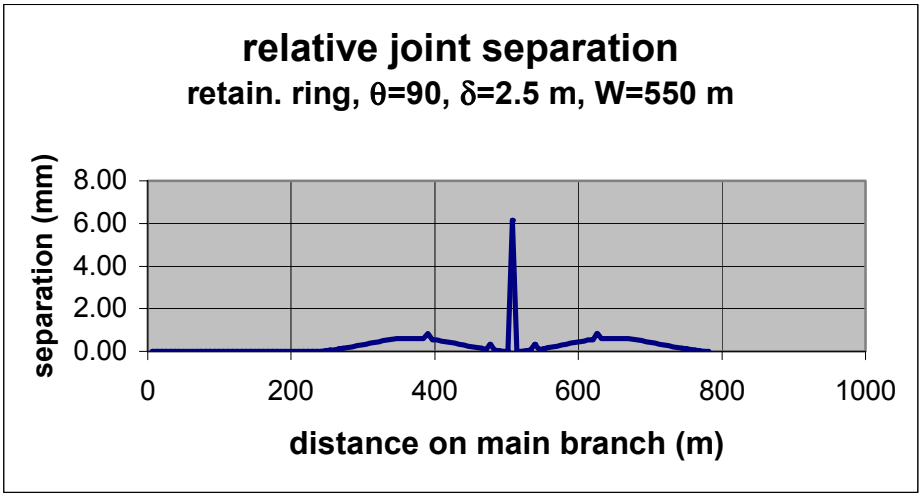

Figure 5-25 Joint Separation for Retaining Ring Joints on the Main Branch Loaded in the θ = 90 Direction (Global Y)

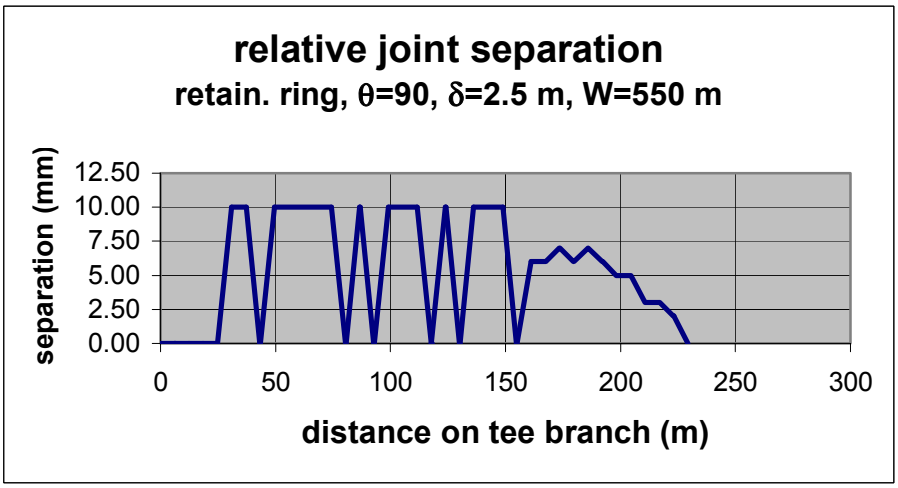

Figure 5-26 Joint Separation for Retaining Ring Joints on the Tee Branch Loaded in the θ = 90 Direction (Global Y)

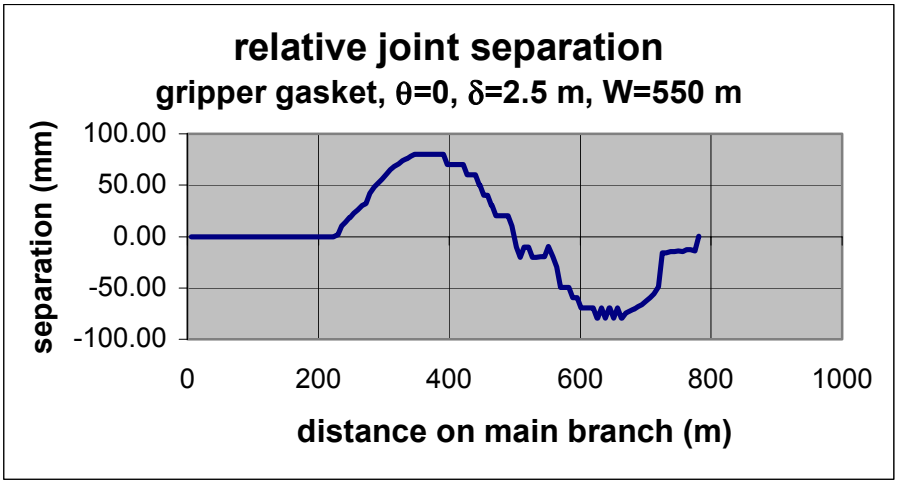

Figure 5-27 Joint Separation for Gripper Gasket Joints on the Main Branch Loaded in the θ = 0 Direction (Global X)

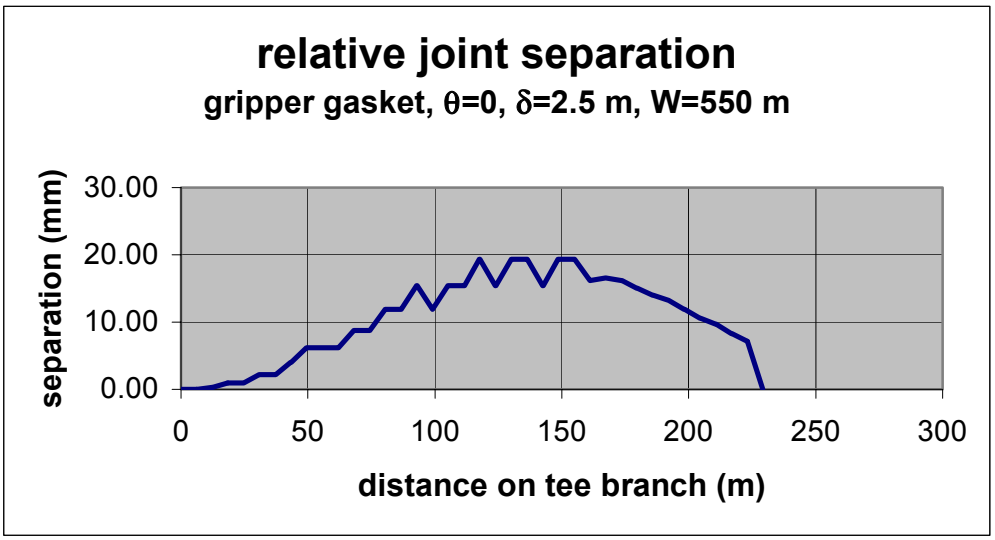

Figure 5-28 Joint Separation for Gripper Gasket Joints on the Tee Branch Loaded in the θ = 0 Direction (Global X)

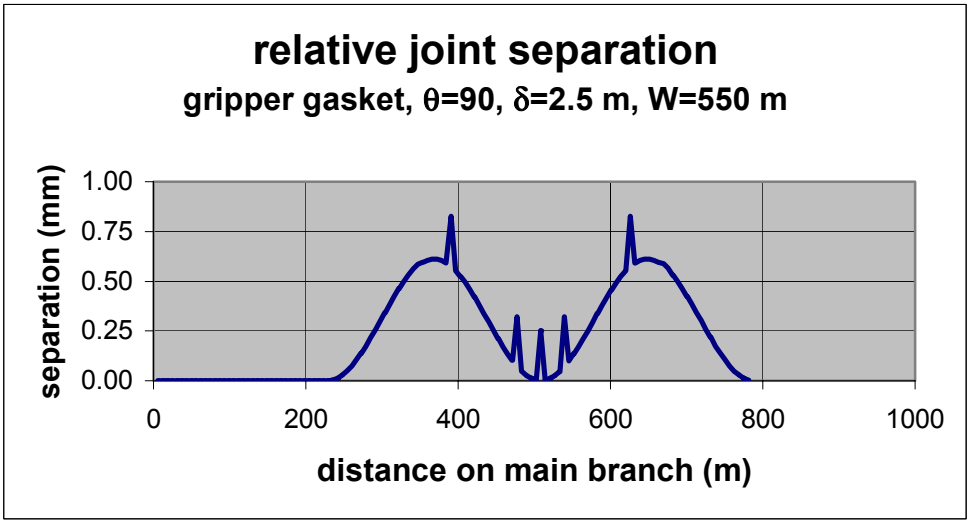

Figure 5-29 Joint Separation for Gripper Gasket Joints on the Main Branch Loaded in the θ = 90 Direction (Global Y)

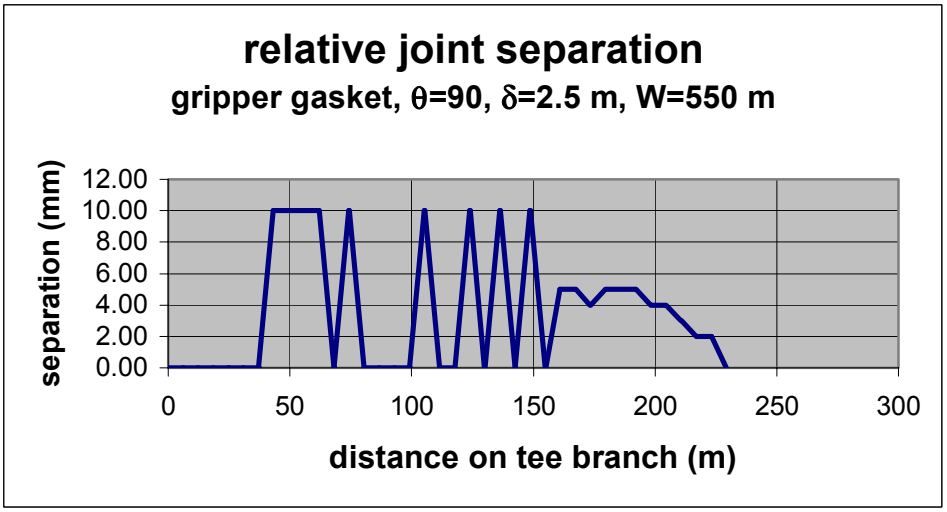

Figure 5-30 Joint Separation for Gripper Gasket Joints on the Tee Branch Loaded in the θ = 90 Direction (Global Y)

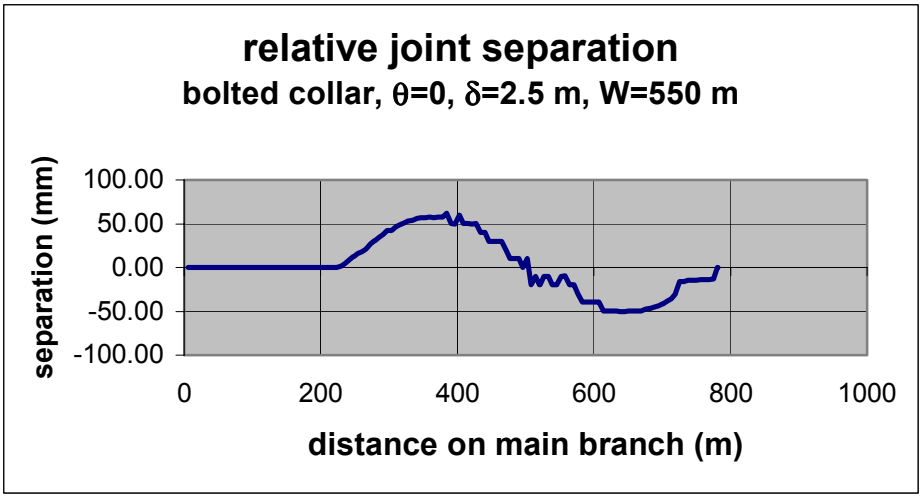

Figure 5-31 Joint Separation for Bolted Collar Joints on the Main Branch Loaded in the θ = 0 Direction (Global X)

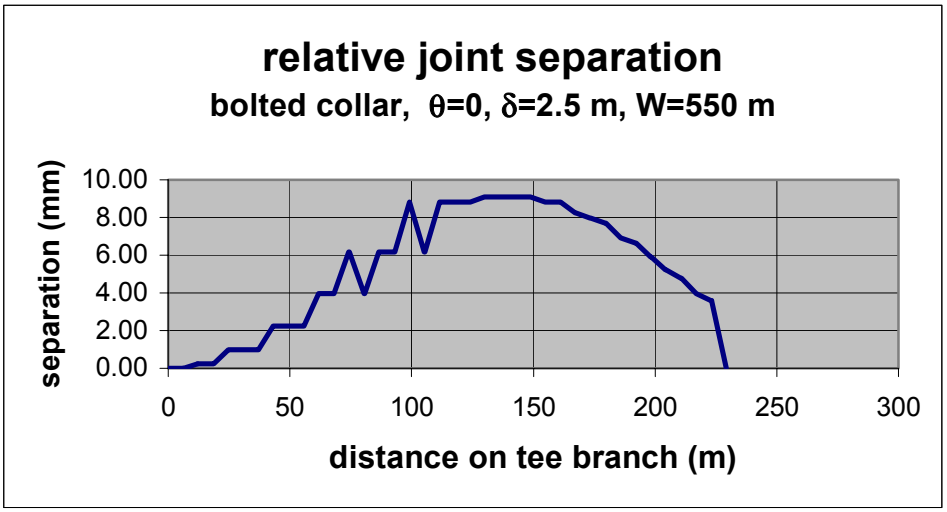

Figure 5-32 Joint Separation for Bolted Collar Joints on the Tee Branch Loaded in the θ = 0 Direction (Global X)

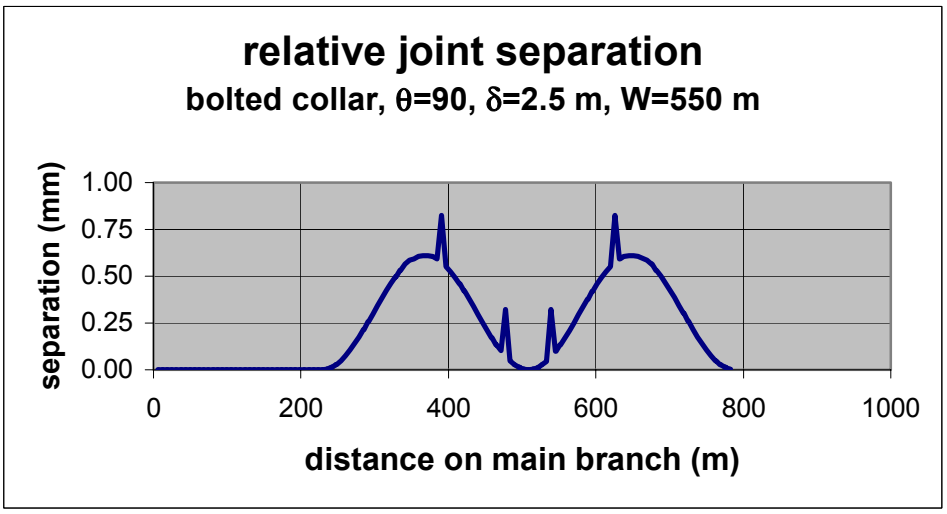

Figure 5-33 Joint Separation for Bolted Collar Joints on the Main Branch Loaded in the θ = 90 Direction (Global Y)

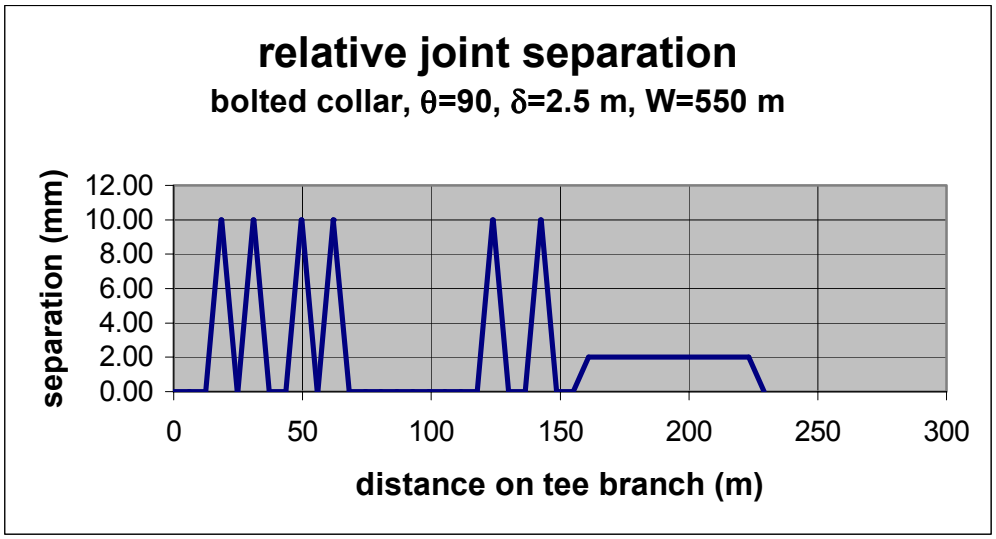

Figure 5-34 Joint Separation for Bolted Collar Joints on the Tee Branch Loaded in the θ = 90 Direction (Global Y)

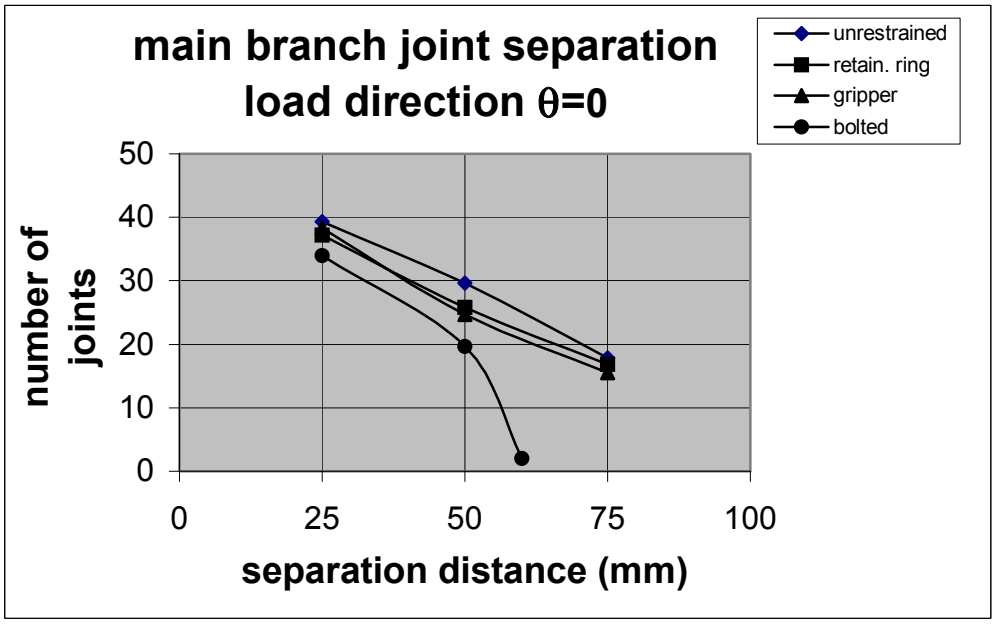

Figure 5-35 Number of Joints and Corresponding Separation Distance for Main Branch Loaded in the θ = 0 Direction (Global X)

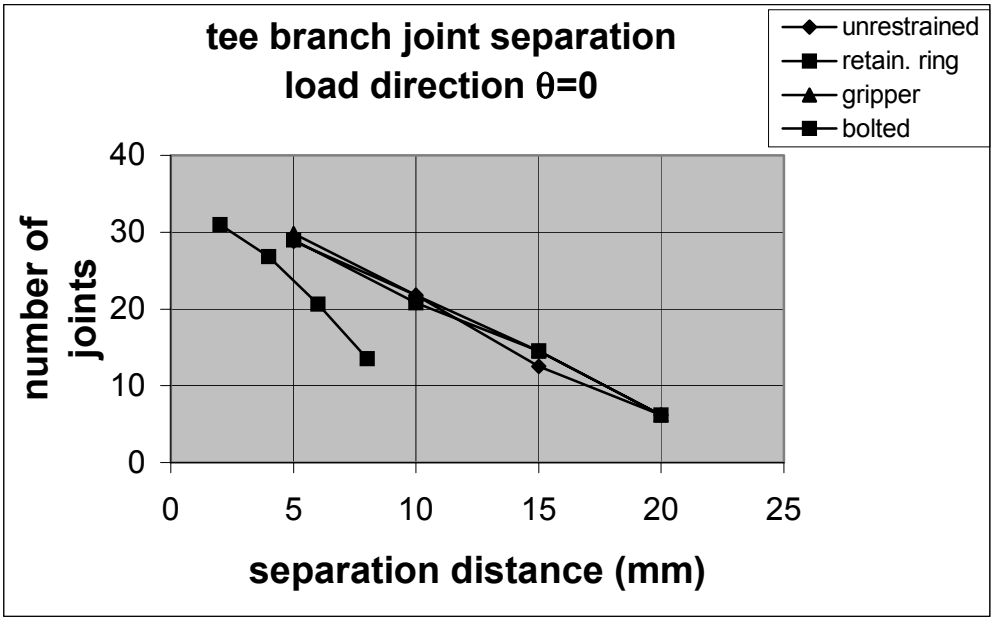

Figure 5-36 Number of Joints and Corresponding Separation Distance for Tee Branch Loaded in the θ = 0 Direction (Global X)

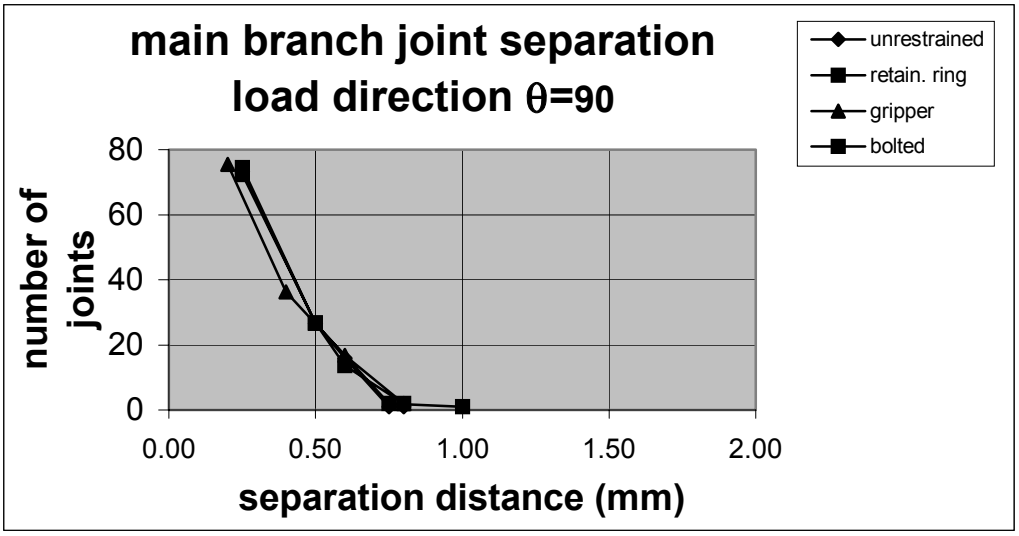

Figure 5-37 Number of Joints and Corresponding Separation Distance for Main Branch Loaded in the θ = 90 Direction (Global Y)

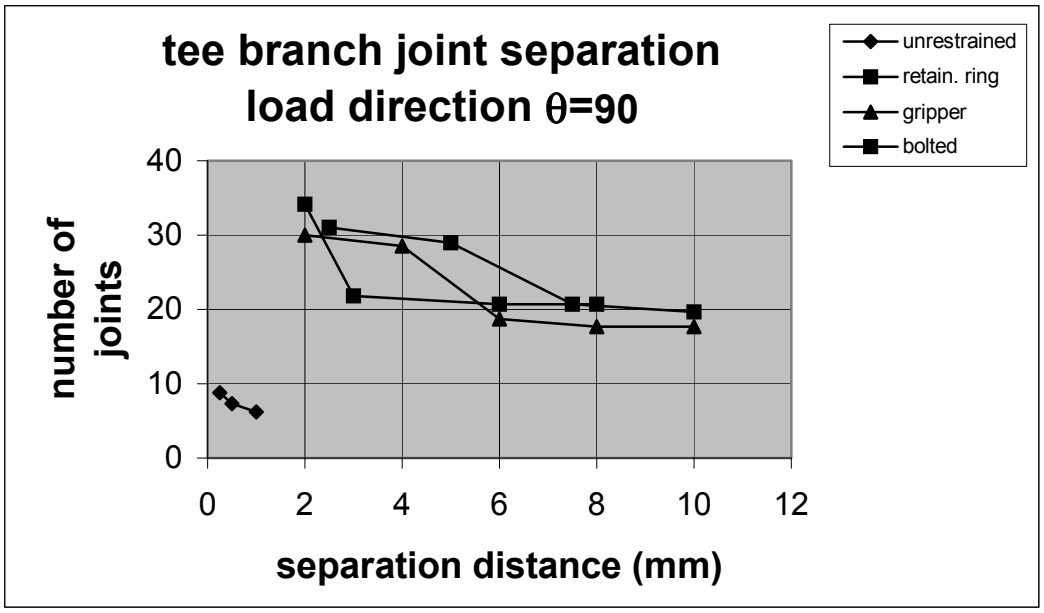

Figure 5-38 Number of Joints and Corresponding Separation Distance for Tee Branch Loaded in the θ = 90 Direction (Global Y)

5.4.6 Example Summary

The methodology and procedures for a finite element computer analysis of a simple piping system has been undertaken. Each step and each piece of required data has been described with an explanation of how it was developed or derived. The objective of this example was to demonstrate the use of joint stiffness data obtained in this experimental testing project for a practical application. The analysis presented here used realistic material properties and modeling. However, the interpretation of results is limited to the cases considered. The procedures describe for the analysis of PGD loadings can be adapted to a variety of situations such as the analysis of transient or time-dependent motions resulting from seismic motions.

The ultimate goal of any analytical procedure is to create a simplification of an actual physical system by creating a mathematical model that can be understood and analyzed using approximate properties, either derived by empirical investigation or by a

mathematical derivation. The end result should be close enough within reasonable engineering tolerance to the response of the real structure so that a trained designer is able to make decisions that result in a structure that will maintain its structural integrity and remain within strength and service limits set by an established criteria. The physical data obtained in this experimental testing project and the methodologies described in this example were designed to help in achieving this goal.

SECTION 6
OBSERVATIONS and CONCLUSIONS

This research establishes axial and rotational stiffness characteristics and maximum force/moment capacity levels for several different types of restrained and unrestrained pipe joints, pipe materials, and pipe diameters. The joint stiffness values can be used as input data for a computerized finite element analysis of piping systems, and the maximum force capacity values can be used in a simplified pipeline risk assessment analysis (see Section 5). The development and implementation of this testing program and the results have led to several observations and conclusions as described below:

- Investigations by other researchers have shown that pipe joints have suffered damage from past earthquakes and are vulnerable to future earthquakes.

- It has been established that unrestrained joints have a very low capacity to resist tension pull-out and are therefore, vulnerable to pull-out failure from seismic motions. Restraining devices can significantly increase a joint's capacity to withstand pull-out, and therefore, decrease the probably of joint failure.

- The static axial testing phase was done under displacement control by incrementally increasing the applied displacements, then relaxing the displacement allowing for a partial unloading. It would have been of value to have a much greater level of unloading to better monitor the unload and reload slopes and the continuation of the loading curve. This should be considered in future experiments of this type.

- For the static axial testing phase, a self-contained, stand alone test assembly proved to be extremely valuable. It allowed specimens to be easily installed and removed within a reasonable amount of time and effort.

- A specimen length of approximately 60 cm (24 in.) is a suitable and convenient length to be used for axial testing. Axial strains monitored along the length of the specimen show that any stress concentrations that may have developed near the joint or at a change of the cross-section were not present at locations away from the joint.

- Monitoring of internal water pressure by a pressure transducer was not a valuable piece of information. Actual pressure levels vary during the testing due to changes in the internal volume of the specimen as axial deformation takes place. Any leakage of consequence is easily detected visually.

- The axial compressive force capacity of cast iron and ductile iron pipes is very high and unless there are motions that cause concurrent bending, failure due to axial compressive thrust is unlikely.

- The maximum axial force capacity of steel pipe with lap-welded joints, ductile iron pipe with retaining ring joints, and ductile iron pipe with gripper gasket joints is significantly influenced by the pipe diameter. This is due to the fact that the force resistance is distributed around the circumference of the joint, and therefore, the greater the circumference, the greater the total resistance.

- The maximum axial force capacity of ductile iron pipe with bolted collar joints is not greatly affected by the pipe diameter. For bolted collar restraints, the resistance is through the bolts and the gripping power of the wedge screw teeth. Since the number of wedge screws is approximately the same for the different diameters of pipe, the total resistance is not significantly different.

- Polyethylene (PE) pipe with butt-fused joints will remain extremely ductile for both axial and bending loadings. PE pipe is a ductile, plastic material and can withstand major distortions without failure, as was seen during this testing program. The severe deformations that occur will restrict the resistance levels, and therefore, if all diameters of PE pipe have severe distortions, there will not be a significant difference in the resisting force between them.

- Simplified risk assessment charts have been developed, and along with the maximum joint force capacities as determined in this research, seismic risk can be evaluated. Pipeline owners can use this methodology to perform preliminary analysis of proposed system alignments, or to review existing systems to determine the most vulnerable zones within their system and to prioritize their upgrade plans.

- The comparison of axial ultimate force capacities for static and axial dynamic loadings for joints with tensile restraint devices shows that they are approximately equal. This indicates that static testing is able to capture the dynamic force characteristics of pipe joints. However, the static loading curves have a definite elastic section and a post-yield section, while the dynamic loading has only an apparent elastic curve up to the failure point.

- The comparison of axial elastic stiffness between static loading and dynamic loading indicates that there is an effect of the dynamic loading, and therefore, static testing cannot capture the dynamic behavior of pipe joints, and dynamic testing is essential in obtaining realistic dynamic stiffness characteristics for pipe joints.

- For bending loading, providing some level of joint restraint can greatly decrease the probability of joint failure due to the prevention of incremental creep of withdrawal.

- Stiffness characteristics have been established through the use of load-displacement and moment-theta curves from approximated bi-linear plots. These values can be used as input data for a computerized finite element analysis of piping systems.

SECTION 7
FUTURE RESEARCH and INVESTIGATION

Although there has been extensive research on the subject of seismic response of pipelines, there is much left to do. A piping system is made up of a number of components, fittings and attachments. The characteristics of each element need to be investigated to determine how they affect the overall system and which component is most vulnerable to failure. Some areas of needed future research are listed below:

- This research project tested a single specimen for each joint type, material type and pipe diameter. In order to gain statistical meaningful data on joint characteristics, a greater population of samples for each specimen needs to tested.

- This research project tested only a limited range of joint types and restraining devices. Testing of additional joint types, restraint devices, and a wider range of pipe diameters should be undertaken to get a more comprehensive database of joint types and their characteristics.

- The objective of this testing program was to examine pipe joints. There are individual components of a piping system, such as “tees” and “elbows”, that need to be tested as individual components in order to determine their influence on the whole system.

- There has been assumption that the buried pipe and the soil have perfect bond up to a frictional limit. In reality, there is a flexibility between the two that can be modeled as a spring element that depends on a number of parameters such as burial depth and soil type. This soil-pipe interaction needs to be examined further, especially under dynamic loading conditions.

- The bending testing phase for this research project was limited to static loading conditions and unrestrained rotation levels for dynamic loading. Bending testing that examines the behavior of restrained joints at higher amplitudes under dynamic loading needs to be done.

- A number of reported pipeline failures were due to shear. This mode of behavior needs to examined more thoroughly in order to get a complete view of a joint's response to seismic motions. No shear tests were performed in this research described in this report.

- The restraining devices tested were not designed specifically for seismic applications. Research and testing should be directed toward the development of a low cost, seismically resistant joint that would provide a greater level of safety against failures.

- Engineering computer software is used for technology transfer. Software should be developed that can use data developed in this and future research in a specific-use program to analyze piping systems for both transient analysis and permanent ground deformation analysis.

- Design criteria and standards for the design of pipelines and pipe joints subjected to seismic motions need to be developed so that the potential for major damage and failure to these system can be reduced.

- Further analytical research on the seismic behavior of segmental pipelines extending through different soil types needs to be performed.

SECTION 8
REFERENCES

ASCE, (1983), "Seismic Response of Buried Pipes and Structural Components", Committee on Seismic Analysis of the ASCE Structural Division Committee on Nuclear Structures and Materials, American Society of Civil Engineers, 1983, pp. 1-56.

ASCE, (1984), "Guidelines for the Seismic Design of Oil and Gas Pipeline Systems", Committee on Gas and Liquid Fuel Lifeline, American Society of Civil Engineers.

Fuchida, K., Wang, L., Akiyoshi, T., (1994), "Parametric Analysis of Buried Pipelines Subjected to Liquefied Ground Movements", Fifth U.S. National Conference on Earthquake Engineering, Proceedings, Earthquake Engineering Research Institute, Oakland, Calif., Vol. IV, 1994, pp. 959-968.

Hamada, M., Yasuda, S., Isoyama, R., and Emoto, K., (1986), "Study on Liquefaction Induced Permanent Ground Displacements", Association for the Development of Earthquake Prediction, Japan.

Iwamatu, J., et al., (1998), "Damage to Buried Water Distribution Pipelines and Ground Deformations from the 1995 Hyogoken-Nanbu Earthquake", Proceedings of Workshop for Anti-Seismic Measures on Water Supply, International Water Services Association (IWSA), Tokyo, Japan, 1998.

Iwamoto, T., (1995), "Summary of Damaged Pipelines for Waterwork System by the 1995 Hyogoken-Nanbu (Kobe) Earthquake", Proceedings of the 4th U.S. Conference on Lifeline Earthquake Engineering, ASCE, Aug. 1995, supplement pp. 1-8.

Kitaura, M., Miyajima, M., (1996), "Damage to Water Supply Pipelines", Special Issue of Soils and Foundation, Japanese Geotechnical Society, Jan. 1996, pp. 325-333.

Kuruswamy, S., (2002) “Nonlinear Analysis of Buried Restrained and Unrestrained Pipelines Subjected to Permanent Ground Deformation”, Masters Thesis, Civil Engineering Dept., University of Nevada, Reno.

LADWP, (1999), personal letter to Ronald Meis in response to request for information about damage during the Northridge earthquake.

Matsubara, K., Hoshiya, M., (2000), “Soil Spring Constants of Buried Pipelines for Seismic Design”, Journal of Engineering Mechanics, Jan. 2000, pp. 76-83.

Newmark, N.M., (1967), “Problems in Wave Propagation in Soil and Rock”, International Symposium on Wave Propagation and Dynamic Properties of Earth Materials, University of New Mexico Press, Aug. 1967, pp. 7-26.

O'Rouke, M., (1996), “Response of Buried Pipelines to Wave Propagation”, NCEER Bulletin Vol. 10, Number 3, July 1996, pp. 1-5.

O‘Rouke, M., Castro, G., Naneen, C., (1980), “Effects of Seismic Wave Propagation Upon Buried Pipelines”, Earthquake Engineering and Structural Dynamics, Vol. 8, 1980, pp. 455-467.

O’Rourke, M., Liu, X., (1999), “Response of Buried Pipelines Subjected to Earthquake Effects”, Monograph Series, Multidisciplinary Center for Earthquake Engineering Research (MCEER), 1999.

O'Rourke, T., (1996), “Lessons Learned for Lifeline Engineering from Major Urban Earthquakes”, Eleventh World Conference on Earthquake Engineering Proceedings, Pergamon, Elsevier Science Ltd., Oxford, England, 1996, Disk 4, paper No. 2172.

O'Rourke, T., Palmer, M., (1996), “Earthquake Performance of Gas Transmission Pipelines”, Earthquake Spectra Vol. 12(3), August 1996, pp. 493-527.

Singhal, A., (1984), “Nonlinear Behavior of Ductile Iron Pipeline Joints”, Journal of Technical Topics in Civil Engineering, Vol. 110 No. 1, May 1984, pp. 29-47.

Trifunac, M., Lee, V., (1996), “Peak Surface Strains During Strong Earthquake Motion”, Soil Dynamics and Earthquake Engineering (15), 1996, pp. 311-319.

Trifunac, M., Todorovska, M., (1997), “Northridge, California, Earthquake of 1994: Density of Pipe Breaks and Surface Strains”, Soil Dynamics and Earthquake Engineering 16 (1997), pp. 193-207.

Wang, L., (1979), “Seismic Vulnerability, Behavior and Design of Buried Pipelines”, SVBDUPS Project Technical Report 9, Dept. of Civil Engineering, Rensselaer Polytechnic Institute, Troy, NY, 1979, pp. 295-302.

Wang, L., Cheng, K., (1979), “Seismic Response Behavior of Buried Pipelines”, Journal of Pressure Vessel Technology, Vol. II, February 1979, pp. 21-30.

Wang, L., Li, H., (1994), “Experimental Study on the Damping and Resistant Characteristics of Conventional Pipe Joints”, Fifth U.S. National Conference on Earthquake Engineering, Proceedings, Earthquake Engineering Research Institute, Oakland, Calif., Vol. II, 1994, pp. 837-846.

APPENDIX A

AXIAL STATIC EXPERIMENTS

TEST REPORTS and LOAD-DISPLACEMENT PLOTS

Nominclature:

OD	pipe outside diameter
ID	pipe inside diameter
Wall thick	pipe wall thickness
Bell OD	pipe bell section outside diameter
Bell ID	pipe bell section inside diameter
Cross area	pipe section cross sectional area of material
Flow area	pipe section cross section of open area
Flange thick	flange section thickness at end of the specimen
Length (OTO)	actual overall length of the specimen, out-to-out of the end flanges
Length segment	actual length of the specimen not including the end flanges

1. Cast Iron Pipe with Lead Caulked Joint .

Material	cast iron
Nominal dia.	200 mm (8”)
Joint type	bell-spigot, lead caulked
Material Characteristics	cast iron pipe with lead caulked joint (in-service segment)
Ultimate stress	552 MPa compression
Modulus	96530 MPa
Cross-Sectional Dimensions	
OD	229 mm
ID	203 mm
Wall thick	12.7 mm
Bell OD	305 mm
Bell ID	229 mm
Bell thick	38.1 mm
Cross Area	8579 sq.mm
Flow area	32424 sq.mm
Flange thick	3.175 cm
Length (OTO)	61 cm
Length segment	54.65 cm
Loading	compression only (incremental displacement control)
Ultimate Load	2046 kN
Ultimate Disp	2.6 cm
Failure mechanism	fracture of barrel toward segment end

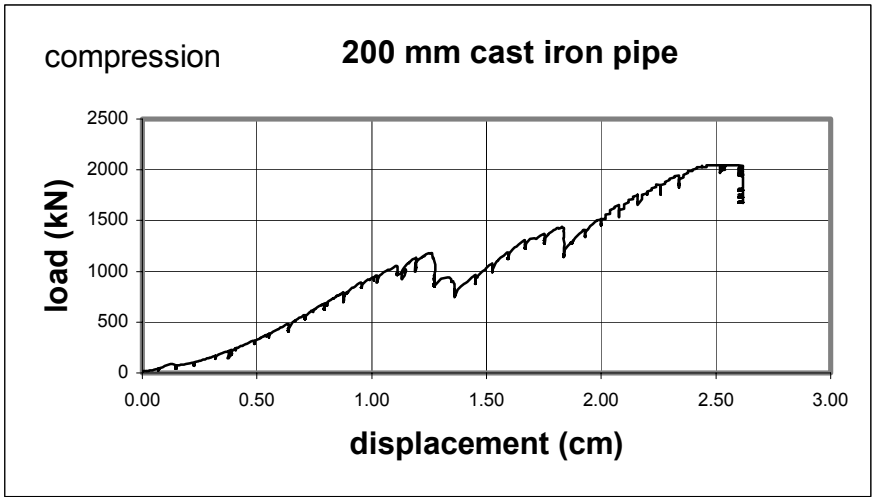

Figure A-1 Load-Displacement Plot for 200 mm Cast Iron Pipe

2. Ductile Iron Pipe with Push-On Rubber Gasket Joint

Material	ductile iron
Nominal dia.	100 mm (4”)
Joint type	push-on bell-spigot, rubber gasket
Material Characteristics	ductile iron pipe with push-on rubber gasket joint
Yield stress	310 MPa
Modulus	165480 MPa
Cross-Sectional Dimensions	
ID	109.2 mm
OD	121.9 mm
Wall thick	6.35 mm
Bell OD	179.1 mm
Bell ID	146.1 mm
Bell thick	16.5 mm
Cross Area	2302 sq.mm
Flow area	9365 sq.mm
Flange thick	none
Length (OTO)	61.0 cm
Length segment	61.0 cm
Loading	compression only (incremental load control)
Ultimate Load	792 kN
Ultimate Disp	.41 cm
Failure mechanism	telescoping of spigot into bell; fracture and buckling of spigot end

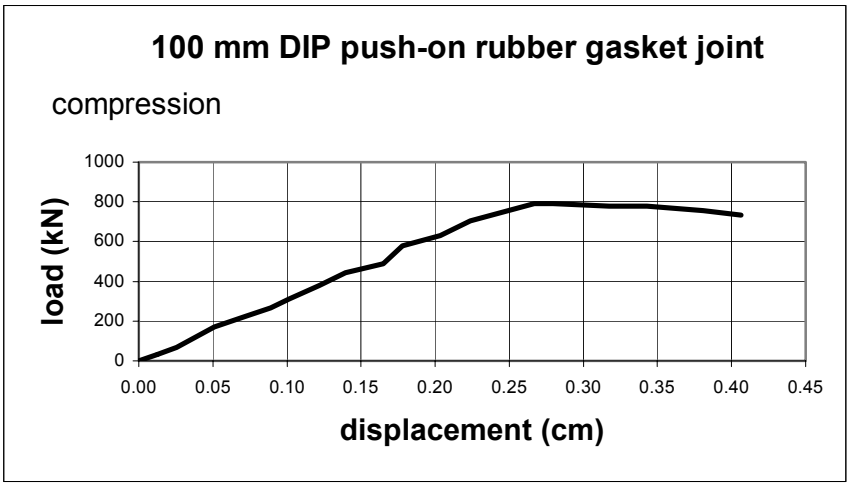

Figure A-2 Load-Displacement for 100 mm DIP with Push-On Rubber Gasket Joint

3. Ductile Iron Pipe with Push-On Rubber Gasket Joint

Material	ductile iron
Nominal dia.	150 mm (6”)
Joint type	push-on bell-spigot, rubber gasket
Material Characteristics	ductile iron pipe with push-on rubber gasket joint
Yield stress	310 MPa
Modulus	165480 MPa
Cross-Sectional Dimensions	
ID	162.6 mm
OD	175.3 mm
Wall thick	6.35 mm
Bell OD	235.0 mm
Bell ID	199.4 mm
Bell thick	17.8 mm
Cross Area	3367 sq.mm
Flow area	20750 sq.mm
Flange thick	2.54 cm
Flange thick	none
Length (OTO)	61.0 cm
Length segment	61.0 cm
Loading	compression only (incremental load control)
Ultimate Load	1054 kN
Ultimate Disp	.46 cm
Failure mechanism	telescoping of spigot into bell; fracture and buckling of spigot end

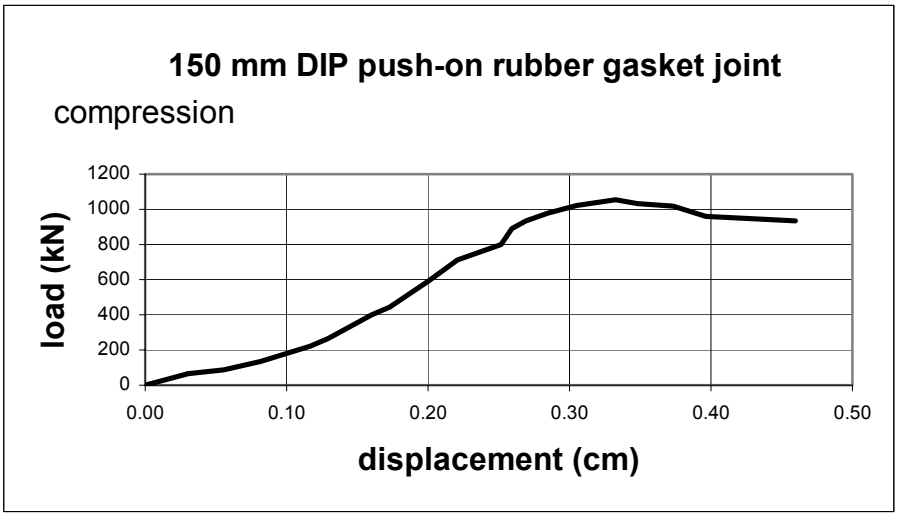

Figure A-3 Load-Displacement for 150 mm DIP with Push-On Rubber Gasket Joint

4. Ductile Iron Pipe with Push-On Rubber Gasket Joint

Material Characteristics	ductile iron
Nominal dia.	200 mm (8”)
Joint type	push-on bell-spigot, rubber gasket

Material Characteristics	ductile iron pipe with push-on rubber gasket joint
Yield stress	310 MPa
Modulus	165480 MPa

Cross-Sectional Dimensions

ID	217.2 mm
OD	229.9 mm
Wall thick	6.35 mm
Bell OD	296.7 mm
Bell ID	258.6 mm
Bell thick	19.1 mm
Cross Area	4457 sq.mm
Flow area	37029 sq.mm
Flange thick	none
Length (OTO)	61.0 cm
Length segment	61.0 cm

Loading	compression only (incremental load control)
Ultimate Load	1112 kN
Ultimate Disp	.84 cm
Failure mechanism	telescoping of spigot into bell; fracture and buckling of spigot end

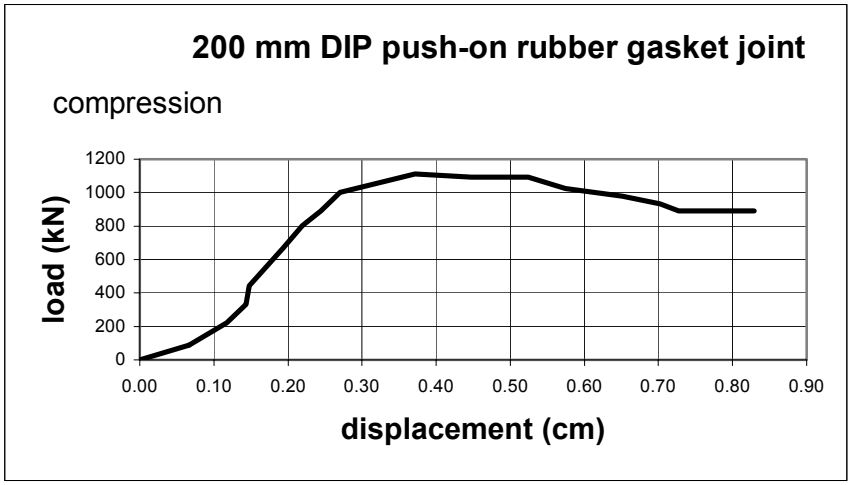

Figure A-4 Load-Displacement for 200 mm DIP with Push-On Rubber Gasket Joint

5. Ductile Iron Pipe with Push-On Rubber Gasket Joint

Material	ductile iron
Nominal dia.	250 mm (10”)
Joint type	push-on bell-spigot, rubber gasket
Material Characteristics	ductile iron pipe with push-on rubber gasket joint
Yield stress	310 MPa
Modulus	165480 MPa
Cross-Sectional Dimensions	
ID	269.2 mm
OD	281.9 mm
Wall thick	6.35 mm
Bell OD	351.3 mm
Bell ID	310.6 mm
Bell thick	20.3 mm
Cross Area	5708 sq.mm
Flow area	56702 sq.mm
Flange thick	none
Length (OTO)	61.0 cm
Length segment	61.0 cm
Loading	compression only (incremental load control)
Ultimate Load	1557 kN
Ultimate Disp	.48 cm
Failure mechanism	telescoping of spigot into bell; fracture and buckling of spigot end

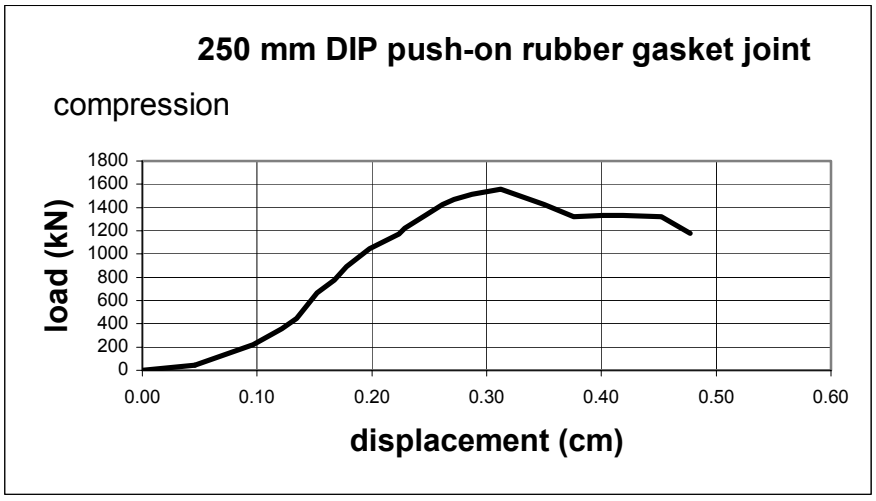

Figure A-5 Load-Displacement for 250 mm DIP with Push-on Rubber Gasket Joint

6. Ductile Iron Pipe with Gripper Gasket

Material	ductile iron
Nominal dia.	150 mm (6”)
Joint type	bell-spigot; gripper gasket
Material Characteristics	ductile iron pipe with gripper gasket
Yield stress	310 MPa
Modulus	165480 MPa
Cross-Sectional Dimensions	
ID	162.6 mm
OD	175.3 mm
Wall thick	6.35 mm
Bell OD	235.0 mm
Bell ID	199.4 mm
Bell thick	17.8 mm
Cross Area	3367 sq.mm
Flow area	20750 sq.mm
Flange thick	2.54 cm
Length (OTO)	61.9 cm
Length segment	56.83 cm
Loading	tension only (incremental displacement control)
Ultimate Load	253 kN
Ultimate Disp	8.44 cm
Failure mechanism	failure of metal teeth

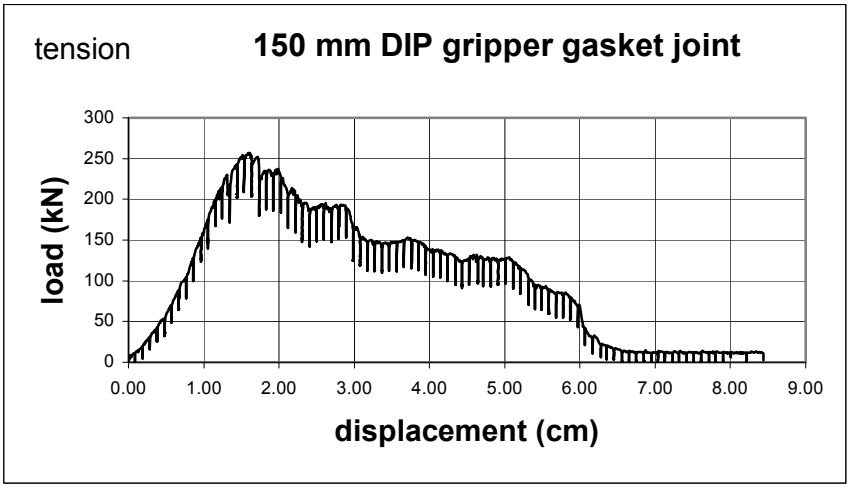

Figure A-6 Load-Displacement for 150 mm DIP with Gripper Gasket Joint

7. Ductile Iron Pipe with Gripper Gasket

Material	ductile iron
Nominal dia.	200 mm (8")
Joint type	bell-spigot; gripper gasket
Material Characteristics	ductile iron pipe with gripper gasket
Yield stress	310 MPa
Modulus	165480 MPa
Cross-Sectional Dimensions	
ID	217.2 mm
OD	229.9 mm
Wall thick	6.35 mm
Bell OD	296.7 mm
Bell ID	258.6 mm
Bell thick	19.1 mm
Cross Area	4457 sq.mm
Flow area	37029 sq.mm
Flange thick	2.54 cm
Length (OTO)	61.0 cm
Length segment	55.88 cm
Loading	tension only (incremental displacement control)
Ultimate Load	539 kN
Ultimate Disp	4.70 cm
Failure mechanism	failure of metal teeth

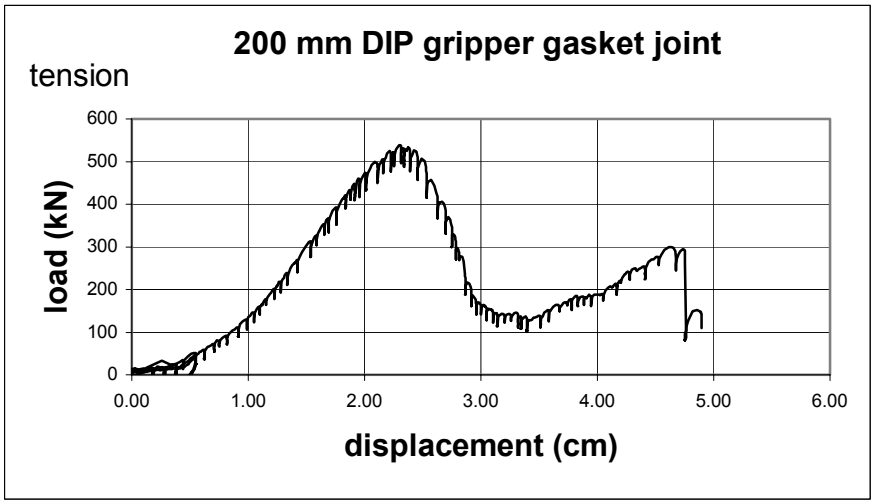

Figure A-7 Load-Displacement for 200 mm DIP with Gripper Gasket Joint

8. Ductile Iron Pipe with Gripper Gasket

Material	ductile iron
Nominal dia.	300 mm (12”)
Joint type	bell-spigot; gripper gasket
Material Characteristics	ductile iron pipe with gripper gasket
Yield stress	310 MPa
Modulus	165480 MPa
Cross-Sectional Dimensions	
OD	335 mm
ID	3211 mm
Wall thick	7.11 mm
Bell OD	414 mm
Bell ID	364 mm
Bell	22 mm
Cross Area	7335 sq.mm
Flow area	80955 sq.mm
Flange thick	2.54 cm
Length (OTO)	62 cm
Length segment	56.83 cm
Loading	tension only (incremental displacement control)
Ultimate Load	488 kN
Ultimate Disp	1.88 cm
Failure mechanism	failure of metal teeth

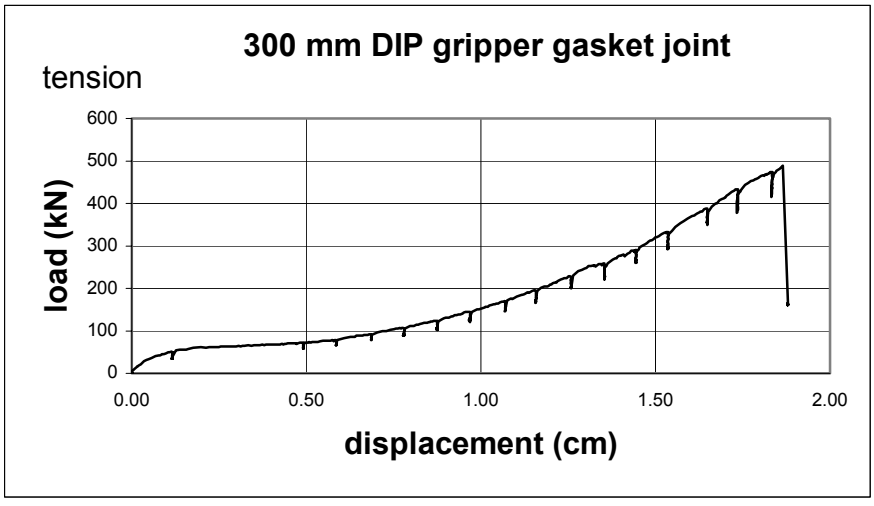

Figure A-8 Load-Displacement for 300 mm DIP with Gripper Gasket Joint

9. Ductile Iron Pipe with Retaining Ring Joint

Material	ductile iron
Nominal dia.	150 mm (6”)
Joint type	bell and spigot; retaining ring
Material Characteristics	ductile iron pipe with retaining ring joint
Yield stress	310 MPa
Modulus	165480 MPa
Cross-Sectional Dimensions	
ID	162.6 mm
OD	175.3 mm
Wall thick	6.35 mm
Bell OD	235.0 mm
Bell ID	199.4 mm
Bell thick	17.8 mm
Cross Area	3367 sq.mm
Flow area	20750 sq.mm
Flange thick	2.54 cm
Length (OTO)	67.31 cm
Length segment	64.77 cm
Loading	compression only (incremental displacement control)
Ultimate Load	538 MPa compression
Ultimate Disp	1.17 cm compression
Failure mechanism	block shear at bell

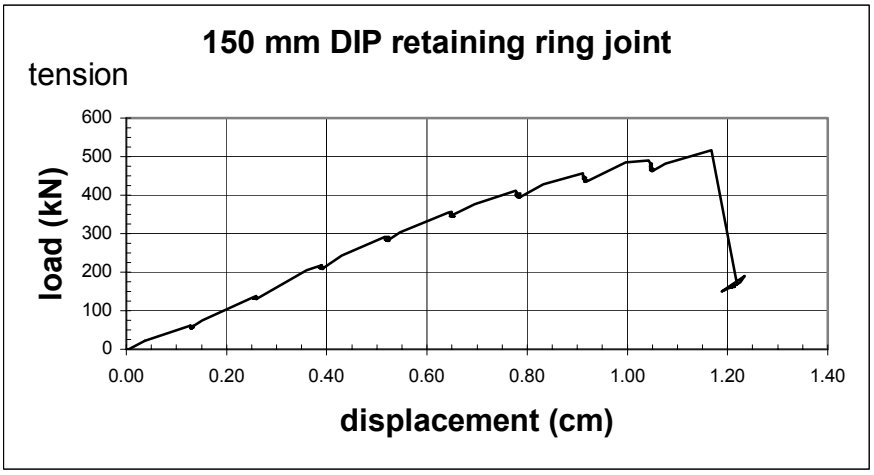

Figure A-9 Load-Displacement for 150 mm DIP with Retaining Ring Joint

10. Ductile Iron Pipe with Retaining Ring Joint

Material	ductile iron
Nominal dia.	200 mm (8”)
Joint type	bell and spigot; retaining ring
Material Characteristics	ductile iron pipe with retaining ring joint
Yield stress	310 MPa
Modulus	165480 MPa
Cross-Sectional Dimensions	
ID	217.2 mm
OD	229.9 mm
Wall thick	6.35 mm
Bell OD	296.7 mm
Bell ID	258.6 mm
Bell thick	19.1 mm
Cross Area	4457 sq.mm
Flow area	37029 sq.mm
Flange thick	2.54 cm
Length (OTO)	67.31 cm
Length segment	62.23 cm
Loading	compression only (incremental displacement control)
Ultimate Load	795 MPa compression
Ultimate Disp	2.89 cm compression
Failure mechanism	fracture in bell

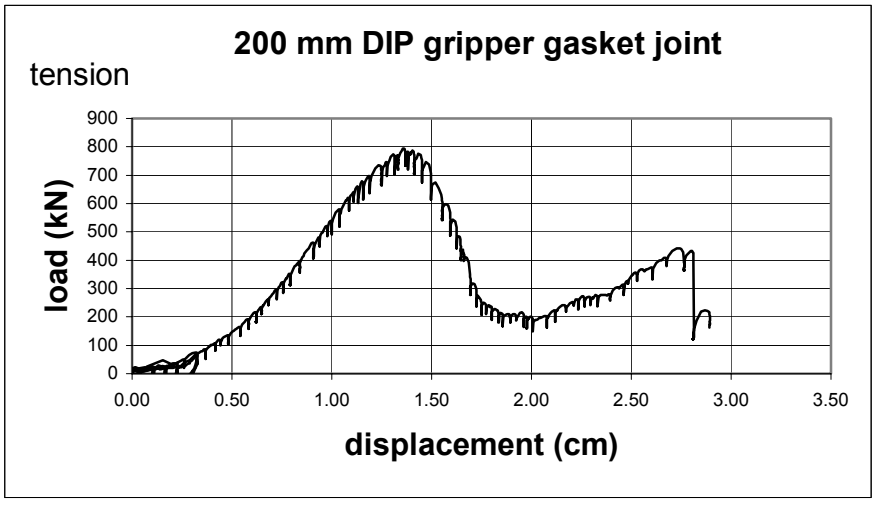

Figure A-10 Load-Displacement for 200 mm DIP with Retaining Ring Joint

11. Ductile Iron Pipe with Retaining Ring Joint

Material	ductile iron
Nominal dia.	300 mm (12”)
Joint type	bell and spigot; retaining ring
Material Characteristics	ductile iron pipe with retaining ring joint
Yield stress	310 MPa
Modulus	165480 MPa
Cross-Sectional Dimensions	
OD	335 mm
ID	3211 mm
Wall thick	7.11 mm
Bell OD	414 mm
Bell ID	364 mm
Bell	22 mm
Cross Area	7335 sq.mm
Flow area	80955 sq.mm
Flange thick	2.54 cm
Length (OTO)	67.31 cm
Length segment	62.23 cm
Loading	compression only (incremental displacement control)
Ultimate Load	750 compression
Ultimate Disp	2.39 cm compression
Failure mechanism	fracture in bell

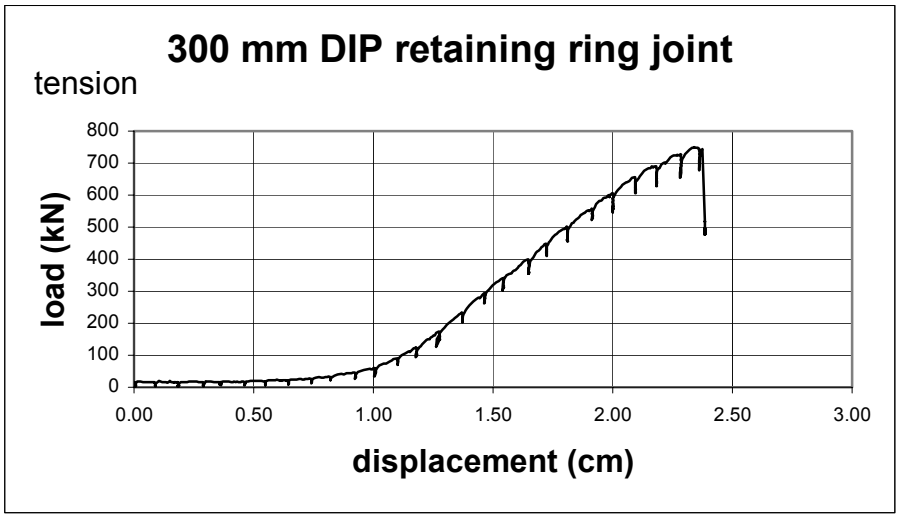

Figure A-11 Load-Displacement for 300 mm DIP with Retaining Ring Joint

12. Ductile Iron Pipe with Bolted Collar Joint

Material	ductile iron
Nominal dia.	150 mm (6”)
Joint type	bell-spigot, bolted collar
Material Characteristics	ductile iron pipe with bolted collar joint
Yield stress	310 MPa
Modulus	165480 MPa
Cross-Sectional Dimensions	
ID	162.6 mm
OD	175.3 mm
Wall thick	6.35 mm
Bell OD	235.0 mm
Bell ID	199.4 mm
Bell thick	17.8 mm
Cross Area	3367 sq.mm
Flow area	20750 sq.mm
Flange thick	2.54 cm
Length (OTO)	61.0 cm
Length segment	55.9 cm
Loading	tension only (incremental displacement control)
Ultimate Load	195 kN
Ultimate Disp	2.9 cm
Failure mechanism	failure of cast iron collar at wedge screw hole

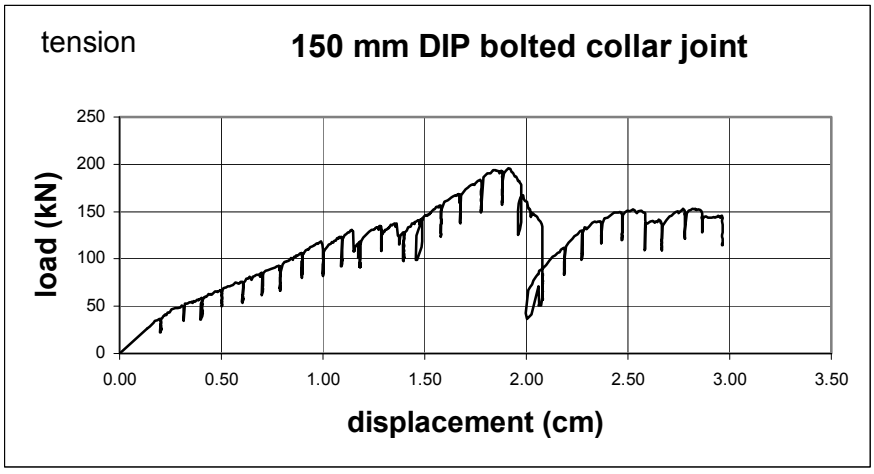

Figure A-12 Load-Displacement for 150 mm DIP with Bolted Collar Joint

13. Ductile Iron Pipe with Bolted Collar Joint

Material	ductile iron
Nominal dia.	200 mm (8”)
Joint type	bell-spigot, bolted collar restrained joint
Material Characteristics	ductile iron pipe with bolted collar joint
Yield stress	310 MPa
Modulus	165480 MPa
Cross-Sectional Dimensions	
ID	217.2 mm
OD	229.9 mm
Wall thick	6.35 mm
Bell OD	296.7 mm
Bell ID	258.6 mm
Bell thick	19.1 mm
Cross Area	4457 sq.mm
Flow area	37029 sq.mm
Flange thick	2.54 cm
Length (OTO)	61.0 cm
Length segment	55.9 cm
Loading	tension only (incremental displacement control)
Ultimate Load	280 kN
Ultimate Disp	4.95 cm in
Failure mechanism	failure of cast iron collar at wedge screw hole

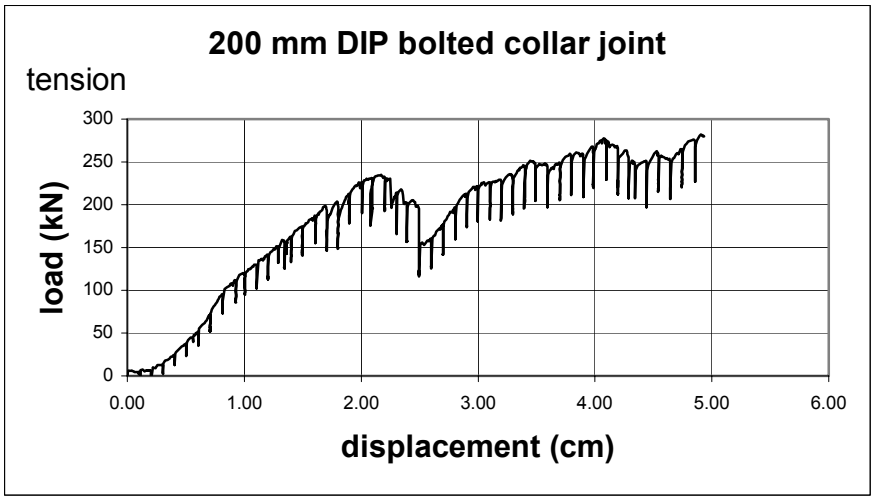

Figure A-13 Load-Displacement for 200 mm DIP with Bolted Collar Joint

14. Steel Pipe with Lap-Welded Joint

Material	steel
Nominal dia.	100 mm (4”)
Joint type	bell-spigot; lap-welded
Material Characteristics	steel pipe with lap-welded joint C-200 Grade A A53
Yield stress	207 MPa
Modulus	200000 MPa
Cross-Sectional Dimensions	
OD	108 mm
ID	102 mm
Wall thick	3.40 mm (10ga.)
Bell OD	108 mm
Bell ID	102 mm
Bell thick	3.40 mm (10ga.)
Cross Area	1109 sq.mm
Flow area	8108 sq.mm
Flange thick	1.91 cm
Length (OTO)	49.53 cm
Length segment	45.71 cm
Loading	bi-directional (incremental alternating displacement control)
Ultimate Load	536 kN compression; 522 kN tension
Ultimate Disp	1.13 cm. compression; 1.29 cm tension
Failure mechanism	fracture in tension in spigot end behind weld

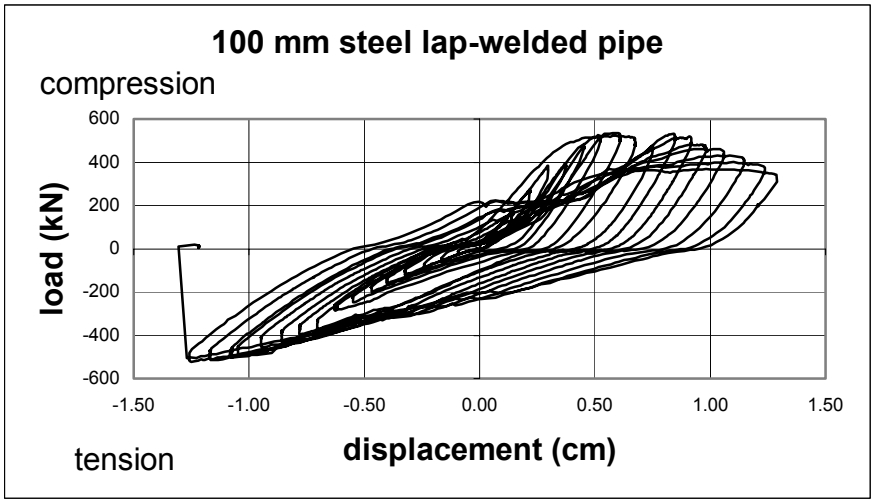

Figure A-14 Load-Displacement for 100 mm Steel Lap-Welded Pipe

15. Steel Pipe with Lap-Welded Joint

Material	steel
Nominal dia.	150 mm (6”)
Joint type	bell-spigot; lap-welded
Material Characteristics	steel pipe with lap-welded joint C-200 Grade A A53
Yield stress	207 MPa
Modulus	200000 MPa
Cross-Sectional Dimensions	
OD	159 mm
ID	152 mm
Wall thick	3.40 mm (10ga.)
Bell OD	159 mm
Bell ID	152 mm
Bell thick	3.40 mm (10ga.)
Cross Area	1664 sq.mm
Flow area	18234 sq.mm
Flange thick	1.9 mm
Length (OTO)	47.3 mm
Length segment	43.51 cm
Loading	bi-directional (incremental alternating displacement control)
Ultimate Load	491 kN compression; 554 kN tension
Ultimate Disp	1.19 cm. compression; 1.17 cm tension
Failure mechanism	fracture in tension in spigot end behind weld

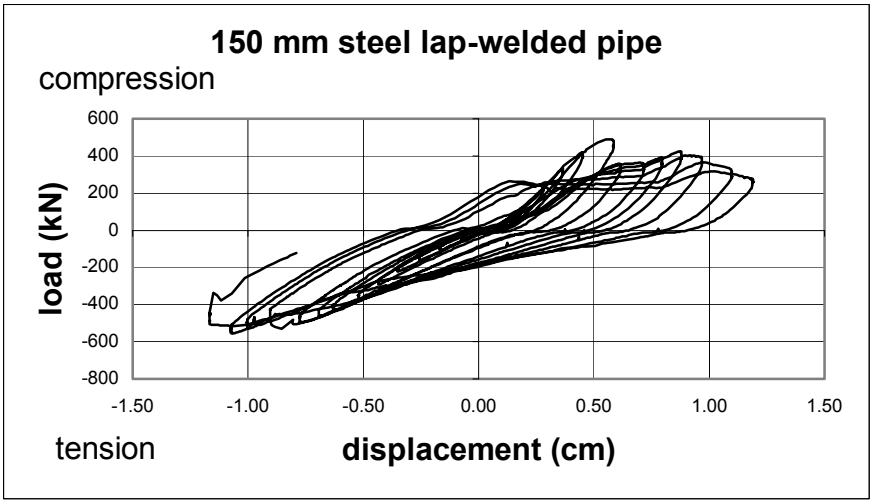

Figure A-15 Load-Displacement for 150 mm Steel Lap-Welded Pipe

16. Steel Pipe with Lap-Welded Joint

Material	steel
Nominal dia.	200 mm (8”)
Joint type	bell-spigot; lap-welded
Material Characteristics	steel pipe with lap-welded joint C-200 Grade A A53
Yield stress	207 MPa
Modulus	200000 MPa
Cross-Sectional Dimension	
OD	210 mm
ID	203 mm
Wall thick	3.40 mm (10ga.)
Bell OD	210 mm
Bell ID	203 mm
Bell thick	3.40 mm (10ga.)
Cross Area	2206 sq.mm
Flow area	32424 sq.mm
Flange thick	1.9 cm
Length (OTO)	47.31 cm
Length segment	43.51 cm
Loading	bi-directional (incremental alternating displacement control)
Ultimate Load	401 kN compression; 711 kN tension
Ultimate Disp	.70 cm compression; 1.50 cm tension
Failure mechanism	fracture in tension through water inlet hole.

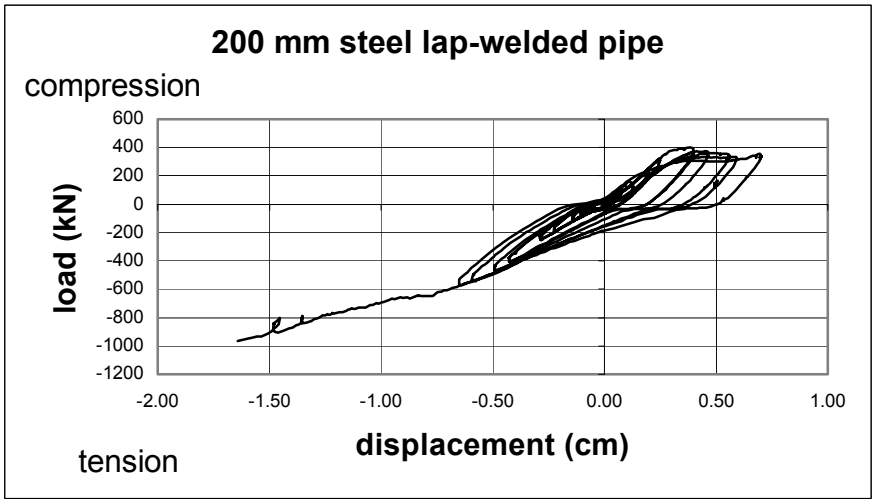

Figure A-16 Load-Displacement for 200 mm Steel Lap-Welded Pipe

17. Steel Pipe with Lap-Welded Joint

Material	steel
Nominal dia.	250 mm (10”)
Joint type	bell-spigot; lap-welded joint
Material Characteristics	steel pipe with lap-welded joint C-200 Grade A A53
Yield stress	207 MPa
Modulus	200000 MPa
Cross-Sectional Dimensions	
OD	261 mm
ID	254 mm
Wall thick	3.40 mm (10ga.)
Bell OD	261 mm
Bell ID	254 mm
Bell thick	3.40 mm (10ga.)
Cross Area	2754 sq.mm
Flow area	50658 sq.mm
Flange thick	1.9 cm
Length (OTO)	47.3 cm
Length segment	43.5 cm
Loading	bi-directional (incremental alternating displacement control)
Ultimate Load	546 kN compression; 761 kN tension
Ultimate Disp	1.3 cm compression; 1.4 cm tension
Failure mechanism	fracture in tension through water inlet hole.

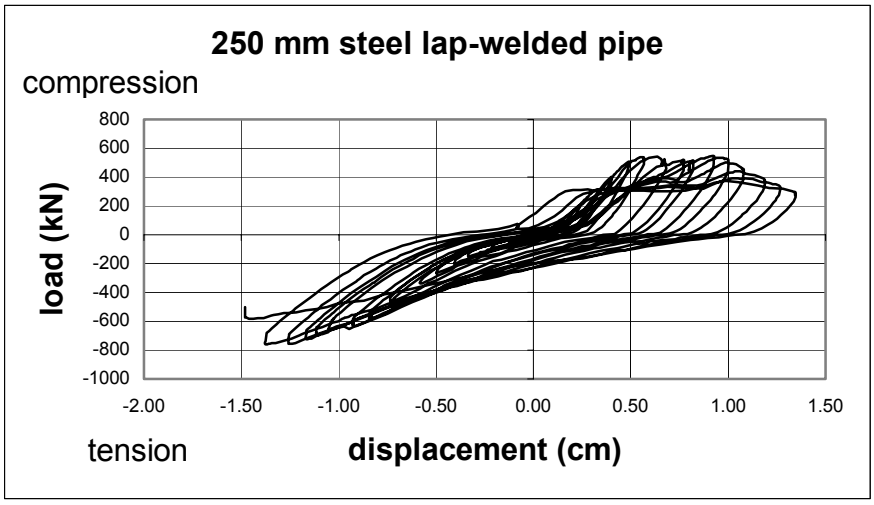

Figure A-17 Load-Displacement for 250 mm Steel Lap-Welded Pipe

18. PVC Pipe with Push-On Rubber Gasket Joint

Material	PVC
Nominal dia.	150 mm (6”)
Joint type	push-on bell-spigot; rubber gask**et**
Material Characteristics	PVC pipe with push-on rubber gasket joint C-900
Yield stress	41 MPa
Modulus	2100 MPa
Cross-Sectional Dimensions	
OD	175 mm
ID	152 mm
Wall thick	11.4 mm
Bell OD	251 mm
Bell ID	178 mm
Bell thick	36.6 mm
Cross Area	5882 sq.mm
Flow area	18241 sq.mm
Flange thick	none
Length (OTO)	61 cm
Length segment	61 cm
Loading	compression only (incremental displacement control)
Ultimate Load	15 kN compression
Ultimate Disp	10 cm
Failure mechanism	no observable failure; spigot end extruded into the bell end

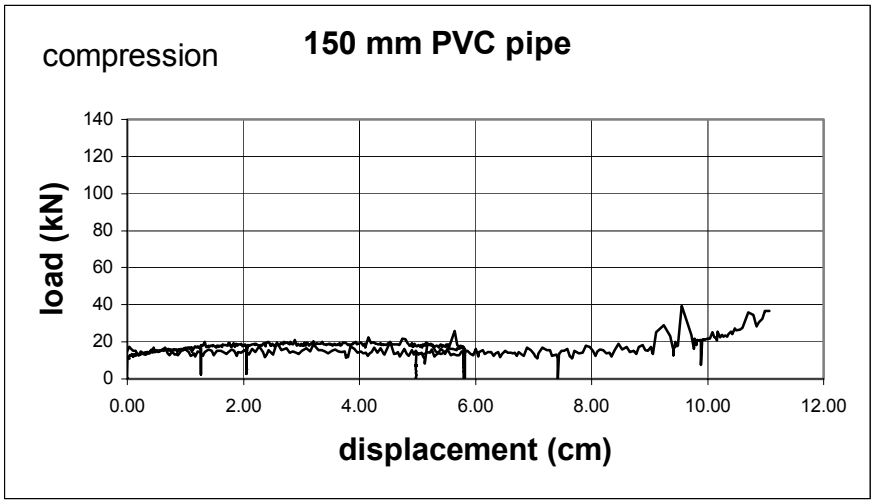

Figure A-18 Load-Displacement for 150 mm PVC Pipe

19. PVC Pipe with Push-On Rubber Gasket Joint

Material	PVC
Nominal dia.	200 mm (8”)
Joint type	push-on bell-spigot; rubber gask**et**
Material Characteristics	PVC pipe with push-on rubber gasket joint C-900
Yield stress	41MPa
Modulus	2100 MPa
Cross-Sectional Dimensions	
OD	229 mm
ID	203 mm
Wall thick	12.7 mm
Bell OD	305 mm
Bell ID	229 mm
Bell thick	36.6 mm
Cross Area	8611 sq.mm
Flow area	32424 sq.mm
Flange thick	none
Length (OTO)	50.5 cm
Length segment	50.5 cm
Loading	compression only (incremental displacement control)
Ultimate Load	13 kN compression
Ultimate Disp	12 cm
Failure mechanism	no observable failure; spigot end extruded into the bell end

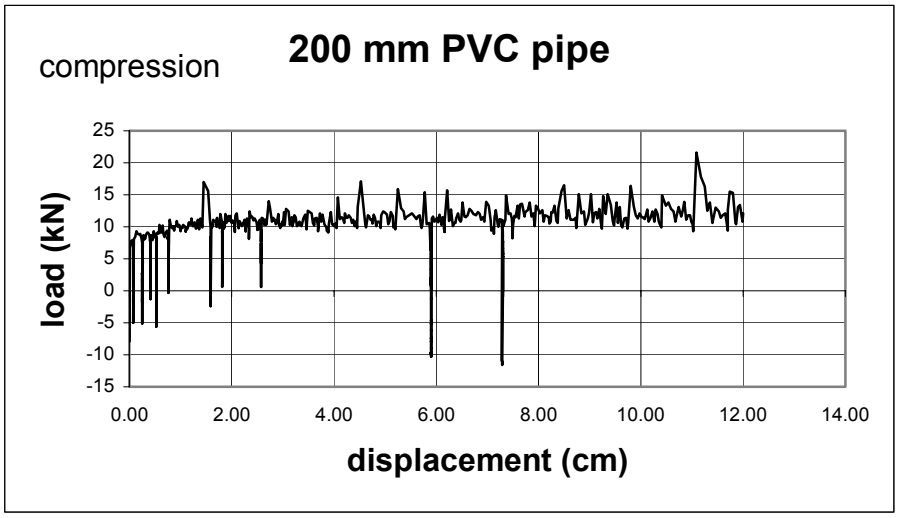

Figure A-19 Load-Displacement for 200 mm PVC Pipe

20. PVC Pipe with Push-On Rubber Gasket Joint

Material	PVC
Nominal dia.	300 mm (12”)
Joint type	push-on bell-spigot; rubber gask**et**
Material Characteristics	PVC pipe with push-on rubber gasket joint C-900
Yield stress	41MPa
Modulus	2100 MPa
Cross-Sectional Dimensions	
OD	335 mm
ID	305 mm
Wall thick	15.2 mm
Bell OD	406 mm
Bell ID	330 mm
Bell thick	38.1 mm
Cross Area	15319 sq.mm
Flow area	72950 sq. mm
Flange thick	none
Length (OTO)	61 mm
Length segment	61 mm
Loading	compression only (incremental displacement control)
Ultimate Load	6 kN compression
Ultimate Disp	6 cm
Failure mechanism	no observable failure; spigot end extruded into the bell end

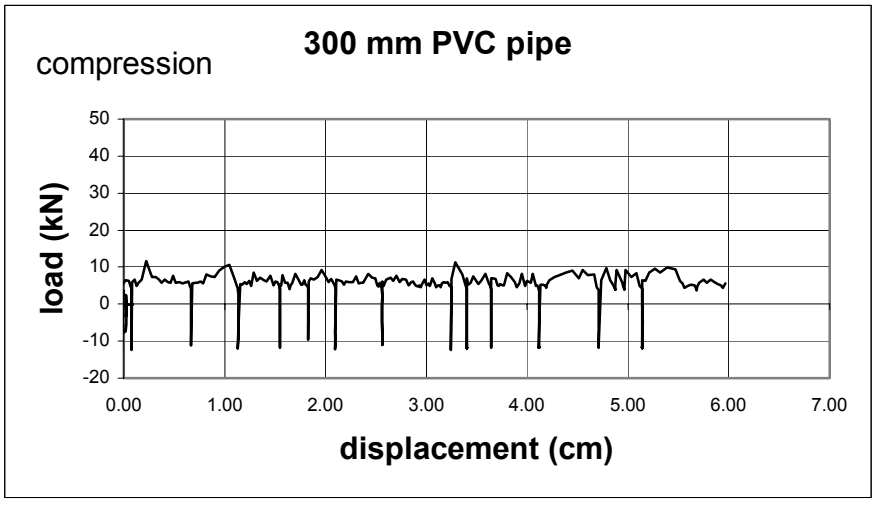

Figure A-20 Load-Displacement for 300 mm PVC Pipe

21. PE Pipe with Butt-Fused Joint

Material	PE polyethylene, high-density
Nominal dia.	150 mm (6”)
Joint type	butt-fused joint
Material Characteristics	PE pipe with butt-fused joint C-906
Yield stress	17 MPa
Modulus	827 MPa
Cross-Sectional Dimensions	
OD	178 mm
ID	152 mm
Wall thick	12.7 mm
Bell OD	178 mm
Bell ID	152 mm
Bell thick	12.7 mm
Cross Area	6585 sq.mm
Flow area	18234 sq.mm
Flange thick	none
Length (OTO)	61 mm
Length segment	61 mm
Loading	bi-directional (incremental alternating displacement control)
Ultimate Load	186 kN compression; 157 kN tension
Ultimate Disp	5.7 cm compression; 7.4 cm tension
Failure mechanism	fracture of the pipe at its end flange

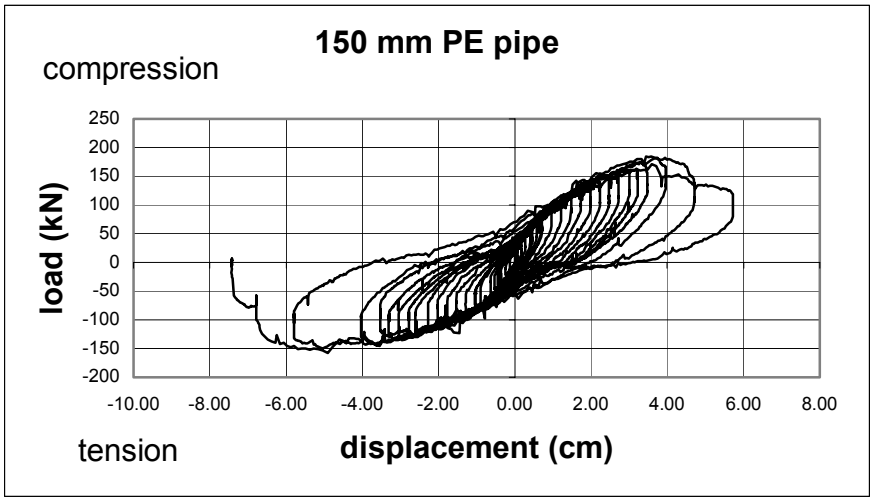

Figure A-21 Load-Displacement for 150 mm PE Pipe

22. PE Pipe with Butt-Fused Joint

Material	PE polyethylene, high-density
Nominal dia.	200 mm (8")
Joint type	butt-fused joint
Material Characteristics	PE pipe with butt-fused joint C-906
Yield stress	17 MPa
Modulus	827 MPa
Cross-Sectional Dimensions	
OD	229 mm
ID	203 mm
Wall thick	12.7 mm
Bell OD	229 mm
Bell ID	203 mm
Bell thick	12.7 mm
Cross Area	8611 sq.mm
Flow area	32424 sq.mm
Flange thick	none
Length (OTO)	61 cm
Length segment	61 cm
Loading	bi-directional (incremental alternating displacement control)
Ultimate Load	307 kN compression; 232 kN tension
Ultimate Disp	6.1 cm compression; 5.5 cm tension
Failure mechanism	fracture of the pipe at its end flange

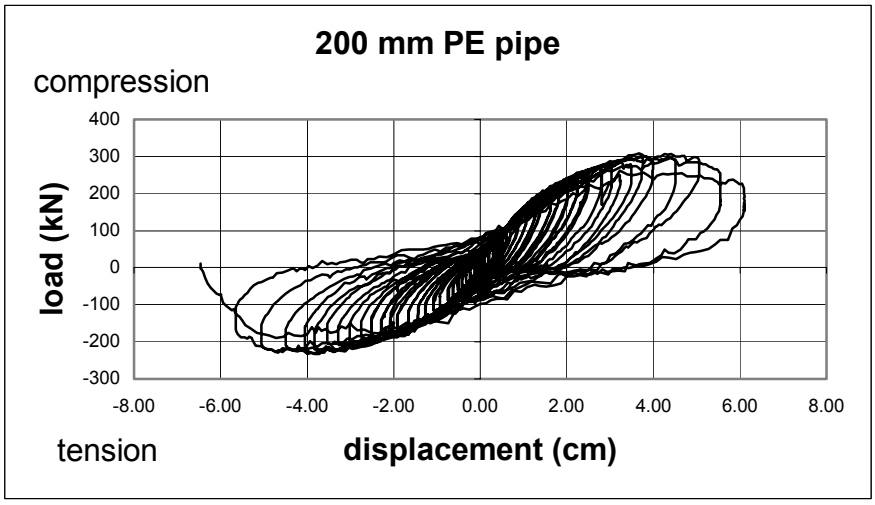

Figure A-22 Load-Displacement for 200 mm PE Pipe

APPENDIX B

AXIAL DYNAMIC EXPERIMENTS

TEST REPORTS and LOAD-DISPLACEMENT PLOTS

Nominclature:

OD	pipe outside diameter
ID	pipe inside diameter
Wall thick	pipe wall thickness
Bell OD	pipe bell section outside diameter
Bell ID	pipe bell section inside diameter
Cross area	pipe section cross sectional area of material
Flow area	pipe section cross section of open area
Flange thick	flange section thickness at end of the specimen
Length (OTO)	actual overall length of the specimen, out-to-out of the end flanges
Length segment	actual length of the specimen not including the end flanges

1. Cast Iron Pipe with Lead Caulked Joint .

Material	cast iron
Nominal dia.	200 mm (8")
Joint type	bell-spigot, lead caulked
Material Characteristics	cast iron pipe with lead caulked joint (in-service segment)
Ultimate stress	552 MPa compression
Modulus	96530 MPa
Cross-Sectional Dimensions	
OD	229 mm
ID	203 mm
Wall thick	12.7 mm
Bell OD	305 mm
Bell ID	229 mm
Bell thick	38.1 mm
Cross Area	8579 sq.mm
Flow area	32424 sq.mm
Flange thick	2.54 cm
Length (OTO)	61 cm
Length segment	55.9 cm
Loading	dynamic Arleta, Sylmar, Laholl records
Ultimate Load	549 kN compression; 108 kN tension
Ultimate Disp	.18 cm compression; 1.48 cm tension
Failure mechanism	no failure

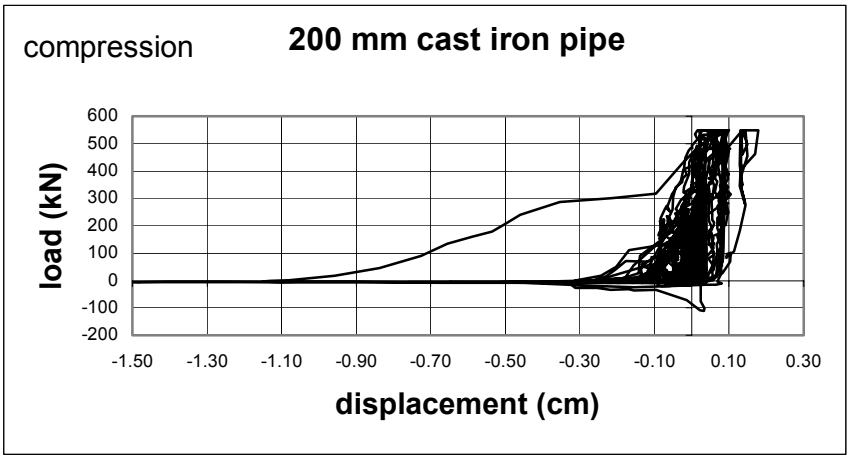

Figure B-1 Load-Displacement for 200 mm Cast Iron Pipe

2. Ductile Iron Pipe with Push-On Rubber Gasket Joint

Material	ductile iron
Nominal dia.	150 mm (6")
Joint type	push-on bell-spigot, rubber gasket
Material Characteristics	ductile iron pipe with push-on rubber gasket joint
Yield stress	310 MPa
Modulus	165480 MPa
Cross-Sectional Dimensions	
ID	162.6 mm
OD	175.3 mm
Wall thick	6.35 mm
Bell OD	235.0 mm
Bell ID	199.4 mm
Bell thick	17.8 mm
Cross Area	3367 sq.mm
Flow area	20750 sq.mm
Flange thick	2.54 cm
Flange thick	none
Length (OTO)	61.0 cm
Length segment	61.0 cm
Loading	dynamic Arleta, Sylmar, Laholl records
Ultimate Load	7 kN compression; 2.6 kN tension
Ultimate Disp	1.0 cm compression; 1.63 cm tension
Failure mechanism	no failure

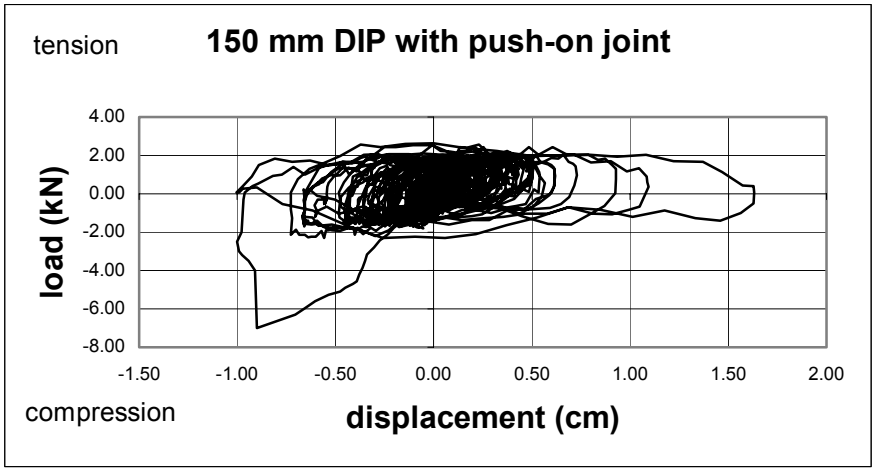

Figure B-2 Load-Displacement for 150 mm DIP with Push-On Rubber Gasket Joint

3. Ductile Iron Pipe with Push-On Rubber Gasket Joint

Material	ductile iron
Nominal dia.	200 mm (8")
Joint type	push-on bell-spigot, rubber gasket
Material Characteristics	ductile iron pipe with push-on rubber gasket joint
Yield stress	310 MPa
Modulus	165480 MPa
Cross-Sectional Dimensions	
ID	217.2 mm
OD	229.9 mm
Wall thick	6.35 mm
Bell OD	296.7 mm
Bell ID	258.6 mm
Bell thick	19.1 mm
Cross Area	4457 sq.mm
Flow area	37029 sq.mm
Flange thick	none
Length (OTO)	61.0 cm
Length segment	61.0 cm
Loading	dynamic Arleta, Sylmar, Laholl records
Ultimate Load	6.6 kN compression; 2.35 kN tension
Ultimate Disp	.9 cm compression; 1.56 cm tension
Failure mechanism	no failure

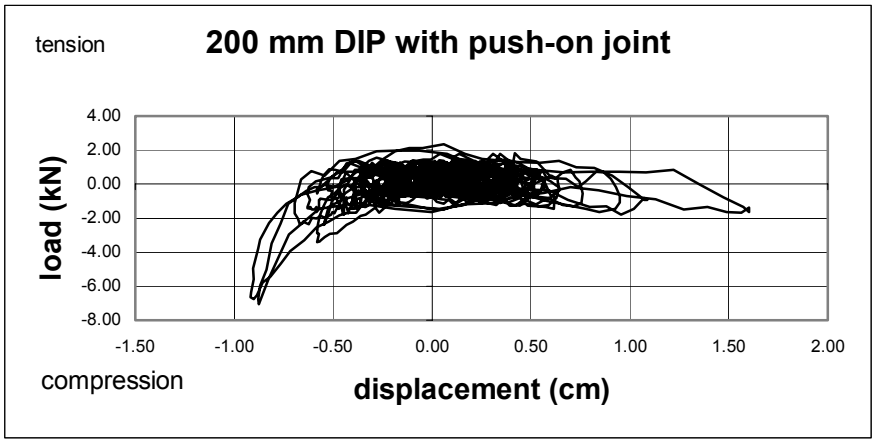

Figure B-3 Load-Displacement for 200 mm DIP with Push-On Rubber Gasket Joint

4. Ductile Iron Pipe with Gripper Gasket

Material	ductile iron
Nominal dia.	150 mm (6”)
Joint type	bell-spigot; gripper gasket
Material Characteristics	ductile iron pipe with gripper gasket
Yield stress	310 MPa
Modulus	165480 MPa
Cross-Sectional Dimensions	
ID	162.6 mm
OD	175.3 mm
Wall thick	6.35 mm
Bell OD	235.0 mm
Bell ID	199.4 mm
Bell thick	17.8 mm
Cross Area	3367 sq.mm
Flow area	20750 sq.mm
Flange thick	2.54 cm
Length (OTO)	61.9 cm
Length segment	56.83 cm
Loading	dynamic Arleta, Sylmar, Laholl records
Ultimate Load	110 kN tension; 3.0 kN compression (no compression engagement)
Ultimate Disp	.56 cm tension; .33 cm compression
Failure mechanism	fracture and dislodgement of metal teeth

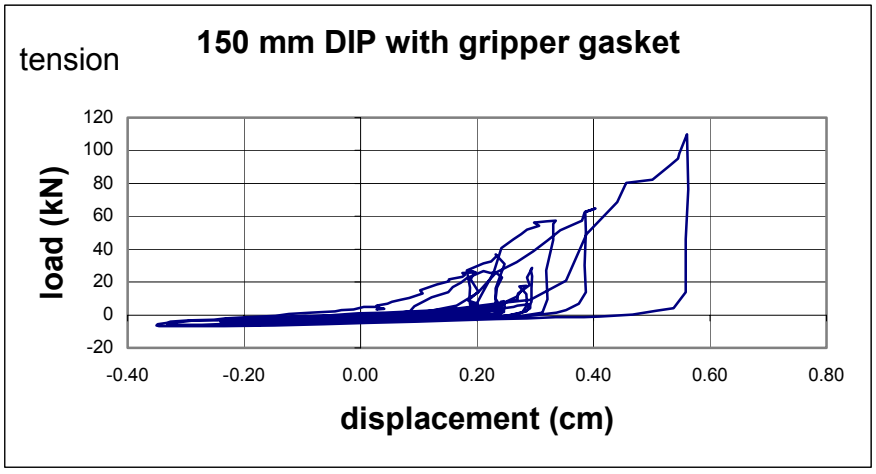

Figure B-4 Load-Displacement for 150 mm DIP with Gripper Gasket Joint

5. Ductile Iron Pipe with Gripper Gasket

Material	ductile iron
Nominal dia.	200mm (8")
Joint type	bell-spigot; gripper gasket
Material Characteristics	ductile iron pipe with gripper gasket
Yield stress	310 MPa
Modulus	165480 MPa
Cross-Sectional Dimensions	
ID	217.2 mm
OD	229.9 mm
Wall thick	6.35 mm
Bell OD	296.7 mm
Bell ID	258.6 mm
Bell thick	19.1 mm
Cross Area	4457 sq.mm
Flow area	37029 sq.mm
Flange thick	2.54 cm
Length (OTO)	61.0 cm
Length segment	55.88 cm
Loading	dynamic Arleta, Sylmar, Laholl records
Ultimate Load	343 kN tension; 171 kN compression (no compression engagement)
Ultimate Disp	2.52 cm tension; 1.78 cm compression
Failure mechanism	fracture and dislodgement of metal teeth

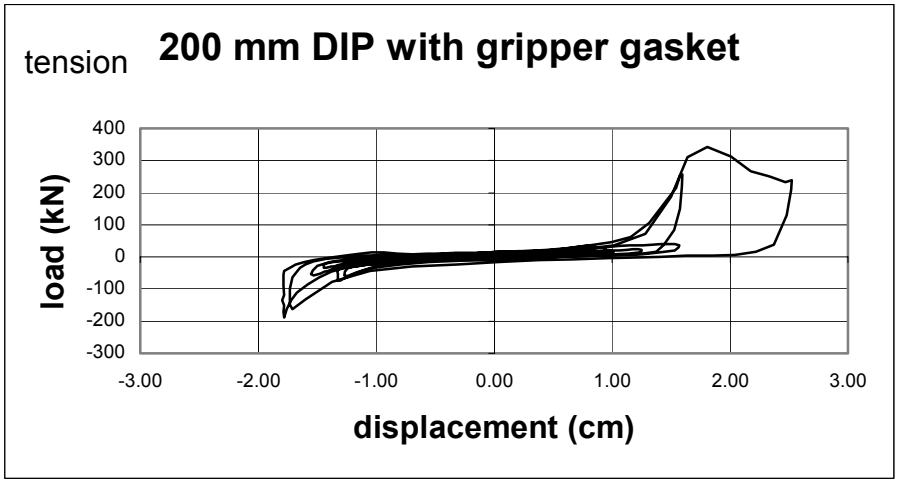

Figure B-5 Load-Displacement for 200 mm DIP with Gripper Gasket Joint

6. Ductile Iron Pipe with Retaining Ring Joint

Material	ductile iron
Nominal dia.	150 mm (6”)
Joint type	bell and spigot; retaining ring
Material Characteristics	ductile iron pipe with retaining ring joint
Yield stress	310 MPa
Modulus	165480 MPa
Cross-Sectional Dimensions	
ID	162.6 mm
OD	175.3 mm
Wall thick	6.35 mm
Bell OD	235.0 mm
Bell ID	199.4 mm
Bell thick	17.8 mm
Cross Area	3367 sq.mm
Flow area	20750 sq.mm
Flange thick	2.54 cm
Length (OTO)	67.31 cm
Length segment	64.77 cm
Loading	dynamic Arleta, Sylmar, Laholl records
Ultimate Load	441 kN tension; 1.1 kN compression
Ultimate Disp	.83 cm tension; .93 cm compression
Failure mechanism	cracking at bell

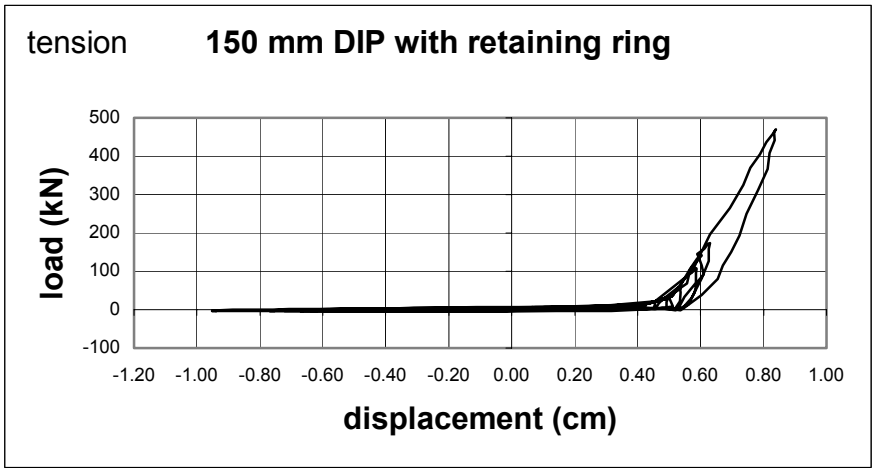

Figure B-6 Load-Displacement for 150 mm DIP with Retaining Ring Joint

7. Ductile Iron Pipe with Retaining Ring Joint

Material	ductile iron
Nominal dia.	200mm (8")
Joint type	bell and spigot, retaining ring
Material Characteristics	ductile iron pipe with retaining ring joint
Yield stress	310 MPa
Modulus	165480 MPa
Cross-Sectional Dimensions	
ID	217.2 mm
OD	229.9 mm
Wall thick	6.35 mm
Bell OD	296.7 mm
Bell ID	258.6 mm
Bell thick	19.1 mm
Cross Area	4457 sq.mm
Flow area	37029 sq.mm
Flange thick	2.54 cm
Length (OTO)	67.31 cm
Length segment	62.23 cm
Loading	dynamic Arleta, Sylmar, Laholl records
Ultimate Load	551 kN tension; 13 kN compression
Ultimate Disp	.80 cm tension; 1.01 cm compression
Failure mechanism	fracture at the bell

.

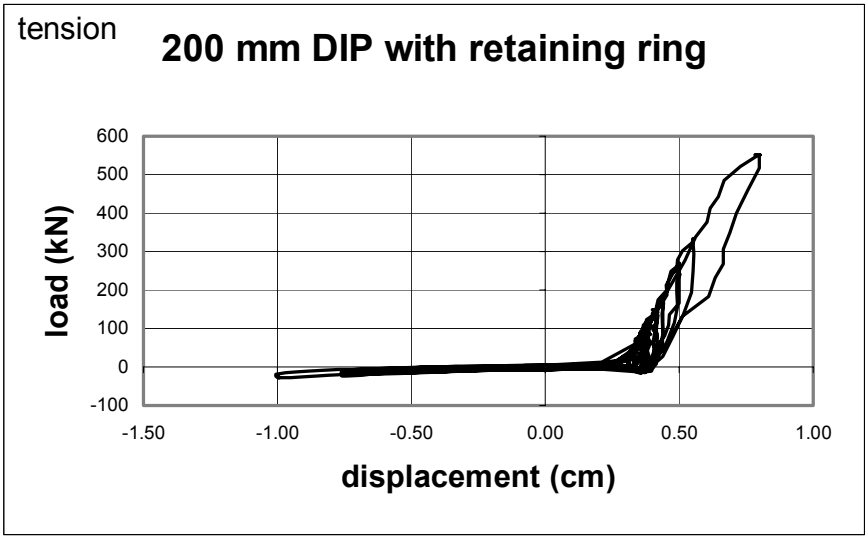

Figure B-7 Load-Displacement for 200 mm DIP with Retaining Ring Joint

8. Ductile Iron Pipe with Bolted Collar Joint

Material	ductile iron
Nominal dia.	150 mm (6”)
Joint type	bell-spigot, bolted collar
Material Characteristics	ductile iron pipe with bolted collar joint
Yield stress	310 MPa
Modulus	165480 MPa
Cross-Sectional Dimensions	
ID	162.6 mm
OD	175.3 mm
Wall thick	6.35 mm
Bell OD	235.0 mm
Bell ID	199.4 mm
Bell thick	17.8 mm
Cross Area	3367 sq.mm
Flow area	20750 sq.mm
Flange thick	2.54 cm
Length (OTO)	61.0 cm
Length segment	55.9 cm
Loading	dynamic Arleta, Sylmar, Laholl records
Ultimate Load	201 kN tension; 3.1 kN compression
Ultimate Disp	2.53 cm tension; 1.7 cm compression
Failure mechanism	fracture at the wedge screw holes

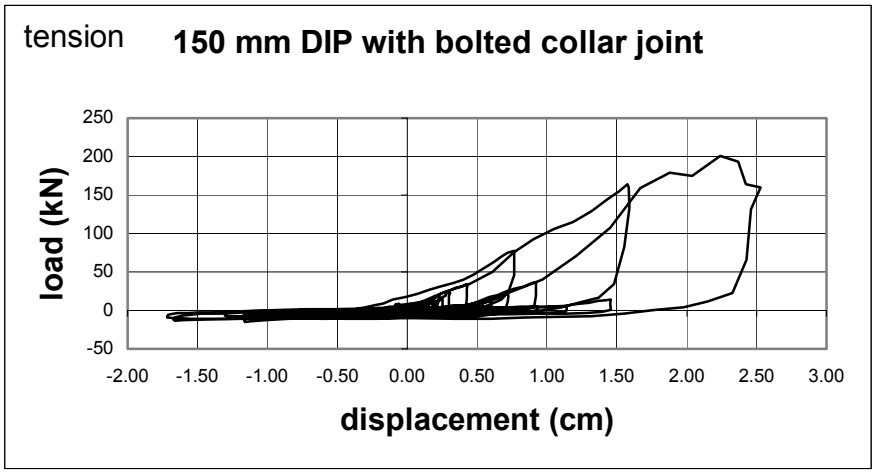

Figure B-8 Load-Displacement for 150 mm DIP with Bolted Collar Joint

9. Ductile Iron Pipe with Bolted Collar Joint

Material	ductile iron
Nominal dia.	200 mm (8”)
Joint type	bell-spigot, bolted collar restrained joint
Material Characteristics	ductile iron pipe with bolted collar joint
Yield stress	310 MPa
Modulus	165480 MPa
Cross-Sectional Dimensions	
ID	217.2 mm
OD	229.9 mm
Wall thick	6.35 mm
Bell OD	296.7 mm
Bell ID	258.6 mm
Bell thick	19.1 mm
Cross Area	4457 sq.mm
Flow area	37029 sq.mm
Flange thick	2.54 cm
Length (OTO)	61.0 cm
Length segment	55.9 cm
Loading	dynamic Arleta, Sylmar, Laholl records
Ultimate Load	212 kN tension; 23.5 kN compression
Ultimate Disp	1.23 cm tension; 1.0 cm compression
Failure mechanism	fracture at the wedge screw holes

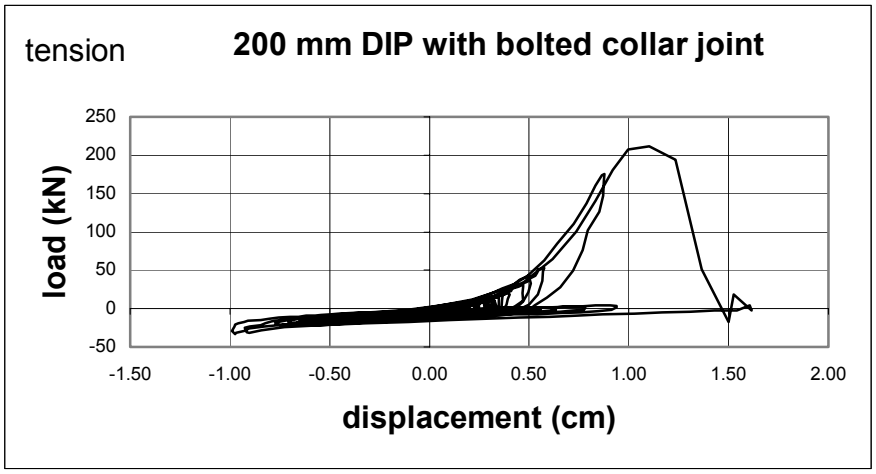

Figure B-9 Load-Displacement for 200 mm DIP with Bolted Collar Joint

10. Steel Pipe with Lap-Welded Joint

Material	steel
Nominal dia.	150 mm (6”)
Joint type	bell-spigot; lap-welded
Material Characteristics	steel pipe with lap-welded joint C-200 Grade A A53
Yield stress	207 MPa
Modulus	200000 MPa
Cross-Sectional Dimensions	
OD	159 mm
ID	152 mm
Wall thick	3.40 mm (10ga.)
Bell OD	159 mm
Bell ID	152 mm
Bell thick	3.40 mm (10ga.)
Cross Area	1664 sq.mm
Flow area	18234 sq.mm
Flange thick	1.9 mm
Length (OTO)	47.3 mm
Length segment	43.51 cm
Loading	dynamic Arleta, Sylmar, Laholl records
Ultimate Load	472 kN tension; 516 kN compression
Ultimate Disp	.9 cm tension; .71 cm compression
Failure mechanism	no failure

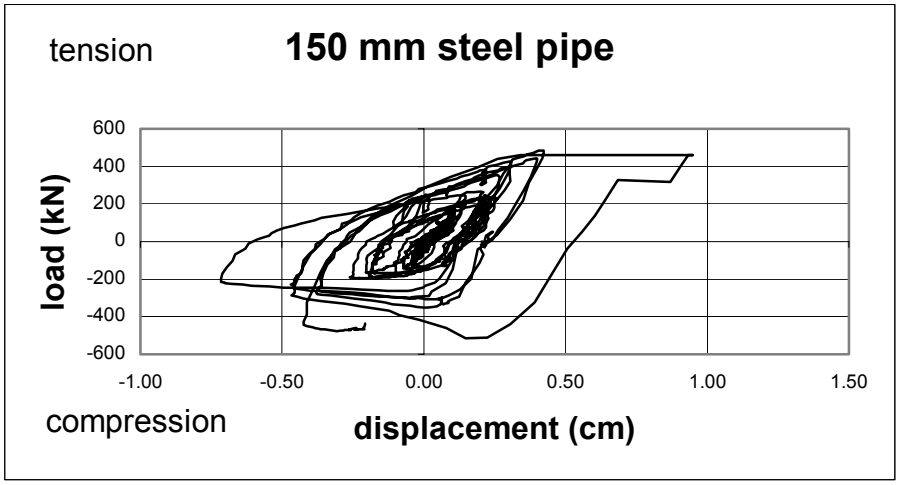

Figure B-10 Load-Displacement for 150 mm Steel Pipe

11. Steel Pipe with Lap-Welded Joint

Material	steel
Nominal dia.	200mm (8")
Joint type	bell-spigot; lap-welded
Material Characteristics	steel pipe with lap-welded joint C-200 Grade A A53
Yield stress	207 MPa
Modulus	200000 MPa
Cross-Sectional Dimensions	
OD	210 mm
ID	203 mm
Wall thick	3.40 mm (10ga.)
Bell OD	210 mm
Bell ID	203 mm
Bell thick	3.40 mm (10ga.)
Cross Area	2206 sq.mm
Flow area	32424 sq.mm
Flange thick	1.9 cm
Length (OTO)	47.31 cm
Length segment	43.51 cm
Loading	dynamic Arleta, Sylmar, Laholl records
Ultimate Load	551 kN tension; 558 kN compression
Ultimate Disp	.29 cm tension; .11 cm compression
Failure mechanism	no failure

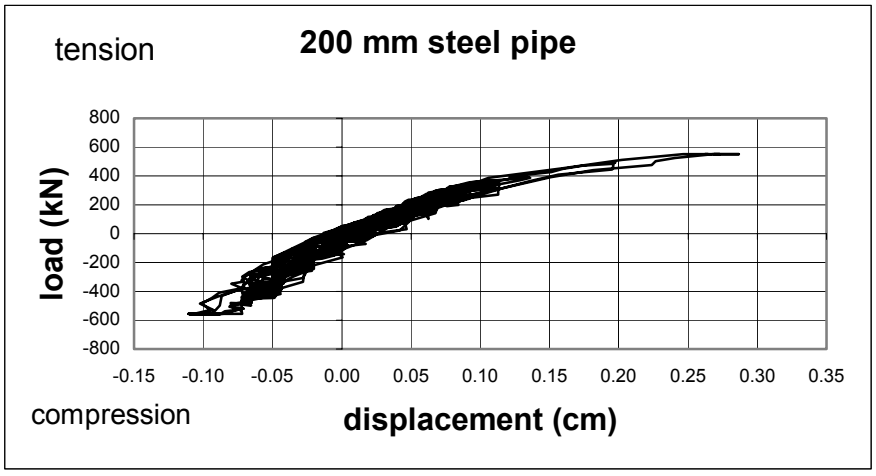

Figure B-11 Load-Displacement for 200 mm Steel Pipe

12. PVC Pipe with Push-On Rubber Gasket Joint

Material	PVC
Nominal dia.	150 mm (6”)
Joint type	push-on bell-spigot; rubber gask**et**
Material Characteristics	PVC pipe with push-on rubber gasket joint C-900
Yield stress	41 MPa
Modulus	2100 MPa
Cross-Sectional Dimensions	
OD	175 mm
ID	152 mm
Wall thick	11.4 mm
Bell OD	251 mm
Bell ID	178 mm
Bell thick	36.6 mm
Cross Area	5882 sq.mm
Flow area	18241 sq.mm
Flange thick	none
Length (OTO)	61 cm
Length segment	61 cm
Loading	dynamic Arleta, Sylmar, Laholl records
Ultimate Load	1.4 kN tension; 2.8 kN compression
Ultimate Disp	1.57 cm tension; .9 cm compression
Failure mechanism	no failure

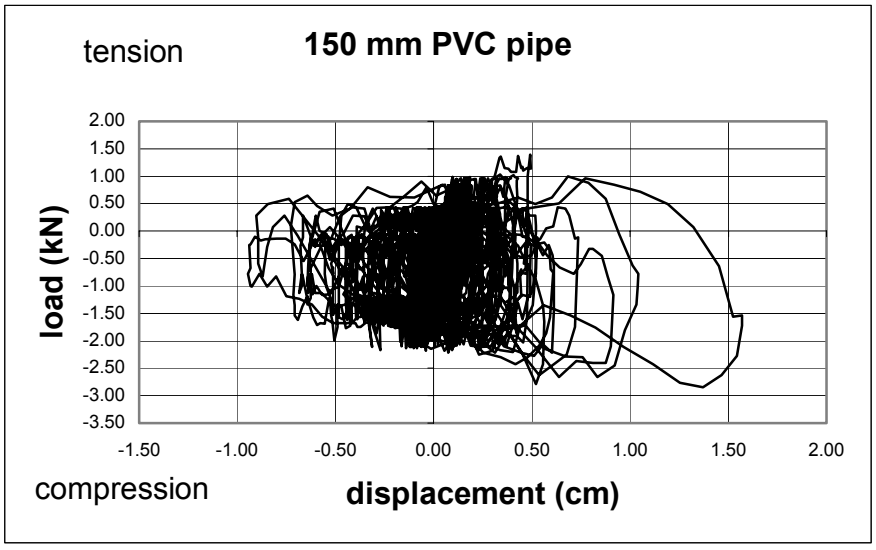

Figure B-12 Load-Displacement for 150 mm PVC Pipe

13. PVC Pipe with Push-On Rubber Gasket Joint

Material	PVC
Nominal dia.	200 mm (8")
Joint type	push-on bell-spigot; rubber gask**et**
Material Characteristics	PVC pipe with push-on rubber gasket joint C-900
Yield stress	41MPa
Modulus	2100 MPa
Cross-Sectional Dimensions	
OD	229 mm
ID	203 mm
Wall thick	12.7 mm
Bell OD	305 mm
Bell ID	229 mm
Bell thick	36.6 mm
Cross Area	8611 sq.mm
Flow area	32424 sq.mm
Flange thick	none
Length (OTO)	50.5 cm
Length segment	50.5 cm
Loading	dynamic Arleta, Sylmar, Laholl records
Ultimate Load	7 kN compression; 1.6 kN tension
Ultimate Disp	.96 cm compression; 1.56 cm tension
Failure mechanism	no failure

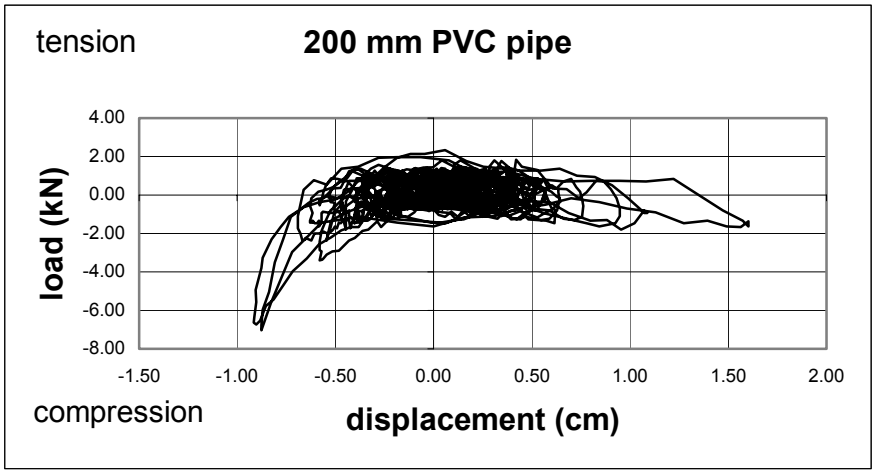

Figure B-13 Load-Displacement for 200 mm PVC Pipe

14. PE Pipe with Butt-Fused Joint

Material	PE polyethylene, high-density
Nominal dia.	150 mm (6”)
Joint type	butt-fused joint
Material Characteristics	PE pipe with butt-fused joint C-906
Yield stress	17 MPa
Modulus	827 MPa
Cross-Sectional Dimensions	
OD	178 mm
ID	152 mm
Wall thick	12.7 mm
Bell OD	178 mm
Bell ID	152 mm
Bell thick	12.7 mm
Cross Area	6585 sq.mm
Flow area	18234 sq.mm
Flange thick	none
Length (OTO)	61 mm
Length segment	61 mm
Loading	dynamic Arleta, Sylmar, Laholl records
Ultimate Load	150 kN tension; 151 kN compression
Ultimate Disp	2.27 cm tension; 1.83 cm compression
Failure mechanism	no failure at joint

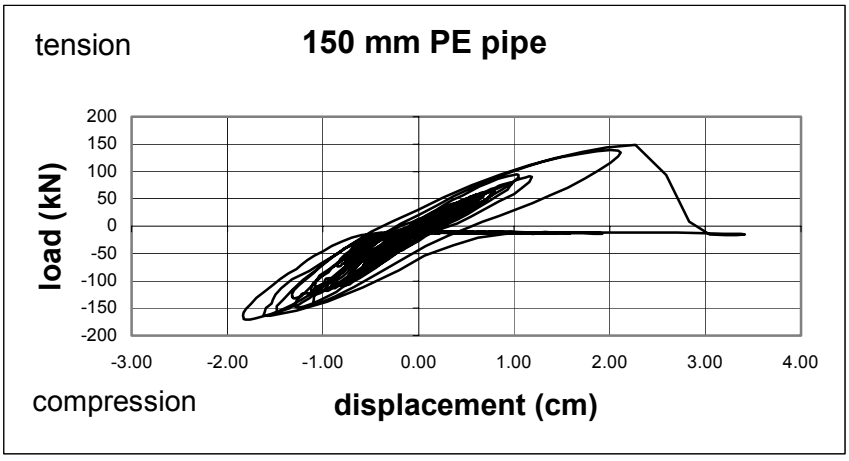

Figure B-14 Load-Displacement for 150 mm PE Pipe

15. PE Pipe with Butt-Fused Joint

Material	PE polyethylene, high-density
Nominal dia.	200 mm (8")
Joint type	butt-fused joint
Material Characteristics	PE pipe with butt-fused joint C-906
Yield stress	17 MPa
Modulus	827 MPa
Cross-Sectional Dimensions	
OD	229 mm
ID	203 mm
Wall thick	12.7 mm
Bell OD	229 mm
Bell ID	203 mm
Bell thick	12.7 mm
Cross Area	8611 sq.mm
Flow area	32424 sq.mm
Flange thick	none
Length (OTO)	61 cm
Length segment	61 cm
Loading	dynamic Arleta, Sylmar, Laholl records
Ultimate Load	220 kN tension; 300 kN compression
Ultimate Disp	3.89 cm tension; 3.28 cm compression
Failure mechanism	no failure at joint

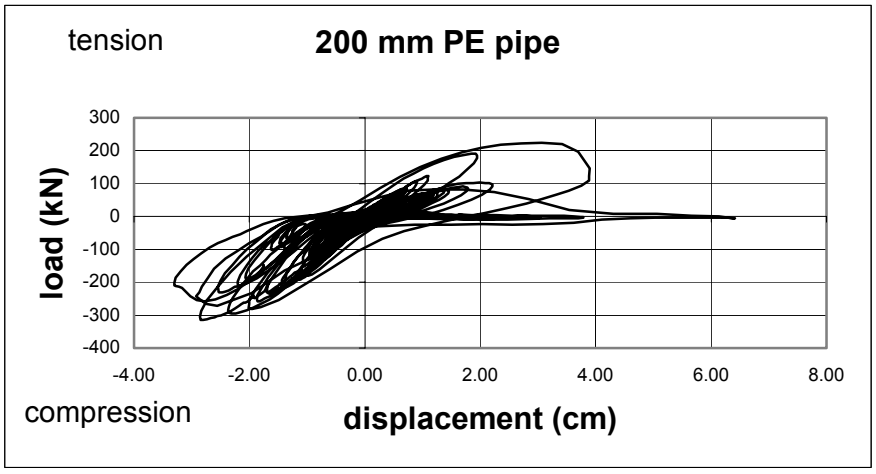

Figure B-15 Load-Displacement for 200 mm PE Pipe

APPENDIX C

STATIC AND DYNAMIC BENDING EXPERIMENTS

TEST REPORTS and MOMENT-THETA PLOTS

Nomenclature:

OD	pipe outside diameter
ID	pipe inside diameter
Wall thick	pipe wall thickness
Bell OD	pipe bell section outside diameter
Bell ID	pipe bell section inside diameter
Cross area	pipe section cross sectional area of material
Flow area	pipe section cross section of open area
Flange thick	flange section thickness at end of the specimen
Length (OTO)	actual overall length of the specimen, out-to-out of the end flanges
Length segment	actual length of the specimen not including the end flanges
Theta	joint rotation in radians

1. Cast Iron Pipe with Lead Caulked Joint

Material	cast iron
Nominal dia.	200 mm (8”)
Joint type	bell-spigot, lead caulked
Material Characteristics	cast iron pipe with lead caulked joint (in-service segment)
Ultimate stress	552 MPa compression
Modulus	96530 MPa
Cross-Sectional Dimensions	
OD	229 mm
ID	203 mm
Wall thick	12.7 mm
Bell OD	305 mm
Bell ID	229 mm
Bell thick	38.1 mm
Cross Area	8579 sq.mm
Flow area	32424 sq.mm
Flange thick	none
Length (OTO)	137 cm
Length segment	137 cm
Loading	dynamic, Arleta record; static cyclic
Ultimate Moment	2490 kN-cm
Ultimate Rotation	.0456 rad.
Failure mechanism	failure of pipe barrel in supporting pipe

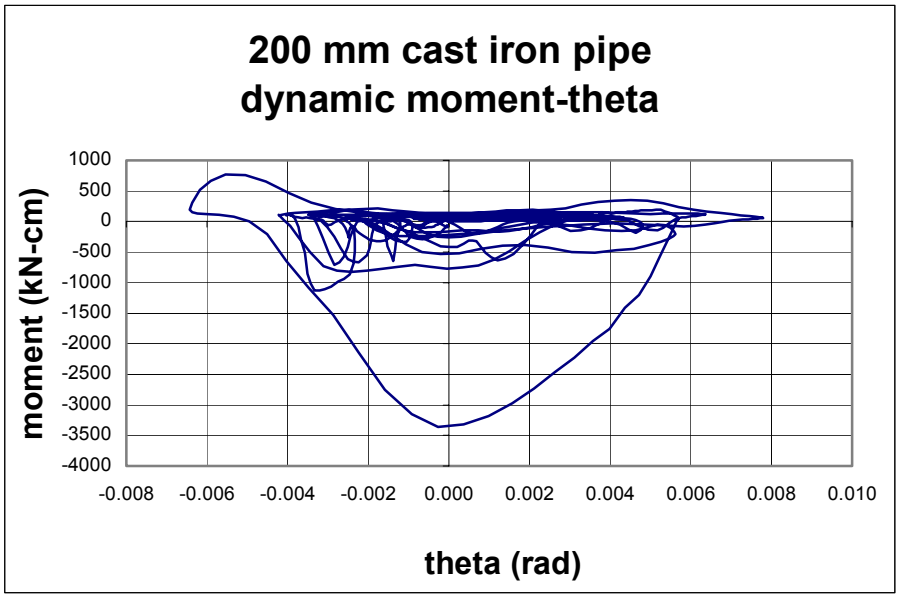

Figure C-1 Dynamic Moment-Theta for 200 mm Cast Iron Pipe

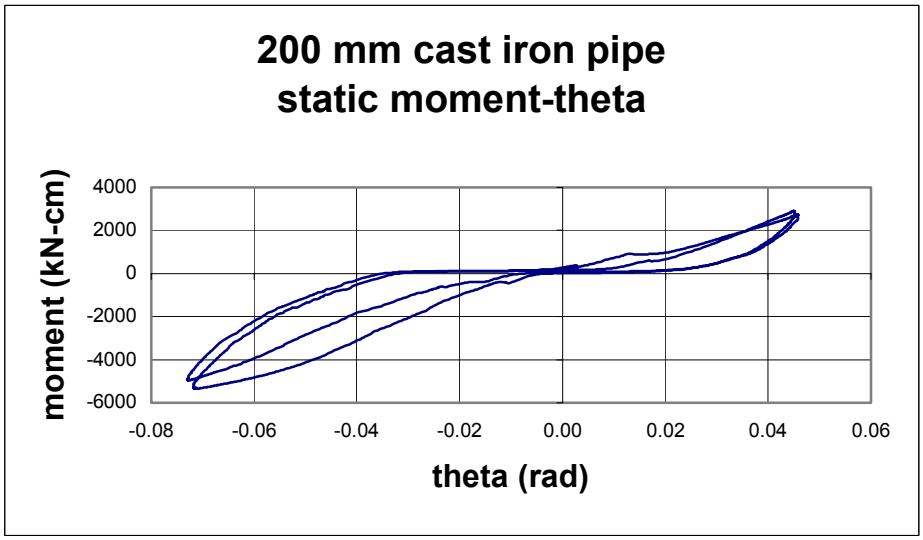

Figure C-2 Static Moment-Theta for 200 mm Cast Iron Pipe

2. Ductile Iron Pipe with Push-On Rubber Gasket Joint

Material	ductile iron
Nominal dia.	150 mm (6”)
Joint type	push-on bell-spigot, rubber gasket
Material Characteristics	ductile iron pipe with push-on rubber gasket joint
Yield stress	310 MPa
Modulus	165480 MPa
Cross-Sectional Dimensions	
ID	162.6 mm
OD	175.3 mm
Wall thick	6.35 mm
Bell OD	235.0 mm
Bell ID	199.4 mm
Bell thick	17.8 mm
Cross Area	3367 sq.mm
Flow area	20750 sq.mm
Flange thick	2.54 cm
Flange thick	2.5 cm
Length (OTO)	137 cm
Length segment	132 cm
Loading	dynamic, Arleta record; static cyclic
Ultimate Moment	301 kN-cm
Ultimate Rotation	.10 rad
Failure mechanism	leakage at .08 radian rotation

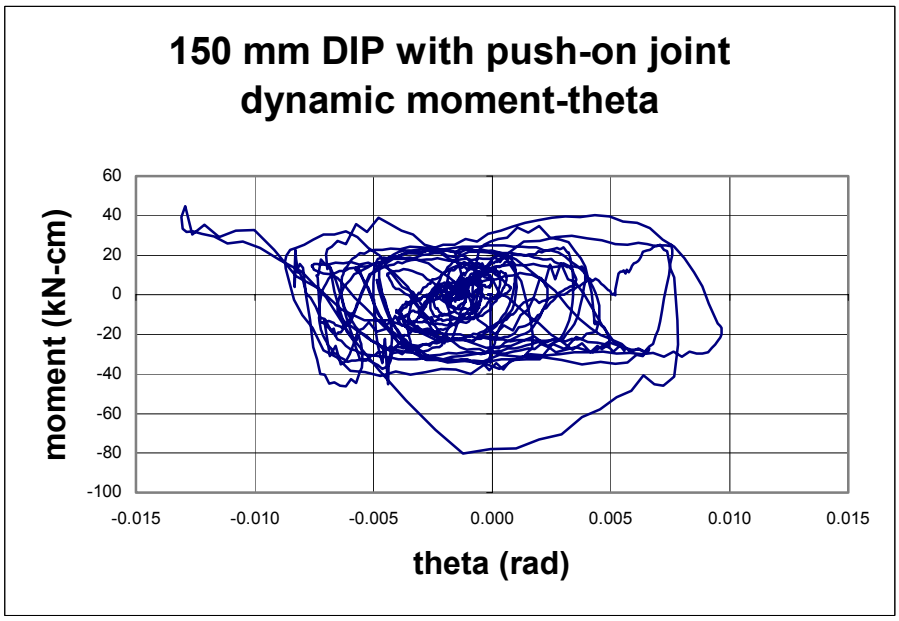

Figure C-3 Dynamic Moment-Theta for 150 mm DIP with Push-On Gasket

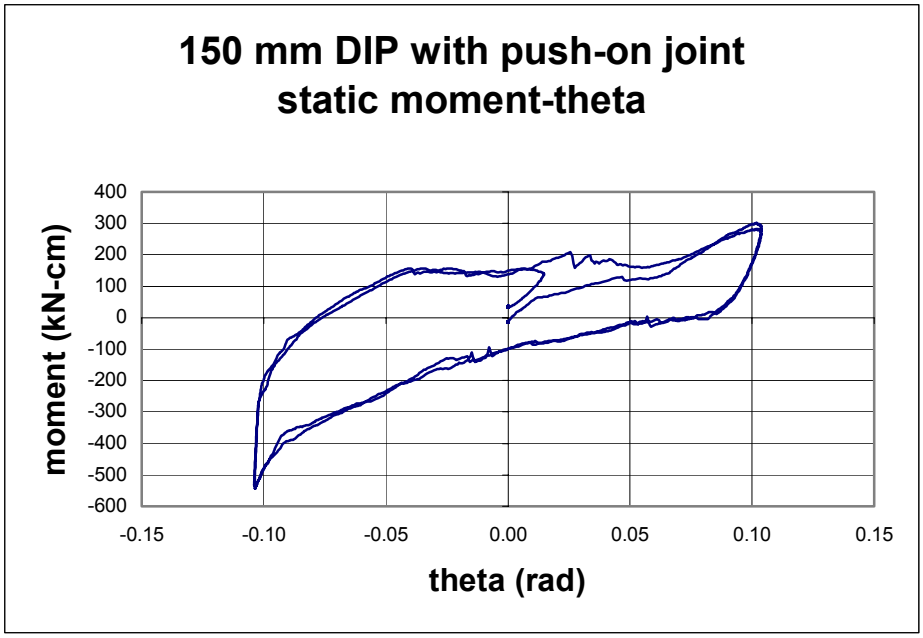

Figure C-4 Static Moment-Theta for 150 mm DIP with Push-On Gasket

3. Ductile Iron Pipe with Push-On Rubber Gasket Joint

Material	ductile iron
Nominal dia.	200 mm (8”)
Joint type	push-on bell-spigot, rubber gasket
Material Characteristics	ductile iron pipe with push-on rubber gasket joint
Yield stress	310 MPa
Modulus	165480 MPa
Cross-Sectional Dimensions	
ID	217.2 mm
OD	229.9 mm
Wall thick	6.35 mm
Bell OD	296.7 mm
Bell ID	258.6 mm
Bell thick	19.1 mm
Cross Area	4457 sq.mm
Flow area	37029 sq.mm
Flange thick	2.5 cm
Length (OTO)	137 cm
Length segment	137 cm
Loading	dynamic, Arleta record; static cyclic
Ultimate Moment	227 kN-cm
Ultimate Rotation	.12 rad.
Failure mechanism	leakage at .08 rad. rotation

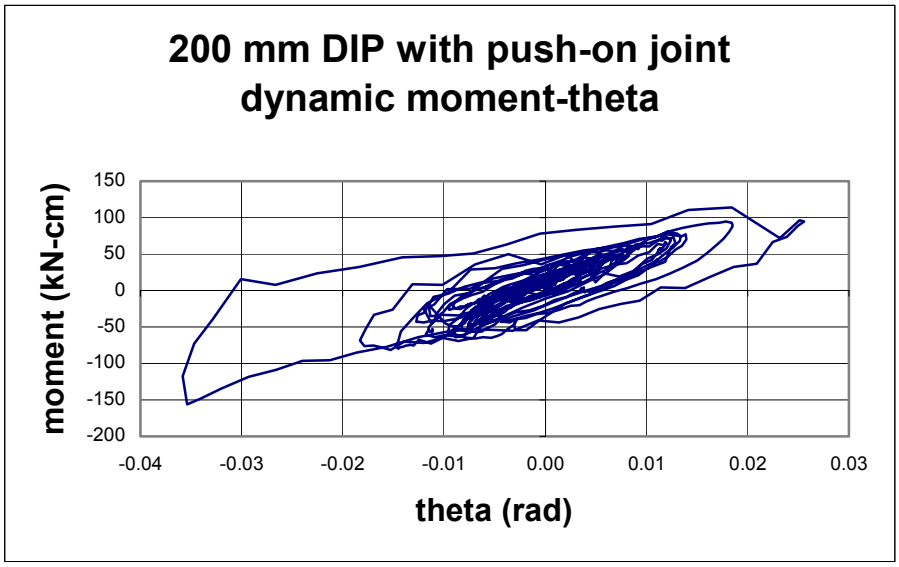

Figure C-5 Dynamic Moment-Theta for 200 mm DIP with Push-On Gasket

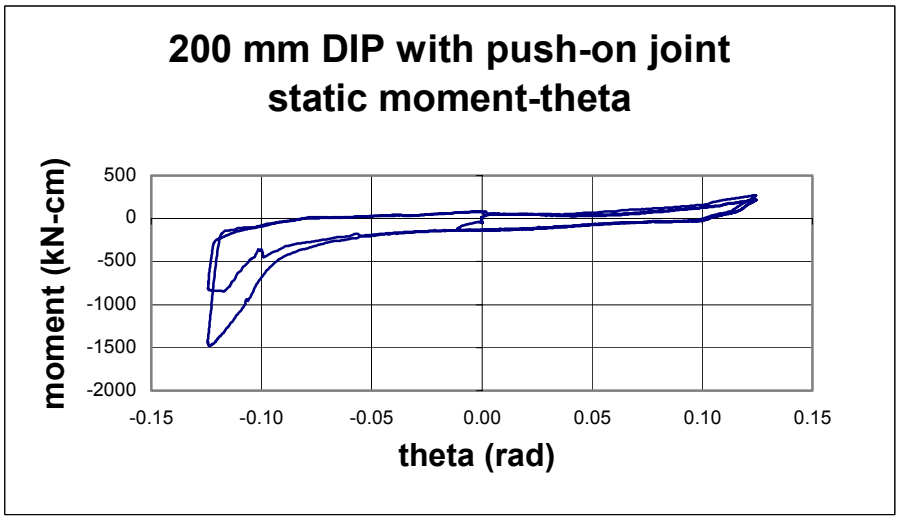

Figure C-6 Static Moment-Theta for 200 mm DIP with Push-On Gasket

4. Ductile Iron Pipe with Gripper Gasket

Material	ductile iron
Nominal dia.	150 mm (6”)
Joint type	bell-spigot; gripper gasket
Material Characteristics	ductile iron pipe with gripper gasket
Yield stress	310 MPa
Modulus	165480 MPa
Cross-Sectional Dimensions	
ID	162.6 mm
OD	175.3 mm
Wall thick	6.35 mm
Bell OD	235.0 mm
Bell ID	199.4 mm
Bell thick	17.8 mm
Cross Area	3367 sq.mm
Flow area	20750 sq.mm
Flange thick	2.54 cm
Length (OTO)	137 cm
Length segment	135 cm
Loading	dynamic, Arleta record; static cyclic
Ultimate Moment	2580 kN-cm
Ultimate Rotation	.09 rad.
Failure mechanism	leakage at .08 radian rotation

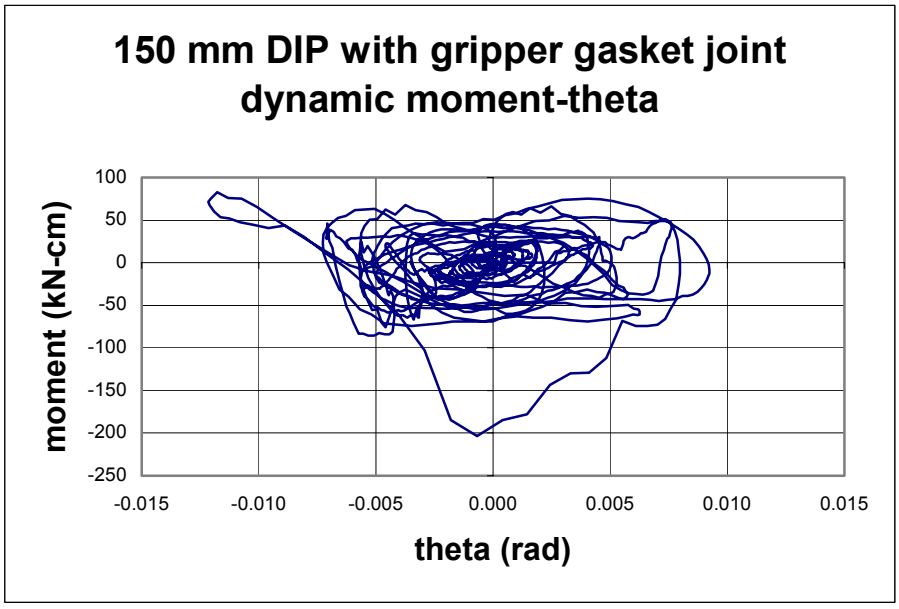

Figure C-7 Dynamic Moment-Theta for 150 mm DIP with Gripper Gasket Joint

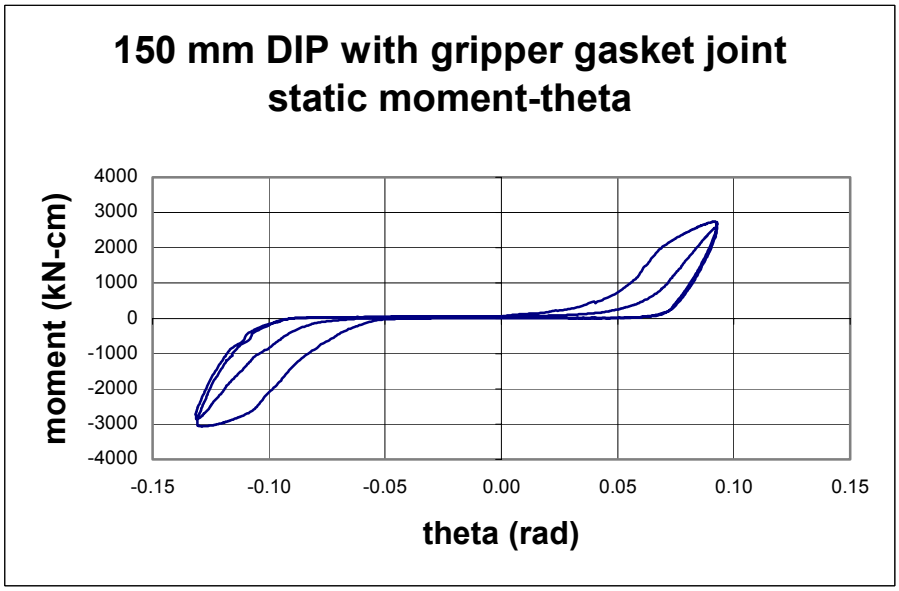

Figure C-8 Static Moment-Theta for 150 mm DIP with Gripper Gasket Joint

5. Ductile Iron Pipe with Gripper Gasket

Material	ductile iron
Nominal dia.	200 mm (8”)
Joint type	bell-spigot; gripper gasket
Material Characteristics	ductile iron pipe with gripper gasket
Yield stress	310 MPa
Modulus	165480 MPa
Cross-Sectional Dimensions	
ID	217.2 mm
OD	229.9 mm
Wall thick	6.35 mm
Bell OD	296.7 mm
Bell ID	258.6 mm
Bell thick	19.1 mm
Cross Area	4457 sq.mm
Flow area	37029 sq.mm
Flange thick	2.54 cm
Length (OTO)	61.0 cm
Length segment	55.88 cm
Loading	dynamic, Arleta record; static cyclic
Ultimate Moment	3150 kN-cm
Ultimate Rotation	.10 rad.
Failure mechanism	leakage at .08 radian rotation

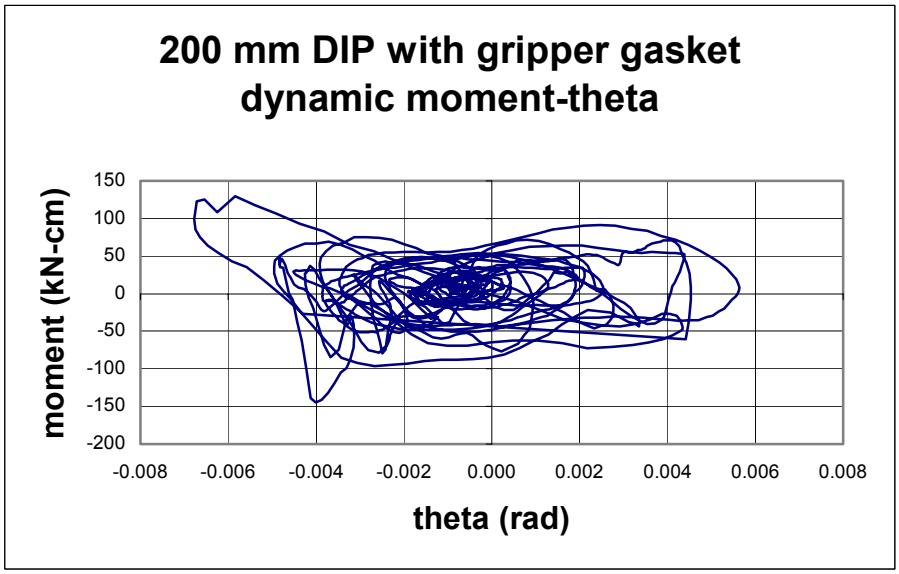

Figure C-9 Dynamic Moment-Theta for 200 mm DIP with Gripper Gasket Joint

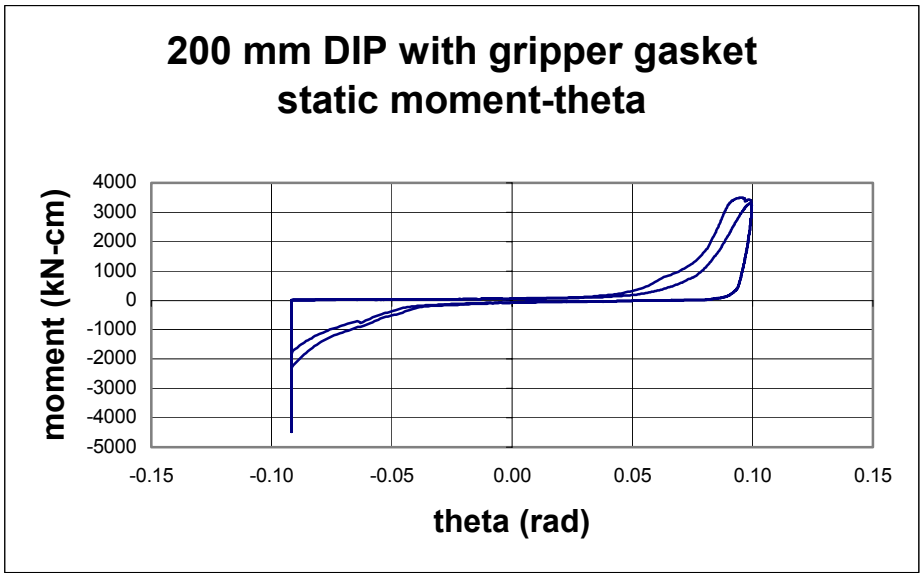

Figure C-10 Static Moment-Theta for 200 mm DIP with Gripper Gasket Joint

6. Ductile Iron Pipe with Retaining Ring Joint

Material	ductile iron
Nominal dia.	150 mm (6”)
Joint type	bell and spigot; retaining ring
Material Characteristics	ductile iron pipe with retaining ring joint
Yield stress	310 MPa
Modulus	165480 MPa
Cross-Sectional Dimensions	
ID	162.6 mm
OD	175.3 mm
Wall thick	6.35 mm
Bell OD	235.0 mm
Bell ID	199.4 mm
Bell thick	17.8 mm
Cross Area	3367 sq.mm
Flow area	20750 sq.mm
Flange thick	2.54 cm
Length (OTO)	67.31 cm
Length segment	64.77 cm
Loading	dynamic, Arleta record; static cyclic
Ultimate Moment	3060 kN-cm
Ultimate Rotation	.11 rad
Failure mechanism	leakage at .08 radian rotation

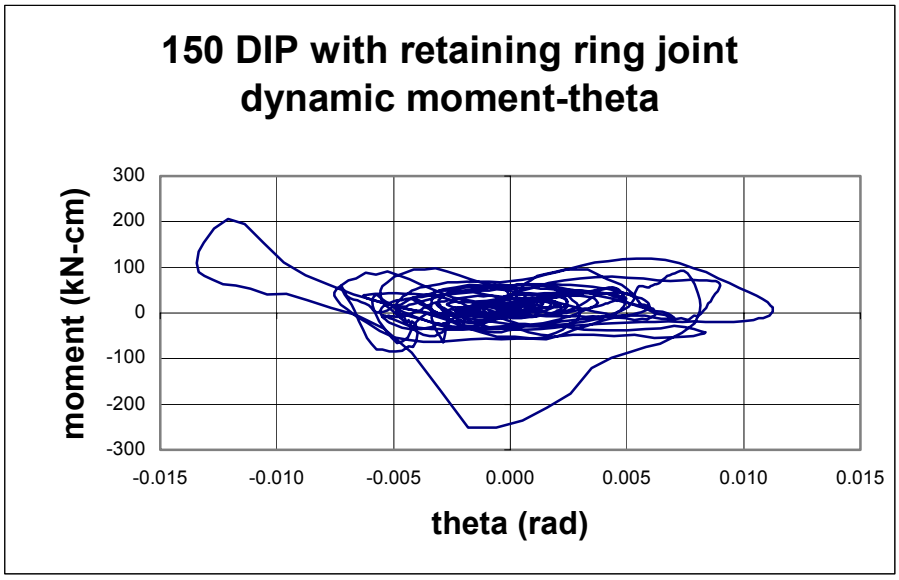

Figure C-11 Dynamic Moment-Theta for 150 mm DIP with Retaining Ring Joint

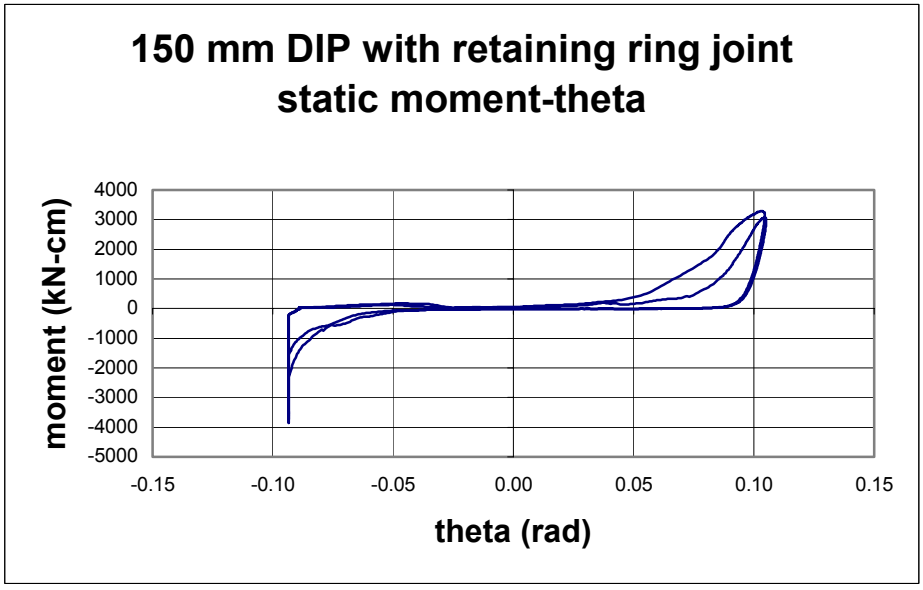

Figure C-12 Static Moment-Theta for 150 mm DIP with Retaining Ring Joint

7. Ductile Iron Pipe with Retaining Ring Joint

Material	ductile iron
Nominal dia.	200 mm (8”)
Joint type	bell and spigot; retaining ring
Material Characteristics	ductile iron pipe with retaining ring joint
Yield stress	310 MPa
Modulus	165480 MPa
Cross-Sectional Dimensions	
ID	217.2 mm
OD	229.9 mm
Wall thick	6.35 mm
Bell OD	296.7 mm
Bell ID	258.6 mm
Bell thick	19.1 mm
Cross Area	4457 sq.mm
Flow area	37029 sq.mm
Flange thick	2.54 cm
Length (OTO)	67.31 cm
Length segment	62.23 cm
Loading	dynamic, Arleta record; static cyclic
Ultimate Moment	3000 kN-cm
Ultimate Rotation	.095 rad
Failure mechanism	leakage at .08 radian rotation

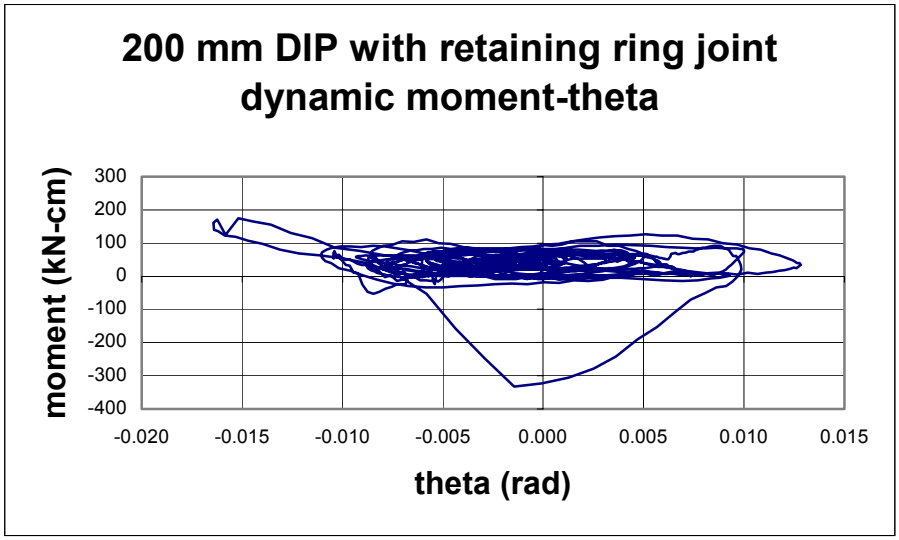

Figure C-13 Dynamic Moment-Theta for 200 mm DIP with Retaining Ring Joint

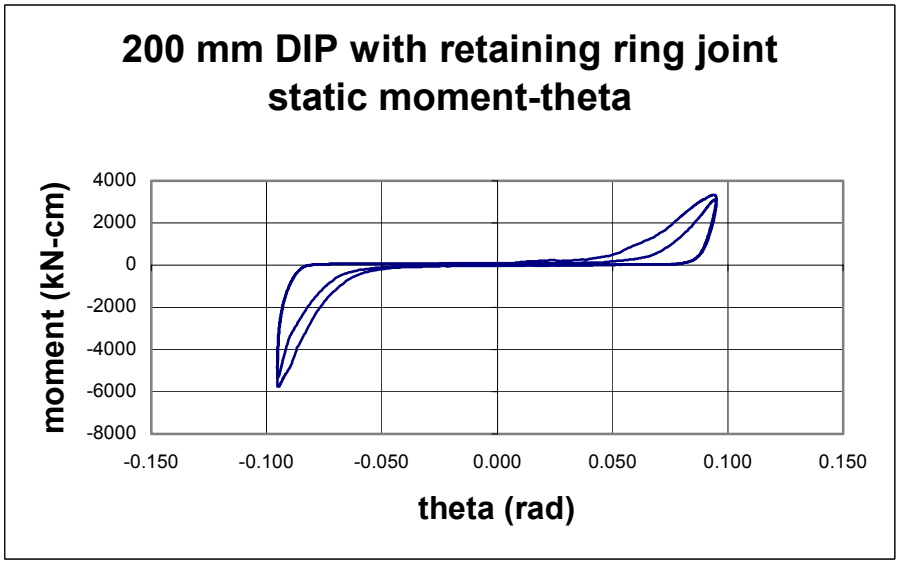

Figure C-14 Static Moment-Theta for 200 mm DIP with Retaining Ring Joint

8. Ductile Iron Pipe with Bolted Collar Joint

Material	ductile iron
Nominal dia.	150 mm (6”)
Joint type	bell-spigot, bolted collar
Material Characteristics	ductile iron pipe with bolted collar joint
Yield stress	310 MPa
Modulus	165480 MPa
Cross-Sectional Dimensions	
ID	162.6 mm
OD	175.3 mm
Wall thick	6.35 mm
Bell OD	235.0 mm
Bell ID	199.4 mm
Bell thick	17.8 mm
Cross Area	3367 sq.mm
Flow area	20750 sq.mm
Flange thick	2.54 cm
Length (OTO)	61.0 cm
Length segment	55.9 cm
Loading	dynamic, Arleta record; static cyclic
Ultimate Moment	1950 kN-cm
Ultimate Rotation	.09 rad.
Failure mechanism	leakage at .08 radian rotation

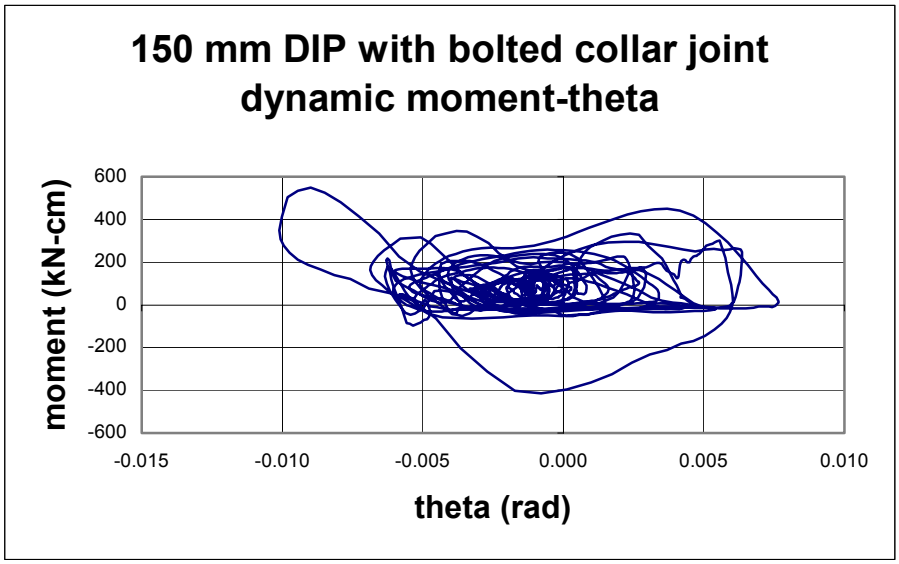

Figure C-15 Dynamic Moment-Theta for 150 mm DIP with Bolted Collar Joint

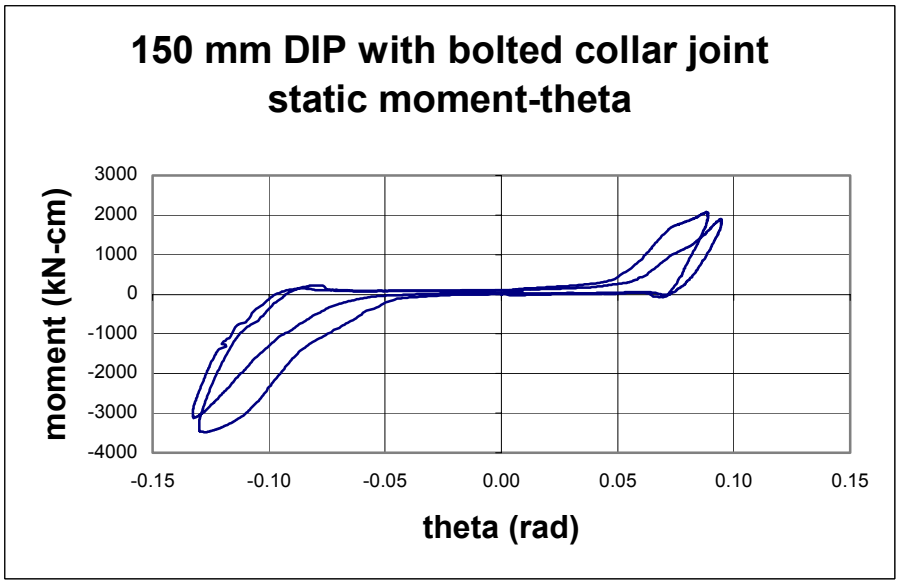

Figure C-16 Static Moment-Theta for 150 mm DIP with Bolted Collar Joint

9. Ductile Iron Pipe with Bolted Collar Joint

Material	ductile iron
Nominal dia.	200 mm (8”)
Joint type	bell-spigot, bolted collar restrained joint
Material Characteristics	ductile iron pipe with bolted collar joint
Yield stress	310 MPa
Modulus	165480 MPa
Cross-Sectional Dimensions	
ID	217.2 mm
OD	229.9 mm
Wall thick	6.35 mm
Bell OD	296.7 mm
Bell ID	258.6 mm
Bell thick	19.1 mm
Cross Area	4457 sq.mm
Flow area	37029 sq.mm
Flange thick	2.54 cm
Length (OTO)	61.0 cm
Length segment	55.9 cm
Loading	dynamic, Arleta record; static cyclic
Ultimate Moment	2950 kN-cm
Ultimate Rotation	.10 rad.
Failure mechanism	leakage at .08 radian rotation

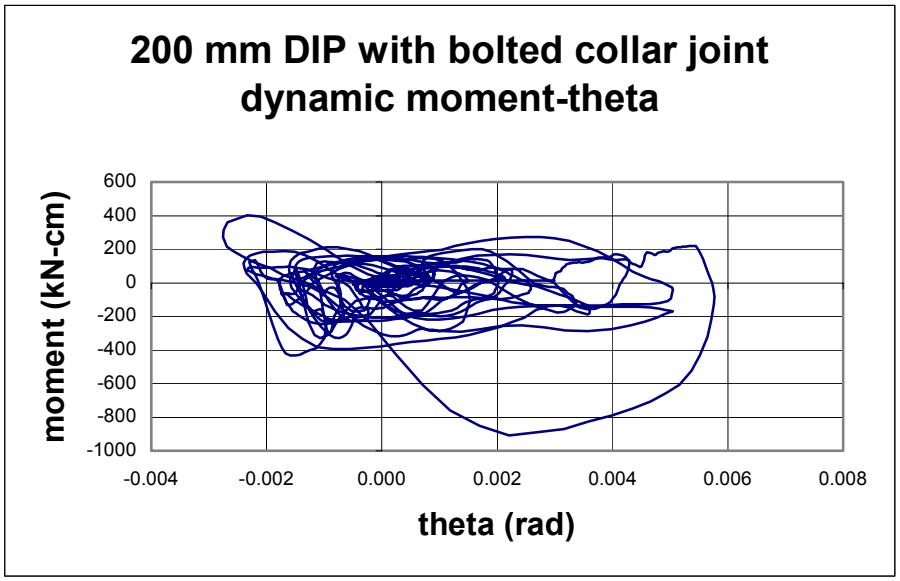

Figure C-17 Dynamic Moment-Theta for 200 mm DIP with Bolted Collar Joint

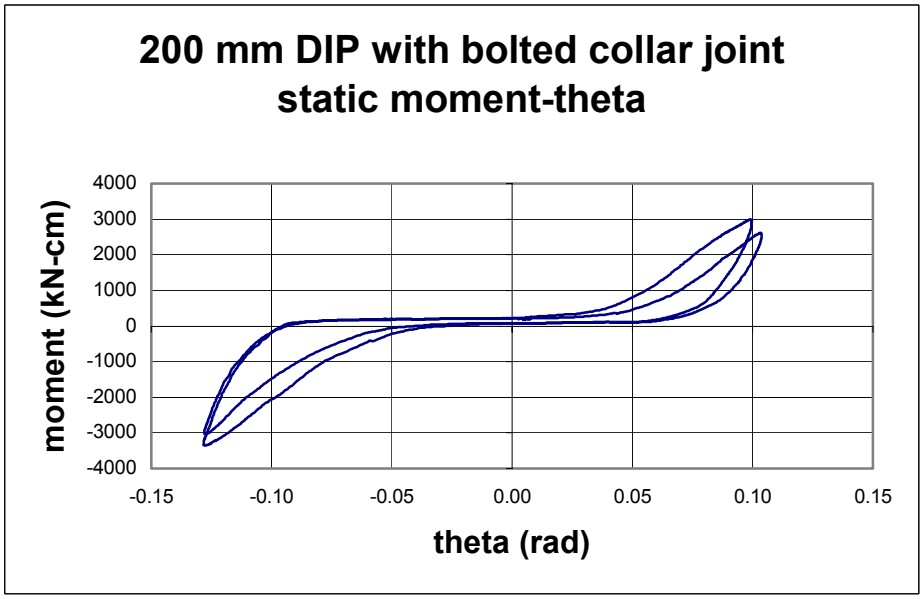

Figure C-18 Static Moment-Theta for 200 mm DIP with Bolted Collar Joint

10. Steel Pipe with Lap-Welded Joint

Material	steel
Nominal dia.	150 mm (6”)
Joint type	bell-spigot; lap-welded
Material Characteristics	steel pipe with lap-welded joint C-200 Grade A A53
Yield stress	207 MPa
Modulus	200000 MPa
Cross-Sectional Dimensions	
OD	159 mm
ID	152 mm
Wall thick	3.40 mm (10ga.)
Bell OD	159 mm
Bell ID	152 mm
Bell thick	3.40 mm (10ga.)
Cross Area	1664 sq.mm
Flow area	18234 sq.mm
Flange thick	1.25 cm
Length (OTO)	137 mm
Length segment	136.5 cm
Loading	dynamic, Arleta record; static cyclic
Ultimate Moment	560 kN-cm
Ultimate Rotation	.017 rad.
Failure mechanism	no failure at joint

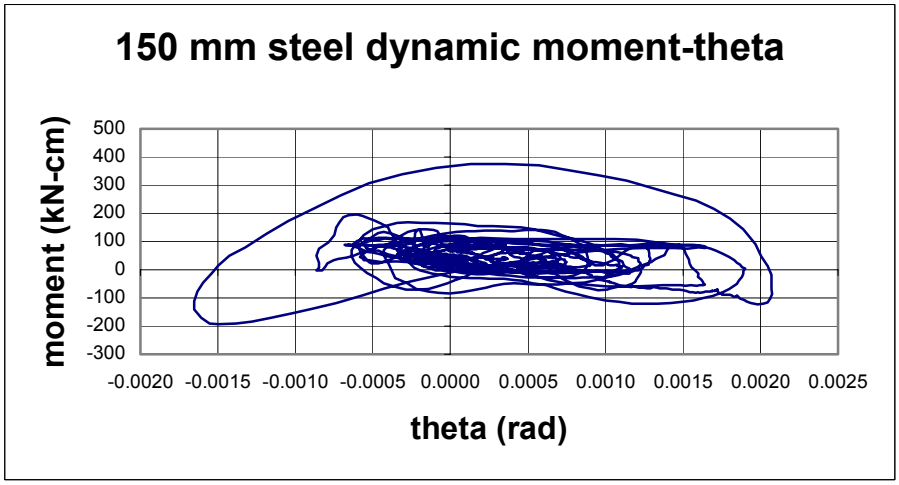

Figure C-19 Dynamic Moment-Theta for 150 mm Steel Pipe

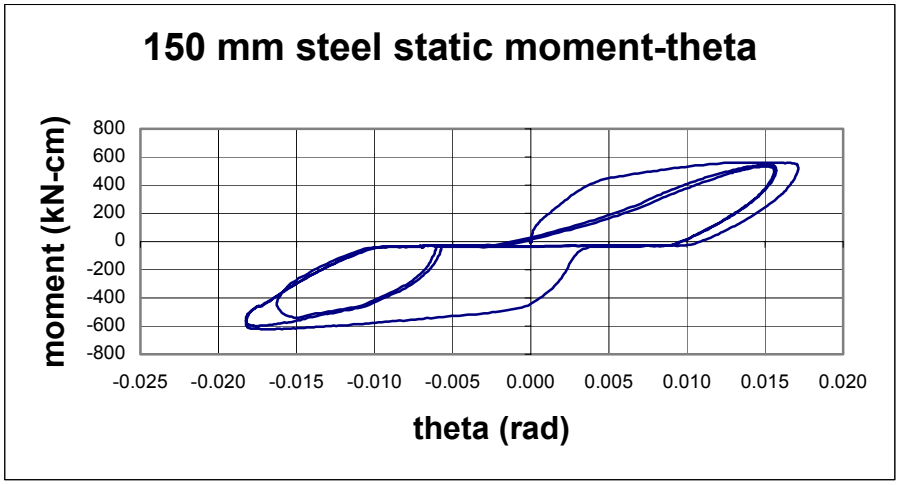

Figure C-20 Static Moment-Theta for 150 mm Steel Pipe

11. Steel Pipe with Lap-Welded Joint

Material	steel
Nominal dia.	200 mm (8”)
Joint type	bell-spigot; lap-welded
Material Characteristics	steel pipe with lap-welded joint C-200 Grade A A53
Yield stress	207 MPa
Modulus	200000 MPa
Cross-Sectional Dimensions	
OD	210 mm
ID	203 mm
Wall thick	3.40 mm (10ga.)
Bell OD	210 mm
Bell ID	203 mm
Bell thick	3.40 mm (10ga.)
Cross Area	2206 sq.mm
Flow area	32424 sq.mm
Flange thick	1.25 cm
Length (OTO)	137 mm
Length segment	136.5 cm
Loading	dynamic, Arleta record; static cyclic
Ultimate Moment	1264 kN-cm
Ultimate Rotation	.016 rad.
Failure mechanism	no failure at joint

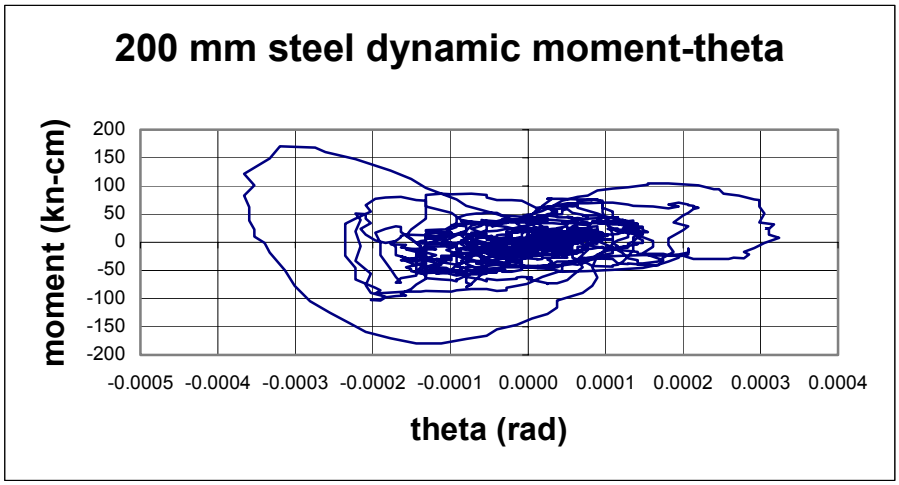

Figure C-21 Dynamic Moment-Theta for 200 mm Steel Pipe

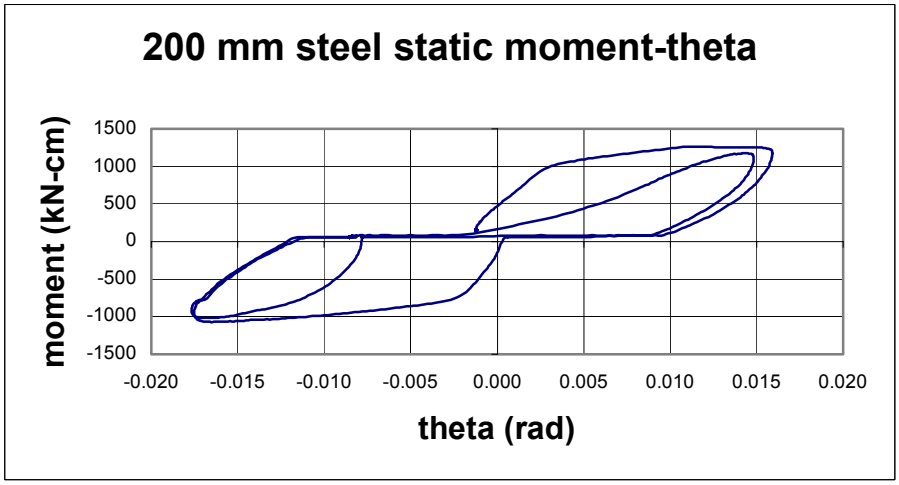

Figure C-22 Static Moment-Theta for 200 mm Steel Pipe

12. PVC Pipe with Push-On Rubber Gasket Joint

Material	PVC
Nominal dia.	150 mm (6”)
Joint type	push-on bell-spigot; rubber gask**et**
Material Characteristics	PVC pipe with push-on rubber gasket joint C-900
Yield stress	41 MPa
Modulus	2100 MPa
Cross-Sectional Dimensions	
OD	175 mm
ID	152 mm
Wall thick	11.4 mm
Bell OD	251 mm
Bell ID	178 mm
Bell thick	36.6 mm
Cross Area	5882 sq.mm
Flow area	18241 sq.mm
Flange thick	none
Length (OTO)	137 cm
Length segment	137 cm
Loading	dynamic, Arleta record; static cyclic
Ultimate Moment	384 kN-cm
Ultimate Rotation	.08 rad.
Failure mechanism	no failure at joint

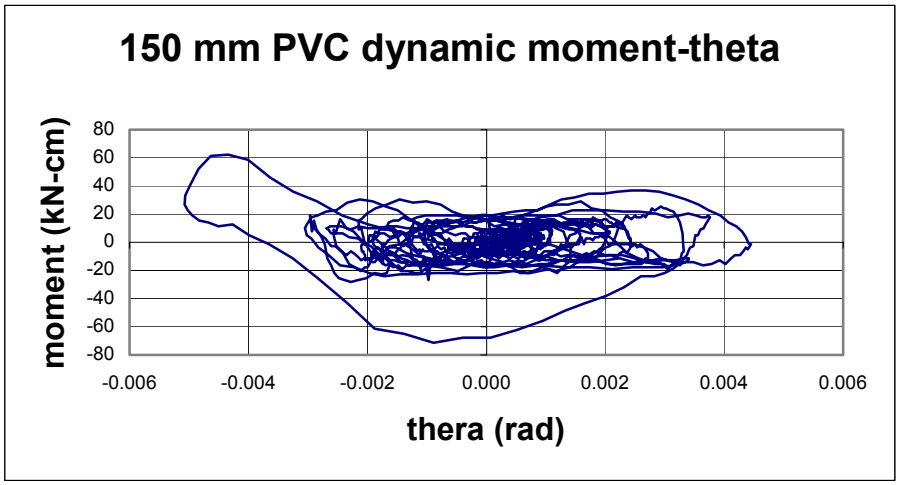

Figure C-23 Dynamic Moment-Theta for 150 mm PVC Pipe

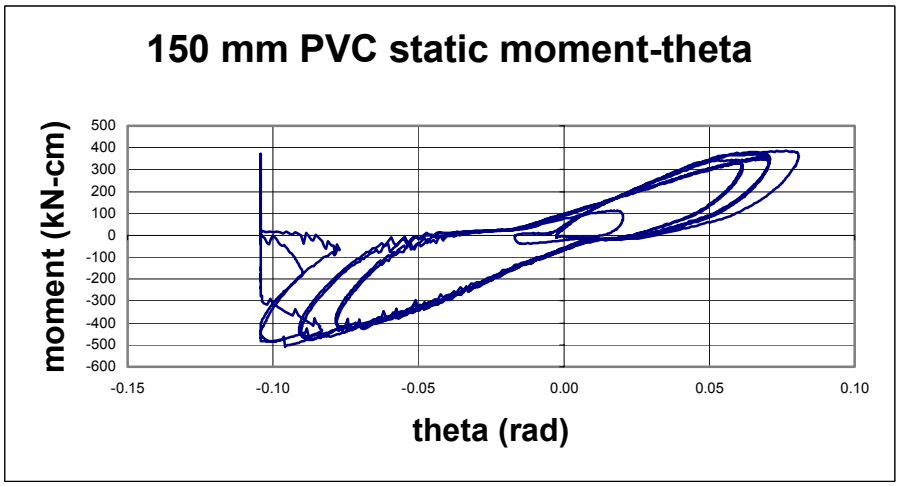

Figure C-24 Static Moment-Theta for 150 mm PVC Pipe

13. PVC Pipe with Push-On Rubber Gasket Joint

Material	PVC
Nominal dia.	200 mm (8”)
Joint type	push-on bell-spigot; rubber gask**et**
Material Characteristics	PVC pipe with push-on rubber gasket joint C-900
Yield stress	41MPa
Modulus	2100 MPa
Cross-Sectional Dimensions	
OD	229 mm
ID	203 mm
Wall thick	12.7 mm
Bell OD	305 mm
Bell ID	229 mm
Bell thick	36.6 mm
Cross Area	8611 sq.mm
Flow area	32424 sq.mm
Flange thick	none
Length (OTO)	137 cm
Length segment	137 cm
Loading	dynamic, Arleta record; static cyclic
Ultimate Moment	410 kN-cm
Ultimate Rotation	.036 rad.
Failure mechanism	no failure at joint

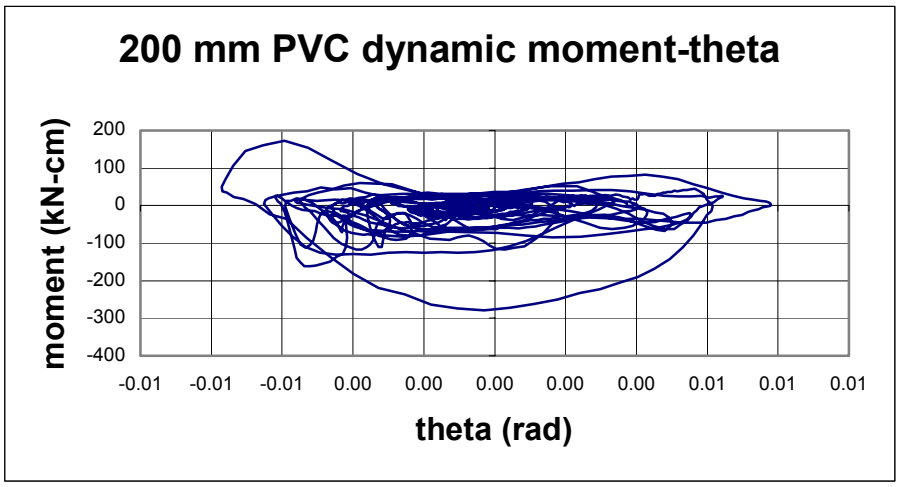

Figure C-25 Dynamic Moment-Theta for 200 mm PVC Pipe

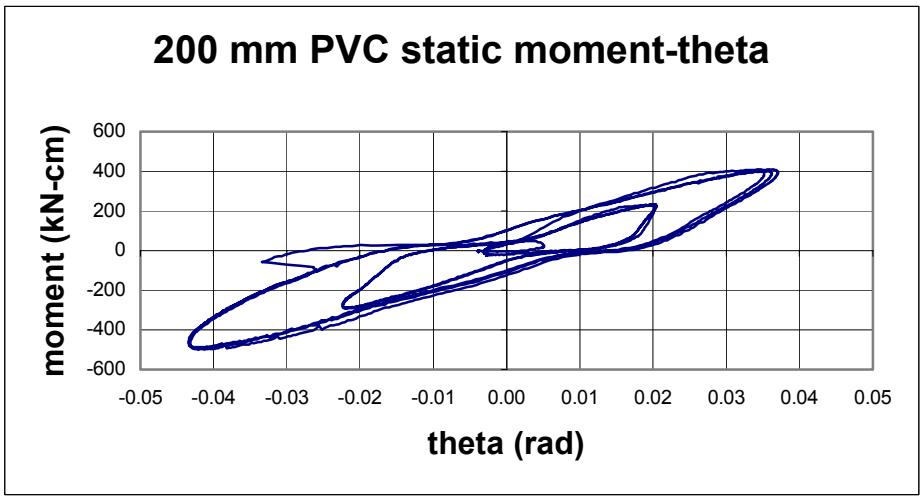

Figure C-26 Static Moment-Theta for 200 mm PVC Pipe

14. PE Pipe with Butt-Fused Joint

Material	PE polyethylene, high-density
Nominal dia.	150 mm (6”)
Joint type	butt-fused joint
Material Characteristics	PE pipe with butt-fused joint C-906
Yield stress	17 MPa
Modulus	827 MPa
Cross-Sectional Dimensions	
OD	178 mm
ID	152 mm
Wall thick	12.7 mm
Bell OD	178 mm
Bell ID	152 mm
Bell thick	12.7 mm
Cross Area	6585 sq.mm
Flow area	18234 sq.mm
Flange thick	none
Length (OTO)	137 mm
Length segment	137 mm
Loading	dynamic, Arleta record; static cyclic
Ultimate Moment	254 kN-cm
Ultimate Rotation	.06 rad.
Failure mechanism	no failure at joint

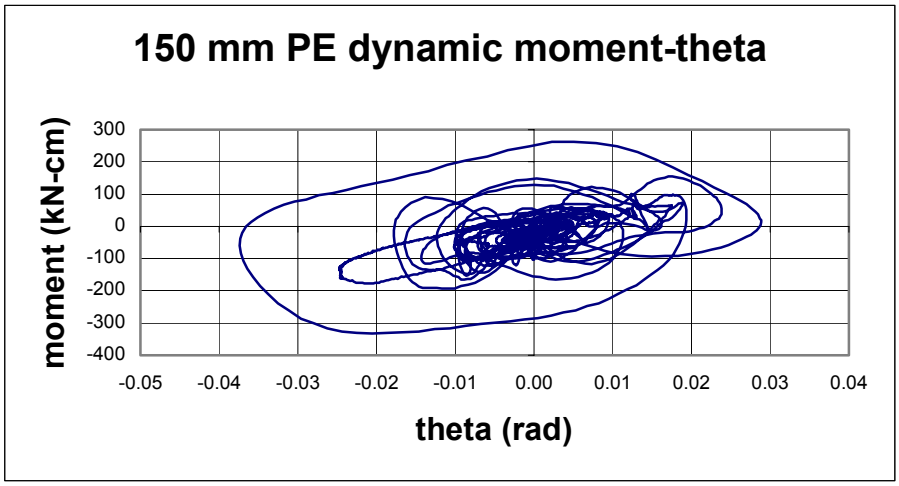

Figure C-27 Dynamic Moment-Theta for 150 mm PE Pipe

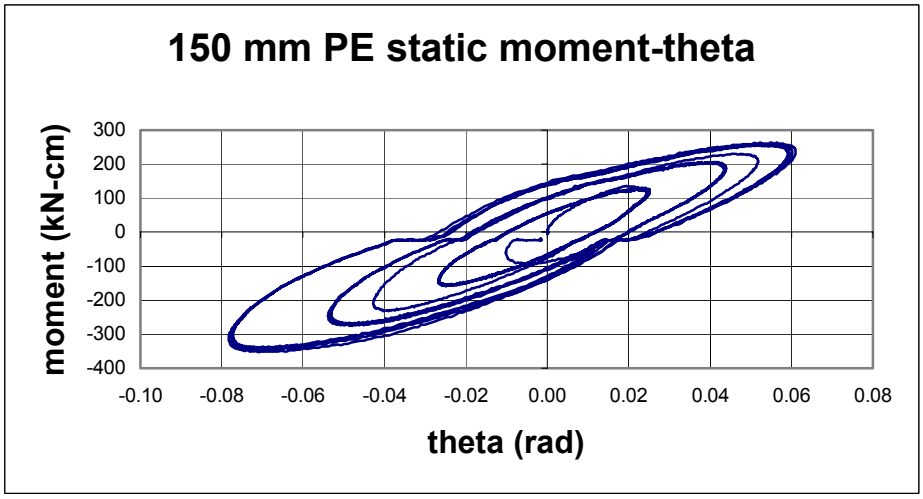

Figure C-28 Static Moment-Theta for 150 mm PE Pipe

15. PE Pipe with Butt-Fused Joint

Material	PE polyethylene, high-density
Nominal dia.	200 mm (8”)
Joint type	butt-fused joint
Material Characteristics	PE pipe with butt-fused joint C-906
Yield stress	17 MPa
Modulus	827 MPa
Cross-Sectional Dimensions	
OD	229 mm
ID	203 mm
Wall thick	12.7 mm
Bell OD	229 mm
Bell ID	203 mm
Bell thick	12.7 mm
Cross Area	8611 sq.mm
Flow area	32424 sq.mm
Flange thick	none
Length (OTO)	61 cm
Length segment	61 cm
Loading	dynamic, Arleta record; static cyclic
Ultimate Moment	814 kN-cm
Ultimate Rotation	.08 rad.
Failure mechanism	no failure at joint

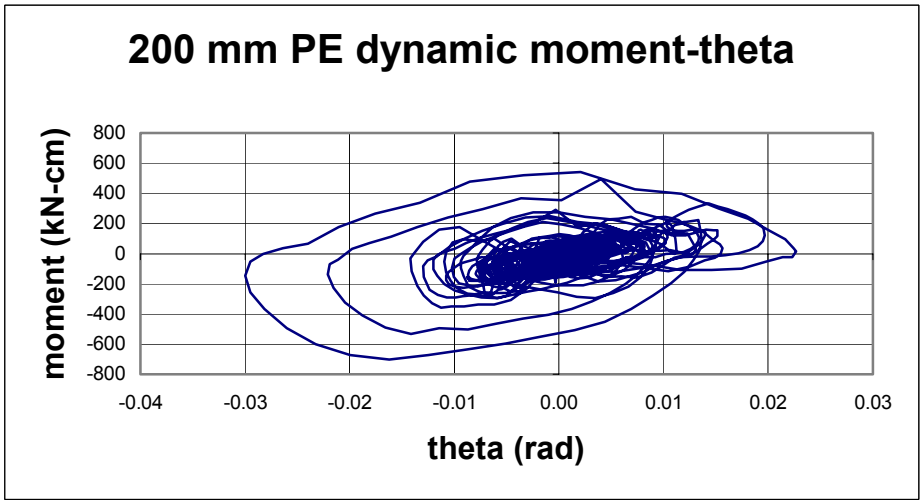

Figure C-29 Dynamic Moment-Theta for 200 mm PE Pipe

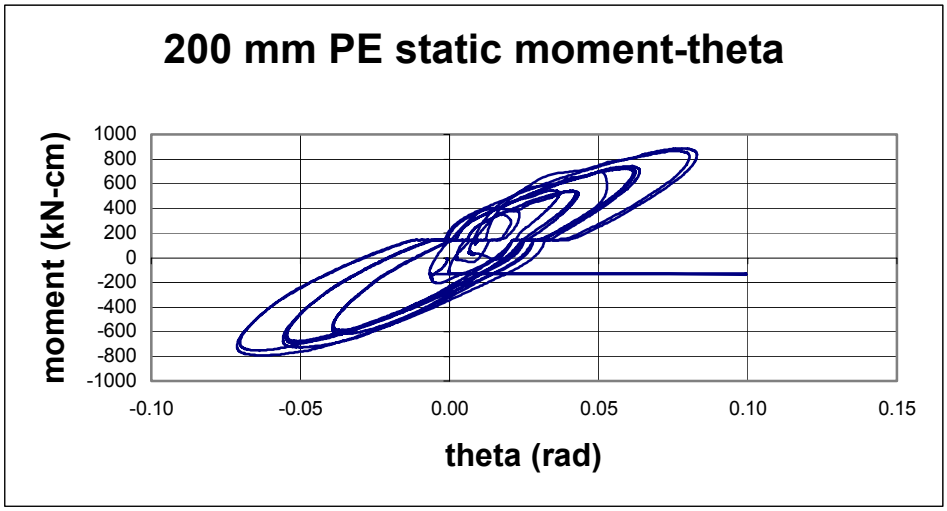

Figure C-30 Static Moment-Theta for 200 mm PE Pipe

APPENDIX D
RISK ASSESSMENT EVALUATION DEVELOPMENT

T. O'Rourke (1996) has developed a simplified risk evaluation procedure that compares the imposed force on a pipe joint from a seismic motion and the force level that is able to be transferred to the pipe surface from the soil by interface friction to the force resistance capacity of the joint. Although this procedure was originally designed for piping systems with continuous joints, it is also applicable to systems with segmented joints that have a tensile restraint capacity. This procedure has been modified for this research project to allow the use of the force capacities determined from this experimental testing project. The following is the development of risk assessment charts (Figures 5-1 and 5-2). Site specific and pipe joint specific parameters are computed and plotted on the risk assessment charts to determine the probability of a "fail" or a "no fail" condition.

The strains in the soil can be determined from the seismic and soil properties. From Newmark (1967) the soil strains can be expressed as:

$$\varepsilon_{pipe} = \frac{V}{c} \qquad \text{(D-1)}$$

where:

ε_{pipe} = pipe or soil strain

V = particle velocity from the seismic motion

c = soil wave propagation velocity

From this relationship, T. O'Rourke (1966) expands the expression to an imposed force:

$$F_s = \frac{V\ A\ E}{c} \qquad \text{(D-2)}$$

where:

F_s	=	imposed force from the seismic motion
V	=	particle velocity from the seismic motion
c	=	soil wave propagation velocity
A	=	cross sectional area of the pipe
E	=	Young's modulus of the pipe material

The maximum possible force transfer by interface friction can be determined from the expression:

$$F_f = \frac{f\ T\ c}{4} \qquad \text{(D-3)}$$

where:

F_f	=	maximum possible force transfer from the soil to the pipe
f	=	maximum friction force per unit length that can be transferred from the soil to the pipe (see Eq. D-5)
T	=	predominate period of the seismic motion
c	=	soil wave propagation velocity

Note that the length of the seismic wave is from the expression:

$$\text{wave length} = T \times c \qquad \text{(D-4)}$$

The effective length of pipe over which the frictional force acts that effects the force level at a joint is ¼ of the length of a cycle of the seismic wave (¼ T x c).

The variable f, is the friction force per unit length and is determined from the expression:

$$f = \frac{(k_o+1)}{2} \gamma z \tan\phi D_o \qquad \text{(D-5)}$$

where:

f	=	maximum friction force per unit length that can be transferred from the soil to the pipe
k_o	=	at rest lateral earth pressure coefficient
γ	=	soil density
z	=	centerline depth of pipe
ϕ	=	soil friction angle
D_o	=	outside diameter of the pipe

The relationships for "fail" a condition are:

$$\text{if} \quad F_s > F_{max} \quad \Rightarrow \quad \text{potential fail condition} \qquad \text{(D-6)}$$

and

$$\text{if} \quad F_f > F_{max} \quad \Rightarrow \quad \text{potential fail condition} \qquad \text{(D-7)}$$

where: F_{max} = joint force capacity as determined in this experimental testing project

Note: for a probable overall joint failure condition, both criteria must have a "fail condition".

Rearranging equations D-6 and D-7 gives:

$$\text{if} \quad \frac{V\,A\,E}{c} > F_{max} \Rightarrow \text{potential fail condition} \qquad \text{(D-8)}$$

and

$$\text{if} \quad \frac{f\,T\,c}{4} > F_{max} \Rightarrow \text{potential fail condition} \qquad \text{(D-9)}$$

Rearranging equations D-8 and D-9 gives:

$$\left(\frac{V}{c}\right)\cdot\left(\frac{A\,E}{F_{max}}\right) \geq 1 \text{ for fail condition} \qquad \text{(D - 10)}$$

$$(T\,c)\cdot\left(\frac{f}{4\cdot F_{max}}\right) \geq 1 \text{ for fail condition} \qquad \text{(D - 11)}$$

Using equations D-10 and D-11 as a basis, risk assessment charts with computed site specific and earthquake parameters V/c for Figure 5-1 and T x c for Figure 5-2, are developed and used for a risk assessment evaluation of a pipeline.

APPENDIX E
DEVELOPMENT OF SOIL STRAIN – SEISMIC VELOCITY RELATIONSHIP

The basis of the behavior of pipelines and pipe joints is the relationship between the seismic motion and the resulting soil strains as developed by Newmark (1967). Since this is such an important concept, it needs to be fully developed in order to understand each element in the expression. The development of the wave equation and the strain velocity relationship is as follows:

Consider a soil element with an imposed strain:

recall: $\varepsilon_x = \frac{\delta u}{\delta x}$ (E-1)

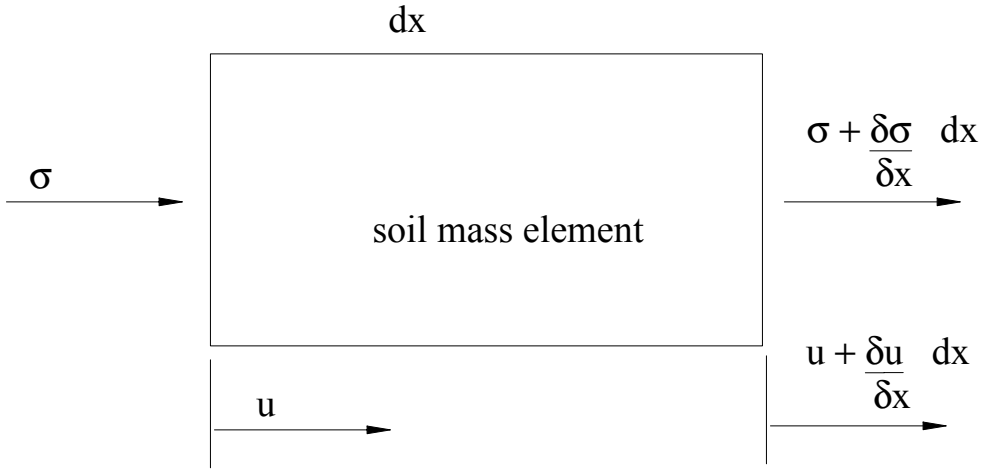

expand: $\sigma_x = G\,\varepsilon_x = G\,\frac{\delta u}{\delta x}$ (E-2)

where: G = soil shear modulus

differentiate (E-2): $\frac{\sigma_x}{\delta x} = G\,\frac{\delta^2 u}{\delta x^2}$ (E-3)

recall basic equation of motion: $\Sigma F = M\,a$ (E-4)

referring to the diagram: $\Sigma F = [\sigma - (\sigma + \frac{\delta \sigma}{\delta x}\,dx)]\,dA$ (E-5)

and $M\,a = [\rho\,dA\,dx][\frac{\delta^2 u}{\delta t^2}]$ (E-6)

substituting (E-5) and (E-6) into (E-4):

$$[\sigma - (\sigma + \frac{\delta \sigma}{\delta x}\,dx)]\,dA = [\rho\,dA\,dx][\frac{\delta^2 u}{\delta t^2}] \quad \text{(E-7)}$$

reducing (E-7): $\frac{\delta \sigma}{\delta x} = \rho\,\frac{\delta^2 u}{\delta t^2}$ (E-8)

substituting (E-3) into (E-8) gives the wave equation:

$$G\,\frac{\delta^2 u}{\delta x^2} = \rho\,\frac{\delta^2 u}{\delta t^2} \quad \text{(E-9)}$$

recall from geotechnical relationships:

$$c = \sqrt{\frac{G}{\rho}} \quad \text{(E.10)}$$

where: c = shear wave propagation velocity
ρ = soil density
G = soil shear modulus

rearranging: $\frac{G}{\rho} = c^2$ (E-11)

rearranging (E-11), and substituting into (E-9) give the differential equation:

$$c^2 \frac{\delta^2 u}{\delta x^2} = \frac{\delta^2 u}{\delta t^2} \quad \text{(E-12)}$$

assume a solution for "u"

$$u(t) = u_0 e^{i\lambda(x-ct)} \quad \text{(E-13)}$$

differentiate (E-13) to get the particle velocity from the seismic motion:

$$\frac{du}{dx} = V = u_0(i\lambda c)\, e^{i\lambda(x-ct)} \quad \text{(E-14)}$$

differentiate again to get the particle acceleration:

$$\frac{d^2u}{dx^2} = A = u_0(i\lambda c)^2\, e^{i\lambda(x-ct)} \quad \text{(E-15)}$$

for maximum value, set $e^{i\lambda(x-Vt)} = 1$

$$A = u_0\, c^2\, (i\lambda)^2 \quad \text{(E-16)}$$

reducing (E-16):

$$A = u_0\, c^2\, \lambda^2 \quad \text{(E-17)}$$

from (E-14):

$$V = u_0\, (-i\lambda c) e^{i\lambda(x-ct)} \quad \text{(E-18)}$$

for maximum value, set $e^{i\lambda(x-ct)} = 1$

$$V = u_0\, (-i\lambda c) \quad \text{(E-19)}$$

differentiate (E-13), the expression for strain:

$$\varepsilon = \frac{\delta u}{\delta x} = u_0 (i\lambda) e^{i\lambda(x-ct)} \qquad \text{(E-20)}$$

for maximum value of strain, set $e^{i\lambda(x-ct)} = 1$

$$\varepsilon = u_0 (i\lambda) \qquad \text{(E-21)}$$

divide (E-21) by (E-19)

$$\frac{\varepsilon}{V} = \frac{u_0 (i\lambda)}{u_0 (-i\lambda c)} \qquad \text{(E-22)}$$

rearranging and reducing (E-22) gives the strain-velocity relationship:

$$\varepsilon = \frac{V}{c} \qquad \text{(E-23)}$$

where:

ε = strain in the soil

V = particle velocity of the seismic motion

c = shear wave velocity of the soil

Multidisciplinary Center for Earthquake Engineering Research
List of Technical Reports

The Multidisciplinary Center for Earthquake Engineering Research (MCEER) publishes technical reports on a variety of subjects related to earthquake engineering written by authors funded through MCEER. These reports are available from both MCEER Publications and the National Technical Information Service (NTIS). Requests for reports should be directed to MCEER Publications, Multidisciplinary Center for Earthquake Engineering Research, State University of New York at Buffalo, Red Jacket Quadrangle, Buffalo, New York 14261. Reports can also be requested through NTIS, 5285 Port Royal Road, Springfield, Virginia 22161. NTIS accession numbers are shown in parenthesis, if available.

NCEER-87-0001 "First-Year Program in Research, Education and Technology Transfer," 3/5/87, (PB88-134275, A04, MF-A01).

NCEER-87-0002 "Experimental Evaluation of Instantaneous Optimal Algorithms for Structural Control," by R.C. Lin, T.T. Soong and A.M. Reinhorn, 4/20/87, (PB88-134341, A04, MF-A01).

NCEER-87-0003 "Experimentation Using the Earthquake Simulation Facilities at University at Buffalo," by A.M. Reinhorn and R.L. Ketter, to be published.

NCEER-87-0004 "The System Characteristics and Performance of a Shaking Table," by J.S. Hwang, K.C. Chang and G.C. Lee, 6/1/87, (PB88-134259, A03, MF-A01). This report is available only through NTIS (see address given above).

NCEER-87-0005 "A Finite Element Formulation for Nonlinear Viscoplastic Material Using a Q Model," by O. Gyebi and G. Dasgupta, 11/2/87, (PB88-213764, A08, MF-A01).

NCEER-87-0006 "Symbolic Manipulation Program (SMP) - Algebraic Codes for Two and Three Dimensional Finite Element Formulations," by X. Lee and G. Dasgupta, 11/9/87, (PB88-218522, A05, MF-A01).

NCEER-87-0007 "Instantaneous Optimal Control Laws for Tall Buildings Under Seismic Excitations," by J.N. Yang, A. Akbarpour and P. Ghaemmaghami, 6/10/87, (PB88-134333, A06, MF-A01). This report is only available through NTIS (see address given above).

NCEER-87-0008 "IDARC: Inelastic Damage Analysis of Reinforced Concrete Frame - Shear-Wall Structures," by Y.J. Park, A.M. Reinhorn and S.K. Kunnath, 7/20/87, (PB88-134325, A09, MF-A01). This report is only available through NTIS (see address given above).

NCEER-87-0009 "Liquefaction Potential for New York State: A Preliminary Report on Sites in Manhattan and Buffalo," by M. Budhu, V. Vijayakumar, R.F. Giese and L. Baumgras, 8/31/87, (PB88-163704, A03, MF-A01). This report is available only through NTIS (see address given above).

NCEER-87-0010 "Vertical and Torsional Vibration of Foundations in Inhomogeneous Media," by A.S. Veletsos and K.W. Dotson, 6/1/87, (PB88-134291, A03, MF-A01). This report is only available through NTIS (see address given above).

NCEER-87-0011 "Seismic Probabilistic Risk Assessment and Seismic Margins Studies for Nuclear Power Plants," by Howard H.M. Hwang, 6/15/87, (PB88-134267, A03, MF-A01). This report is only available through NTIS (see address given above).

NCEER-87-0012 "Parametric Studies of Frequency Response of Secondary Systems Under Ground-Acceleration Excitations," by Y. Yong and Y.K. Lin, 6/10/87, (PB88-134309, A03, MF-A01). This report is only available through NTIS (see address given above).

NCEER-87-0013 "Frequency Response of Secondary Systems Under Seismic Excitation," by J.A. HoLung, J. Cai and Y.K. Lin, 7/31/87, (PB88-134317, A05, MF-A01). This report is only available through NTIS (see address given above).

NCEER-87-0014 "Modelling Earthquake Ground Motions in Seismically Active Regions Using Parametric Time Series Methods," by G.W. Ellis and A.S. Cakmak, 8/25/87, (PB88-134283, A08, MF-A01). This report is only available through NTIS (see address given above).

NCEER-87-0015 "Detection and Assessment of Seismic Structural Damage," by E. DiPasquale and A.S. Cakmak, 8/25/87, (PB88-163712, A05, MF-A01). This report is only available through NTIS (see address given above).

NCEER-87-0016 "Pipeline Experiment at Parkfield, California," by J. Isenberg and E. Richardson, 9/15/87, (PB88-163720, A03, MF-A01). This report is available only through NTIS (see address given above).

NCEER-87-0017 "Digital Simulation of Seismic Ground Motion," by M. Shinozuka, G. Deodatis and T. Harada, 8/31/87, (PB88-155197, A04, MF-A01). This report is available only through NTIS (see address given above).

NCEER-87-0018 "Practical Considerations for Structural Control: System Uncertainty, System Time Delay and Truncation of Small Control Forces," J.N. Yang and A. Akbarpour, 8/10/87, (PB88-163738, A08, MF-A01). This report is only available through NTIS (see address given above).

NCEER-87-0019 "Modal Analysis of Nonclassically Damped Structural Systems Using Canonical Transformation," by J.N. Yang, S. Sarkani and F.X. Long, 9/27/87, (PB88-187851, A04, MF-A01).

NCEER-87-0020 "A Nonstationary Solution in Random Vibration Theory," by J.R. Red-Horse and P.D. Spanos, 11/3/87, (PB88-163746, A03, MF-A01).

NCEER-87-0021 "Horizontal Impedances for Radially Inhomogeneous Viscoelastic Soil Layers," by A.S. Veletsos and K.W. Dotson, 10/15/87, (PB88-150859, A04, MF-A01).

NCEER-87-0022 "Seismic Damage Assessment of Reinforced Concrete Members," by Y.S. Chung, C. Meyer and M. Shinozuka, 10/9/87, (PB88-150867, A05, MF-A01). This report is available only through NTIS (see address given above).

NCEER-87-0023 "Active Structural Control in Civil Engineering," by T.T. Soong, 11/11/87, (PB88-187778, A03, MF-A01).

NCEER-87-0024 "Vertical and Torsional Impedances for Radially Inhomogeneous Viscoelastic Soil Layers," by K.W. Dotson and A.S. Veletsos, 12/87, (PB88-187786, A03, MF-A01).

NCEER-87-0025 "Proceedings from the Symposium on Seismic Hazards, Ground Motions, Soil-Liquefaction and Engineering Practice in Eastern North America," October 20-22, 1987, edited by K.H. Jacob, 12/87, (PB88-188115, A23, MF-A01). This report is available only through NTIS (see address given above).

NCEER-87-0026 "Report on the Whittier-Narrows, California, Earthquake of October 1, 1987," by J. Pantelic and A. Reinhorn, 11/87, (PB88-187752, A03, MF-A01). This report is available only through NTIS (see address given above).

NCEER-87-0027 "Design of a Modular Program for Transient Nonlinear Analysis of Large 3-D Building Structures," by S. Srivastav and J.F. Abel, 12/30/87, (PB88-187950, A05, MF-A01). This report is only available through NTIS (see address given above).

NCEER-87-0028 "Second-Year Program in Research, Education and Technology Transfer," 3/8/88, (PB88-219480, A04, MF-A01).

NCEER-88-0001 "Workshop on Seismic Computer Analysis and Design of Buildings With Interactive Graphics," by W. McGuire, J.F. Abel and C.H. Conley, 1/18/88, (PB88-187760, A03, MF-A01). This report is only available through NTIS (see address given above).

NCEER-88-0002 "Optimal Control of Nonlinear Flexible Structures," by J.N. Yang, F.X. Long and D. Wong, 1/22/88, (PB88-213772, A06, MF-A01).

NCEER-88-0003 "Substructuring Techniques in the Time Domain for Primary-Secondary Structural Systems," by G.D. Manolis and G. Juhn, 2/10/88, (PB88-213780, A04, MF-A01).

NCEER-88-0004 "Iterative Seismic Analysis of Primary-Secondary Systems," by A. Singhal, L.D. Lutes and P.D. Spanos, 2/23/88, (PB88-213798, A04, MF-A01).

NCEER-88-0005 "Stochastic Finite Element Expansion for Random Media," by P.D. Spanos and R. Ghanem, 3/14/88, (PB88-213806, A03, MF-A01).

NCEER-88-0006 "Combining Structural Optimization and Structural Control," by F.Y. Cheng and C.P. Pantelides, 1/10/88, (PB88-213814, A05, MF-A01).

NCEER-88-0007 "Seismic Performance Assessment of Code-Designed Structures," by H.H-M. Hwang, J-W. Jaw and H-J. Shau, 3/20/88, (PB88-219423, A04, MF-A01). This report is only available through NTIS (see address given above).

NCEER-88-0008 "Reliability Analysis of Code-Designed Structures Under Natural Hazards," by H.H-M. Hwang, H. Ushiba and M. Shinozuka, 2/29/88, (PB88-229471, A07, MF-A01). This report is only available through NTIS (see address given above).

NCEER-88-0009 "Seismic Fragility Analysis of Shear Wall Structures," by J-W Jaw and H.H-M. Hwang, 4/30/88, (PB89-102867, A04, MF-A01).

NCEER-88-0010 "Base Isolation of a Multi-Story Building Under a Harmonic Ground Motion - A Comparison of Performances of Various Systems," by F-G Fan, G. Ahmadi and I.G. Tadjbakhsh, 5/18/88, (PB89-122238, A06, MF-A01). This report is only available through NTIS (see address given above).

NCEER-88-0011 "Seismic Floor Response Spectra for a Combined System by Green's Functions," by F.M. Lavelle, L.A. Bergman and P.D. Spanos, 5/1/88, (PB89-102875, A03, MF-A01).

NCEER-88-0012 "A New Solution Technique for Randomly Excited Hysteretic Structures," by G.Q. Cai and Y.K. Lin, 5/16/88, (PB89-102883, A03, MF-A01).

NCEER-88-0013 "A Study of Radiation Damping and Soil-Structure Interaction Effects in the Centrifuge," by K. Weissman, supervised by J.H. Prevost, 5/24/88, (PB89-144703, A06, MF-A01).

NCEER-88-0014 "Parameter Identification and Implementation of a Kinematic Plasticity Model for Frictional Soils," by J.H. Prevost and D.V. Griffiths, to be published.

NCEER-88-0015 "Two- and Three- Dimensional Dynamic Finite Element Analyses of the Long Valley Dam," by D.V. Griffiths and J.H. Prevost, 6/17/88, (PB89-144711, A04, MF-A01).

NCEER-88-0016 "Damage Assessment of Reinforced Concrete Structures in Eastern United States," by A.M. Reinhorn, M.J. Seidel, S.K. Kunnath and Y.J. Park, 6/15/88, (PB89-122220, A04, MF-A01). This report is only available through NTIS (see address given above).

NCEER-88-0017 "Dynamic Compliance of Vertically Loaded Strip Foundations in Multilayered Viscoelastic Soils," by S. Ahmad and A.S.M. Israil, 6/17/88, (PB89-102891, A04, MF-A01).

NCEER-88-0018 "An Experimental Study of Seismic Structural Response With Added Viscoelastic Dampers," by R.C. Lin, Z. Liang, T.T. Soong and R.H. Zhang, 6/30/88, (PB89-122212, A05, MF-A01). This report is available only through NTIS (see address given above).

NCEER-88-0019 "Experimental Investigation of Primary - Secondary System Interaction," by G.D. Manolis, G. Juhn and A.M. Reinhorn, 5/27/88, (PB89-122204, A04, MF-A01).

NCEER-88-0020 "A Response Spectrum Approach For Analysis of Nonclassically Damped Structures," by J.N. Yang, S. Sarkani and F.X. Long, 4/22/88, (PB89-102909, A04, MF-A01).

NCEER-88-0021 "Seismic Interaction of Structures and Soils: Stochastic Approach," by A.S. Veletsos and A.M. Prasad, 7/21/88, (PB89-122196, A04, MF-A01). This report is only available through NTIS (see address given above).

NCEER-88-0022 "Identification of the Serviceability Limit State and Detection of Seismic Structural Damage," by E. DiPasquale and A.S. Cakmak, 6/15/88, (PB89-122188, A05, MF-A01). This report is available only through NTIS (see address given above).

NCEER-88-0023 "Multi-Hazard Risk Analysis: Case of a Simple Offshore Structure," by B.K. Bhartia and E.H. Vanmarcke, 7/21/88, (PB89-145213, A05, MF-A01).

NCEER-88-0024 "Automated Seismic Design of Reinforced Concrete Buildings," by Y.S. Chung, C. Meyer and M. Shinozuka, 7/5/88, (PB89-122170, A06, MF-A01). This report is available only through NTIS (see address given above).

NCEER-88-0025 "Experimental Study of Active Control of MDOF Structures Under Seismic Excitations," by L.L. Chung, R.C. Lin, T.T. Soong and A.M. Reinhorn, 7/10/88, (PB89-122600, A04, MF-A01).

NCEER-88-0026 "Earthquake Simulation Tests of a Low-Rise Metal Structure," by J.S. Hwang, K.C. Chang, G.C. Lee and R.L. Ketter, 8/1/88, (PB89-102917, A04, MF-A01).

NCEER-88-0027 "Systems Study of Urban Response and Reconstruction Due to Catastrophic Earthquakes," by F. Kozin and H.K. Zhou, 9/22/88, (PB90-162348, A04, MF-A01).

NCEER-88-0028 "Seismic Fragility Analysis of Plane Frame Structures," by H.H-M. Hwang and Y.K. Low, 7/31/88, (PB89-131445, A06, MF-A01).

NCEER-88-0029 "Response Analysis of Stochastic Structures," by A. Kardara, C. Bucher and M. Shinozuka, 9/22/88, (PB89-174429, A04, MF-A01).

NCEER-88-0030 "Nonnormal Accelerations Due to Yielding in a Primary Structure," by D.C.K. Chen and L.D. Lutes, 9/19/88, (PB89-131437, A04, MF-A01).

NCEER-88-0031 "Design Approaches for Soil-Structure Interaction," by A.S. Veletsos, A.M. Prasad and Y. Tang, 12/30/88, (PB89-174437, A03, MF-A01). This report is available only through NTIS (see address given above).

NCEER-88-0032 "A Re-evaluation of Design Spectra for Seismic Damage Control," by C.J. Turkstra and A.G. Tallin, 11/7/88, (PB89-145221, A05, MF-A01).

NCEER-88-0033 "The Behavior and Design of Noncontact Lap Splices Subjected to Repeated Inelastic Tensile Loading," by V.E. Sagan, P. Gergely and R.N. White, 12/8/88, (PB89-163737, A08, MF-A01).

NCEER-88-0034 "Seismic Response of Pile Foundations," by S.M. Mamoon, P.K. Banerjee and S. Ahmad, 11/1/88, (PB89-145239, A04, MF-A01).

NCEER-88-0035 "Modeling of R/C Building Structures With Flexible Floor Diaphragms (IDARC2)," by A.M. Reinhorn, S.K. Kunnath and N. Panahshahi, 9/7/88, (PB89-207153, A07, MF-A01).

NCEER-88-0036 "Solution of the Dam-Reservoir Interaction Problem Using a Combination of FEM, BEM with Particular Integrals, Modal Analysis, and Substructuring," by C-S. Tsai, G.C. Lee and R.L. Ketter, 12/31/88, (PB89-207146, A04, MF-A01).

NCEER-88-0037 "Optimal Placement of Actuators for Structural Control," by F.Y. Cheng and C.P. Pantelides, 8/15/88, (PB89-162846, A05, MF-A01).

NCEER-88-0038 "Teflon Bearings in Aseismic Base Isolation: Experimental Studies and Mathematical Modeling," by A. Mokha, M.C. Constantinou and A.M. Reinhorn, 12/5/88, (PB89-218457, A10, MF-A01). This report is available only through NTIS (see address given above).

NCEER-88-0039 "Seismic Behavior of Flat Slab High-Rise Buildings in the New York City Area," by P. Weidlinger and M. Ettouney, 10/15/88, (PB90-145681, A04, MF-A01).

NCEER-88-0040 "Evaluation of the Earthquake Resistance of Existing Buildings in New York City," by P. Weidlinger and M. Ettouney, 10/15/88, to be published.

NCEER-88-0041 "Small-Scale Modeling Techniques for Reinforced Concrete Structures Subjected to Seismic Loads," by W. Kim, A. El-Attar and R.N. White, 11/22/88, (PB89-189625, A05, MF-A01).

NCEER-88-0042 "Modeling Strong Ground Motion from Multiple Event Earthquakes," by G.W. Ellis and A.S. Cakmak, 10/15/88, (PB89-174445, A03, MF-A01).

NCEER-88-0043 "Nonstationary Models of Seismic Ground Acceleration," by M. Grigoriu, S.E. Ruiz and E. Rosenblueth, 7/15/88, (PB89-189617, A04, MF-A01).

NCEER-88-0044 "SARCF User's Guide: Seismic Analysis of Reinforced Concrete Frames," by Y.S. Chung, C. Meyer and M. Shinozuka, 11/9/88, (PB89-174452, A08, MF-A01).

NCEER-88-0045 "First Expert Panel Meeting on Disaster Research and Planning," edited by J. Pantelic and J. Stoyle, 9/15/88, (PB89-174460, A05, MF-A01).

NCEER-88-0046 "Preliminary Studies of the Effect of Degrading Infill Walls on the Nonlinear Seismic Response of Steel Frames," by C.Z. Chrysostomou, P. Gergely and J.F. Abel, 12/19/88, (PB89-208383, A05, MF-A01).

NCEER-88-0047 "Reinforced Concrete Frame Component Testing Facility - Design, Construction, Instrumentation and Operation," by S.P. Pessiki, C. Conley, T. Bond, P. Gergely and R.N. White, 12/16/88, (PB89-174478, A04, MF-A01).

NCEER-89-0001 "Effects of Protective Cushion and Soil Compliancy on the Response of Equipment Within a Seismically Excited Building," by J.A. HoLung, 2/16/89, (PB89-207179, A04, MF-A01).

NCEER-89-0002 "Statistical Evaluation of Response Modification Factors for Reinforced Concrete Structures," by H.H-M. Hwang and J-W. Jaw, 2/17/89, (PB89-207187, A05, MF-A01).

NCEER-89-0003 "Hysteretic Columns Under Random Excitation," by G-Q. Cai and Y.K. Lin, 1/9/89, (PB89-196513, A03, MF-A01).

NCEER-89-0004 "Experimental Study of `Elephant Foot Bulge' Instability of Thin-Walled Metal Tanks," by Z-H. Jia and R.L. Ketter, 2/22/89, (PB89-207195, A03, MF-A01).

NCEER-89-0005 "Experiment on Performance of Buried Pipelines Across San Andreas Fault," by J. Isenberg, E. Richardson and T.D. O'Rourke, 3/10/89, (PB89-218440, A04, MF-A01). This report is available only through NTIS (see address given above).

NCEER-89-0006 "A Knowledge-Based Approach to Structural Design of Earthquake-Resistant Buildings," by M. Subramani, P. Gergely, C.H. Conley, J.F. Abel and A.H. Zaghw, 1/15/89, (PB89-218465, A06, MF-A01).

NCEER-89-0007 "Liquefaction Hazards and Their Effects on Buried Pipelines," by T.D. O'Rourke and P.A. Lane, 2/1/89, (PB89-218481, A09, MF-A01).

NCEER-89-0008 "Fundamentals of System Identification in Structural Dynamics," by H. Imai, C-B. Yun, O. Maruyama and M. Shinozuka, 1/26/89, (PB89-207211, A04, MF-A01).

NCEER-89-0009 "Effects of the 1985 Michoacan Earthquake on Water Systems and Other Buried Lifelines in Mexico," by A.G. Ayala and M.J. O'Rourke, 3/8/89, (PB89-207229, A06, MF-A01).

NCEER-89-R010 "NCEER Bibliography of Earthquake Education Materials," by K.E.K. Ross, Second Revision, 9/1/89, (PB90-125352, A05, MF-A01). This report is replaced by NCEER-92-0018.

NCEER-89-0011 "Inelastic Three-Dimensional Response Analysis of Reinforced Concrete Building Structures (IDARC-3D), Part I - Modeling," by S.K. Kunnath and A.M. Reinhorn, 4/17/89, (PB90-114612, A07, MF-A01). This report is available only through NTIS (see address given above).

NCEER-89-0012 "Recommended Modifications to ATC-14," by C.D. Poland and J.O. Malley, 4/12/89, (PB90-108648, A15, MF-A01).

NCEER-89-0013 "Repair and Strengthening of Beam-to-Column Connections Subjected to Earthquake Loading," by M. Corazao and A.J. Durrani, 2/28/89, (PB90-109885, A06, MF-A01).

NCEER-89-0014 "Program EXKAL2 for Identification of Structural Dynamic Systems," by O. Maruyama, C-B. Yun, M. Hoshiya and M. Shinozuka, 5/19/89, (PB90-109877, A09, MF-A01).

NCEER-89-0015 "Response of Frames With Bolted Semi-Rigid Connections, Part I - Experimental Study and Analytical Predictions," by P.J. DiCorso, A.M. Reinhorn, J.R. Dickerson, J.B. Radziminski and W.L. Harper, 6/1/89, to be published.

NCEER-89-0016 "ARMA Monte Carlo Simulation in Probabilistic Structural Analysis," by P.D. Spanos and M.P. Mignolet, 7/10/89, (PB90-109893, A03, MF-A01).

NCEER-89-P017 "Preliminary Proceedings from the Conference on Disaster Preparedness - The Place of Earthquake Education in Our Schools," Edited by K.E.K. Ross, 6/23/89, (PB90-108606, A03, MF-A01).

NCEER-89-0017 "Proceedings from the Conference on Disaster Preparedness - The Place of Earthquake Education in Our Schools," Edited by K.E.K. Ross, 12/31/89, (PB90-207895, A012, MF-A02). This report is available only through NTIS (see address given above).

NCEER-89-0018 "Multidimensional Models of Hysteretic Material Behavior for Vibration Analysis of Shape Memory Energy Absorbing Devices, by E.J. Graesser and F.A. Cozzarelli, 6/7/89, (PB90-164146, A04, MF-A01).

NCEER-89-0019 "Nonlinear Dynamic Analysis of Three-Dimensional Base Isolated Structures (3D-BASIS)," by S. Nagarajaiah, A.M. Reinhorn and M.C. Constantinou, 8/3/89, (PB90-161936, A06, MF-A01). This report has been replaced by NCEER-93-0011.

NCEER-89-0020 "Structural Control Considering Time-Rate of Control Forces and Control Rate Constraints," by F.Y. Cheng and C.P. Pantelides, 8/3/89, (PB90-120445, A04, MF-A01).

NCEER-89-0021 "Subsurface Conditions of Memphis and Shelby County," by K.W. Ng, T-S. Chang and H-H.M. Hwang, 7/26/89, (PB90-120437, A03, MF-A01).

NCEER-89-0022 "Seismic Wave Propagation Effects on Straight Jointed Buried Pipelines," by K. Elhmadi and M.J. O'Rourke, 8/24/89, (PB90-162322, A10, MF-A02).

NCEER-89-0023 "Workshop on Serviceability Analysis of Water Delivery Systems," edited by M. Grigoriu, 3/6/89, (PB90-127424, A03, MF-A01).

NCEER-89-0024 "Shaking Table Study of a 1/5 Scale Steel Frame Composed of Tapered Members," by K.C. Chang, J.S. Hwang and G.C. Lee, 9/18/89, (PB90-160169, A04, MF-A01).

NCEER-89-0025 "DYNA1D: A Computer Program for Nonlinear Seismic Site Response Analysis - Technical Documentation," by Jean H. Prevost, 9/14/89, (PB90-161944, A07, MF-A01). This report is available only through NTIS (see address given above).

NCEER-89-0026 "1:4 Scale Model Studies of Active Tendon Systems and Active Mass Dampers for Aseismic Protection," by A.M. Reinhorn, T.T. Soong, R.C. Lin, Y.P. Yang, Y. Fukao, H. Abe and M. Nakai, 9/15/89, (PB90-173246, A10, MF-A02). This report is available only through NTIS (see address given above).

NCEER-89-0027 "Scattering of Waves by Inclusions in a Nonhomogeneous Elastic Half Space Solved by Boundary Element Methods," by P.K. Hadley, A. Askar and A.S. Cakmak, 6/15/89, (PB90-145699, A07, MF-A01).

NCEER-89-0028 "Statistical Evaluation of Deflection Amplification Factors for Reinforced Concrete Structures," by H.H.M. Hwang, J-W. Jaw and A.L. Ch'ng, 8/31/89, (PB90-164633, A05, MF-A01).

NCEER-89-0029 "Bedrock Accelerations in Memphis Area Due to Large New Madrid Earthquakes," by H.H.M. Hwang, C.H.S. Chen and G. Yu, 11/7/89, (PB90-162330, A04, MF-A01).

NCEER-89-0030 "Seismic Behavior and Response Sensitivity of Secondary Structural Systems," by Y.Q. Chen and T.T. Soong, 10/23/89, (PB90-164658, A08, MF-A01).

NCEER-89-0031 "Random Vibration and Reliability Analysis of Primary-Secondary Structural Systems," by Y. Ibrahim, M. Grigoriu and T.T. Soong, 11/10/89, (PB90-161951, A04, MF-A01).

NCEER-89-0032 "Proceedings from the Second U.S. - Japan Workshop on Liquefaction, Large Ground Deformation and Their Effects on Lifelines, September 26-29, 1989," Edited by T.D. O'Rourke and M. Hamada, 12/1/89, (PB90-209388, A22, MF-A03).

NCEER-89-0033 "Deterministic Model for Seismic Damage Evaluation of Reinforced Concrete Structures," by J.M. Bracci, A.M. Reinhorn, J.B. Mander and S.K. Kunnath, 9/27/89, (PB91-108803, A06, MF-A01).

NCEER-89-0034 "On the Relation Between Local and Global Damage Indices," by E. DiPasquale and A.S. Cakmak, 8/15/89, (PB90-173865, A05, MF-A01).

NCEER-89-0035 "Cyclic Undrained Behavior of Nonplastic and Low Plasticity Silts," by A.J. Walker and H.E. Stewart, 7/26/89, (PB90-183518, A10, MF-A01).

NCEER-89-0036 "Liquefaction Potential of Surficial Deposits in the City of Buffalo, New York," by M. Budhu, R. Giese and L. Baumgrass, 1/17/89, (PB90-208455, A04, MF-A01).

NCEER-89-0037 "A Deterministic Assessment of Effects of Ground Motion Incoherence," by A.S. Veletsos and Y. Tang, 7/15/89, (PB90-164294, A03, MF-A01).

NCEER-89-0038 "Workshop on Ground Motion Parameters for Seismic Hazard Mapping," July 17-18, 1989, edited by R.V. Whitman, 12/1/89, (PB90-173923, A04, MF-A01).

NCEER-89-0039 "Seismic Effects on Elevated Transit Lines of the New York City Transit Authority," by C.J. Costantino, C.A. Miller and E. Heymsfield, 12/26/89, (PB90-207887, A06, MF-A01).

NCEER-89-0040 "Centrifugal Modeling of Dynamic Soil-Structure Interaction," by K. Weissman, Supervised by J.H. Prevost, 5/10/89, (PB90-207879, A07, MF-A01).

NCEER-89-0041 "Linearized Identification of Buildings With Cores for Seismic Vulnerability Assessment," by I-K. Ho and A.E. Aktan, 11/1/89, (PB90-251943, A07, MF-A01).

NCEER-90-0001 "Geotechnical and Lifeline Aspects of the October 17, 1989 Loma Prieta Earthquake in San Francisco," by T.D. O'Rourke, H.E. Stewart, F.T. Blackburn and T.S. Dickerman, 1/90, (PB90-208596, A05, MF-A01).

NCEER-90-0002 "Nonnormal Secondary Response Due to Yielding in a Primary Structure," by D.C.K. Chen and L.D. Lutes, 2/28/90, (PB90-251976, A07, MF-A01).

NCEER-90-0003 "Earthquake Education Materials for Grades K-12," by K.E.K. Ross, 4/16/90, (PB91-251984, A05, MF-A05). This report has been replaced by NCEER-92-0018.

NCEER-90-0004 "Catalog of Strong Motion Stations in Eastern North America," by R.W. Busby, 4/3/90, (PB90-251984, A05, MF-A01).

NCEER-90-0005 "NCEER Strong-Motion Data Base: A User Manual for the GeoBase Release (Version 1.0 for the Sun3)," by P. Friberg and K. Jacob, 3/31/90 (PB90-258062, A04, MF-A01).

NCEER-90-0006 "Seismic Hazard Along a Crude Oil Pipeline in the Event of an 1811-1812 Type New Madrid Earthquake," by H.H.M. Hwang and C-H.S. Chen, 4/16/90, (PB90-258054, A04, MF-A01).

NCEER-90-0007 "Site-Specific Response Spectra for Memphis Sheahan Pumping Station," by H.H.M. Hwang and C.S. Lee, 5/15/90, (PB91-108811, A05, MF-A01).

NCEER-90-0008 "Pilot Study on Seismic Vulnerability of Crude Oil Transmission Systems," by T. Ariman, R. Dobry, M. Grigoriu, F. Kozin, M. O'Rourke, T. O'Rourke and M. Shinozuka, 5/25/90, (PB91-108837, A06, MF-A01).

NCEER-90-0009 "A Program to Generate Site Dependent Time Histories: EQGEN," by G.W. Ellis, M. Srinivasan and A.S. Cakmak, 1/30/90, (PB91-108829, A04, MF-A01).

NCEER-90-0010 "Active Isolation for Seismic Protection of Operating Rooms," by M.E. Talbott, Supervised by M. Shinozuka, 6/8/9, (PB91-110205, A05, MF-A01).

NCEER-90-0011 "Program LINEARID for Identification of Linear Structural Dynamic Systems," by C-B. Yun and M. Shinozuka, 6/25/90, (PB91-110312, A08, MF-A01).

NCEER-90-0012 "Two-Dimensional Two-Phase Elasto-Plastic Seismic Response of Earth Dams," by A.N. Yiagos, Supervised by J.H. Prevost, 6/20/90, (PB91-110197, A13, MF-A02).

NCEER-90-0013 "Secondary Systems in Base-Isolated Structures: Experimental Investigation, Stochastic Response and Stochastic Sensitivity," by G.D. Manolis, G. Juhn, M.C. Constantinou and A.M. Reinhorn, 7/1/90, (PB91-110320, A08, MF-A01).

NCEER-90-0014 "Seismic Behavior of Lightly-Reinforced Concrete Column and Beam-Column Joint Details," by S.P. Pessiki, C.H. Conley, P. Gergely and R.N. White, 8/22/90, (PB91-108795, A11, MF-A02).

NCEER-90-0015 "Two Hybrid Control Systems for Building Structures Under Strong Earthquakes," by J.N. Yang and A. Danielians, 6/29/90, (PB91-125393, A04, MF-A01).

NCEER-90-0016 "Instantaneous Optimal Control with Acceleration and Velocity Feedback," by J.N. Yang and Z. Li, 6/29/90, (PB91-125401, A03, MF-A01).

NCEER-90-0017 "Reconnaissance Report on the Northern Iran Earthquake of June 21, 1990," by M. Mehrain, 10/4/90, (PB91-125377, A03, MF-A01).

NCEER-90-0018 "Evaluation of Liquefaction Potential in Memphis and Shelby County," by T.S. Chang, P.S. Tang, C.S. Lee and H. Hwang, 8/10/90, (PB91-125427, A09, MF-A01).

NCEER-90-0019 "Experimental and Analytical Study of a Combined Sliding Disc Bearing and Helical Steel Spring Isolation System," by M.C. Constantinou, A.S. Mokha and A.M. Reinhorn, 10/4/90, (PB91-125385, A06, MF-A01). This report is available only through NTIS (see address given above).

NCEER-90-0020 "Experimental Study and Analytical Prediction of Earthquake Response of a Sliding Isolation System with a Spherical Surface," by A.S. Mokha, M.C. Constantinou and A.M. Reinhorn, 10/11/90, (PB91-125419, A05, MF-A01).

NCEER-90-0021 "Dynamic Interaction Factors for Floating Pile Groups," by G. Gazetas, K. Fan, A. Kaynia and E. Kausel, 9/10/90, (PB91-170381, A05, MF-A01).

NCEER-90-0022 "Evaluation of Seismic Damage Indices for Reinforced Concrete Structures," by S. Rodriguez-Gomez and A.S. Cakmak, 9/30/90, PB91-171322, A06, MF-A01).

NCEER-90-0023 "Study of Site Response at a Selected Memphis Site," by H. Desai, S. Ahmad, E.S. Gazetas and M.R. Oh, 10/11/90, (PB91-196857, A03, MF-A01).

NCEER-90-0024 "A User's Guide to Strongmo: Version 1.0 of NCEER's Strong-Motion Data Access Tool for PCs and Terminals," by P.A. Friberg and C.A.T. Susch, 11/15/90, (PB91-171272, A03, MF-A01).

NCEER-90-0025 "A Three-Dimensional Analytical Study of Spatial Variability of Seismic Ground Motions," by L-L. Hong and A.H.-S. Ang, 10/30/90, (PB91-170399, A09, MF-A01).

NCEER-90-0026 "MUMOID User's Guide - A Program for the Identification of Modal Parameters," by S. Rodriguez-Gomez and E. DiPasquale, 9/30/90, (PB91-171298, A04, MF-A01).

NCEER-90-0027 "SARCF-II User's Guide - Seismic Analysis of Reinforced Concrete Frames," by S. Rodriguez-Gomez, Y.S. Chung and C. Meyer, 9/30/90, (PB91-171280, A05, MF-A01).

NCEER-90-0028 "Viscous Dampers: Testing, Modeling and Application in Vibration and Seismic Isolation," by N. Makris and M.C. Constantinou, 12/20/90 (PB91-190561, A06, MF-A01).

NCEER-90-0029 "Soil Effects on Earthquake Ground Motions in the Memphis Area," by H. Hwang, C.S. Lee, K.W. Ng and T.S. Chang, 8/2/90, (PB91-190751, A05, MF-A01).

NCEER-91-0001 "Proceedings from the Third Japan-U.S. Workshop on Earthquake Resistant Design of Lifeline Facilities and Countermeasures for Soil Liquefaction, December 17-19, 1990," edited by T.D. O'Rourke and M. Hamada, 2/1/91, (PB91-179259, A99, MF-A04).

NCEER-91-0002 "Physical Space Solutions of Non-Proportionally Damped Systems," by M. Tong, Z. Liang and G.C. Lee, 1/15/91, (PB91-179242, A04, MF-A01).

NCEER-91-0003 "Seismic Response of Single Piles and Pile Groups," by K. Fan and G. Gazetas, 1/10/91, (PB92-174994, A04, MF-A01).

NCEER-91-0004 "Damping of Structures: Part 1 - Theory of Complex Damping," by Z. Liang and G. Lee, 10/10/91, (PB92-197235, A12, MF-A03).

NCEER-91-0005 "3D-BASIS - Nonlinear Dynamic Analysis of Three Dimensional Base Isolated Structures: Part II," by S. Nagarajaiah, A.M. Reinhorn and M.C. Constantinou, 2/28/91, (PB91-190553, A07, MF-A01). This report has been replaced by NCEER-93-0011.

NCEER-91-0006 "A Multidimensional Hysteretic Model for Plasticity Deforming Metals in Energy Absorbing Devices," by E.J. Graesser and F.A. Cozzarelli, 4/9/91, (PB92-108364, A04, MF-A01).

NCEER-91-0007 "A Framework for Customizable Knowledge-Based Expert Systems with an Application to a KBES for Evaluating the Seismic Resistance of Existing Buildings," by E.G. Ibarra-Anaya and S.J. Fenves, 4/9/91, (PB91-210930, A08, MF-A01).

NCEER-91-0008 "Nonlinear Analysis of Steel Frames with Semi-Rigid Connections Using the Capacity Spectrum Method," by G.G. Deierlein, S-H. Hsieh, Y-J. Shen and J.F. Abel, 7/2/91, (PB92-113828, A05, MF-A01).

NCEER-91-0009 "Earthquake Education Materials for Grades K-12," by K.E.K. Ross, 4/30/91, (PB91-212142, A06, MF-A01). This report has been replaced by NCEER-92-0018.

NCEER-91-0010 "Phase Wave Velocities and Displacement Phase Differences in a Harmonically Oscillating Pile," by N. Makris and G. Gazetas, 7/8/91, (PB92-108356, A04, MF-A01).

NCEER-91-0011 "Dynamic Characteristics of a Full-Size Five-Story Steel Structure and a 2/5 Scale Model," by K.C. Chang, G.C. Yao, G.C. Lee, D.S. Hao and Y.C. Yeh," 7/2/91, (PB93-116648, A06, MF-A02).

NCEER-91-0012 "Seismic Response of a 2/5 Scale Steel Structure with Added Viscoelastic Dampers," by K.C. Chang, T.T. Soong, S-T. Oh and M.L. Lai, 5/17/91, (PB92-110816, A05, MF-A01).

NCEER-91-0013 "Earthquake Response of Retaining Walls; Full-Scale Testing and Computational Modeling," by S. Alampalli and A-W.M. Elgamal, 6/20/91, to be published.

NCEER-91-0014 "3D-BASIS-M: Nonlinear Dynamic Analysis of Multiple Building Base Isolated Structures," by P.C. Tsopelas, S. Nagarajaiah, M.C. Constantinou and A.M. Reinhorn, 5/28/91, (PB92-113885, A09, MF-A02).

NCEER-91-0015 "Evaluation of SEAOC Design Requirements for Sliding Isolated Structures," by D. Theodossiou and M.C. Constantinou, 6/10/91, (PB92-114602, A11, MF-A03).

NCEER-91-0016 "Closed-Loop Modal Testing of a 27-Story Reinforced Concrete Flat Plate-Core Building," by H.R. Somaprasad, T. Toksoy, H. Yoshiyuki and A.E. Aktan, 7/15/91, (PB92-129980, A07, MF-A02).

NCEER-91-0017 "Shake Table Test of a 1/6 Scale Two-Story Lightly Reinforced Concrete Building," by A.G. El-Attar, R.N. White and P. Gergely, 2/28/91, (PB92-222447, A06, MF-A02).

NCEER-91-0018 "Shake Table Test of a 1/8 Scale Three-Story Lightly Reinforced Concrete Building," by A.G. El-Attar, R.N. White and P. Gergely, 2/28/91, (PB93-116630, A08, MF-A02).

NCEER-91-0019 "Transfer Functions for Rigid Rectangular Foundations," by A.S. Veletsos, A.M. Prasad and W.H. Wu, 7/31/91, to be published.

NCEER-91-0020 "Hybrid Control of Seismic-Excited Nonlinear and Inelastic Structural Systems," by J.N. Yang, Z. Li and A. Danielians, 8/1/91, (PB92-143171, A06, MF-A02).

NCEER-91-0021 "The NCEER-91 Earthquake Catalog: Improved Intensity-Based Magnitudes and Recurrence Relations for U.S. Earthquakes East of New Madrid," by L. Seeber and J.G. Armbruster, 8/28/91, (PB92-176742, A06, MF-A02).

NCEER-91-0022 "Proceedings from the Implementation of Earthquake Planning and Education in Schools: The Need for Change - The Roles of the Changemakers," by K.E.K. Ross and F. Winslow, 7/23/91, (PB92-129998, A12, MF-A03).

NCEER-91-0023 "A Study of Reliability-Based Criteria for Seismic Design of Reinforced Concrete Frame Buildings," by H.H.M. Hwang and H-M. Hsu, 8/10/91, (PB92-140235, A09, MF-A02).

NCEER-91-0024 "Experimental Verification of a Number of Structural System Identification Algorithms," by R.G. Ghanem, H. Gavin and M. Shinozuka, 9/18/91, (PB92-176577, A18, MF-A04).

NCEER-91-0025 "Probabilistic Evaluation of Liquefaction Potential," by H.H.M. Hwang and C.S. Lee," 11/25/91, (PB92-143429, A05, MF-A01).

NCEER-91-0026 "Instantaneous Optimal Control for Linear, Nonlinear and Hysteretic Structures - Stable Controllers," by J.N. Yang and Z. Li, 11/15/91, (PB92-163807, A04, MF-A01).

NCEER-91-0027 "Experimental and Theoretical Study of a Sliding Isolation System for Bridges," by M.C. Constantinou, A. Kartoum, A.M. Reinhorn and P. Bradford, 11/15/91, (PB92-176973, A10, MF-A03).

NCEER-92-0001 "Case Studies of Liquefaction and Lifeline Performance During Past Earthquakes, Volume 1: Japanese Case Studies," Edited by M. Hamada and T. O'Rourke, 2/17/92, (PB92-197243, A18, MF-A04).

NCEER-92-0002 "Case Studies of Liquefaction and Lifeline Performance During Past Earthquakes, Volume 2: United States Case Studies," Edited by T. O'Rourke and M. Hamada, 2/17/92, (PB92-197250, A20, MF-A04).

NCEER-92-0003 "Issues in Earthquake Education," Edited by K. Ross, 2/3/92, (PB92-222389, A07, MF-A02).

NCEER-92-0004 "Proceedings from the First U.S. - Japan Workshop on Earthquake Protective Systems for Bridges," Edited by I.G. Buckle, 2/4/92, (PB94-142239, A99, MF-A06).

NCEER-92-0005 "Seismic Ground Motion from a Haskell-Type Source in a Multiple-Layered Half-Space," A.P. Theoharis, G. Deodatis and M. Shinozuka, 1/2/92, to be published.

NCEER-92-0006 "Proceedings from the Site Effects Workshop," Edited by R. Whitman, 2/29/92, (PB92-197201, A04, MF-A01).

NCEER-92-0007 "Engineering Evaluation of Permanent Ground Deformations Due to Seismically-Induced Liquefaction," by M.H. Baziar, R. Dobry and A-W.M. Elgamal, 3/24/92, (PB92-222421, A13, MF-A03).

NCEER-92-0008 "A Procedure for the Seismic Evaluation of Buildings in the Central and Eastern United States," by C.D. Poland and J.O. Malley, 4/2/92, (PB92-222439, A20, MF-A04).

NCEER-92-0009 "Experimental and Analytical Study of a Hybrid Isolation System Using Friction Controllable Sliding Bearings," by M.Q. Feng, S. Fujii and M. Shinozuka, 5/15/92, (PB93-150282, A06, MF-A02).

NCEER-92-0010 "Seismic Resistance of Slab-Column Connections in Existing Non-Ductile Flat-Plate Buildings," by A.J. Durrani and Y. Du, 5/18/92, (PB93-116812, A06, MF-A02).

NCEER-92-0011 "The Hysteretic and Dynamic Behavior of Brick Masonry Walls Upgraded by Ferrocement Coatings Under Cyclic Loading and Strong Simulated Ground Motion," by H. Lee and S.P. Prawel, 5/11/92, to be published.

NCEER-92-0012 "Study of Wire Rope Systems for Seismic Protection of Equipment in Buildings," by G.F. Demetriades, M.C. Constantinou and A.M. Reinhorn, 5/20/92, (PB93-116655, A08, MF-A02).

NCEER-92-0013 "Shape Memory Structural Dampers: Material Properties, Design and Seismic Testing," by P.R. Witting and F.A. Cozzarelli, 5/26/92, (PB93-116663, A05, MF-A01).

NCEER-92-0014 "Longitudinal Permanent Ground Deformation Effects on Buried Continuous Pipelines," by M.J. O'Rourke, and C. Nordberg, 6/15/92, (PB93-116671, A08, MF-A02).

NCEER-92-0015 "A Simulation Method for Stationary Gaussian Random Functions Based on the Sampling Theorem," by M. Grigoriu and S. Balopoulou, 6/11/92, (PB93-127496, A05, MF-A01).

NCEER-92-0016 "Gravity-Load-Designed Reinforced Concrete Buildings: Seismic Evaluation of Existing Construction and Detailing Strategies for Improved Seismic Resistance," by G.W. Hoffmann, S.K. Kunnath, A.M. Reinhorn and J.B. Mander, 7/15/92, (PB94-142007, A08, MF-A02).

NCEER-92-0017 "Observations on Water System and Pipeline Performance in the Limón Area of Costa Rica Due to the April 22, 1991 Earthquake," by M. O'Rourke and D. Ballantyne, 6/30/92, (PB93-126811, A06, MF-A02).

NCEER-92-0018 "Fourth Edition of Earthquake Education Materials for Grades K-12," Edited by K.E.K. Ross, 8/10/92, (PB93-114023, A07, MF-A02).

NCEER-92-0019 "Proceedings from the Fourth Japan-U.S. Workshop on Earthquake Resistant Design of Lifeline Facilities and Countermeasures for Soil Liquefaction," Edited by M. Hamada and T.D. O'Rourke, 8/12/92, (PB93-163939, A99, MF-E11).

NCEER-92-0020 "Active Bracing System: A Full Scale Implementation of Active Control," by A.M. Reinhorn, T.T. Soong, R.C. Lin, M.A. Riley, Y.P. Wang, S. Aizawa and M. Higashino, 8/14/92, (PB93-127512, A06, MF-A02).

NCEER-92-0021 "Empirical Analysis of Horizontal Ground Displacement Generated by Liquefaction-Induced Lateral Spreads," by S.F. Bartlett and T.L. Youd, 8/17/92, (PB93-188241, A06, MF-A02).

NCEER-92-0022 "IDARC Version 3.0: Inelastic Damage Analysis of Reinforced Concrete Structures," by S.K. Kunnath, A.M. Reinhorn and R.F. Lobo, 8/31/92, (PB93-227502, A07, MF-A02).

NCEER-92-0023 "A Semi-Empirical Analysis of Strong-Motion Peaks in Terms of Seismic Source, Propagation Path and Local Site Conditions, by M. Kamiyama, M.J. O'Rourke and R. Flores-Berrones, 9/9/92, (PB93-150266, A08, MF-A02).

NCEER-92-0024 "Seismic Behavior of Reinforced Concrete Frame Structures with Nonductile Details, Part I: Summary of Experimental Findings of Full Scale Beam-Column Joint Tests," by A. Beres, R.N. White and P. Gergely, 9/30/92, (PB93-227783, A05, MF-A01).

NCEER-92-0025 "Experimental Results of Repaired and Retrofitted Beam-Column Joint Tests in Lightly Reinforced Concrete Frame Buildings," by A. Beres, S. El-Borgi, R.N. White and P. Gergely, 10/29/92, (PB93-227791, A05, MF-A01).

NCEER-92-0026 "A Generalization of Optimal Control Theory: Linear and Nonlinear Structures," by J.N. Yang, Z. Li and S. Vongchavalitkul, 11/2/92, (PB93-188621, A05, MF-A01).

NCEER-92-0027 "Seismic Resistance of Reinforced Concrete Frame Structures Designed Only for Gravity Loads: Part I - Design and Properties of a One-Third Scale Model Structure," by J.M. Bracci, A.M. Reinhorn and J.B. Mander, 12/1/92, (PB94-104502, A08, MF-A02).

NCEER-92-0028 "Seismic Resistance of Reinforced Concrete Frame Structures Designed Only for Gravity Loads: Part II - Experimental Performance of Subassemblages," by L.E. Aycardi, J.B. Mander and A.M. Reinhorn, 12/1/92, (PB94-104510, A08, MF-A02).

NCEER-92-0029 "Seismic Resistance of Reinforced Concrete Frame Structures Designed Only for Gravity Loads: Part III - Experimental Performance and Analytical Study of a Structural Model," by J.M. Bracci, A.M. Reinhorn and J.B. Mander, 12/1/92, (PB93-227528, A09, MF-A01).

NCEER-92-0030 "Evaluation of Seismic Retrofit of Reinforced Concrete Frame Structures: Part I - Experimental Performance of Retrofitted Subassemblages," by D. Choudhuri, J.B. Mander and A.M. Reinhorn, 12/8/92, (PB93-198307, A07, MF-A02).

NCEER-92-0031 "Evaluation of Seismic Retrofit of Reinforced Concrete Frame Structures: Part II - Experimental Performance and Analytical Study of a Retrofitted Structural Model," by J.M. Bracci, A.M. Reinhorn and J.B. Mander, 12/8/92, (PB93-198315, A09, MF-A03).

NCEER-92-0032 "Experimental and Analytical Investigation of Seismic Response of Structures with Supplemental Fluid Viscous Dampers," by M.C. Constantinou and M.D. Symans, 12/21/92, (PB93-191435, A10, MF-A03). This report is available only through NTIS (see address given above).

NCEER-92-0033 "Reconnaissance Report on the Cairo, Egypt Earthquake of October 12, 1992," by M. Khater, 12/23/92, (PB93-188621, A03, MF-A01).

NCEER-92-0034 "Low-Level Dynamic Characteristics of Four Tall Flat-Plate Buildings in New York City," by H. Gavin, S. Yuan, J. Grossman, E. Pekelis and K. Jacob, 12/28/92, (PB93-188217, A07, MF-A02).

NCEER-93-0001 "An Experimental Study on the Seismic Performance of Brick-Infilled Steel Frames With and Without Retrofit," by J.B. Mander, B. Nair, K. Wojtkowski and J. Ma, 1/29/93, (PB93-227510, A07, MF-A02).

NCEER-93-0002 "Social Accounting for Disaster Preparedness and Recovery Planning," by S. Cole, E. Pantoja and V. Razak, 2/22/93, (PB94-142114, A12, MF-A03).

NCEER-93-0003 "Assessment of 1991 NEHRP Provisions for Nonstructural Components and Recommended Revisions," by T.T. Soong, G. Chen, Z. Wu, R-H. Zhang and M. Grigoriu, 3/1/93, (PB93-188639, A06, MF-A02).

NCEER-93-0004 "Evaluation of Static and Response Spectrum Analysis Procedures of SEAOC/UBC for Seismic Isolated Structures," by C.W. Winters and M.C. Constantinou, 3/23/93, (PB93-198299, A10, MF-A03).

NCEER-93-0005 "Earthquakes in the Northeast - Are We Ignoring the Hazard? A Workshop on Earthquake Science and Safety for Educators," edited by K.E.K. Ross, 4/2/93, (PB94-103066, A09, MF-A02).

NCEER-93-0006 "Inelastic Response of Reinforced Concrete Structures with Viscoelastic Braces," by R.F. Lobo, J.M. Bracci, K.L. Shen, A.M. Reinhorn and T.T. Soong, 4/5/93, (PB93-227486, A05, MF-A02).

NCEER-93-0007 "Seismic Testing of Installation Methods for Computers and Data Processing Equipment," by K. Kosar, T.T. Soong, K.L. Shen, J.A. HoLung and Y.K. Lin, 4/12/93, (PB93-198299, A07, MF-A02).

NCEER-93-0008 "Retrofit of Reinforced Concrete Frames Using Added Dampers," by A. Reinhorn, M. Constantinou and C. Li, to be published.

NCEER-93-0009 "Seismic Behavior and Design Guidelines for Steel Frame Structures with Added Viscoelastic Dampers," by K.C. Chang, M.L. Lai, T.T. Soong, D.S. Hao and Y.C. Yeh, 5/1/93, (PB94-141959, A07, MF-A02).

NCEER-93-0010 "Seismic Performance of Shear-Critical Reinforced Concrete Bridge Piers," by J.B. Mander, S.M. Waheed, M.T.A. Chaudhary and S.S. Chen, 5/12/93, (PB93-227494, A08, MF-A02).

NCEER-93-0011 "3D-BASIS-TABS: Computer Program for Nonlinear Dynamic Analysis of Three Dimensional Base Isolated Structures," by S. Nagarajaiah, C. Li, A.M. Reinhorn and M.C. Constantinou, 8/2/93, (PB94-141819, A09, MF-A02).

NCEER-93-0012 "Effects of Hydrocarbon Spills from an Oil Pipeline Break on Ground Water," by O.J. Helweg and H.H.M. Hwang, 8/3/93, (PB94-141942, A06, MF-A02).

NCEER-93-0013 "Simplified Procedures for Seismic Design of Nonstructural Components and Assessment of Current Code Provisions," by M.P. Singh, L.E. Suarez, E.E. Matheu and G.O. Maldonado, 8/4/93, (PB94-141827, A09, MF-A02).

NCEER-93-0014 "An Energy Approach to Seismic Analysis and Design of Secondary Systems," by G. Chen and T.T. Soong, 8/6/93, (PB94-142767, A11, MF-A03).

NCEER-93-0015 "Proceedings from School Sites: Becoming Prepared for Earthquakes - Commemorating the Third Anniversary of the Loma Prieta Earthquake," Edited by F.E. Winslow and K.E.K. Ross, 8/16/93, (PB94-154275, A16, MF-A02).

NCEER-93-0016 "Reconnaissance Report of Damage to Historic Monuments in Cairo, Egypt Following the October 12, 1992 Dahshur Earthquake," by D. Sykora, D. Look, G. Croci, E. Karaesmen and E. Karaesmen, 8/19/93, (PB94-142221, A08, MF-A02).

NCEER-93-0017 "The Island of Guam Earthquake of August 8, 1993," by S.W. Swan and S.K. Harris, 9/30/93, (PB94-141843, A04, MF-A01).

NCEER-93-0018 "Engineering Aspects of the October 12, 1992 Egyptian Earthquake," by A.W. Elgamal, M. Amer, K. Adalier and A. Abul-Fadl, 10/7/93, (PB94-141983, A05, MF-A01).

NCEER-93-0019 "Development of an Earthquake Motion Simulator and its Application in Dynamic Centrifuge Testing," by I. Krstelj, Supervised by J.H. Prevost, 10/23/93, (PB94-181773, A-10, MF-A03).

NCEER-93-0020 "NCEER-Taisei Corporation Research Program on Sliding Seismic Isolation Systems for Bridges: Experimental and Analytical Study of a Friction Pendulum System (FPS)," by M.C. Constantinou, P. Tsopelas, Y-S. Kim and S. Okamoto, 11/1/93, (PB94-142775, A08, MF-A02).

NCEER-93-0021 "Finite Element Modeling of Elastomeric Seismic Isolation Bearings," by L.J. Billings, Supervised by R. Shepherd, 11/8/93, to be published.

NCEER-93-0022 "Seismic Vulnerability of Equipment in Critical Facilities: Life-Safety and Operational Consequences," by K. Porter, G.S. Johnson, M.M. Zadeh, C. Scawthorn and S. Eder, 11/24/93, (PB94-181765, A16, MF-A03).

NCEER-93-0023 "Hokkaido Nansei-oki, Japan Earthquake of July 12, 1993, by P.I. Yanev and C.R. Scawthorn, 12/23/93, (PB94-181500, A07, MF-A01).

NCEER-94-0001 "An Evaluation of Seismic Serviceability of Water Supply Networks with Application to the San Francisco Auxiliary Water Supply System," by I. Markov, Supervised by M. Grigoriu and T. O'Rourke, 1/21/94, (PB94-204013, A07, MF-A02).

NCEER-94-0002 "NCEER-Taisei Corporation Research Program on Sliding Seismic Isolation Systems for Bridges: Experimental and Analytical Study of Systems Consisting of Sliding Bearings, Rubber Restoring Force Devices and Fluid Dampers," Volumes I and II, by P. Tsopelas, S. Okamoto, M.C. Constantinou, D. Ozaki and S. Fujii, 2/4/94, (PB94-181740, A09, MF-A02 and PB94-181757, A12, MF-A03).

NCEER-94-0003 "A Markov Model for Local and Global Damage Indices in Seismic Analysis," by S. Rahman and M. Grigoriu, 2/18/94, (PB94-206000, A12, MF-A03).

NCEER-94-0004 "Proceedings from the NCEER Workshop on Seismic Response of Masonry Infills," edited by D.P. Abrams, 3/1/94, (PB94-180783, A07, MF-A02).

NCEER-94-0005 "The Northridge, California Earthquake of January 17, 1994: General Reconnaissance Report," edited by J.D. Goltz, 3/11/94, (PB193943, A10, MF-A03).

NCEER-94-0006 "Seismic Energy Based Fatigue Damage Analysis of Bridge Columns: Part I - Evaluation of Seismic Capacity," by G.A. Chang and J.B. Mander, 3/14/94, (PB94-219185, A11, MF-A03).

NCEER-94-0007 "Seismic Isolation of Multi-Story Frame Structures Using Spherical Sliding Isolation Systems," by T.M. Al-Hussaini, V.A. Zayas and M.C. Constantinou, 3/17/94, (PB193745, A09, MF-A02).

NCEER-94-0008 "The Northridge, California Earthquake of January 17, 1994: Performance of Highway Bridges," edited by I.G. Buckle, 3/24/94, (PB94-193851, A06, MF-A02).

NCEER-94-0009 "Proceedings of the Third U.S.-Japan Workshop on Earthquake Protective Systems for Bridges," edited by I.G. Buckle and I. Friedland, 3/31/94, (PB94-195815, A99, MF-A06).

NCEER-94-0010 "3D-BASIS-ME: Computer Program for Nonlinear Dynamic Analysis of Seismically Isolated Single and Multiple Structures and Liquid Storage Tanks," by P.C. Tsopelas, M.C. Constantinou and A.M. Reinhorn, 4/12/94, (PB94-204922, A09, MF-A02).

NCEER-94-0011 "The Northridge, California Earthquake of January 17, 1994: Performance of Gas Transmission Pipelines," by T.D. O'Rourke and M.C. Palmer, 5/16/94, (PB94-204989, A05, MF-A01).

NCEER-94-0012 "Feasibility Study of Replacement Procedures and Earthquake Performance Related to Gas Transmission Pipelines," by T.D. O'Rourke and M.C. Palmer, 5/25/94, (PB94-206638, A09, MF-A02).

NCEER-94-0013 "Seismic Energy Based Fatigue Damage Analysis of Bridge Columns: Part II - Evaluation of Seismic Demand," by G.A. Chang and J.B. Mander, 6/1/94, (PB95-18106, A08, MF-A02).

NCEER-94-0014 "NCEER-Taisei Corporation Research Program on Sliding Seismic Isolation Systems for Bridges: Experimental and Analytical Study of a System Consisting of Sliding Bearings and Fluid Restoring Force/Damping Devices," by P. Tsopelas and M.C. Constantinou, 6/13/94, (PB94-219144, A10, MF-A03).

NCEER-94-0015 "Generation of Hazard-Consistent Fragility Curves for Seismic Loss Estimation Studies," by H. Hwang and J-R. Huo, 6/14/94, (PB95-181996, A09, MF-A02).

NCEER-94-0016 "Seismic Study of Building Frames with Added Energy-Absorbing Devices," by W.S. Pong, C.S. Tsai and G.C. Lee, 6/20/94, (PB94-219136, A10, A03).

NCEER-94-0017 "Sliding Mode Control for Seismic-Excited Linear and Nonlinear Civil Engineering Structures," by J. Yang, J. Wu, A. Agrawal and Z. Li, 6/21/94, (PB95-138483, A06, MF-A02).

NCEER-94-0018 "3D-BASIS-TABS Version 2.0: Computer Program for Nonlinear Dynamic Analysis of Three Dimensional Base Isolated Structures," by A.M. Reinhorn, S. Nagarajaiah, M.C. Constantinou, P. Tsopelas and R. Li, 6/22/94, (PB95-182176, A08, MF-A02).

NCEER-94-0019 "Proceedings of the International Workshop on Civil Infrastructure Systems: Application of Intelligent Systems and Advanced Materials on Bridge Systems," Edited by G.C. Lee and K.C. Chang, 7/18/94, (PB95-252474, A20, MF-A04).

NCEER-94-0020 "Study of Seismic Isolation Systems for Computer Floors," by V. Lambrou and M.C. Constantinou, 7/19/94, (PB95-138533, A10, MF-A03).

NCEER-94-0021 "Proceedings of the U.S.-Italian Workshop on Guidelines for Seismic Evaluation and Rehabilitation of Unreinforced Masonry Buildings," Edited by D.P. Abrams and G.M. Calvi, 7/20/94, (PB95-138749, A13, MF-A03).

NCEER-94-0022 "NCEER-Taisei Corporation Research Program on Sliding Seismic Isolation Systems for Bridges: Experimental and Analytical Study of a System Consisting of Lubricated PTFE Sliding Bearings and Mild Steel Dampers," by P. Tsopelas and M.C. Constantinou, 7/22/94, (PB95-182184, A08, MF-A02).

NCEER-94-0023 “Development of Reliability-Based Design Criteria for Buildings Under Seismic Load,” by Y.K. Wen, H. Hwang and M. Shinozuka, 8/1/94, (PB95-211934, A08, MF-A02).

NCEER-94-0024 “Experimental Verification of Acceleration Feedback Control Strategies for an Active Tendon System,” by S.J. Dyke, B.F. Spencer, Jr., P. Quast, M.K. Sain, D.C. Kaspari, Jr. and T.T. Soong, 8/29/94, (PB95-212320, A05, MF-A01).

NCEER-94-0025 “Seismic Retrofitting Manual for Highway Bridges,” Edited by I.G. Buckle and I.F. Friedland, published by the Federal Highway Administration (PB95-212676, A15, MF-A03).

NCEER-94-0026 “Proceedings from the Fifth U.S.-Japan Workshop on Earthquake Resistant Design of Lifeline Facilities and Countermeasures Against Soil Liquefaction,” Edited by T.D. O’Rourke and M. Hamada, 11/7/94, (PB95-220802, A99, MF-E08).

NCEER-95-0001 “Experimental and Analytical Investigation of Seismic Retrofit of Structures with Supplemental Damping: Part 1 - Fluid Viscous Damping Devices,” by A.M. Reinhorn, C. Li and M.C. Constantinou, 1/3/95, (PB95-266599, A09, MF-A02).

NCEER-95-0002 “Experimental and Analytical Study of Low-Cycle Fatigue Behavior of Semi-Rigid Top-And-Seat Angle Connections,” by G. Pekcan, J.B. Mander and S.S. Chen, 1/5/95, (PB95-220042, A07, MF-A02).

NCEER-95-0003 “NCEER-ATC Joint Study on Fragility of Buildings,” by T. Anagnos, C. Rojahn and A.S. Kiremidjian, 1/20/95, (PB95-220026, A06, MF-A02).

NCEER-95-0004 “Nonlinear Control Algorithms for Peak Response Reduction,” by Z. Wu, T.T. Soong, V. Gattulli and R.C. Lin, 2/16/95, (PB95-220349, A05, MF-A01).

NCEER-95-0005 “Pipeline Replacement Feasibility Study: A Methodology for Minimizing Seismic and Corrosion Risks to Underground Natural Gas Pipelines,” by R.T. Eguchi, H.A. Seligson and D.G. Honegger, 3/2/95, (PB95-252326, A06, MF-A02).

NCEER-95-0006 “Evaluation of Seismic Performance of an 11-Story Frame Building During the 1994 Northridge Earthquake,” by F. Naeim, R. DiSulio, K. Benuska, A. Reinhorn and C. Li, to be published.

NCEER-95-0007 “Prioritization of Bridges for Seismic Retrofitting,” by N. Basöz and A.S. Kiremidjian, 4/24/95, (PB95-252300, A08, MF-A02).

NCEER-95-0008 “Method for Developing Motion Damage Relationships for Reinforced Concrete Frames,” by A. Singhal and A.S. Kiremidjian, 5/11/95, (PB95-266607, A06, MF-A02).

NCEER-95-0009 “Experimental and Analytical Investigation of Seismic Retrofit of Structures with Supplemental Damping: Part II - Friction Devices,” by C. Li and A.M. Reinhorn, 7/6/95, (PB96-128087, A11, MF-A03).

NCEER-95-0010 “Experimental Performance and Analytical Study of a Non-Ductile Reinforced Concrete Frame Structure Retrofitted with Elastomeric Spring Dampers,” by G. Pekcan, J.B. Mander and S.S. Chen, 7/14/95, (PB96-137161, A08, MF-A02).

NCEER-95-0011 “Development and Experimental Study of Semi-Active Fluid Damping Devices for Seismic Protection of Structures,” by M.D. Symans and M.C. Constantinou, 8/3/95, (PB96-136940, A23, MF-A04).

NCEER-95-0012 “Real-Time Structural Parameter Modification (RSPM): Development of Innervated Structures,” by Z. Liang, M. Tong and G.C. Lee, 4/11/95, (PB96-137153, A06, MF-A01).

NCEER-95-0013 “Experimental and Analytical Investigation of Seismic Retrofit of Structures with Supplemental Damping: Part III - Viscous Damping Walls,” by A.M. Reinhorn and C. Li, 10/1/95, (PB96-176409, A11, MF-A03).

NCEER-95-0014 “Seismic Fragility Analysis of Equipment and Structures in a Memphis Electric Substation,” by J-R. Huo and H.H.M. Hwang, (PB96-128087, A09, MF-A02), 8/10/95.

NCEER-95-0015 “The Hanshin-Awaji Earthquake of January 17, 1995: Performance of Lifelines,” Edited by M. Shinozuka, 11/3/95, (PB96-176383, A15, MF-A03).

NCEER-95-0016 “Highway Culvert Performance During Earthquakes,” by T.L. Youd and C.J. Beckman, available as NCEER-96-0015.

NCEER-95-0017 “The Hanshin-Awaji Earthquake of January 17, 1995: Performance of Highway Bridges,” Edited by I.G. Buckle, 12/1/95, to be published.

NCEER-95-0018 “Modeling of Masonry Infill Panels for Structural Analysis,” by A.M. Reinhorn, A. Madan, R.E. Valles, Y. Reichmann and J.B. Mander, 12/8/95, (PB97-110886, MF-A01, A06).

NCEER-95-0019 “Optimal Polynomial Control for Linear and Nonlinear Structures,” by A.K. Agrawal and J.N. Yang, 12/11/95, (PB96-168737, A07, MF-A02).

NCEER-95-0020 "Retrofit of Non-Ductile Reinforced Concrete Frames Using Friction Dampers," by R.S. Rao, P. Gergely and R.N. White, 12/22/95, (PB97-133508, A10, MF-A02).

NCEER-95-0021 "Parametric Results for Seismic Response of Pile-Supported Bridge Bents," by G. Mylonakis, A. Nikolaou and G. Gazetas, 12/22/95, (PB97-100242, A12, MF-A03).

NCEER-95-0022 "Kinematic Bending Moments in Seismically Stressed Piles," by A. Nikolaou, G. Mylonakis and G. Gazetas, 12/23/95, (PB97-113914, MF-A03, A13).

NCEER-96-0001 "Dynamic Response of Unreinforced Masonry Buildings with Flexible Diaphragms," by A.C. Costley and D.P. Abrams," 10/10/96, (PB97-133573, MF-A03, A15).

NCEER-96-0002 "State of the Art Review: Foundations and Retaining Structures," by I. Po Lam, to be published.

NCEER-96-0003 "Ductility of Rectangular Reinforced Concrete Bridge Columns with Moderate Confinement," by N. Wehbe, M. Saiidi, D. Sanders and B. Douglas, 11/7/96, (PB97-133557, A06, MF-A02).

NCEER-96-0004 "Proceedings of the Long-Span Bridge Seismic Research Workshop," edited by I.G. Buckle and I.M. Friedland, to be published.

NCEER-96-0005 "Establish Representative Pier Types for Comprehensive Study: Eastern United States," by J. Kulicki and Z. Prucz, 5/28/96, (PB98-119217, A07, MF-A02).

NCEER-96-0006 "Establish Representative Pier Types for Comprehensive Study: Western United States," by R. Imbsen, R.A. Schamber and T.A. Osterkamp, 5/28/96, (PB98-118607, A07, MF-A02).

NCEER-96-0007 "Nonlinear Control Techniques for Dynamical Systems with Uncertain Parameters," by R.G. Ghanem and M.I. Bujakov, 5/27/96, (PB97-100259, A17, MF-A03).

NCEER-96-0008 "Seismic Evaluation of a 30-Year Old Non-Ductile Highway Bridge Pier and Its Retrofit," by J.B. Mander, B. Mahmoodzadegan, S. Bhadra and S.S. Chen, 5/31/96, (PB97-110902, MF-A03, A10).

NCEER-96-0009 "Seismic Performance of a Model Reinforced Concrete Bridge Pier Before and After Retrofit," by J.B. Mander, J.H. Kim and C.A. Ligozio, 5/31/96, (PB97-110910, MF-A02, A10).

NCEER-96-0010 "IDARC2D Version 4.0: A Computer Program for the Inelastic Damage Analysis of Buildings," by R.E. Valles, A.M. Reinhorn, S.K. Kunnath, C. Li and A. Madan, 6/3/96, (PB97-100234, A17, MF-A03).

NCEER-96-0011 "Estimation of the Economic Impact of Multiple Lifeline Disruption: Memphis Light, Gas and Water Division Case Study," by S.E. Chang, H.A. Seligson and R.T. Eguchi, 8/16/96, (PB97-133490, A11, MF-A03).

NCEER-96-0012 "Proceedings from the Sixth Japan-U.S. Workshop on Earthquake Resistant Design of Lifeline Facilities and Countermeasures Against Soil Liquefaction, Edited by M. Hamada and T. O'Rourke, 9/11/96, (PB97-133581, A99, MF-A06).

NCEER-96-0013 "Chemical Hazards, Mitigation and Preparedness in Areas of High Seismic Risk: A Methodology for Estimating the Risk of Post-Earthquake Hazardous Materials Release," by H.A. Seligson, R.T. Eguchi, K.J. Tierney and K. Richmond, 11/7/96, (PB97-133565, MF-A02, A08).

NCEER-96-0014 "Response of Steel Bridge Bearings to Reversed Cyclic Loading," by J.B. Mander, D-K. Kim, S.S. Chen and G.J. Premus, 11/13/96, (PB97-140735, A12, MF-A03).

NCEER-96-0015 "Highway Culvert Performance During Past Earthquakes," by T.L. Youd and C.J. Beckman, 11/25/96, (PB97-133532, A06, MF-A01).

NCEER-97-0001 "Evaluation, Prevention and Mitigation of Pounding Effects in Building Structures," by R.E. Valles and A.M. Reinhorn, 2/20/97, (PB97-159552, A14, MF-A03).

NCEER-97-0002 "Seismic Design Criteria for Bridges and Other Highway Structures," by C. Rojahn, R. Mayes, D.G. Anderson, J. Clark, J.H. Hom, R.V. Nutt and M.J. O'Rourke, 4/30/97, (PB97-194658, A06, MF-A03).

NCEER-97-0003 “Proceedings of the U.S.-Italian Workshop on Seismic Evaluation and Retrofit,” Edited by D.P. Abrams and G.M. Calvi, 3/19/97, (PB97-194666, A13, MF-A03).

NCEER-97-0004 "Investigation of Seismic Response of Buildings with Linear and Nonlinear Fluid Viscous Dampers," by A.A. Seleemah and M.C. Constantinou, 5/21/97, (PB98-109002, A15, MF-A03).

NCEER-97-0005 "Proceedings of the Workshop on Earthquake Engineering Frontiers in Transportation Facilities," edited by G.C. Lee and I.M. Friedland, 8/29/97, (PB98-128911, A25, MR-A04).

NCEER-97-0006 "Cumulative Seismic Damage of Reinforced Concrete Bridge Piers," by S.K. Kunnath, A. El-Bahy, A. Taylor and W. Stone, 9/2/97, (PB98-108814, A11, MF-A03).

NCEER-97-0007 "Structural Details to Accommodate Seismic Movements of Highway Bridges and Retaining Walls," by R.A. Imbsen, R.A. Schamber, E. Thorkildsen, A. Kartoum, B.T. Martin, T.N. Rosser and J.M. Kulicki, 9/3/97, (PB98-108996, A09, MF-A02).

NCEER-97-0008 "A Method for Earthquake Motion-Damage Relationships with Application to Reinforced Concrete Frames," by A. Singhal and A.S. Kiremidjian, 9/10/97, (PB98-108988, A13, MF-A03).

NCEER-97-0009 "Seismic Analysis and Design of Bridge Abutments Considering Sliding and Rotation," by K. Fishman and R. Richards, Jr., 9/15/97, (PB98-108897, A06, MF-A02).

NCEER-97-0010 "Proceedings of the FHWA/NCEER Workshop on the National Representation of Seismic Ground Motion for New and Existing Highway Facilities," edited by I.M. Friedland, M.S. Power and R.L. Mayes, 9/22/97, (PB98-128903, A21, MF-A04).

NCEER-97-0011 "Seismic Analysis for Design or Retrofit of Gravity Bridge Abutments," by K.L. Fishman, R. Richards, Jr. and R.C. Divito, 10/2/97, (PB98-128937, A08, MF-A02).

NCEER-97-0012 "Evaluation of Simplified Methods of Analysis for Yielding Structures," by P. Tsopelas, M.C. Constantinou, C.A. Kircher and A.S. Whittaker, 10/31/97, (PB98-128929, A10, MF-A03).

NCEER-97-0013 "Seismic Design of Bridge Columns Based on Control and Repairability of Damage," by C-T. Cheng and J.B. Mander, 12/8/97, (PB98-144249, A11, MF-A03).

NCEER-97-0014 "Seismic Resistance of Bridge Piers Based on Damage Avoidance Design," by J.B. Mander and C-T. Cheng, 12/10/97, (PB98-144223, A09, MF-A02).

NCEER-97-0015 “Seismic Response of Nominally Symmetric Systems with Strength Uncertainty,” by S. Balopoulou and M. Grigoriu, 12/23/97, (PB98-153422, A11, MF-A03).

NCEER-97-0016 “Evaluation of Seismic Retrofit Methods for Reinforced Concrete Bridge Columns,” by T.J. Wipf, F.W. Klaiber and F.M. Russo, 12/28/97, (PB98-144215, A12, MF-A03).

NCEER-97-0017 “Seismic Fragility of Existing Conventional Reinforced Concrete Highway Bridges,” by C.L. Mullen and A.S. Cakmak, 12/30/97, (PB98-153406, A08, MF-A02).

NCEER-97-0018 “Loss Asssessment of Memphis Buildings,” edited by D.P. Abrams and M. Shinozuka, 12/31/97, (PB98-144231, A13, MF-A03).

NCEER-97-0019 “Seismic Evaluation of Frames with Infill Walls Using Quasi-static Experiments,” by K.M. Mosalam, R.N. White and P. Gergely, 12/31/97, (PB98-153455, A07, MF-A02).

NCEER-97-0020 “Seismic Evaluation of Frames with Infill Walls Using Pseudo-dynamic Experiments,” by K.M. Mosalam, R.N. White and P. Gergely, 12/31/97, (PB98-153430, A07, MF-A02).

NCEER-97-0021 “Computational Strategies for Frames with Infill Walls: Discrete and Smeared Crack Analyses and Seismic Fragility,” by K.M. Mosalam, R.N. White and P. Gergely, 12/31/97, (PB98-153414, A10, MF-A02).

NCEER-97-0022 "Proceedings of the NCEER Workshop on Evaluation of Liquefaction Resistance of Soils," edited by T.L. Youd and I.M. Idriss, 12/31/97, (PB98-155617, A15, MF-A03).

MCEER-98-0001 "Extraction of Nonlinear Hysteretic Properties of Seismically Isolated Bridges from Quick-Release Field Tests," by Q. Chen, B.M. Douglas, E.M. Maragakis and I.G. Buckle, 5/26/98, (PB99-118838, A06, MF-A01).

MCEER-98-0002 "Methodologies for Evaluating the Importance of Highway Bridges," by A. Thomas, S. Eshenaur and J. Kulicki, 5/29/98, (PB99-118846, A10, MF-A02).

MCEER-98-0003 "Capacity Design of Bridge Piers and the Analysis of Overstrength," by J.B. Mander, A. Dutta and P. Goel, 6/1/98, (PB99-118853, A09, MF-A02).

MCEER-98-0004 "Evaluation of Bridge Damage Data from the Loma Prieta and Northridge, California Earthquakes," by N. Basoz and A. Kiremidjian, 6/2/98, (PB99-118861, A15, MF-A03).

MCEER-98-0005 "Screening Guide for Rapid Assessment of Liquefaction Hazard at Highway Bridge Sites," by T. L. Youd, 6/16/98, (PB99-118879, A06, not available on microfiche).

MCEER-98-0006 "Structural Steel and Steel/Concrete Interface Details for Bridges," by P. Ritchie, N. Kauhl and J. Kulicki, 7/13/98, (PB99-118945, A06, MF-A01).

MCEER-98-0007 "Capacity Design and Fatigue Analysis of Confined Concrete Columns," by A. Dutta and J.B. Mander, 7/14/98, (PB99-118960, A14, MF-A03).

MCEER-98-0008 "Proceedings of the Workshop on Performance Criteria for Telecommunication Services Under Earthquake Conditions," edited by A.J. Schiff, 7/15/98, (PB99-118952, A08, MF-A02).

MCEER-98-0009 "Fatigue Analysis of Unconfined Concrete Columns," by J.B. Mander, A. Dutta and J.H. Kim, 9/12/98, (PB99-123655, A10, MF-A02).

MCEER-98-0010 "Centrifuge Modeling of Cyclic Lateral Response of Pile-Cap Systems and Seat-Type Abutments in Dry Sands," by A.D. Gadre and R. Dobry, 10/2/98, (PB99-123606, A13, MF-A03).

MCEER-98-0011 "IDARC-BRIDGE: A Computational Platform for Seismic Damage Assessment of Bridge Structures," by A.M. Reinhorn, V. Simeonov, G. Mylonakis and Y. Reichman, 10/2/98, (PB99-162919, A15, MF-A03).

MCEER-98-0012 "Experimental Investigation of the Dynamic Response of Two Bridges Before and After Retrofitting with Elastomeric Bearings," by D.A. Wendichansky, S.S. Chen and J.B. Mander, 10/2/98, (PB99-162927, A15, MF-A03).

MCEER-98-0013 "Design Procedures for Hinge Restrainers and Hinge Sear Width for Multiple-Frame Bridges," by R. Des Roches and G.L. Fenves, 11/3/98, (PB99-140477, A13, MF-A03).

MCEER-98-0014 "Response Modification Factors for Seismically Isolated Bridges," by M.C. Constantinou and J.K. Quarshie, 11/3/98, (PB99-140485, A14, MF-A03).

MCEER-98-0015 "Proceedings of the U.S.-Italy Workshop on Seismic Protective Systems for Bridges," edited by I.M. Friedland and M.C. Constantinou, 11/3/98, (PB2000-101711, A22, MF-A04).

MCEER-98-0016 "Appropriate Seismic Reliability for Critical Equipment Systems: Recommendations Based on Regional Analysis of Financial and Life Loss," by K. Porter, C. Scawthorn, C. Taylor and N. Blais, 11/10/98, (PB99-157265, A08, MF-A02).

MCEER-98-0017 "Proceedings of the U.S. Japan Joint Seminar on Civil Infrastructure Systems Research," edited by M. Shinozuka and A. Rose, 11/12/98, (PB99-156713, A16, MF-A03).

MCEER-98-0018 "Modeling of Pile Footings and Drilled Shafts for Seismic Design," by I. PoLam, M. Kapuskar and D. Chaudhuri, 12/21/98, (PB99-157257, A09, MF-A02).

MCEER-99-0001 "Seismic Evaluation of a Masonry Infilled Reinforced Concrete Frame by Pseudodynamic Testing," by S.G. Buonopane and R.N. White, 2/16/99, (PB99-162851, A09, MF-A02).

MCEER-99-0002 "Response History Analysis of Structures with Seismic Isolation and Energy Dissipation Systems: Verification Examples for Program SAP2000," by J. Scheller and M.C. Constantinou, 2/22/99, (PB99-162869, A08, MF-A02).

MCEER-99-0003 "Experimental Study on the Seismic Design and Retrofit of Bridge Columns Including Axial Load Effects," by A. Dutta, T. Kokorina and J.B. Mander, 2/22/99, (PB99-162877, A09, MF-A02).

MCEER-99-0004 "Experimental Study of Bridge Elastomeric and Other Isolation and Energy Dissipation Systems with Emphasis on Uplift Prevention and High Velocity Near-source Seismic Excitation," by A. Kasalanati and M. C. Constantinou, 2/26/99, (PB99-162885, A12, MF-A03).

MCEER-99-0005 "Truss Modeling of Reinforced Concrete Shear-flexure Behavior," by J.H. Kim and J.B. Mander, 3/8/99, (PB99-163693, A12, MF-A03).

MCEER-99-0006 "Experimental Investigation and Computational Modeling of Seismic Response of a 1:4 Scale Model Steel Structure with a Load Balancing Supplemental Damping System," by G. Pekcan, J.B. Mander and S.S. Chen, 4/2/99, (PB99-162893, A11, MF-A03).

MCEER-99-0007 "Effect of Vertical Ground Motions on the Structural Response of Highway Bridges," by M.R. Button, C.J. Cronin and R.L. Mayes, 4/10/99, (PB2000-101411, A10, MF-A03).

MCEER-99-0008 "Seismic Reliability Assessment of Critical Facilities: A Handbook, Supporting Documentation, and Model Code Provisions," by G.S. Johnson, R.E. Sheppard, M.D. Quilici, S.J. Eder and C.R. Scawthorn, 4/12/99, (PB2000-101701, A18, MF-A04).

MCEER-99-0009 "Impact Assessment of Selected MCEER Highway Project Research on the Seismic Design of Highway Structures," by C. Rojahn, R. Mayes, D.G. Anderson, J.H. Clark, D'Appolonia Engineering, S. Gloyd and R.V. Nutt, 4/14/99, (PB99-162901, A10, MF-A02).

MCEER-99-0010 "Site Factors and Site Categories in Seismic Codes," by R. Dobry, R. Ramos and M.S. Power, 7/19/99, (PB2000-101705, A08, MF-A02).

MCEER-99-0011 "Restrainer Design Procedures for Multi-Span Simply-Supported Bridges," by M.J. Randall, M. Saiidi, E. Maragakis and T. Isakovic, 7/20/99, (PB2000-101702, A10, MF-A02).

MCEER-99-0012 "Property Modification Factors for Seismic Isolation Bearings," by M.C. Constantinou, P. Tsopelas, A. Kasalanati and E. Wolff, 7/20/99, (PB2000-103387, A11, MF-A03).

MCEER-99-0013 "Critical Seismic Issues for Existing Steel Bridges," by P. Ritchie, N. Kauhl and J. Kulicki, 7/20/99, (PB2000-101697, A09, MF-A02).

MCEER-99-0014 "Nonstructural Damage Database," by A. Kao, T.T. Soong and A. Vender, 7/24/99, (PB2000-101407, A06, MF-A01).

MCEER-99-0015 "Guide to Remedial Measures for Liquefaction Mitigation at Existing Highway Bridge Sites," by H.G. Cooke and J. K. Mitchell, 7/26/99, (PB2000-101703, A11, MF-A03).

MCEER-99-0016 "Proceedings of the MCEER Workshop on Ground Motion Methodologies for the Eastern United States," edited by N. Abrahamson and A. Becker, 8/11/99, (PB2000-103385, A07, MF-A02).

MCEER-99-0017 "Quindío, Colombia Earthquake of January 25, 1999: Reconnaissance Report," by A.P. Asfura and P.J. Flores, 10/4/99, (PB2000-106893, A06, MF-A01).

MCEER-99-0018 "Hysteretic Models for Cyclic Behavior of Deteriorating Inelastic Structures," by M.V. Sivaselvan and A.M. Reinhorn, 11/5/99, (PB2000-103386, A08, MF-A02).

MCEER-99-0019 "Proceedings of the 7th U.S.- Japan Workshop on Earthquake Resistant Design of Lifeline Facilities and Countermeasures Against Soil Liquefaction," edited by T.D. O'Rourke, J.P. Bardet and M. Hamada, 11/19/99, (PB2000-103354, A99, MF-A06).

MCEER-99-0020 "Development of Measurement Capability for Micro-Vibration Evaluations with Application to Chip Fabrication Facilities," by G.C. Lee, Z. Liang, J.W. Song, J.D. Shen and W.C. Liu, 12/1/99, (PB2000-105993, A08, MF-A02).

MCEER-99-0021 "Design and Retrofit Methodology for Building Structures with Supplemental Energy Dissipating Systems," by G. Pekcan, J.B. Mander and S.S. Chen, 12/31/99, (PB2000-105994, A11, MF-A03).

MCEER-00-0001 "The Marmara, Turkey Earthquake of August 17, 1999: Reconnaissance Report," edited by C. Scawthorn; with major contributions by M. Bruneau, R. Eguchi, T. Holzer, G. Johnson, J. Mander, J. Mitchell, W. Mitchell, A. Papageorgiou, C. Scaethorn, and G. Webb, 3/23/00, (PB2000-106200, A11, MF-A03).

MCEER-00-0002 "Proceedings of the MCEER Workshop for Seismic Hazard Mitigation of Health Care Facilities," edited by G.C. Lee, M. Ettouney, M. Grigoriu, J. Hauer and J. Nigg, 3/29/00, (PB2000-106892, A08, MF-A02).

MCEER-00-0003 "The Chi-Chi, Taiwan Earthquake of September 21, 1999: Reconnaissance Report," edited by G.C. Lee and C.H. Loh, with major contributions by G.C. Lee, M. Bruneau, I.G. Buckle, S.E. Chang, P.J. Flores, T.D. O'Rourke, M. Shinozuka, T.T. Soong, C-H. Loh, K-C. Chang, Z-J. Chen, J-S. Hwang, M-L. Lin, G-Y. Liu, K-C. Tsai, G.C. Yao and C-L. Yen, 4/30/00.

MCEER-00-0004 "Seismic Retrofit of End-Sway Frames of Steel Deck-Truss Bridges with a Supplemental Tendon System: Experimental and Analytical Investigation," by G. Pekcan, J.B. Mander and S.S. Chen, 7/1/00.

MCEER-00-0005 "Sliding Fragility of Unrestrained Equipment in Critical Facilities," by W.H. Chong and T.T. Soong, 7/5/00.

MCEER-00-0006 "Seismic Response of Reinforced Concrete Bridge Pier Walls in the Weak Direction," by N. Abo-Shadi, M. Saiidi and D. Sanders, 7/17/00.

MCEER-00-0007 "Low-Cycle Fatigue Behavior of Longitudinal Reinforcement in Reinforced Concrete Bridge Columns," by J. Brown and S.K. Kunnath, 7/23/00.

MCEER-00-0008 "Soil Structure Interaction of Bridges for Seismic Analysis," I. PoLam and H. Law, 9/25/00.

MCEER-00-0009 "Proceedings of the First MCEER Workshop on Mitigation of Earthquake Disaster by Advanced Technologies (MEDAT-1), edited by M. Shinozuka, D.J. Inman and T.D. O'Rourke, 11/10/00.

MCEER-00-0010 "Development and Evaluation of Simplified Procedures for Analysis and Design of Buildings with Passive Energy Dissipation Systems," by O.M. Ramirez, M.C. Constantinou, C.A. Kircher, A.S. Whittaker, M.W. Johnson, J.D. Gomez and C. Chrysostomou, 11/16/01.

MCEER-00-0011 "Dynamic Soil-Foundation-Structure Interaction Analyses of Large Caissons," by C-Y. Chang, C-M. Mok, Z-L. Wang, R. Settgast, F. Waggoner, M.A. Ketchum, H.M. Gonnermann and C-C. Chin, 12/30/00.

MCEER-00-0012 "Experimental Evaluation of Seismic Performance of Bridge Restrainers," by A.G. Vlassis, E.M. Maragakis and M. Saiid Saiidi, 12/30/00.

MCEER-00-0013 "Effect of Spatial Variation of Ground Motion on Highway Structures," by M. Shinozuka, V. Saxena and G. Deodatis, 12/31/00.

MCEER-00-0014 "A Risk-Based Methodology for Assessing the Seismic Performance of Highway Systems," by S.D. Werner, C.E. Taylor, J.E. Moore, II, J.S. Walton and S. Cho, 12/31/00.

MCEER-01-0001 “Experimental Investigation of P-Delta Effects to Collapse During Earthquakes,” by D. Vian and M. Bruneau, 6/25/01.

MCEER-01-0002 “Proceedings of the Second MCEER Workshop on Mitigation of Earthquake Disaster by Advanced Technologies (MEDAT-2),” edited by M. Bruneau and D.J. Inman, 7/23/01.

MCEER-01-0003 "Sensitivity Analysis of Dynamic Systems Subjected to Seismic Loads," by C. Roth and M. Grigoriu, 9/18/01.

MCEER-01-0004 "Overcoming Obstacles to Implementing Earthquake Hazard Mitigation Policies: Stage 1 Report," by D.J. Alesch and W.J. Petak, 12/17/01.

MCEER-01-0005 "Updating Real-Time Earthquake Loss Estimates: Methods, Problems and Insights," by C.E. Taylor, S.E. Chang and R.T. Eguchi, 12/17/01.

MCEER-01-0006 "Experimental Investigation and Retrofit of Steel Pile Foundations and Pile Bents Under Cyclic Lateral Loadings," by A. Shama, J. Mander, B. Blabac and S. Chen, 12/31/01.

MCEER-02-0001 "Assessment of Performance of Bolu Viaduct in the 1999 Duzce Earthquake in Turkey" by P.C. Roussis, M.C. Constantinou, M. Erdik, E. Durukal and M. Dicleli, 5/8/02.

MCEER-02-0002 "Seismic Behavior of Rail Counterweight Systems of Elevators in Buildings," by M.P. Singh, Rildova and L.E. Suarez, 5/27/02.

MCEER-02-0003 "Development of Analysis and Design Procedures for Spread Footings," by G. Mylonakis, G. Gazetas, S. Nikolaou and A. Chauncey, 10/02/02.

MCEER-02-0004 "Bare-Earth Algorithms for Use with SAR and LIDAR Digital Elevation Models," by C.K. Huyck, R.T. Eguchi and B. Houshmand, 10/16/02.

MCEER-02-0005 "Review of Energy Dissipation of Compression Members in Concentrically Braced Frames," by K.Lee and M. Bruneau, 10/18/02.

MCEER-03-0001 "Experimental Investigation of Light-Gauge Steel Plate Shear Walls for the Seismic Retrofit of Buildings" by J. Berman and M. Bruneau, 5/2/03.

MCEER-03-0002 "Statistical Analysis of Fragility Curves," by M. Shinozuka, M.Q. Feng, H. Kim, T. Uzawa and T. Ueda, 6/16/03.

MCEER-03-0003 "Proceedings of the Eighth U.S.-Japan Workshop on Earthquake Resistant Design f Lifeline Facilities and Countermeasures Against Liquefaction," edited by M. Hamada, J.P. Bardet and T.D. O'Rourke, 6/30/03.

MCEER-03-0004 "Proceedings of the PRC-US Workshop on Seismic Analysis and Design of Special Bridges," edited by L.C. Fan and G.C. Lee, 7/15/03.

MCEER-03-0005 "Urban Disaster Recovery: A Framework and Simulation Model," by S.B. Miles and S.E. Chang, 7/25/03.

MCEER-03-0006 "Behavior of Underground Piping Joints Due to Static and Dynamic Loading," by R.D. Meis, M. Maragakis and R. Siddharthan, 11/17/03.

University at Buffalo, State University of New York
Red Jacket Quadrangle ■ Buffalo, New York 14261
Phone: (716) 645-3391 ■ Fax: (716) 645-3399
E-mail: *mceer@mceermail.buffalo.edu* ■ WWW Site *http://mceer.buffalo.edu*

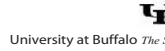

University at Buffalo *The State University of New York*

ISSN 1520-295X